NONREDUCTIVE BIOMINERALIZATION OF URANIUM(VI) AS A RESULT OF MICROBIAL PHOSPHATASE ACTIVITY

A Dissertation
Presented to
The Academic Faculty

by

Melanie J Beazley

In Partial Fulfillment
of the Requirements for the Degree
Doctor of Philosophy in the
School of Earth and Atmospheric Sciences

Georgia Institute of Technology
August 2009

NONREDUCTIVE BIOMINERALIZATION OF URANIUM(VI) AS A RESULT OF MICROBIAL PHOSPHATASE ACTIVITY

Approved by:

Dr. Martial Taillefert, Advisor
School of Earth and Atmospheric Sciences
Georgia Institute of Technology

Dr. Patricia A. Sobecky
School of Biology
Georgia Institute of Technology

Dr. Thomas J. DiChristina
School of Biology
Georgia Institute of Technology

Dr. Philippe Van Cappellen
School of Earth and Atmospheric Sciences
Georgia Institute of Technology

Dr. Samuel M. Webb
Stanford Synchrotron Radiation Lightsource

Date Approved: June 17, 2009

ACKNOWLEDGEMENTS

I would especially like to thank my advisor, Dr. Martial Taillefert, for his continued support over the past years. His commitment to science and independent thinking has been an inspiration and I am a much better scientist because of his example. I wish to thank my committee members, Dr. Patricia Sobecky, Dr. Thomas DiChristina, Dr. Samuel Webb, and Dr. Philippe Van Cappellen, whose recommendations have improved this dissertation. A special thanks to Dr. Samuel Webb for beamline support, help in EXAFS fittings, and hospitality at SSRL.

Thank you to all my past and present lab mates who have made life in the Taillefert Group a lot of fun and above all interesting: Stephanie, Morris, Jordon, Deidre, Lin, Kate, and Gwen. I especially thank Rob Martinez for all his microbiological help and friendship. A very special thank you to all my fellow graduate students in EAS and Biology for your friendship and encouragement, especially Poulomi, JFK, Arsineh, Katia, Jason Dale, Justin, Tracy, and Jason Landrum. Alyce, thanks for listening!

I would like to thank the School of Earth & Atmospheric Sciences for providing me with a teaching assistantship. I especially wish to thank Judy Curry for her support and advice early in my graduate career. Thank you to Susan Ryan, Laura Cederquist, Kathy Plummer, and Rita Anderson for all your help. I also wish to thank Dr. Michael Kuperberg for travel fellowships to DOE ERSP meetings.

And finally, I want to thank my family for their love and support.

TABLE OF CONTENTS

LIST OF TABLES

LIST OF FIGURES

LIST OF SYMBOLS AND ABBREVIATIONS

BGE	Background Electrolyte
DOE	Department of Energy
CE	Capillary Electrophoresis
EOF	Electroosmosis Flow
EXAFS	Extended X-ray Absorption Fine Structure
FRC	Field Research Center
IC	Ion Chromatography
ICP-MS	Inductively-coupled Plasma Mass Spectrometry
MDL	Minimum Detection Limit
μ-XANES	Micro X-ray Absorption Near-Edge Spectroscopy
NSAP	Non-specific Acid Phosphatase
ORFRC	Oak Ridge Field Research Center
ORNL	Oak Ridge National Laboratory
SIXPACK	Sam's Interface for XAS Package
SSRL	Stanford Synchrotron Radiation Lightsource
XANES	X-ray Absorption Near-Edge Spectroscopy
XAS	X-ray Absorption Spectroscopy

SUMMARY

Uranium contamination of soils and groundwater at Department of Energy facilities across the United States is a primary environmental concern and the development of effective remediation strategies is a major challenge. Bioremediation, or the use of microbial enzymatic activity to facilitate the remediation of a contaminant, offers a promising in situ approach that may be less invasive than traditional methods, such as pump and treat or excavation.

Environmental conditions at uranium contaminated waste sites impose unique biogeochemical obstacles that must be addressed to successfully remediate uranium contamination. Low pH and high nitrate concentrations in soils and groundwater affect microbial activity and the speciation and mobility of uranium. Microorganisms that are able to survive in such conditions may possess unique abilities that can be exploited in developing new bioremediation strategies. The overall objective of this research is to explore new ways to promote indigenous bacterial processes in contaminated soils and groundwater that immobilize uranium at low pH and high nitrate concentrations.

This study demonstrates for the first time the successful biomineralization of uranium phosphate minerals as a result of microbial phosphatase activity at low pH in both aerobic and anaerobic conditions using pure cultures and soils from a contaminated waste site. Pure cultures of microorganisms isolated from soils of a low pH, high uranium- and nitrate-contaminated waste site, expressed constitutive phosphatase activity in response to an organophosphate addition in aerobic (*Rahnella* sp. and *Bacillus* sp.) and anaerobic (*Rahnella* sp.) incubations. Sufficient phosphate was hydrolyzed to precipitate 73 to 95% total uranium as chernikovite, an autunite-type uranium phosphate mineral,

identified by synchrotron X-ray absorption spectroscopy and X-ray diffraction. Highest rates of uranium precipitation and phosphatase activity were observed between pH 5.0 and 7.0.

Indigenous microorganisms were also stimulated by organophosphate amendment in soils from a contaminated waste site using flow-through reactors. A continuous supply of organophosphate, nitrate, and uranium in synthetic groundwater of the same composition as that at the site was pumped through both high and low pH soils for 30 and 75 days. High phosphate concentrations (0.5 to 3 mmol L^{-1}) in pore water effluents were observed within days of organophosphate addition and throughout the course of the experiment. Highest rates of phosphatase activity occurred at pH 5.5 in naturally low pH soils in the presence of high uranium and nitrate concentrations. Uranyl phosphate precipitation occurred in organophosphate-amended soils at pH 5.5 and 7 as a result of the favorable reaction between negatively-charged phosphate and positively-charged uranyl. The precipitation of uranium phosphate in both soils was identified by a combination of pore water measurements, solid phase extractions, synchrotron-based X-ray spectroscopy, and a reactive transport model.

The results of this study demonstrate that uranium is biomineralized to a highly insoluble uranyl phosphate mineral as a result of enzymatic hydrolysis of an organophosphate compound as sole carbon and phosphorus source over a wide range of pH, in both aerobic and anaerobic conditions, and in the presence of high uranium and nitrate concentrations. The nonreductive biomineralization of U(VI) provides a promising new approach for in situ uranium bioremediation in low pH, high nitrate, and

aerobic conditions that could be complementary to U(VI) bioreduction in high pH, low nitrate, and reducing environments.

CHAPTER 1

OVERVIEW

1.1 Motivation

Between 1942 and the early 1990's, the production of nuclear materials and weapons in the United States generated large volumes of radioactive waste that has left a legacy of contaminated groundwater and soils at over 120 Department of Energy (DOE) sites in 36 states across the United States (NABIR, 2003). Since the shutdown of nuclear weapons production in the 1990's, the mission of the DOE has shifted to environmental restoration and decontamination of over 1.9 million cubic meters of contaminated groundwater and 79 million cubic meters of contaminated solid media (including soils) (DOE, 1997). Groundwater and soil contamination at these sites resulted from direct injection of mixed waste into the subsurface, leakage from storage tanks, and infiltration into the surrounding media from unlined storage ponds that resulted in plumes of mixed waste migrating according to hydrological and geological conditions (DOE, 1997). Heavy metals and radionuclides represent 50 to 60% of the contamination at the majority of these sites including uranium, reported in soils and groundwater at more than 50% of the DOE facilities (NABIR, 2003).

At the Oak Ridge Field Research Center (ORFRC) in Oak Ridge, Tennessee uranium contamination resulted from the migration of groundwater plumes originating from the former S-3 Waste Disposal Ponds located near the Y-12 Plant and the Y-12 Bone Yard/Burn Yard (Figure 1.1) (Brooks, 2001). The unlined ponds received highly acidic uranium nitrate liquid wastes generated at the Y-12 Plant and liquid and sludge

waste from other DOE facilities from 1951 to 1983. The liquid wastes were treated and removed in 1984 and the area capped by asphalt (Figure 1.1). Subsurface groundwater adjacent to the ponds is acidic and contains high concentrations of U (up to 252 μM) and nitrate (up to 645 mM) while solid-phase U can exceed 4 mmol kg^{-1} (Jardine et al., 2006).

Figure 1.1 The former S-3 Waste Disposal Ponds located near the Oak Ridge Y-12 Plant in Bear Creek Valley (left). The unlined ponds received highly acidic uranium nitrate liquid wastes from 1951 to 1983 (Brooks, 2001). The ponds were capped in 1984 after treatment and removal of liquid wastes (right). Picture from http://public.ornl.gov/orifc/orfrc3_site.cfm#Anchor1.

The commitment of the DOE to the restoration of the ORFRC and other contaminated sites has led to a dramatic increase in research over the past 15 years in all areas of remediation (NABIR, 2003). Traditional clean-up methods, such as pump-and-treat (Mackay and Cherry, 1989) and excavation (Dawson and Gilman, 2001) can be cost-prohibitive and infeasible over such large spatial scales and, therefore, the development of in situ remediation methods has received great attention. Bioremediation, or the microbial conversion of a contaminant to a less reactive form, is an area of particular interest.

Organic contaminants in natural systems can be converted to less toxic inorganic products by microbial enzymatic activities. Microorganisms metabolize the carbon substrate to produce energy and the contaminant is simultaneously biodegraded (Alexander, 1981). As many metal contaminants can not be degraded to benign products, microorganisms enzymatically decrease their solubility through detoxification mechanisms (e.g. Lovley et al., 1991; Macaskie and Basnakova, 1998; Macaskie et al., 1992). In turn, the solubility of metal contaminants is also regulated by geochemical processes, including sorption, complexation, precipitation, and redox processes, which have to be considered to effectively study their bioremediation (e.g. Barnett et al., 2000; Bruno et al., 1995; Haas and Northup, 2004; Merroun et al., 2005)

1.2 Uranium occurrence in nature

Uranium is the most abundant of the naturally-occurring actinides with concentrations of 1 to 4 ppm in crustal rocks and sediments (Ewing, 1999), found mainly in enriched deposits in Canada, South Africa, Australia, Namibia, and the United States (Cotton et al., 1999). Natural concentrations of uranium are similar to molybdate and arsenic and exceed mercury, antimony, silver, and cadmium (CRC, 1997). Concentrations in continental surface waters range from ca. 0.001 to 5 μM, while seawater concentrations are constant around 0.03 μM (Langmuir, 1997; Murphy and Shock, 1999). The three main isotopes of uranium are ^{238}U, ^{235}U, and ^{234}U with natural abundances of 99.2745%, 0.720%, and 0.0055% (CRC, 1997). All 23 isotopes of uranium are radioactive with half lives ranging from 10^5 to 10^9 years (CRC, 1997).

1.3 Aqueous Chemistry of Uranium

The chemistry of uranium is complex and, though heavily studied for over a century, remains poorly understood. Uranium complexity is a direct result of its chemical structure. Uranium has an atomic weight of 92 and exists in four different oxidation states +3, +4, +5, and +6. The electronic configuration of these oxidation states is listed below.

U^{0}: [Xe] $4f^{14}\ 5d^{10}\ 6s^{2}\ 6p^{6}\ 5f^{3}\ 6d^{1}\ 7s^{2}$

U^{3+}: [Xe] $4f^{14}\ 5d^{10}\ 6s^{2}\ 6p^{6}\ 5f^{3}$

U^{4+}: [Xe] $4f^{14}\ 5d^{10}\ 6s^{2}\ 6p^{6}\ 5f^{2}$

U^{5+}: [Xe] $4f^{14}\ 5d^{10}\ 6s^{2}\ 6p^{6}\ 5f^{1}$

U^{6+}: [Xe] $4f^{14}\ 5d^{10}\ 6s^{2}\ 6p^{6}\ 5f^{0}$

The most common valence states of uranium in nature are U(IV) and U(VI). Uranium (IV) is highly insoluble, found in reducing environments primarily as the mineral uraninite, $UO_{2(s)}$ (Finch and Murakami, 1999; Langmuir, 1997). In oxygenated aqueous systems, uraninite rapidly oxidizes to the U(VI) species as the uranyl ion, UO_2^{2+}, (Rabinowitch and Belford, 1964) which is highly soluble and stable over a wide pH range (Murphy and Shock, 1999). The uranyl ion is linear $[O = U = O]^{2+}$ with strong covalent bonds between the oxygen and uranium atoms which remain intact during complexation reactions (Chernyaev, 1966; Cotton et al., 1999). *Ab initio* molecular orbital calculations indicate the strength of the O—U bonds is probably due to donations of p-orbital electrons from the oxygen atoms into the empty 6d- and 6f- orbitals of the U^{6+} ion (Burns, 1999). The stereochemistry of UO_2^{2+} is varied with the most common

coordination of 4, 5, or 6 ligands in the equatorial plane (Figure 1.2). These equatorial O—U bonds are longer and weaker than the axial O—U bonds (Chernyaev, 1966; Cotton et al., 1999).

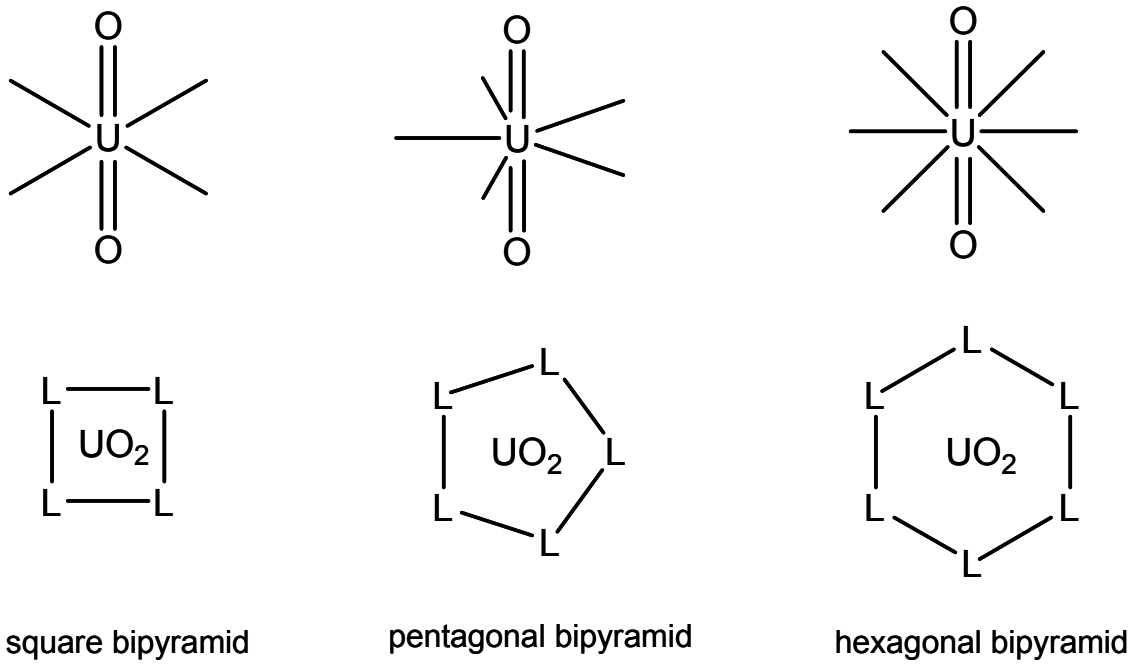

Figure 1.2 The uranyl ion $[O = U = O]^{2+}$ is linear in the axial position with 4, 5 and 6 ligand (L) coordination in the equatorial plane.

The aqueous chemistry of U(VI) is complex due to coordination and hydrolytic reactions. The uranyl ion is a hard acid and preferentially reacts with hard anions, particularly oxygen-containing ligands, and strongly hydrolyzes water (Equation 1-1) (Chernyaev, 1966; Cotton et al., 1999; Finch and Murakami, 1999; Suzuki and Banfield, 1999).

$$xUO_2^{2+} + yH_2O \rightarrow (UO_2)_x(OH)_y^{2x-y} + yH^+ \qquad (1\text{-}1)$$

Water or hydroxyl groups act as ligands filling the inner sphere of the uranyl ion, as well as displacing certain other ligands (Chernyaev, 1966; Cotton et al., 1999). The primary hydrolyzed species of UO_2^{2+} at typical groundwater concentrations of ca. 10^{-8} M and circumneutral pH are UO_2OH^+, $(UO_2)_2(OH)_2^{2+}$, $(UO_2)_3(OH)_5^+$, $UO_2(OH)_2^0$, and $UO_2(OH)_3^-$ (Figure 1.3) (Cotton et al., 1999; Langmuir, 1997).

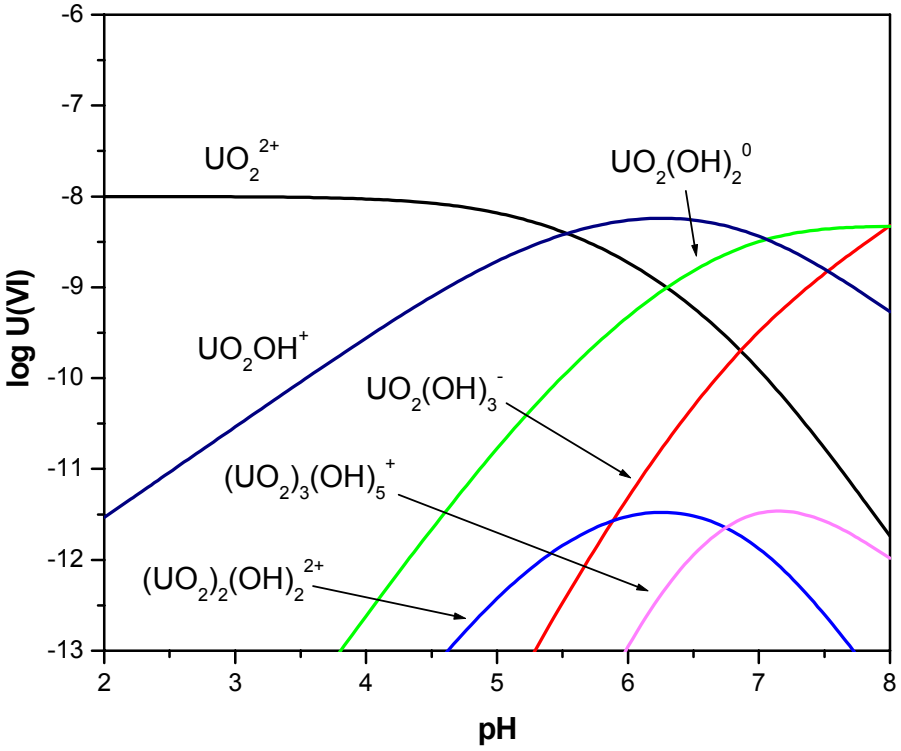

Figure 1.3 Distribution of U(VI) aqueous species for ΣU(VI) = 10^{-8} M at 25°C, I = 0.1 M, and P_{CO2} = 0 bar as predicted using the equilibrium modeling program MINEQL (Schecher and McAvoy, 2001) updated with the thermodynamic stability constants listed in Table 1.1.

Uranyl preferentially forms complexes with functional groups such as, carboxylates, carbonyls, alcohols, and ammonia (Suzuki and Banfield, 1999). Complexes with multidentate ligands, such as CO_3^{2-}, tend to have greater stability than those with monodentate ligands (Stumm and Morgan, 1996).

Table 1.1 Most updated (2006) uranium complexation reactions and thermodynamic stability constants (T = 25°C, I = 0, P = 1 bar)

Reaction	log K	ref.
Hydrolysis Reactions		
$UO_2^{2+} + H_2O = UO_2OH^+ + H^+$	-5.2	a,b,c
$UO_2^{2+} + 2H_2O = UO_2(OH)_2 + 2H^+$	-12.15	c
$UO_2^{2+} + 3H_2O = UO_2(OH)_3^- + 3H^+$	-20.25	c
$UO_2^{2+} + 4H_2O = UO_2(OH)_4^{2-} + 4H^+$	-32.4	c
$2UO_2^{2+} + H_2O = (UO_2)_2OH^{3+} + H^+$	-2.7	b,c
$2UO_2^{2+} + 2H_2O = (UO_2)_2(OH)_2^{2+} + 2H^+$	-5.62	a,b,c
$3UO_2^{2+} + 4H_2O = (UO_2)_3(OH)_4^{2+} + 4H^+$	-11.9	b,c
$3UO_2^{2+} + 5H_2O = (UO_2)_3(OH)_5^+ + 5H^+$	-15.55	a,b,c
$3UO_2^{2+} + 7H_2O = (UO_2)_3(OH)_7^- + 7H^+$	-32.2	c
$4UO_2^{2+} + 7H_2O = (UO_2)_4(OH)_7^+ + 7H^+$	-21.9	a,b,c
Uranium and Carbonate Complexes		
$UO_2^{2+} + CO_3^{2-} = UO_2CO_3$	9.94	c
$UO_2^{2+} + 2CO_3^{2-} = UO_2(CO_3)_2^{2-}$	16.61	c
$UO_2^{2+} + 3CO_3^{2-} = UO_2(CO_3)_3^{4-}$	21.84	c
$Ca^{2+} + UO_2^{2+} + 3CO_3^{2-} = CaUO_2(CO_3)_3^{2-}$	27.18	d
$2Ca^{2+} + UO_2^{2+} + 3CO_3^{2-} = Ca_2UO_2(CO_3)_3^0$	30.7	d
Uranium and Phosphate Aqueous Complexes		
$UO_2^{2+} + PO_4^{3-} = UO_2PO_4^-$	13.23	b,c
$UO_2^{2+} + HPO_4^{2-} = UO_2HPO_4$	7.24	b,c
$UO_2^{2+} + H_3PO_4^0 = UO_2H_2PO_4^+ + H^+$	1.12	a,b,c
Uranium Solids		
$UO_2^{2+} + 3H_2O = UO_3 \cdot 2H_2O + 2H^+$(s) schoepite	-5.2	a
$UO_2^{2+} + PO_4^{3-} + 3H_2O + H_3O^+ = (H_3O)(UO_2)(PO_4)\cdot 3H_2O$(s)	22.73	e
$UO_2^{2+} + H_3PO_4^0 + 4H_2O = 2H^+ + UO_2HPO4 \cdot 4H_2O$(s) H-autunite	2.5	a,b
$Ca^{2+} + 2UO_2^{2+} + 2PO_4^{3-} = Ca(UO_2)_2(PO_4)_2$ (s) autunite	44.7	a

a (Langmuir, 1997)
b (Grenthe et al., 1992)
c (Guillaumont et al., 2003)
d (Dong and Brooks, 2006)
e (Van Haverbeke et al., 1996) mineral described as chernikovite

Uranyl carbonates are highly soluble and play a dominate role in the migration of uranium in neutral to alkaline groundwater (Finch and Murakami, 1999). Carbonate is strongly bound to uranium. It occupies two coordinate positions in the major species $[UO_2(CO_3)_2]^{2-}$ and $[UO_2(CO_3)_3]^{4-}$ (Cotton et al., 1999), forms a highly stable four-member ring with UO_2^{2+} (Chernyaev, 1966), and displaces other ligands, including hydroxyls at pH > 7. Thermodynamic modeling of aqueous U(VI) at atmospheric CO_2 pressure ($10^{-3.5}$ bar) illustrates the importance of carbonate uranyl species near circumneutral pH (Figure 1.4). These uranyl carbonate complexes are highly stable and affect the speciation of U(VI) by displacing other ligands bound to uranyl. Simultaneously, these complexes prevent adsorption to some mineral surfaces (Fox et al., 2006; Langmuir, 1978) and promote dissolution of U(IV) and U(VI) minerals (De Pablo et al., 1999; Sowder et al., 2001). Calcium is common in groundwater and complexes with U(VI) and carbonate to form ternary calcium-uranyl-carbonate species (Bernhard et al., 1996; Dong and Brooks, 2006) that increase the rate of uranyl mineral dissolution (Liu et al., 2007) and decrease the rate and extent of bacterial U(VI) reduction (Brooks et al., 2003; Liu et al., 2007). Brooks et al. (2003) demonstrated that $Ca_2UO_2(CO_3)_3$ is a weaker electron acceptor than $UO_2(CO_3)_3^{4-}$, thereby slowing or inhibiting the bacterial reduction of U(VI) to U(IV). Carbonate exerts a strong influence on U(VI) speciation at circumneutral pH but plays a much less significant role in the speciation of uranium at lower pH because carbonate is primarily protonated below pH 6.

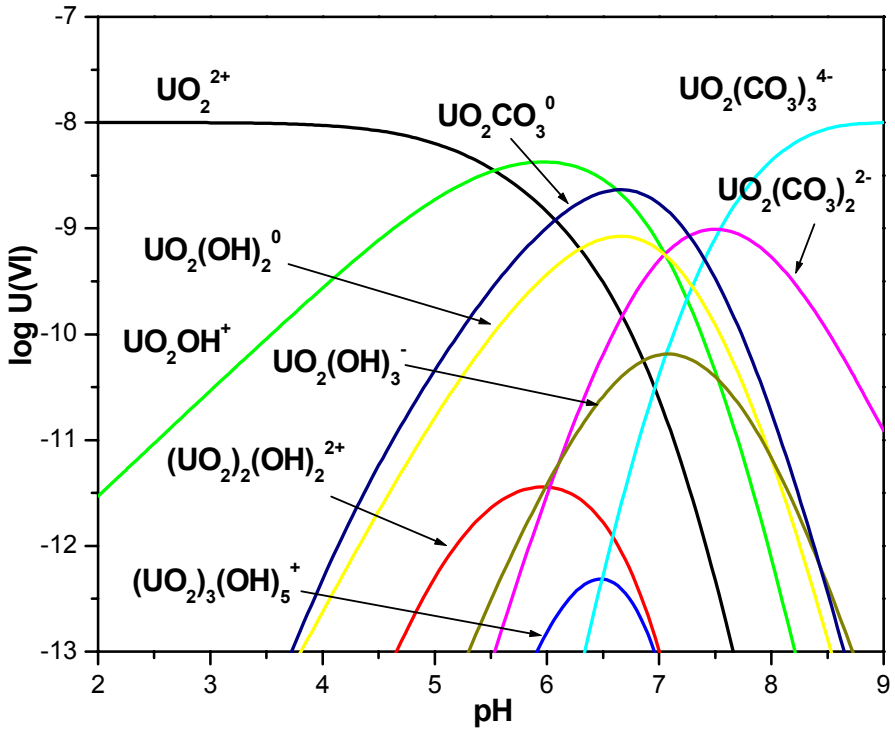

Figure 1.4 Distribution of U(VI) aqueous species for ΣU(VI) = 10^{-8} M at 25°C, I = 0.1 M, and P_{CO2} = -3.5 bar as predicted using the equilibrium modeling program MINEQL (Schecher and McAvoy, 2001) updated with the thermodynamic stability constants listed in Table 1.1.

1.4 Solid-phase Controls on Uranium in Natural System

Adsorption reactions at the mineral-water interface of Fe oxides control the transport of U(VI) through soils and sediments. Fe oxides are ubiquitous in natural systems and provide hydroxyl groups with high surface areas for the adsorption of metal cations (Tessier et al., 1996). The reactivity of these hydroxyl groups is dependent on pH and their charge is determined by the mineral's zero point charge (ZPC). The pH_{ZPC} is the pH at which the surface charge of a mineral changes sign (Langmuir, 1997; Stumm and Morgan, 1996). The pH_{ZPC} for goethite ranges between 5.9 and 6.7 (Langmuir, 1997), and adsorption of U(VI) is most favorable between pH 5 and 7 when uranyl

complexes are positively charged (Hsi and Langmuir, 1985; Langmuir, 1997). The pH_{ZPC} of other important minerals in naturals systems include, silicates (1 to 3), montmorillonite (≤ 2 to 3), kaolinite (≤ 2 to 4.6), hematite (4.2 to 6.9), amorphous $Fe(OH)_3$ (8.5 to 8.8), manganese oxides (1.5 to 7.3), calcite (8.5, 10.8), and hydroxyapatite (≤ 8.5) (Langmuir, 1997; Stumm and Morgan, 1996).

Below circumneutral pH, U(VI) also forms highly stable and insoluble complexes with phosphate. Thermodynamic modeling predicts the formation of solid-phase autunite $[Ca(UO_2)_2(PO_4)_2]$ in the presence of 200 μM U(VI), 200 μM PO_4^{3-}, and 200 μM Ca^{2+} at atmospheric CO_2 pressure ($10^{-3.5}$ bar) (Figure 1.5a) and at 0 bar (Figure 1.5b). Equilibrium calculations demonstrate that the presence of carbonate does not affect the solubility of uranyl phosphate minerals such as autunites which are stable between pH 4 and 8. In turn, mineralization of schoepite, an uranyl hydroxide mineral, is inhibited above pH 8 by the formation of $UO_2(CO_3)_3^{4-}$. In reducing conditions, the formation of uraninite is favored above circumneutral pH (Figure 1.6) and does not thermodynamically affect the formation of uranyl phosphate at high pε and low pH.

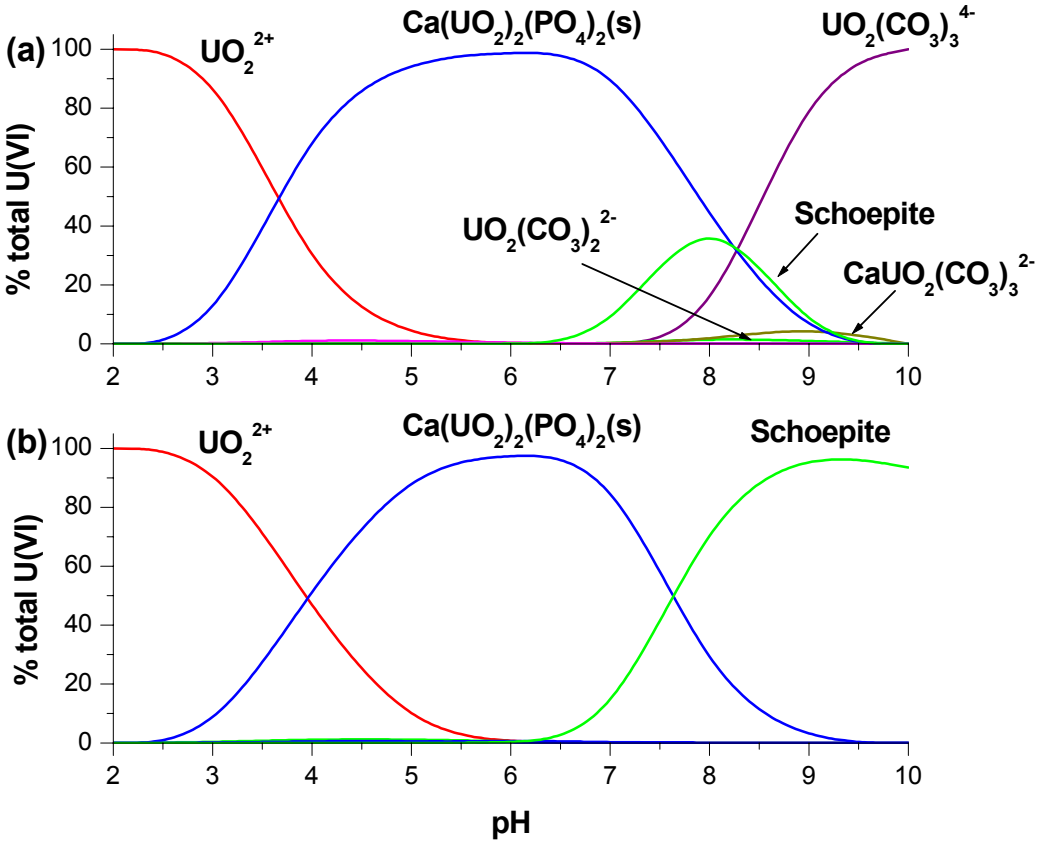

Figure 1.5 Speciation of 200 µM UO_2^{2+}, 200 µM PO_4^{3-}, and 200 µM Ca^{2+} as a function of pH at (a) $P_{CO2} = 10^{-3.5}$ and (b) $P_{CO2} = 0$ as predicted using the equilibrium modeling program MINEQL (Schecher and McAvoy, 2001) updated with the thermodynamic stability constants listed in Table 1.1.

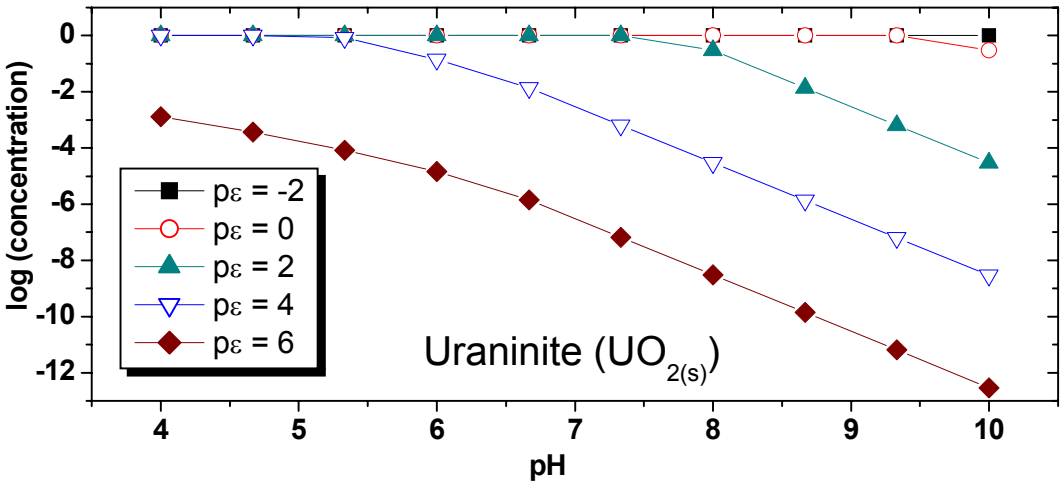

Figure 1.6 Speciation of 50 µM uranium as a function of pH and pε. The formation of uraninite is favored at low pε and high pH.

Phosphate in natural systems can control the mobility of U(VI) in groundwater and soils. Uranyl phosphates are widely distributed in nature with over 70 minerals identified with U:P stoichiometric ratios of 1:1 (autunite and meta-autunite groups), 3:2 (phosphuranylite group), and 1:2 (walpurgite group) (Finch and Murakami, 1999). In fact, uranyl phosphate minerals have been identified in contaminated soils at the ORFRC (Kelly et al., 2005; Roh et al., 2000; Stubbs et al., 2006), at the former uranium production facility at Fernald, Ohio (Bertsch et al., 1994; Morris et al., 1996), and at the Hanford (Washington) DOE facility (Arai et al., 2007; Catalano et al., 2006). Uranyl phosphate minerals are stable over long periods of time as evidenced by assemblages found in bedrock deposits stable for up to 150 ka (Jerden Jr. and Sinha, 2003). Dissolution studies have also demonstrated chernikovite [$(UO_2)H(PO_4)\cdot 4H_2O$] and metaautunite [$Ca(UO_2)_2(PO_4)_2\cdot x$H2O] are resistant to dissolution in 1 mM bicarbonate on yearly time scales (Sowder et al., 2001), and rates of autunite dissolution are minimum at pH 5-6 (Wellman et al., 2007). Thus, the insolubility of uranyl phosphates may provide a long-term sink for U(VI) in natural systems particularly below circumneutral pH.

In addition to forming precipitates with U(VI), phosphate can also control the solubility of U(VI) by adsorption reactions. Phosphate adsorbs strongly to iron oxides across a wide pH range in a monodentate coordination with hydroxyl groups on the Fe(III) surface (Dideriksen and Stipp, 2003) and enhances adsorption of U(VI) through the formation of ternary surface complexes between uranium and phosphate (Cheng et al., 2004). The adsorption of phosphate to ferrihydrite surfaces changes the average surface charge of the iron oxide and moves its sorption edge to a lower pH, thereby promoting the adsorption of U(VI) at lower pH (Payne et al., 1996). Adsorption of

phosphate to iron oxyhydroxides may also inhibit microbial iron reduction by blocking iron surfaces (Borch et al., 2007) that in turn, may also inhibit U bioreduction. Sorption of U(VI) to alumina surfaces is also increased by the presence of phosphate in the pH range 3 to 6 (Zhijun et al., 2006). These findings surmise the possibility that adsorption of U(VI) to mineral surfaces in the presence of phosphate may be a precursor to the precipitation of uranyl phosphate minerals (Sato et al., 1997).

Thus, the adsorption of U(VI) to mineral surfaces in soils and sediments is favorable over a wide pH range and will play an important role in the transport of U(VI) in these systems.

1.5 Remediation of Uranium in Contaminated Subsurfaces

The remediation of uranium from subsurface environments has been extensively studied and includes both abiotic and biotic strategies. Adsorption at mineral-water interfaces (Cheng et al., 2004; Lack et al., 2002; Sato et al., 1997), mineral precipitation/coprecipitation (Bruno et al., 1995; Gu et al., 2003), complexation with organic compounds (Francis et al., 2000; Nash et al., 1998; Robinson et al., 1998), adsorption to zero-valent iron (Noubactep, 2006; Noubactep et al., 2006), and adsorption to hydroxyapatite in permeable reaction barriers (Fuller et al., 2003; Fuller et al., 2002) are chemical methods that can effectively remove uranium from solution. Bioremediation, in which microorganisms actively transform and degrade contaminants, offers an alternative strategy. Bioreduction, the enzymatic reduction of soluble U(VI) to insoluble U(IV), as uraninite ($UO_{2(s)}$), in anaerobic conditions, is one of the most studied biological process of uranium immobilization (e.g. Fredrickson et al., 2000; Ganesh et al.,

1999; Lovley and Phillips, 1992; Lovley et al., 1991; North et al., 2004; Senko et al., 2002; Wade Jr. and DiChristina, 2000). Unfortunately, uraninite is rapidly oxidized to the more mobile and reactive uranyl ion (UO_2^{2+}) in oxic conditions (Langmuir, 1997; Murphy and Shock, 1999), and more slowly oxidized under nitrate-reducing conditions by Fe(III) produced by nitrate-dependent Fe(II)-oxidizing bacteria or by oxidation of Fe(II) by nitrite (Senko et al., 2002; Senko et al., 2005a; Senko et al., 2005b). In addition, bioreduction can only be promoted at circumneutral pH.

Fewer studies are available on the bioremediation of uranium in oxidizing conditions (Macaskie et al., 1994; Powers et al., 2002). Biomineralization, or microbial-mediated mineral precipitation, offers a complementary approach to bioreduction. Resistance to heavy metals has been reported for bacterial strains exhibiting acid phosphatase activity (Jeong et al., 1997; Macaskie et al., 1994; Montgomery et al., 1995). Bacterial non-specific acid phosphatases (NSAPs) are a group of secreted phosphohydrolases (phosphatases) that hydrolyze a number of structurally unrelated organic phosphomonoester substrates in acidic-to-neutral pH conditions (Rossolini et al., 1998). NSAPs are secreted by bacteria, as soluble periplasmic proteins or membrane-bound lipoproteins, to liberate inorganic phosphate from organophosphate substrates and comprise three different molecular families designated Class A, Class B, and Class C (Rossolini et al., 1998). The three classes are distinguished by the conserved amino acid motif and X-ray crystallography and protein comparative modeling has identified the active sites in Class A NSAPs as Lys115, Arg122, Ser148, Gly149, His150, Arg183, His189, and Asp193; Class B NSAPs as Asp44, Asp46, Thr48, Arg114, Asp167, and

Asp171; and Class C NSAPs as Asp84, Asp86, Thr88, Arg146, Asp201, and Asp205 (Martinez et al., 2007).

Phosphorus metabolism by NSAPs is unregulated and much less characterized (Rossolini et al., 1998) compared to alkaline phosphatases regulated by the Pho regulon that induces phosphatase activity in phosphate-limiting conditions (Kertesz et al., 1994; Vershinina and Znamenskaya, 2002; Wanner, 1993). The alkaline phosphatase of *Escherichia coli* (*E. coli*) is the most studied of all bacterial alkaline phosphatase enzymes (Coleman, 1992; Kim and Wyckoff, 1991; Vershinina and Znamenskaya, 2002). The overall reaction mechanism of phosphatase in *E.coli* is demonstrated in Figure 1.7. At acidic pH, the hydrolysis of E-P is rate-limiting and the dissociation of E•P is the rate-determining step at alkaline pH (Kim and Wyckoff, 1991). The enzymatic reaction produces a covalent serine-phosphate (E-P) intermediate that progresses to form inorganic phosphate (P_i) and an alcohol. The active site of the enzyme contains three metal-binding sites (M1, M2, and M3) that are occupied by zinc (M1 and M2) and magnesium (M3) (Stec et al., 2000). Alkaline phosphatase activity in *E. coli* is regulated by the Pho regulon that contains genes involved in the transport and assimilation of phosphate. During phosphate-starvation conditions, the Pho regulon induces *psi* (phosphate starvation-inducible) genes that code for proteins involved in phosphate transport and when phosphate is in excess the Pho regulon is repressed by the formation of the PhoR and PhoU repressor complex. The Pho regulon is found is several other bacterial species, including *Bacillus subtilis* (Vershinina and Znamenskaya, 2002).

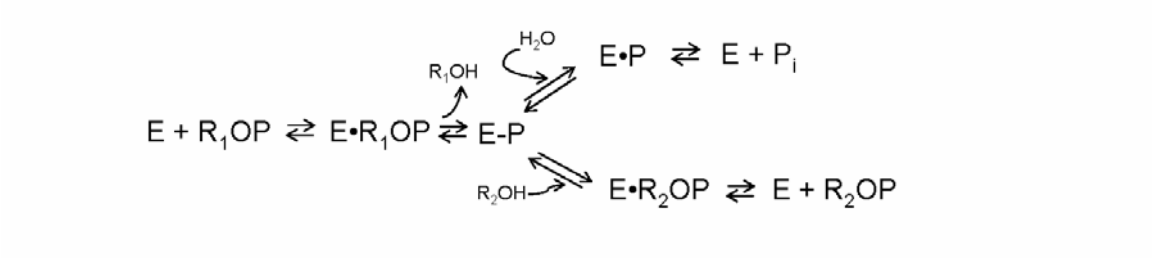

Figure 1.7 The overall reaction scheme of the alkaline phosphatase. The E-P is the phosphoseryl enzyme formed with Ser102 and E•ROP and E•P are the non-covalent complexes with substrate or product (Kim and Wyckoff, 1991).

Several phosphatase-positive microorganisms tolerant to heavy metals have constitutively expressed Class A NSAPs (Macaskie et al., 1992; Macaskie et al., 1995; Yong and Macaskie, 1995) that facilitate the precipitation of cell-bound uranium-phosphate (Macaskie et al., 1994) as $HUO_2PO_4 \cdot 4H_2O$ (Jeong et al., 1997). Significant accumulation of phosphate is observed in the presence of constitutively-expressed phosphatases (Martinez et al., 2007; Powers et al., 2002) suggesting that microbial NSAP activity may play a key role in the biomineralization of uranium.

1.6 Research Scope and Objectives

Environmental conditions in uranium contaminated waste sites impose unique biogeochemical obstacles that must be addressed to successfully remediate uranium contaminations. Low pH and high nitrate concentrations in soils and groundwater affect microbial activity and the speciation and mobility of uranium. Microorganisms that are able to survive in such conditions may possess unique abilities that can be exploited in developing new bioremediation strategies. The overall objective of this research is to explore new ways to promote indigenous bacterial processes in these contaminated waste sites that immobilize U(VI) at low pH and high nitrate concentrations.

Previous work has identified bacterial isolates from U contaminated areas of the ORFRC that exhibit phosphatase activity in the presence of an organophosphate substrate (Martinez et al., 2007). The primary goal of this study is to determine if indigenous microbial communities in contaminated soils from the ORFRC produce enough phosphate through the expression of phosphatase enzymes to precipitate insoluble U(VI) phosphate minerals, as a complementary strategy to the immobilization of U through bioreduction.

It is critical to our overall understanding of U behavior in natural environments to assess changes in the chemical speciation and molecular structure of U(VI). In this work, a combination of state-of-the-art analytical tools was used to monitor the composition of dissolved constituents as a function of time and the speciation of U in the solid phase. Chapter 2 of this dissertation outlines the various analytical techniques used in this study. Concentrations of dissolved chemical constituents were monitored by inductively-coupled plasma mass spectrometry (dissolved uranium and other metals), ion chromatography and capillary electrophoresis (anions and organophosphates), voltammetry (dissolved oxygen, Mn^{2+}, Fe^{2+}, ΣH_2S), and other common techniques (e.g. phosphate and nitrite by spectrophotometry). Synchrotron-based X-ray diffraction and X-ray absorption spectroscopy were used to determine the speciation and the molecular structure of uranium in the solid-phase.

Chapter III investigates the biomineralization of U(VI) in pure culture aerobic incubations with three bacterial species isolated from the ORFRC in the presence of high U(VI) and nitrate concentrations to elucidate the conditions most favorable for successful U remediation. The objectives of this work were to (1) determine whether the strains

hydrolyzed sufficient phosphate from an organophosphate substrate to precipitate uranium, (2) establish whether pH has an effect on phosphatase activity and U(VI) precipitation, and (3) identify the uranium solid phase formed during biomineralization.

The ORFRC subsurface is primarily oxic; however oxygen can be rapidly consumed during microbial respiration. In Chapter IV one of the bacterial isolates from the ORFRC was investigated for its ability to exhibit the same phosphatase activity in anaerobic conditions. The objectives of this work were to determine whether (1) the isolate can grow anaerobically with nitrate as terminal electron acceptor, (2) sufficient phosphate is hydrolyzed to anaerobically precipitate U(VI), and (3) compare the minerals formed in anaerobic and aerobic conditions.

Chapter V focuses on contaminated ORFRC soil studies using flow-through reactors. The primary goal of this work is to determine how soils react to the amendment of an organophosphate compound as sole C and P source. Parameters such as pH and nitrate concentrations were adjusted to assess their effect on phosphatase activity. The chemical composition of pore water effluents was monitored to identify the biogeochemical processes occurring in the soils. At the end of the experiments the chemical speciation and molecular structure of uranium in the soils were determined using a combination of wet chemical extraction and XAS measurements. A one-dimensional transport model was used to determine the advection, dispersion, and retardation factor in the reactors using a conservative tracer. The model was then used with the reactive species involved in U(VI) biomineralization to assess their rates of transformation and estimate the rate of precipitation of uranium phosphate minerals. The objectives of this study were to determine whether (1) indigenous microorganisms in a

contaminated soil hydrolyze an organophosphate substrate as sole C and P source, (2) pH affects natural microbial phosphatase activity, (3) uranium phosphate is precipitated in the soil column, and (4) soil permeability changes as a result of organophosphate amendments.

Finally, Chapter VI synthesizes the findings of this research, discusses whether the biomineralization of uranium phosphate as a result of microbial phosphatase activity appears a valuable approach to uranium bioremediation, provides new questions identified by these studies, and presents a number of recommendations for future investigations.

Appendices are found at the end of the thesis. Appendix A contains supporting information and additional data relevant to Chapter 3. Appendix B describes the Matlab™ code used for the one-dimensional advection-dispersion and reactive transport models used in Chapter 5 to determine transport parameters and rates of transformation in flow-through reactors. Appendix C provides additional analytical and transport model data from the flow-through experiments in Chapter 5.

CHAPTER 2

ANALYTICAL TECHNIQUES

2.1 Inductively-Coupled Plasma Mass Spectrometry

Total dissolved uranium concentrations were measured by inductively-coupled plasma mass spectrometry (ICP-MS) with an Agilent 7500a Series system. Samples were filtered (0.2 μm pore size, AcetatePlus; GE Water and Process Technologies) and acidified with 2% nitric acid (trace metal grade, Fisher) diluted in Nanopure water (Barnstead). Uranium standards and samples contained holmium and bismuth (SPEX certiPrep) as internal standards. Samples were corrected by the averaged holmium and bismuth response normalized to calibration response. The detection limit of uranium was 0.1 nM. Calibration standards (0 to 4000 ppt) were analyzed every 30 samples and at the start and completion of each run cycle to account for instrument drift. Blanks, calibration check standards (95-105% recovery), and River Water Certified Reference Material for Trace Metals (SLRS-4, National Research Council Canada, Ottawa, Canada) were analyzed for quality controls. The analytical error on triplicate samples was < 3% relative standard deviation (RSD).

2.2 Colorimetry

2.2.1 Phosphate

Phosphate concentrations were determined by colorimetric analysis based on the method of Murphy and Riley (1962). Measurements were conducted at 885 nm on a

Milton Roy Spectronic 601 spectrophotometer with standards of 0 to 25 μM made from a stock solution of KH_2PO_4 (Fisher) in Nanopure water. Reagents used included ammonium molybdate (0.023 M), sulfuric acid (2.8 M), potassium antimonyl tartrate (4.2 mM), and ascorbic acid (0.31 M). All chemicals used were reagent grade (Fisher). Reagents were stored in the refrigerator and stable for months, except ascorbic acid which was stable for only 2 weeks. Immediately prior to analysis 1.6 mL ammonium molybdate, 4 mL sulfuric acid, 0.8 mL potassium antimonyl tartrate, and 1.6 mL ascorbic acid were combined. An aliquot of this mixture (100 μL) was added to 1 mL of each standard and sample. The blue color was allowed to develop for 20 minutes and the samples were analyzed at 885 nm. Minimum detection was 2 μM and analytical error on duplicate samples was < 4% RSD.

2.2.2 Nitrite

Nitrite concentrations were determined by colorimetric analysis (Grasshoff, 1983). Measurements were conducted at 540 nm on a Milton Roy Spectronic 601 spectrophotometer with standards of 0 to 20 μM made from a stock solution of anhydrous $NaNO_2$ (Fisher) in Nanopure water. The $NaNO_2$ was dried at 100°C for 1 hour prior to preparation. The reagents used included sulphanilamide (Fisher) and N-1-napthylethylenediamine dihydrochloride (NED) (Sigma). Sulphanilamide (0.25 g) was added to 2.5 mL of concentrated HCl (trace metal grade; Fisher) in 25 mL Nanopure water (5.8 mM) and stored in the refrigerator. NED (0.025 g) was added to Nanopure water to a total volume of 25 mL (0.97 mM) and stored in a dark bottle in the refrigerator. Sulphanilamide (20 μL) was added to 1 mL of each standard and sample, mixed, and allowed to react for 1 minute. NED (20 μL) was then added and the sample allowed to

develop for 15 minutes before analysis at 530 nm. Minimum detection was 2.5 μM and analytical error on duplicate samples was < 5% RSD.

2.2.3 Ammonium

Ammonium concentrations were determined by colorimetric analysis based on Strickland and Parsons (1972). Measurements were conducted at 640 nm on a Milton Roy Spectronic 601 spectrophotometer with standards of 0 to 20 μM made from a stock solution of NH_4Cl (Fisher) in Nanopure water. The NH_4Cl was dried at 55°C overnight prior to preparation. Reagents used included phenol (8.5 mM; Sigma), nitroprusside (2.5 mM in 95% ethanol (Aldrich; Sigma), and an alkaline solution (3.75 g sodium citrate (Sigma Aldrich) and 0.2 g NaOH (Fisher) in 250 mL Nanopure water). Immediately prior to analysis 2.5 mL of 4-6% sodium hypochlorite (NaOCl, Fisher) was added to 10 mL of the alkaline reagent to create an oxidizing reagent. The reagents were added in the following order to 1 mL of each sample and standard: phenol (500 μL), nitroprusside (500 μL), and oxidizing reagent (1 mL). The glass sample vials were parafilmed and heated at 45°C for 1 hour before analysis at 640 nm.

2.3 Capillary Electrophoresis

Concentrations of bromide (Br^-), chloride (Cl^-), nitrate (NO_3^-), and sulfate (SO_4^{2-}) for a portion of the work presented in Chapter 5 of this dissertation were determined by capillary electrophoresis (CE).

2.3.1 Overview of technique

Electrophoresis is the movement of charged chemical species under the influence of an electric field along a capillary column, most commonly made of bare fused-silica,

connected to a cathode at one end and an anode at the other. Analysis of chemical species by CE is based on (1) electroosmosis mobility and (2) electrophoretic mobility (Weinberger, 2000).

The electroosmosis flow (EOF) is the bulk flow of a conducting background electrolyte buffer (BGE) solution through the capillary when a large difference of potential (10-30 kV) is applied between both ends of the capillary. The interior capillary wall contains silanol (Si-OH) groups, which at pH > 2 have a negative charge (SiO^-). Positive cations in the buffer solution are attracted to the negatively-charged capillary wall and form an electric double layer and a potential difference (zeta potential). The cations in the diffuse layer are moved with the EOF toward the cathode. The mobility of the EOF is dependent on the pH and ionic strength of the buffer. At high pH, silanol groups on the capillary wall are completely ionized and mobility is greatest. At low pH the surface is protonated (SiOH), diminishing the velocity of the EOF. At pH 4 the EOF is suppressed. The diffuse double layer is compressed at high ionic strength, decreasing the zeta potential and reducing the EOF mobility. The charge on the capillary wall, and therefore the EOF, may also be controlled by the addition of either permanent or temporary (dynamic) coatings to the column. Chemicals coat the interior wall of the capillary and produce a stable surface whose charge is not affected by electrolytes or pH.

Electrophoretic mobility describes how fast an ion moves through the BGE in the capillary, and is determined by the positive motion of the electrical force and the retarding frictional force. Electrophoretic mobility of a given ion is determined by its charge-to-size ratio and the average charge along the capillary walls. Small ions of high

charge have a greater mobility than large ions of low charge. Mixtures of different ions and solutes may be separated due to the difference in their electrophoretic mobilities.

The sample is injected at the anode end of the column and moves along with the EOF toward the cathode. Anions in the sample migrate against the EOF toward the anode, and cations migrate with the EOF to the cathode. A detector (UV or fluorescence) is located at the cathode end and records the passage of the ions on an electropherogram, which represents graphically migration time vs. detector response.

Detection is either in the direct mode or the indirect mode. Direct detection is employed when the compound to be separated absorbs in the region of the detector. In the indirect mode, the compound does not absorb in the detector region, and an absorbing buffer is used as the BGE. The decrease in absorbance of the BGE is recorded when the analyte passes in front of the detector.

2.3.2 Anion analysis

Anions were detected in indirect mode by UV at 254 nm on a Beckman P/ACE MDQ system equipped with a photo-diode array and a UV/Vis. New columns were conditioned prior to analysis for 10 min at 93.8 kPa with 1 M NaOH and then Nanopure water for 8 min. The chromate buffer used as the BGE was prepared with K_2CrO_4 (ICN Biomedicals), a surfactant cetyltrimethylammoniumbromide (CTAB; Acros), and methanol (Diress and Lucy, 2005). Stock solutions of K_2CrO_4 (50 mM) and CTAB (2.5 mM) were prepared with Nanopure water and filtered (0.2 μm pore size, AcetatePlus; GE Water and Process Technologies). The K_2CrO_4 solution was adjusted to pH 8 with 1 M HCl prior to filtering. The BGE was prepared daily by adding 1 mL K_2CrO_4, 1 mL

CTAB, 3 mL methanol, and 5 mL Nanopure water. The solution was mixed carefully so as not to create bubbles.

During analysis, the column was conditioned before each run cycle as follows: 0.1 M NaOH for 2 min, Nanopure water for 2 min, and then BGE buffer for 3 min all at 93.8 kPa. Samples were injected for 2.0 s at 5 kPa and detected indirectly at -15 kV in chromate buffer for 10 min by UV at 254 nm. The chromate buffer was replaced every 6 sample runs. Anion standards of 0 to 1 mM were prepared from stock solutions of NaBr (Sigma), KCl (Sigma), $NaNO_3$ (Sigma), and $MgSO_4$ (Sigma). Detection limits for all anions was 50 µM and >95% recovery on calibration check standards. Anion electropherograms (baseline corrected) and calibration curves are shown in Figure 2.1.

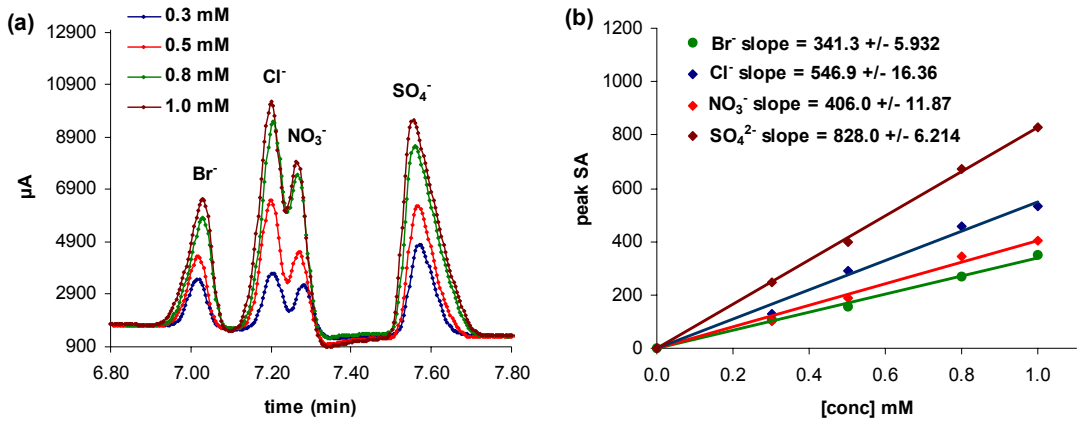

Figure 2.1 (a) Electropherograms (baseline corrected) and (b) calibration curves of Br^-, Cl^-, NO_3^-, and SO_4^{2-} as determined by indirect detection in chromate buffer by capillary electrophoresis.

2.4 Ion Chromatography

Concentrations of bromide (Br^-), chloride (Cl^-), nitrate (NO_3^-), sulfate (SO_4^{2-}), glycerol-2-phosphate (G2P) were determined by ion chromatography (IC) for a portion of the work presented in Chapter 5 of this dissertation. All measurements were conducted on a Dionex DX-300 Series IC equipped with a Dionex IonPac® AS14A chromatography column (4 x 250 mm), AG14A guard column (4 x 50 mm), and AMMS 300 (4 mm) suppressor. Anion standards of 0 to 250 µM were prepared from stock solutions of NaBr (Sigma), KCl (Sigma), $NaNO_3$ (Sigma), $MgSO_4$ (Sigma), and G2P (Sigma Aldrich) and Nanopure water. Anions were measured using a bicarbonate buffer (1 mM $NaHCO_3$ and 8 mM Na_2CO_3) as eluent at a flow rate of 1 mL min^{-1} and a regenerant solution of 25.8 mM H_2SO_4.

2.5 Voltammetry

Oxygen and reduced species, such as Fe^{2+}, Mn^{2+}, and ΣH_2S, were analyzed voltammetrically in-line in the flow cell with a computer-operated DLK-100A or DLK-60 potentiostat (Analytical Instrument Systems). All measurements were performed with Au/Hg solid-state microelectrodes fabricated as described in Brendel and Luther (1995), a platinum counter electrode, and an Ag/AgCl reference electrode. The working microelectrodes consisted of a 100-µm-diameter Au wire housed in 3-mm PEEK tubing connected via a copper conducting wire to a potentiostat. The Au surface was polished with diamond pastes of 15, 6, 1, and 0.25 µm (Buehler), mercury plated for 6 min at -0.1 V in a $Hg(NO_3)_2$ solution, and then polarized at -9 V for 90 s to form a good amalgam

between the Au and Hg (Brendel and Luther, 1995). Finally, electrodes were tested for quality and calibrated for dissolved oxygen O_2 by linear sweep voltammetry, then Mn^{2+} by cathodic square wave voltammetry in degassed 0.02 mol L^{-1} NaCl. Both the O_2 (MDL $\approx$ 4 µmol L^{-1}) and Mn^{2+} (MDL $\approx$ 15 µmol L^{-1}) calibrations were run from -0.1 to -1.75 V with a scan rate of 200 mV s^{-1} in 0.02 mol L^{-1} NaCl. A pre-conditioning potential of -0.1 V for 10 s was applied to all O_2 and Mn^{2+} measurements to clean the surface of the microelectrodes between measurements (Brendel and Luther, 1995). The Mn^{2+} calibration curves were used to elucidate the concentrations of other species with the pilot ion method (Brendel and Luther, 1995).

2.6 Synchrotron X-ray Absorption Spectroscopy

2.6.1 X-ray Absorption Spectroscopy (XAS)

Solid uranyl phosphate and soil samples were analyzed by XAS at Stanford Synchrotron Radiation Lightsource (SSRL) on beam lines 11-2 (Fall 2006) and 10-2 (summer 2007, summer 2008, winter 2009). Uranyl phosphate samples were measured in 1.5 mL centrifuge tubes and soil samples were placed in windowed lexan sample holders sealed with Kapton tape. For the XAS analysis presented in Chapter 3 of this dissertation, uranium L_{III}-edge XAS spectra were collected at SSRL beamline 11-2 using a focused X-ray beam with a 23 keV harmonic rejection cutoff. The incident energy was selected with a Si(220) monochromator. Transmission and fluorescence data were collected simultaneously. For the remaining XAS analysis presented in Chapters 4 and 5, uranium L_{III}-edge XAS spectra were collected at SSRL beamline 10-2 using a focused X-ray beam with a 23 keV harmonic rejection cutoff and a 13 element Ge detector. The incident energy was selected with a Si(111) monochromator crystal. Transmission and

fluorescence data were collected simultaneously. All extended X-ray absorption fine structure (EXAFS) data were reduced using Sam's Interface for XAS Package (SIXPACK) (Webb, 2005). Phase and amplitude files for the EXAFS fitting were created with FEFF7 (Ankudinov et al., 1998; Zabinsky et al., 1995). Since the Debye-Waller factors (σ) correlated highly with coordination numbers (N), σ's for some shells were each fixed at their average values.

The structure of U(VI) is distinguished by the linear uranyl ion $[O = U = O]^{2+}$ containing 2 axial oxygen atoms (O_{ax}; Figure 2.2a) surrounded by 4 to 6 equatorial oxygen atoms (O_{eq}; Figure 2.2b) (Cotton et al., 1999). The coordination number of O_{ax} is always 2 and the radial distance, R (in Å), between U and O_{ax} is typically ~1.80 Å (Figure 2.2a). Uranyl equatorial oxygen atoms typically display U-O_{eq} distances of ~2.30 Å; however, uranyl surface complexes can stretch some of the O_{eq} and thus increase bond distances up to ~ 2.45 Å depending on the ligand, which splits the O_{eq} shells (Figure 2.2b and d). Split equatorial oxygen shells are common in uranyl complexes with minerals including, alumina silicates (Hudson et al., 1999; Sylwester et al., 2000), apatite (Fuller et al., 2003), and iron oxides (Waite et al., 1994). In the latter complexes, two of the shorter O_{eq} are bound to two neighboring iron oxide edge oxygens in a bidentate fashion, forming Fe-O_{eq}-U angles of ca. 112º (Figure 2.2d) (Bargar et al., 2000). The uranyl ion is also distinguished by multiple scattering (MS) of photoelectrons between the O_{ax} and U atoms. Therefore, all EXAFS fittings in this study include three U-O_{ax} MS paths with the coordination number (N) set to 2 atoms, the radial distance (R) set to 2 R_{Oax}, and the Debye-Waller factor (σ^2) set to 2 σ^2_{Oax}. A P shell at ~3.6 Å (Figure 2.2c) was included in all samples containing P, along with the MS paths U-O_{eq}-P (~3.7 Å) and U-O_{eq}-P-O_{eq}

(~3.8 Å). U-P minerals are composed of sheets of square bipyramidal uranyl and tetrahedral phosphate $[(UO_2)(PO_4)]^-$ attached by interlayer charge-balancing cations (Catalano and Brown Jr., 2004; Locock and Burns, 2003), and higher P coordination numbers reflect the formation of these structured U-P sheets. O_{eq} atoms at ~2.45 Å are also common in coordination complexes with carbonates (U-C radial distance ~2.80 Å) and indicate the bidentate sharing of two oxygen atoms between uranyl and carbonate (Figure 2.2d). Ternary complexes of Fe-U-C (Bargar et al., 2000) are common in natural systems (Waite et al., 1994) and are observed in ORFRC soils (Bostick et al., 2002). A uranium-carbon shell with radial distance of ~ 2.80 Å (Figure 2.2d) that included the two triangular U-C-O_{eq} MS paths (~3.24 Å) greatly improved the fits. As all samples were natural soils, Fe and Mn (~3.3 to 3.43 Å) shells were also included in fittings where appropriate (Figure 2.2d).

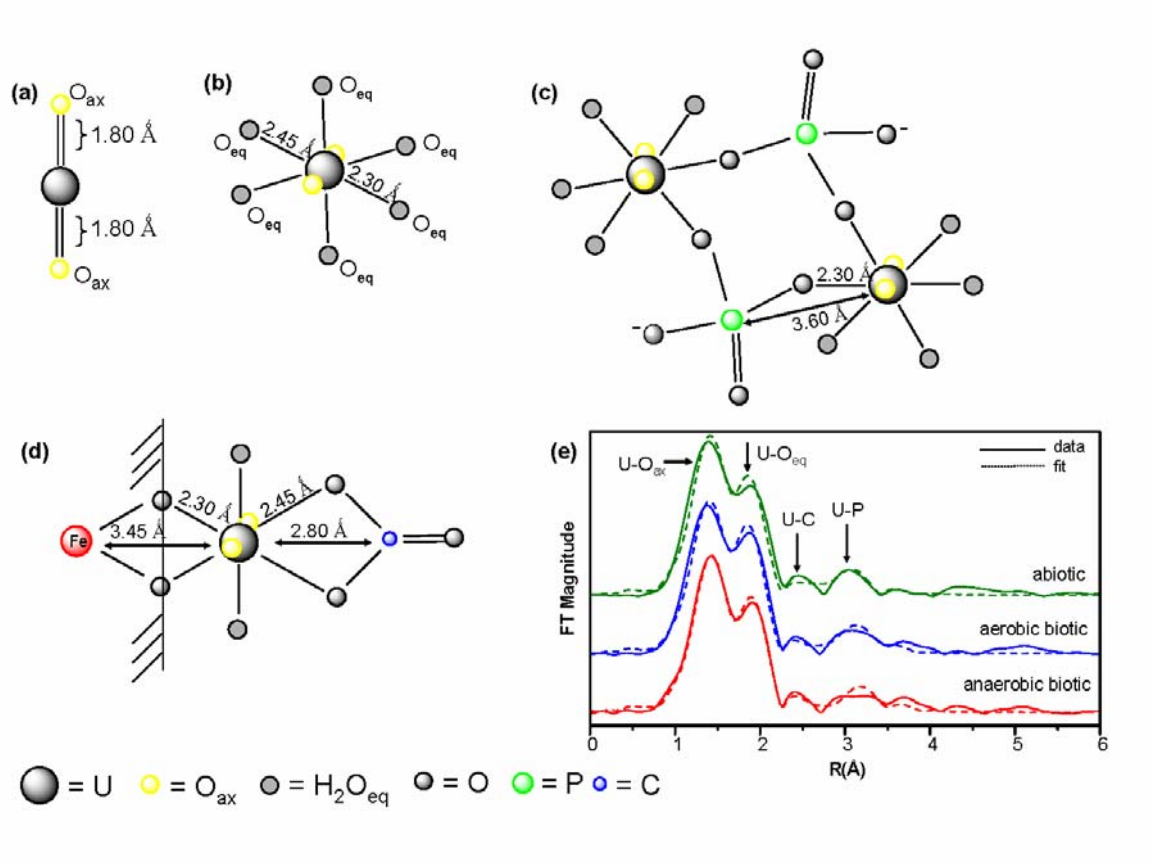

Figure 2.2 U(VI) coordination complexes used in EXAFS fittings included (a) U-O_{ax}, (b) U-O_{eq}, (c) U-P (precipitation), (d) U-Fe (adsorption) and U-C shells. Distances shown in angstroms (Å) are approximate radial bond distances. (e) A typical R-space diagram displaying peaks corresponding to fitted shells. Solid and dashed lines indicate data and fitted data, respectively.

2.6.2 Elemental imaging and µ-XANES

Elemental imaging and µ-XANES analysis was conducted on selected samples at SSRL beam line 2-3 (2009) using a Si(111) monochromator and a motorized three element monolithic Germanium (Ge 3) detector. Elemental data was acquired by continuous scan across the sample grid with a focused beam of 2 µm diameter. Soil samples were thin-sectioned by Spectrum Petrographics, Inc. prior to analysis.

CHAPTER 3

URANIUM BIOMINERALIZATION AS A RESULT OF BACTERIAL PHOSPHATASE ACTIVITY: INSIGHTS FROM BACTERIAL ISOLATES FROM A CONTAMINATED SUBSURFACE

Reproduced in part with permission from Beazley, M. J.; Martinez, R. J.; Sobecky, P. A.; Webb, S. M.; Taillefert, M. Uranium biomineralization as a result of bacterial phosphatase activity: Insights from bacterial isolates from a contaminated subsurface. *Environ. Sci. Technol.* **41**, 5701-5707. Copyright 2007, American Chemical Society.

3.1 Abstract

Uranium contamination is an environmental concern at the Department of Energy's Field Research Center in Oak Ridge, Tennessee. In this study, we investigated whether phosphate biomineralization, or the aerobic precipitation of U(VI)-phosphate phases facilitated by the enzymatic activities of microorganisms, offers an alternative to the more extensively studied anaerobic U(VI) bioreduction. Three heterotrophic bacteria isolated from FRC soils were studied for their ability to grow and liberate phosphate in the presence of U(VI) and an organophosphate between pH 4.5 and 7.0. The objectives were to determine whether the strains hydrolyzed sufficient phosphate to precipitate uranium, to determine whether low pH might have an effect on U(VI) precipitation, and to identify the uranium solid phase formed during biomineralization. Two bacterial strains hydrolyzed sufficient organophosphate to precipitate 73 to 95% total uranium after 120 hours of incubation in simulated groundwater. The highest rates of uranium precipitation and phosphatase activity were observed between pH 5.0 and 7.0. EXAFS

spectra identified the uranyl phosphate precipitate as an autunite/meta-autunite group mineral. The results of this study indicate that aerobic heterotrophic bacteria within a uranium-contaminated environment that can hydrolyze organophosphate, especially in low pH conditions, may play an important role in the bioremediation of uranium.

3.2 Introduction

Radioactive wastes from nuclear weapon production and spent nuclear fuel is a major environmental problem at Department of Energy (DOE) facilities across the United States. Uranium contamination is a particular concern at the DOE Field Research Center (FRC) in the Oak Ridge National Laboratory Reservation at Oak Ridge, Tennessee. Over 30 years of uranium enrichment at the facility produced wastes that have contaminated soil and groundwater adjacent to the disposal ponds with high levels of depleted uranium and nitric acid (Brooks, 2001). The biogeochemical complexities at the FRC site, such as low pH and high concentrations of contaminants (toxic metals, Al, Ni, and nitrate) (Brooks, 2001), make remediation a difficult process, and several different strategies, including both abiotic and biotic approaches, have been examined over the past five years (Istok et al., 2004; North et al., 2004; Wu et al., 2006a; Wu et al., 2006b; Zhou and Gu, 2005).

The fate of uranium in a natural environment is governed by a variety of chemical reactions, including reduction/oxidation, sorption/desorption, precipitation/dissolution, and complexation reactions. The two primary oxidation states of uranium are +4 and +6 (Cotton et al., 1999). U(IV) is stable in anaerobic conditions, mainly in the form of the solid mineral uraninite ($UO_{2(s)}$), but if exposed to dissolved oxygen, uraninite can readily oxidize to the more mobile U(VI) (Finch and Murakami, 1999; Langmuir, 1997). U(VI)

dominates in oxidizing conditions as the highly soluble and stable linear uranyl ion, UO_2^{2+} (Langmuir, 1997; Murphy and Shock, 1999). Uranyl mobility in natural systems below circumneutral pH is controlled primarily by adsorption, precipitation, and complexation reactions (Langmuir, 1978). Uranyl efficiently adsorbs to mineral surfaces, such as iron oxides, over a range of pH, precipitates as insoluble phosphate minerals, such as autunite ($Ca(UO_2)_2(PO_4)_2$), and complexes with organic matter, such as humic and fulvic substances (Finch and Murakami, 1999; Langmuir, 1997). However, above circumneutral pH, uranyl mobility is controlled by carbonates found in most groundwater systems (Langmuir, 1978). Carbonate affects the chemical reactions of uranium through the formation of uranyl carbonate complexes. These strong and highly soluble complexes increase the solubility of uranium by limiting mineral adsorption processes and aiding in the oxidation of U(IV) minerals and dissolution of U(VI) minerals (Langmuir, 1997).

Previous studies on the bioremediation of uranium have focused primarily on the bacterial reduction of U(VI) to uraninite (Istok et al., 2004; Lovley et al., 1991; Wade Jr. and DiChristina, 2000; Wu et al., 2006b). In fact, several bacterial species indigenous to the FRC actively reduce U(VI) (North et al., 2004; Shelobolina et al., 2004). However, much of the uranium contamination at the FRC is within the vadose zone in which oxic conditions prevail (Stubbs et al., 2006). Surprisingly, only a few studies are available on the bioremediation of uranium in aerobic conditions (Macaskie et al., 1994; Powers et al., 2002). In addition, the pH of the contaminated groundwater of the FRC ranges between 3 and 6 which coincides with the highest concentrations of dissolved uranium (Brooks, 2001; Wu et al., 2006a; Wu et al., 2006b). In these pH conditions, carbonates should not

control uranyl solubility and uranyl mineral precipitation may be favored, particularly in the presence of anions such as orthophosphate (Langmuir, 1997). Unfortunately, free orthophosphate is rarely found in soils and aquatic systems. It is instead incorporated in minerals (Langmuir, 1997) or complexed by organic compounds (Turner et al., 2002). In these conditions, microorganisms acquire needed phosphate via phosphatase enzymes which hydrolyze PO_4^{3-} from organophosphate substrates for transport into the cell (Macaskie et al., 1994). We hypothesize that microorganisms in contaminated systems may constitutively express phosphatase genes resulting in enzymatic activity that produces excess orthophosphate and precipitates uranium in a process termed biomineralization. Thus, microbially-mediated mineral precipitation may offer a complementary approach to anaerobic bioreduction in aerobic environments, such as vadose zones.

The objectives of this study were (1) to determine if the phosphatase activity of three aerobic heterotrophic bacterial strains isolated from the FRC promotes the precipitation of solid uranium phosphate in the presence of an organophosphate compound, (2) to investigate if pH and organophosphate concentration affect uranium solubility and phosphatase activity, and (3) to identify the chemical composition of the uranium mineral formed during biomineralization.

3.3 Materials and Methods

3.3.1 Subsurface strains and growth conditions

Three metal-resistant subsurface bacterial strains used in this study, *Arthrobacter* sp. X34, *Bacillus* sp. Y9-2, and *Rahnella* sp. Y9602 were previously isolated from FRC contaminated subsurface soils and identified by 16S rDNA phylogeny (Martinez et al.,

2006). These three genera are commonly found in terrestrial subsurface environments (Balkwill and Boone, 1997; Rozhon et al., 2006). Two of these strains (*Rahnella* sp. and *Bacillus* sp.) exhibited phosphatase-positive phenotypes as determined by histochemical screening (Martinez et al., 2007). Cells were grown in pH-buffered simulated groundwater consisting of 50 mM 2-(*N*-Morpholino)ethanesulfonic acid (MES) (pH 5.5), 2 μM $FeSO_4$, 5 μM $MnCl_2$, 8 μM Na_2MoO_4, 0.8 mM $MgSO_4$, 7.5 mM $NaNO_3$, 0.4 mM KCl, 7.5 mM KNO_3, 0.2 mM $Ca(NO_3)_2$, and amended with 10 mM glycerol-3-phosphate (G3P) (Sigma-Aldrich). Nutrient broth (NB) agar (3 g beef extract, 5 g peptone, 15 g agar per liter) was used for the maintenance of the FRC strains.

3.3.2 Incubations

Incubations with all three bacterial strains were conducted at pH 5.5, the representative pH of contaminated soils at the FRC (Brooks, 2001; Wu et al., 2006a; Wu et al., 2006b). As carbonate is less likely to play a role in the FRC subsurface below circumneutral pH, carbonates were not added to the simulated groundwater. Triplicate flasks containing 250 mL simulated groundwater (pH 5.5) amended with 10 mM G3P as the sole carbon and phosphorus source were inoculated with approximately 10^7 cells mL^{-1} of each strain. Prior to inoculation, FRC strains were grown overnight at 30°C in NB agar (pH 6.8) from frozen stocks (-80°C). The next day, cells from solid medium were grown 16-18 hr in NB broth (pH 5.5) and subsequently diluted 1/50 into fresh NB (pH 5.5) and grown to mid-log phase. Cells were harvested by centrifugation (10,000g for 10 min), washed twice with isotonic saline (8.5 g L^{-1} NaCl), and gently resuspended in simulated groundwater (pH 5.5). Cells resuspended in simulated groundwater were inoculated into experimental flasks and assayed for: (a) viable cell activity; or (b) non-

viable cell activity (i.e., heat-killed cells). Heat-killed cells were held for 30 min at 85°C and allowed to cool to room temperature before inoculation. Abiotic controls contained the exact media components but lacked either a viable or heat-killed cell inoculum. Abiotic control experiments with uranium did not identify any matrix interferences from simulated groundwater and MES. All flasks were incubated at 30°C, 200 rpm, and amended with 200 μM uranyl acetate (Spectrum) after 36 hr of incubation. Subsamples were aseptically removed (24 hr time intervals) to determine (i) culturable cell counts, (ii) orthophosphate concentration, (iii) pH, and (iv) soluble uranium concentrations. Viable cell numbers, reported as colony forming units (CFU), were determined by serially diluting 1 mL subsamples in saline and plating onto NB agar. Further incubations of the *Rahnella* sp. were conducted at pH 4.5, 5.0, and 7.0 to ascertain the most favorable pH for phosphatase activity and uranium phosphate precipitation.

3.3.3 Chemical control experiments and analysis

A direct titration of 10 mM G3P with 1 N NaOH in simulated groundwater (I = 0.02 M) was performed to determine the acid-base properties of G3P with a Thermo Orion 91-06 pH electrode. Equivalence points were determined to calculate the pKa's of G3P (Harris, 1999). In addition, 200 μM uranyl solutions were equilibrated for 48 hr with varying concentrations of G3P to investigate the solubility of uranium in the presence of an organophosphate compound.

Dissolved U(VI) concentrations were measured by inductively-coupled plasma mass spectrometry (ICP-MS) with an Agilent 7500a Series system. Samples were filtered (0.2 μm pore size, AcetatePlus; GE Water and Process Technologies) and acidified with 2% nitric acid (trace metal grade, Fisher) diluted in Nanopure water

(Barnstead). Uranium standards and samples contained holmium and bismuth (SPEX certiPrep) as internal standards. Blanks, calibration check standards (95-105% recovery), and River Water Certified Reference Material for Trace Metals (SLRS-4, National Research Council Canada, Ottawa, Canada) were analyzed for quality controls. The analytical error on triplicate samples was < 3% relative standard deviation (RSD). Total free phosphate (PO_4^{3-}) concentrations were determined by spectrophotometry (Murphy and Riley, 1962). The analytical error on duplicate samples was < 4% RSD. Thermodynamic equilibrium modeling was conducted using MINEQL+ (v. 4.5) updated with the Nuclear Energy Agency's thermodynamic database for uranium (Guillaumont et al., 2003; Schecher and McAvoy, 2001).

At the conclusion of the incubations, the remaining solution was centrifuged and the solid precipitate collected for analysis by X-ray absorption spectroscopy (XAS) at the Stanford Synchrotron Radiation Laboratory (SSRL). Uranium L_{III}-edge XAS spectra were collected at SSRL beamline 11-2 using a focused X-ray beam with a 23 keV harmonic rejection cutoff. The incident energy was selected with a Si(220) monochromator. Transmission and fluorescence data were collected simultaneously. All extended X-ray absorption fine structure (EXAFS) data were reduced using SIXPACK (Webb, 2005). O_{ax} and O_{eq} shells for uranium were fit initially and subtracted from the raw data to create second-shell residual spectra. This technique allows for a more sensitive response of the fitting procedure to the second-shell contributions in the sample spectra. Phase and amplitude files for the EXAFS fitting were created with FEFF7 (Ankudinov et al., 1998; Zabinsky et al., 1995). Since the Debye-Waller factors (σ) correlated highly with coordination numbers (N), σ's for some shells were each fixed at

their average values. The $U{=}O_{ax}{=}U{=}O_{ax}$ transdioxo multiple scattering path (Hudson et al., 1996) was included in all fits.

3.4 Results and Discussion

3.4.1 Speciation of uranium and G3P

Uranyl hydrolysis is well known (Cotton et al., 1999; Langmuir, 1997) and the primary species of uranyl in oxic conditions in the absence of carbonate at and below circumneutral pH are UO_2^{2+}, UO_2OH^+, $(UO_2)_2(OH)_2^{2+}$, and $(UO_2)_3(OH)_5^+$. In contrast, the acid-base properties of G3P and its speciation with U(VI) are not well known. A direct titration of G3P with 1 N NaOH in simulated groundwater identified G3P as a diprotic acid with two equivalence points (Ve_1 = 1.39 mL, Ve_2 = 1.74 mL) corresponding to pKa values of pKa_1 = 2.07 and pKa_2 = 6.4 (Figure 3.1a). The resulting speciation diagram (Figure 3.1b) shows the primary form of G3P between pH 3 and 6 is $HG3P^-$, with one deprotonated phosphate available for binding with the uranyl ion.

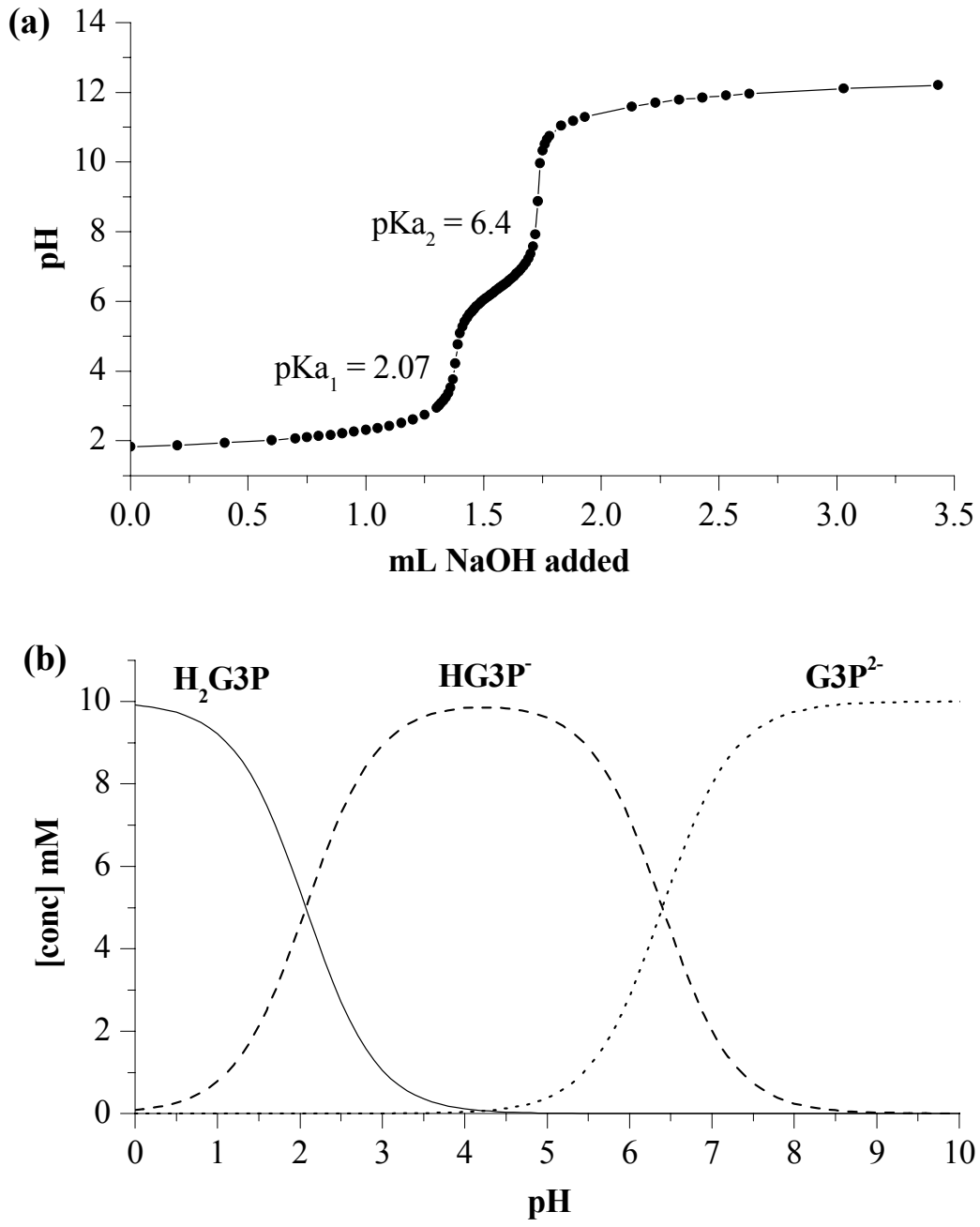

Figure 3.1 . (a) Direct titration of 10 mM G3P in simulated groundwater (I = 0.02 M) with 1 N NaOH indicates a diprotic acid with two equivalence points (Ve_1 = 1.39 mL, Ve_2 = 1.74 mL). (b) The resulting speciation diagram of 10 mM G3P in simulated groundwater.

To demonstrate that the organophosphate ligand does not interfere with uranium abiotically, it was necessary to characterize the nature of the chemical interactions between uranium and G3P. Batch titrations at constant uranyl concentration (200 μM) and varying G3P concentrations revealed that uranyl solubility depends on the concentration of G3P at pH 5.5 (Figure 3.2a). Uranyl precipitated chemically in a mole-to-mole ratio with G3P when the solution [U]:[G3P] molar ratio was greater than or equal to 1:3. These data suggest that a monodentate bond is formed between the uranyl ion and G3P, resulting in a mononuclear U-G3P complex. Monodentate coordination is not uncommon with uranyl; L_{III}-edge EXAFS measurements of uranium(VI) with glucose 6-phosphate (G6P) and fructose 6-phosphate (F6P) at pH 5.5 show monodentate coordination via the oxygen atoms of the phosphate group (Koban et al., 2004). However, uranyl solubility increased when the [U]:[G3P] ratio was smaller than 1:5 and was completely soluble in the presence of 10 mM G3P. The increase in uranyl solubility with increasing organophosphate concentration has been observed with other organophosphates, such as phytic acid (Seaman et al., 2003), and is probably caused by an increase in steric hindrances due to strict ligand coordination requirements within the plane perpendicular to the linear uranyl ion. Interestingly, uranyl solubility did not demonstrate significant dependence on G3P concentration at pH 7 and was insoluble at all ligand concentrations (Figure 3.2a). Therefore, high concentrations of organophosphate and low pHs may favor solubility of uranium.

The same batch reactions were repeated with free orthophosphate to confirm that uranium could be removed by precipitation with orthophosphate once G3P is hydrolyzed. Uranyl precipitation also occurred with free orthophosphate at pH 5.5, and uranyl was

least soluble when the [U]:[P] ratio was greater than or equal to 1:5 (Figure 3.2). In contrast to G3P, the solubility of uranyl did not increase below a [U]:[P] ratio of 1:5, indicating that the removal of uranium could be promoted by orthophosphate. Unfortunately, the concentration of free orthophosphate is often low in groundwater, and most available phosphorus is in the form of organic compounds (Turner et al., 2002). Thus, uranium phosphate precipitation is only a viable remediation strategy if indigenous microorganisms hydrolyze enough organophosphate. More importantly, these microorganisms have to survive and grow in the presence of UO_2^{2+}.

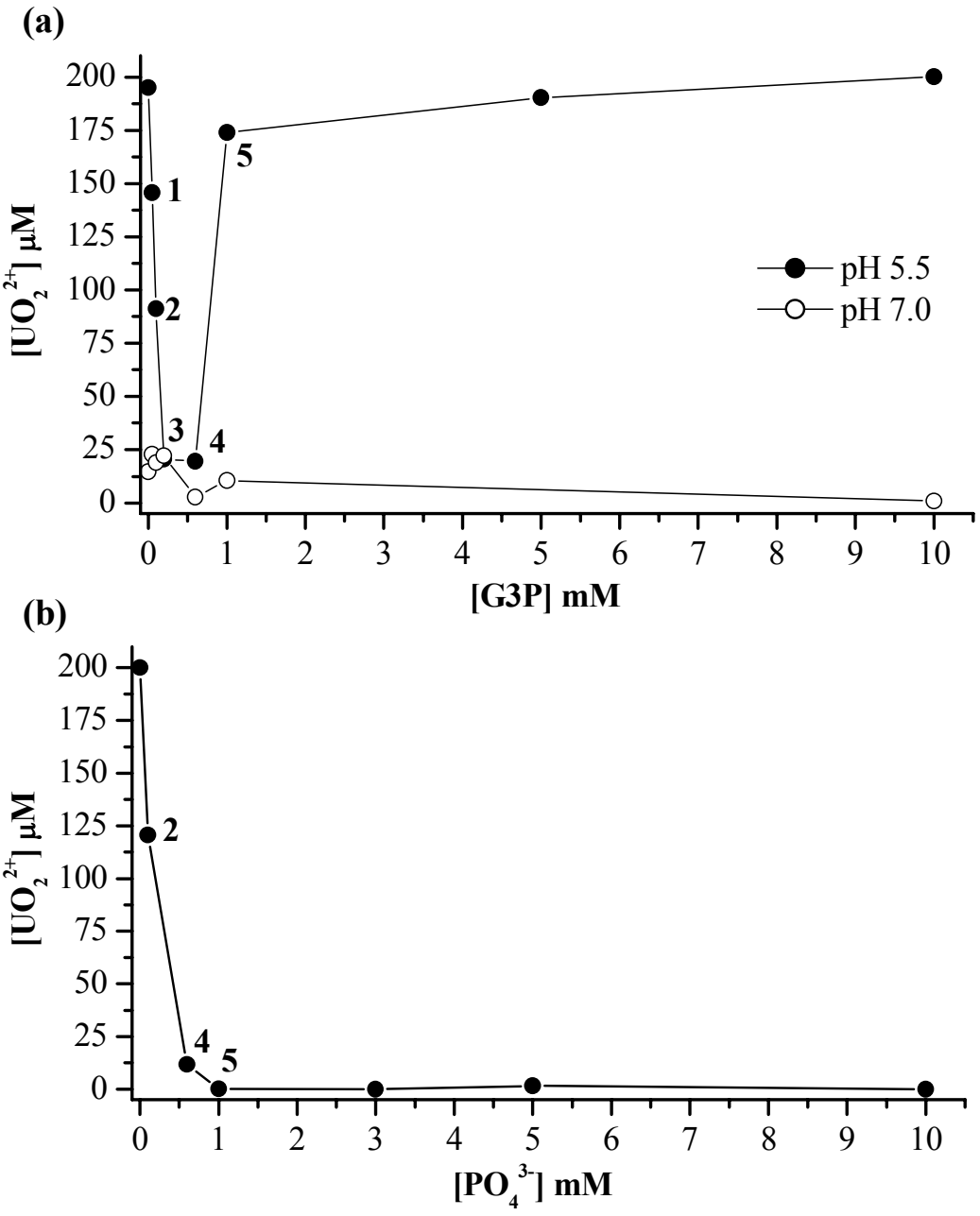

Figure 3.2 Solubility of 200 µM U(VI) as a function of (a) G3P concentration and (b) PO_4^{3-} concentration in simulated groundwater at pH 5.5 and 7.0. Labels 1, 2, 3, 4, and 5 represent [U]:[L] molar ratios of 4:1, 2:1, 1:1, 1:3, and 1:5 with [L] = [G3P] or [PO_4^{3-}].

3.4.2 Incubations

Incubations with strains of *Rahnella*, *Bacillus*, and *Arthrobacter* spp. were conducted at pH 5.5 in the presence of 10 mM G3P (to ensure that G3P was not precipitating chemically with uranium) with 200 μM UO_2^{2+} added at 36 hr. CFU counts were determined to monitor cell viability throughout the 120 hr incubation period. *Arthrobacter* sp. and *Bacillus* sp. CFU counts did not increase during the incubations with or without uranium addition (Figure 3.3a). In contrast, *Rahnella* sp. CFU counts exhibited a significant decrease (10^6-fold) upon the addition of uranium, but by the end of the incubation CFU counts were comparable to the control without uranium (Figure 3.3a).

The rates of uranium precipitation and G3P hydrolysis in the presence of the three bacterial strains are shown in Figure 3.3b and c. *Rahnella* sp. hydrolyzed 9 times more G3P than *Bacillus* sp. after 120 hrs regardless of the presence of uranium (Figure A. 1: A). However, in the presence of uranium both strains hydrolyzed approximately 55% less G3P than in controls without uranium. In *Rahnella* sp. incubations, 34% uranium precipitated within one hour after amendment in the presence of ~ 0.5 mM free orthophosphate. After 12 hours, 78% uranium precipitated while free orthophosphate concentrations doubled (Figure 3.3b and c). After 5 days, 95% of uranium was removed and orthophosphate concentrations increased to 2.4 mM, suggesting that *Rahnella* sp. is not significantly affected by the presence of U(VI). Uranium was not removed in incubations with heat-killed cells of *Rahnella* sp., demonstrating that adsorption of uranium to cell membranes is not significant at pH 5.5 (Figure 3.3b). Simultaneously, *Bacillus* sp. cells did not demonstrate appreciable growth in the simulated groundwater as CFU counts remained constant throughout the incubation in the presence or absence of

uranium (Figure 3.3a). *Bacillus* sp. demonstrated only moderate phosphatase activity (Figure 3.3c), with ~ 300 μM hydrolyzed phosphate in solution at steady-state. Yet, 31% uranium precipitated within one hour after amendment, and 73% of the initial uranium was removed by precipitation after 5 days (Figure 3.3b). Some *Bacillus* strains accumulate uranium on outer cell wall surface layers via inner sphere complexes with cell bound phosphate and carboxyl groups, which function as protective barriers to heavy metals (Merroun et al., 2005; Panak et al., 2002; Panak et al., 2000). As observed with the *Rahnella* strain, uranium was not removed in incubations with heat-killed cells of *Bacillus* sp. (Figure 3.3b), indicating U(VI) did not adsorb or complex with cell surfaces.

In contrast, *Arthrobacter* sp. cells did not demonstrate any measurable phosphatase activity, with zero free phosphate detected at pH 5.5 before and after uranium addition (Figure 3.3c). Dissolved uranium remained stable at initial concentrations in the chemical control, heat-killed cell control, and in the presence of live cells (Figure 3.3b). However, cells remained culturable throughout the incubation though they did not grow, as a function of time (Figure 3.3a), suggesting a different protection mechanism from uranium toxicity. A previous study has shown some *Arthrobacter* strains can accumulate uranium intracellularly and possibly precipitate uranium with polyphosphates as means of detoxification (Suzuki and Banfield, 2004). Altogether, these incubations suggest that bacterial species with phosphatase activity, such as *Rahnella* sp. and *Bacillus* sp., can survive in the presence of UO_2^{2+} and hydrolyze sufficient organophosphate to precipitate U(VI).

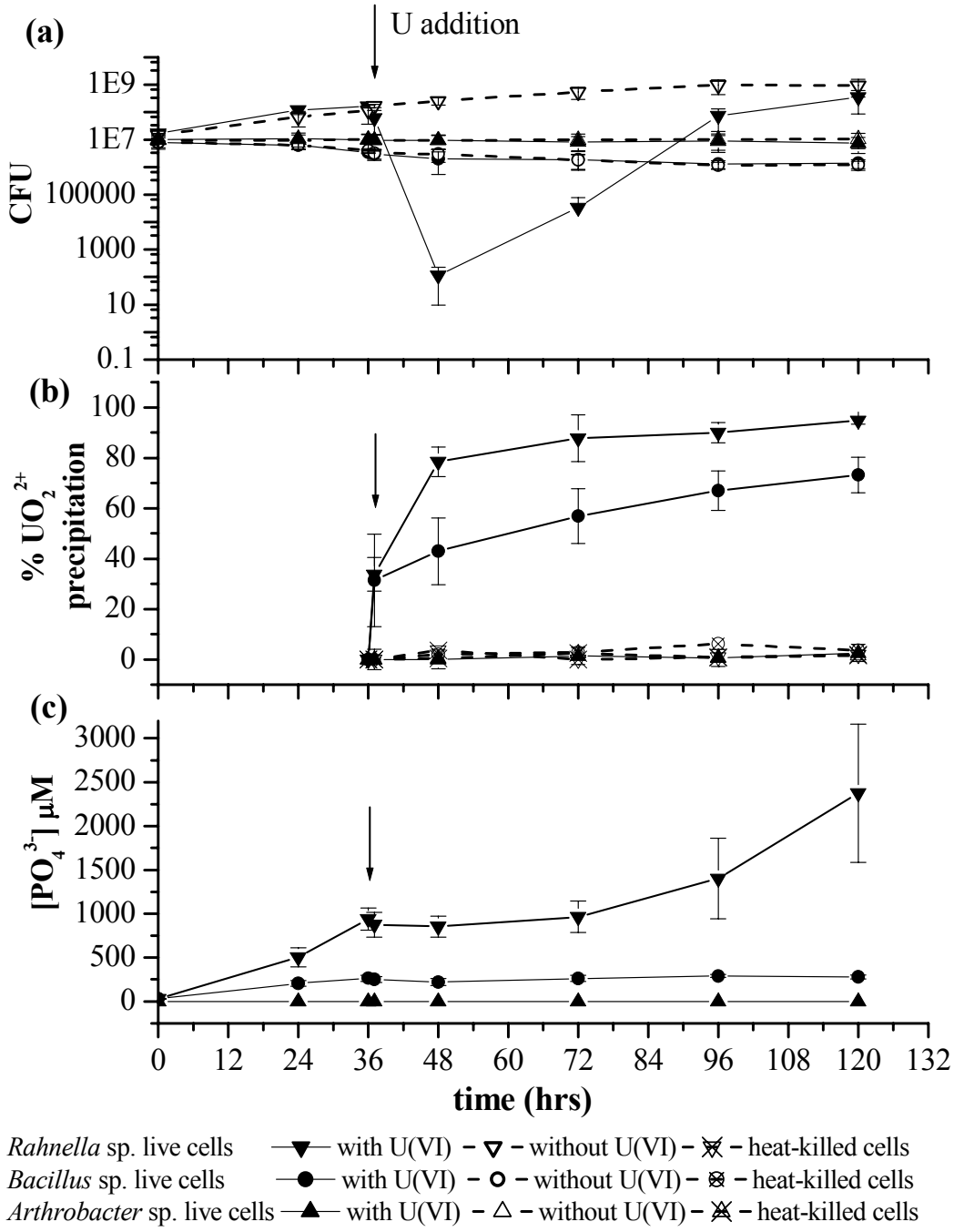

Figure 3.3 (a) Average colony forming units (CFU) from three replicate incubations, (b) percent U(VI) precipitation, and (c) phosphate concentrations in incubations at pH 5.5 with 200 µM UO_2^{2+}, 10 mM G3P, and three bacterial species in simulated groundwater (standard deviation represents variations of triplicate incubations).

Incubations of *Rahnella* sp. were also conducted at different pH to determine the most favorable pH for uranium phosphate precipitation and phosphatase activity and to establish if biomineralization of uranium can occur within the pH range of the FRC groundwater. Uranium precipitation rate was dependent on pH (Figure 3.4a). Uranium precipitation was minimal and cell growth significantly less at pH 4.5, possibly due to the combined stress of low pH and uranium toxicity (Suzuki and Banfield, 2004). Only 28% of initial uranium was precipitated at pH 4.5 at steady-state, compared to 90 and 97% precipitation at pH 5.5 and 7.0, respectively. Chemical and heat-killed cell controls did not demonstrate any abiotic uranium precipitation or adsorption at and below pH 5.5 (Figure A. 2; Appendix A). Chemical precipitation of uranium did occur, however, at pH 7.0 in control samples (Figure 3.2a), suggesting that the precipitation of U(VI) in these incubations with *Rahnella* sp. at pH 7 is chemical.

Hydrolysis of G3P by *Rahnella* sp. demonstrated a dependence on pH and uranium addition (Figure 3.4b and c). In the absence of U(VI), *Rahnella* sp. hydrolyzed 1.5 times more G3P at pH 7.0 compared to pH 4.5 (Figure A. 1;Appendix A) and in the presence of U(VI), 4 times more G3P was hydrolyzed at pH 7.0 than at pH 4.5. The percent phosphate difference between samples with and without U(VI) at each timepoint as a function of pH is shown in Figure 3.4c. After 36 hrs, samples without uranium consistently contained more orthophosphate than samples with uranium throughout the experiments; however, after ~ 97% uranium precipitated, such as at pH 7, the difference in orthophosphate concentrations was minimal.

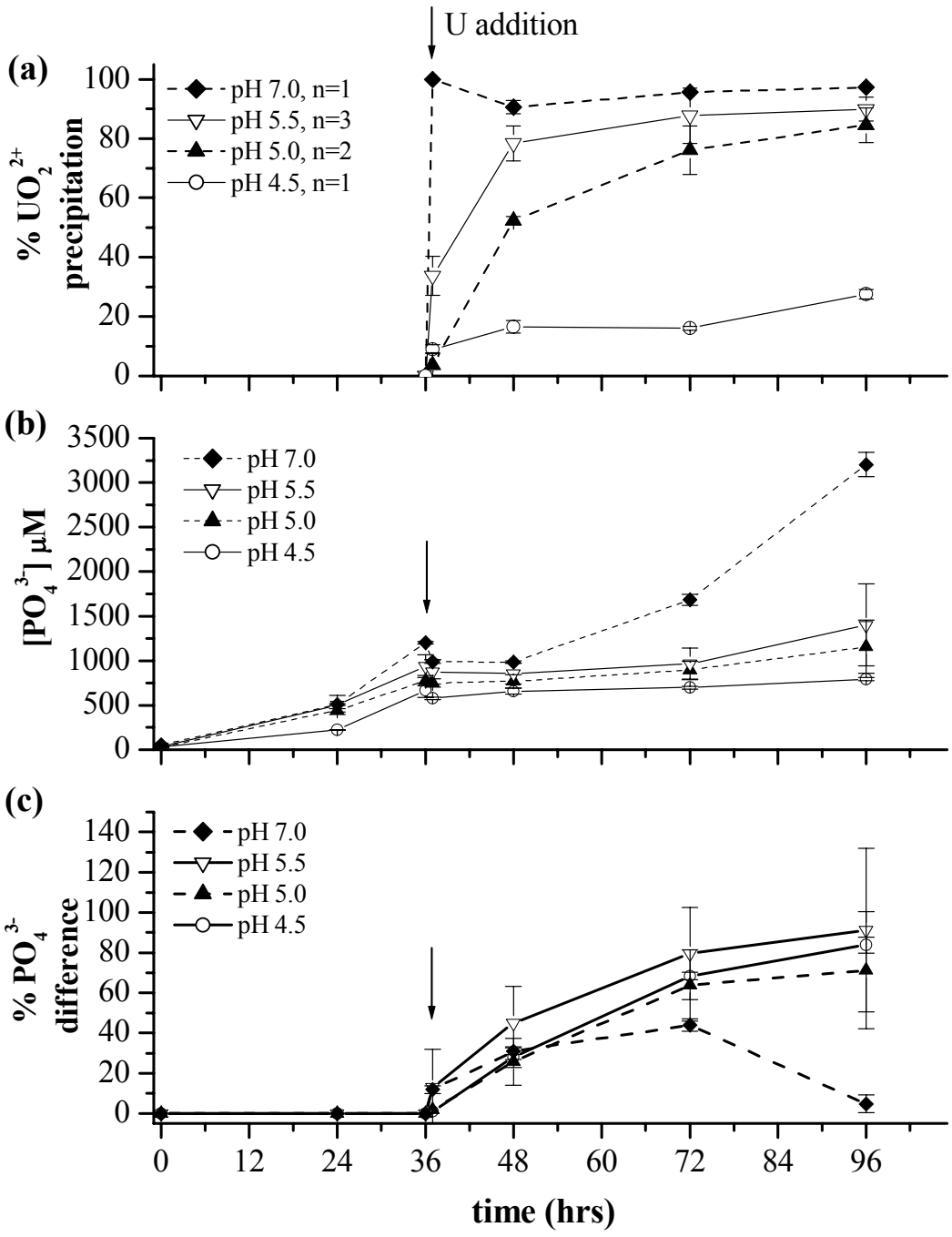

Figure 3.4 (a) Average percent U(VI) precipitation, (b) average phosphate concentrations in the presence of U(VI), and (c) percent phosphate difference between samples with and without U(VI) in incubations of *Rahnella* sp. at different pH in simulated groundwater. U(VI) was added after 36 hours (n represents the number of replicate incubations conducted and averaged).

3.4.3 Solid-phase characterization

Uranium XAS spectra for biological and control bulk precipitates are shown in Figure 3.5 and fitted parameters listed in Table A. 1 (Appendix A). Biological samples included precipitates from incubations with *Rahnella* sp. in the presence of 200 μM UO_2^{2+} and 10 mM G3P in simulated groundwater at pH 5.5 (A) and pH 7.0 (B). Abiotic samples consisted of simulated groundwater amended with 200 μM UO_2^{2+} in the presence of 200 μM NaH_2PO_4 at pH 5.5 (C) and in the presence of 10 mM G3P at pH 7.0 (D).

The XANES structure (Figure 3.5a) in both biological and chemical samples displays a characteristic shoulder between 17180 and 17190 eV consistent with U(VI) oxidation state. The *k*-space region from 8.5 to 10.5 $Å^{-1}$ shows the difference between the samples containing phosphate (A, B, and C) and the sample without phosphate (D). Precipitates with phosphate were characteristic of the closely related autunite and meta-autunite group minerals, while the precipitate without phosphate was a uranium hydroxide mineral. The autunite/meta-autunite group includes minerals such as meta-ankoleite ($K_2(UO_2)_2(PO_4)_2$), autunite ($Ca(UO_2)_2(PO_4)_2$), chernikovite ($H_2(UO_2)_2(PO_4)_2$), and saléeite ($Mg(UO_2)_2(PO_4)_2$. Due to the structural similarities of these autunite-type minerals their EXAFS spectra are difficult to distinguish (Catalano and Brown Jr., 2004; Fuller et al., 2002). These minerals display sheets of square bipyramidal uranyl and tetrahedral phosphate $[(UO_2)(PO_4)]^-$ attached by interlayer charge-balancing cations (Catalano and Brown Jr., 2004; Locock and Burns, 2003). As a result, the polynuclear

structure of autunite may explain the greater stability of autunite precipitates compared to the mononuclear U-G3P complex.

The U-P distances in phosphate precipitates (~ 3.58 Å average) indicate uranyl formed a monodentate complex with phosphate (Table A. 1; Appendix A). The two precipitates formed at pH 5.5 contained an average 2.35 coordinating P molecules compared to 0.75 in the phosphate precipitate formed at pH 7.0 (Table A. 1; Appendix A). The lower coordination number of P molecules at pH 7.0 suggests the existence of a mixture of uranium phosphate and uranium hydroxide minerals, which would be consistent with thermodynamic predictions at higher pH.

The biological uranyl phosphate precipitate (A) had approximately the same EXAFS structure as the chemical uranyl phosphate precipitate (C) at pH 5.5 (Figure 3.5b and c), suggesting little difference between uranium mineralized in the presence of PO_4^{3-} bio-hydrolyzed from an organophosphate substrate and uranium precipitated with free orthophosphate. Interestingly, the chemical precipitation of U(VI)-hydroxide in control samples (Figure 3.5 D and Table A. 1; Appendix A) and the high precipitation rates in live incubations at pH 7.0 suggested that the uranyl precipitation in *Rahnella* sp. incubations was chemical. However, EXAFS measurements (Figure 3.5 B and Table A. 1; Appendix A) identified the precipitate as a mixture of autunite/meta-autunite and uranyl hydroxide indicating a biologically-mediated uranyl phosphate formation at pH 7.0. Thermodynamic modeling using MINEQL+ (v. 4.5) (Schecher and McAvoy, 2001) predicts the principle mineral phase at pH 7.0 as autunite/meta-autunite with uranyl hydroxide comprising only a small percentage of the mineral mixture (Figure 1.5). In contrast, EXAFS identified uranyl hydroxide as the only mineral phase formed at pH 7.0

in chemical control incubations without phosphate (Figure 3.5 D and Table A. 1; Appendix A). The difference in the composition of the uranyl mineral formed in the presence of live cells compared to the mineral formed in chemical controls demonstrates that the precipitation of uranium is driven by biological activities. Thermodynamic modeling of simulated groundwater containing 200 μM UO_2^{2+} and 1 mM PO_4^{3-} (1:5 ratio) identifies a low solubility range for autunite between pH 4 and 8, even in the presence of high concentrations of sulfate and nitrate (not shown). Carbonate that is prevalent in natural systems plays an important role in uranium solubility; however, thermodynamic calculations predict that carbonate should not affect autunite solubility below pH 8. These findings demonstrate the potential applicability of uranium phosphate biomineralization as a bioremediation strategy in aerobic aquifers below circumneutral pH where uranium is a major contaminant.

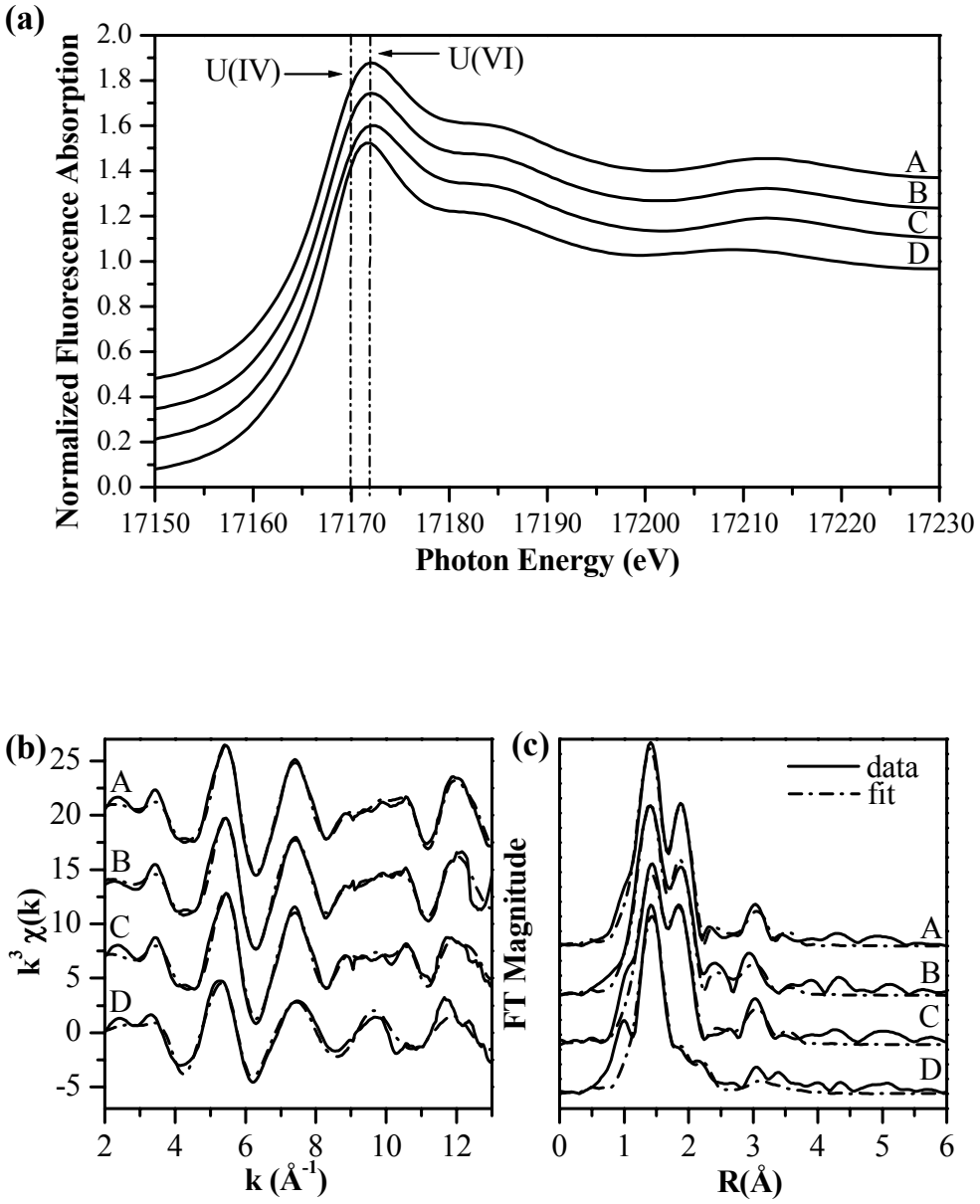

Figure 3.5 Uranium (a) XANES, (b) *k*-space and (c) R-space diagrams of the L_{III}-edge EXAFS from precipitates obtained during incubations with *Rahnella* sp. in the presence of 200 μM UO_2^{2+} and 10 mM G3P in simulated groundwater at pH 5.5 (A) and pH 7.0 (B). Abiotic samples consisted of simulated groundwater amended with 200 μM UO_2^{2+} in the presence of 200 μM NaH_2PO_4 at pH 5.5 (C) and 10 mM G3P at pH 7.0 (D).

The results of this study demonstrate that some aerobic heterotrophic bacteria isolated from a uranium-contaminated environment can catalyze the precipitation of uranium phosphate in oxic conditions through the activity of their phosphatase enzymes. Previous studies have suggested that organisms increase their phosphatase activity as a protection mechanism from heavy metal contamination in toxic environments (Macaskie et al., 1994; Montgomery et al., 1995; Powers et al., 2002; Sobecky et al., 1996; Yong and Macaskie, 1999). In this study, we have demonstrated that two aerobic heterotrophic bacterial species isolated from a contaminated soil sample from Area 3 of the FRC site at Oak Ridge, Tennessee can hydrolyze sufficient organophosphate to precipitate up to 95% total uranium. We are particularly interested in the role these organisms may potentially have in the bioremediation of uranium at the FRC and how pH and organophosphate ligand concentration affect uranium solubility in such a system.

3.4.4 Applications for in situ bioremediation

Soils from Area 3 contain 2 orders of magnitude more uranium, as precipitated uranium phosphate, in shale micropores than uranium adsorbed onto iron oxide surfaces (Stubbs et al., 2006). These findings indicate local saturation of uranium phosphate compared to the bulk groundwater and imply that the pH of the groundwater is too low to favor adsorption of positive uranyl species onto positively charged iron oxides (Stubbs et al., 2006). Indeed, these conditions should be favorable to phosphate adsorption onto iron oxides, and adsorption of phosphate onto goethite-coated sand (Cheng et al., 2004) and ferrihydrite (Payne et al., 1996) below pH 7 can increase the uptake of uranyl via the formation of ternary surface complexes between UO_2^{2+} and PO_4^{3-}. However, free orthophosphate concentrations are usually low in groundwater, and phosphorus is very

often complexed with organic compounds (Turner et al., 2002). If precipitation of uranium phosphate due to localized niches is such a large sink for uranium, microenvironments containing indigenous microorganisms, such as *Rahnella* sp., exhibiting phosphatase activity may produce enough orthophosphate to cause local saturation of uranium phosphates. Thus, uranium phosphate precipitation, either chemically or biologically-mediated, could be enhanced in areas where the uranyl-to-orthophosphate ratio and pH are low.

At the Oak Ridge FRC, where uranium contamination is mostly within the vadose zone and below circumneutral pH, remediation may be promoted, through enhancement of microbial phosphatase activity, by addition of organophosphate compounds. Microbial-mediated hydrolysis of high concentrations of organophosphates may produce enough orthophosphate to significantly reduce the solubility of uranyl. Our findings demonstrate that the aerobic and low pH conditions at the FRC may be ideal for the application of biomineralization of uranium through the activity of phosphatase enzymes.

3.5 Acknowledgements

This research was supported by the Office of Science (BER), U. S. Department of Energy Grant No. DE-FG02-04ER63906. Portions of this research were carried out at the Stanford Synchrotron Radiation Laboratory, a national user facility operated by Stanford University on behalf of the U.S. Department of Energy, Office of Basic Energy Sciences. The SSRL Structural Molecular Biology Program is supported by the Department of Energy, Office of Biological and Environmental Research, and by the National Institutes of Health, National Center for Research Resources, Biomedical Technology Program.

CHAPTER 4

NONREDUCTIVE BIOMINERALIZATION OF URANIUM(VI) PHOSPHATE VIA MICROBIAL PHOSPHATASE ACTIVITY IN ANAEROBIC CONDITIONS

This is a preprint of an article whose final and definitive form has been published in *Geomicrobiology Journal*, authored by Beazley, M. J.; Martinez, R. J.; Sobecky, P. A.; Webb, S. M.; Taillefert, M. entitled Non reductive biomineralization of uranium(VI) phosphate via microbial phosphatase activity in anaerobic conditions.

Geomicrobiology Journal is available online at: http://www.informaworld.com/smpp/.

4.1 Abstract

The remediation of uranium from soils and groundwater at Department of Energy (DOE) sites across the United States represents a major environmental issue, and bioremediation has exhibited great potential as a strategy to immobilize U in the subsurface. The bioreduction of U(VI) to insoluble U(IV) uraninite has been proposed to be an effective bioremediation process in anaerobic conditions. However, high concentrations of nitrate and low pH found in some contaminated areas have been shown to limit the efficiency of microbial reduction of uranium. In the present study, nonreductive uranium biomineralization promoted by microbial phosphatase activity was investigated in anaerobic conditions in the presence of high nitrate and low pH as an alternative approach to the bioreduction of U(VI). A facultative anaerobe, *Rahnella* sp. Y9602, isolated from soils at DOE's Oak Ridge Field Research Center (ORFRC), was able to respire anaerobically on nitrate as a terminal electron acceptor in the presence of glycerol-3-phosphate (G3P) as the sole carbon and phosphorus source and hydrolyzed

sufficient phosphate to precipitate 95% total uranium after 120 hours in synthetic groundwater at pH 5.5. Synchrotron X-ray diffraction and X-ray absorption spectroscopy identified the mineral formed as chernikovite, a U(VI) autunite-type mineral. The results of this study suggest that in contaminated subsurfaces, such as at the ORFRC, where high concentrations of nitrate and low pH may limit uranium bioreduction, the biomineralization of U(VI) phosphate minerals may be a more attractive approach for in situ remediation providing that a source of organophosphate is supplied for bioremediation.

4.2 Introduction

Over thirty years of uranium enrichment at the DOE Oak Ridge, Tennessee site left a legacy of uranium contamination in soils and groundwater (Brooks, 2001). These contaminated systems are characterized by high concentrations of uranium and other toxic metals, as well as, high nitrate and low pH (Brooks, 2001; Wu et al., 2006a). Complete removal of uranium from groundwater and soils through methods such as extraction and pump and treat is infeasible on large spatial scales, and research in recent years has focused on ways to lower the solubility of uranium in situ, thereby stopping and/or slowing its migration through the subsurface (e.g. Arey et al., 1999; Istok et al., 2004; Wu et al., 2006a; Wu et al., 2007).

The solubility of uranium in the subsurface is influenced by the redox conditions, pH, soil matrix, and the presence/absence of organic ligands, phosphate, and carbonate (Langmuir, 1997). Uranium exists in the environment in two primary oxidation states, the soluble uranyl ion (U(VI)) and the insoluble uraninite mineral (U(IV)). Uranium(VI) reduction to U(IV) occurs either chemically by Fe(II) adsorbed onto mineral surfaces

(Boyanov et al., 2007; Jeon et al., 2005; Liger et al., 1999; O'Loughlin et al., 2003) or biologically by dissimilatory metal-reducing bacteria (DMRB) and sulfate-reducing bacteria (SRB) (Fredrickson et al., 2000; Lovley and Phillips, 1992; Lovley et al., 1991; North et al., 2004; Wade Jr. and DiChristina, 2000). Unfortunately, uraninite is rapidly oxidized to the more mobile and reactive uranyl ion ($U^{VI}O_2^{2+}$) in oxic conditions (Langmuir, 1997; Murphy and Shock, 1999), and more slowly oxidized under nitrate-reducing conditions by nitrite or Fe(III) oxyhydroxides (Senko et al., 2002; Senko et al., 2005a; Senko et al., 2005b). Groundwater pH exerts a strong influence on the speciation and solubility of U(VI). Below circumneutral pH, uranyl is positively charged and exists primarily as the soluble species UO_2^{2+} and UO_2OH^+ (Langmuir, 1997). In the presence of phosphate, insoluble uranyl phosphate minerals are thermodynamically stable between pH 4 and 8 (Guillaumont et al., 2003; Schecher and McAvoy, 2001). Uranyl availability in the dissolved phase can also be limited by adsorptive reactions with amorphous Fe(III) oxyhydroxides between pH 4.5 and 8 (Hsi and Langmuir, 1985) and with hydroxyapatite at circumneutral pH even in the presence of uranyl carbonate complexes (Fuller et al., 2002). Above circumneutral pH, uranyl forms strong and highly soluble uranyl carbonate complexes (e.g. $UO_2(CO_2)_3^{4-}$, $UO_2(CO_3)_2^{2-}$) that limit mineral adsorption and promote the oxidative dissolution of uraninite by dissolved oxygen, thus increasing uranium mobility (De Pablo et al., 1999; Langmuir, 1997). It is, therefore, important to consider the pertinent environmental conditions that affect uranium speciation when evaluating a remediation strategy.

The reduction of U(VI) to the insoluble U(IV) uraninite by metal-reducing bacterial species has been demonstrated to immobilize uranium in biostimulated soils at

the Oak Ridge Field Research Center (ORFRC) (Wu et al., 2006a; Wu et al., 2006b; Wu et al., 2007). U(VI) reduction, however, can be limited or hindered by low pH, high concentrations of nitrate, iron and manganese oxides, and infusion of dissolved oxygen through groundwater recharge. Typical uranium-reducing microorganisms, such as *Shewanella* sp. and *Geobacter* sp., grow optimally at and above pH 7 (Venkateswaran et al., 1999), and most remediation strategies include raising the pH to increase microbial activity (Wu et al., 2006a; Wu et al., 2006b). Nitrate is a co-contaminant at the ORFRC with concentrations as high as 160 mM (Wu et al., 2006a) and is an energetically more favorable electron acceptor than U(VI) at circumneutral pH (Edwards et al., 2007) and must be removed before U(VI) can be reduced (Finneran et al., 2002) In addition, high nitrate concentrations may promote the oxidation of U(IV) by anaerobic, nitrate-dependent oxidizers (Beller, 2005) or by Fe(III) produced during nitrite oxidation of Fe(II) (Senko et al., 2005a; Senko et al., 2005b). Metal oxides and oxyhydroxides, such as iron and manganese, can also act as competitive electron acceptors and slow rates of enzymatic reduction of U(VI) (Fredrickson et al., 2002; Wielinga et al., 2000). The effect of bacterial non-specific acid phosphatase (NSAP) activity on uranium solubility (Macaskie et al., 1994; Macaskie et al., 1992) is much less studied compared to bacterial reduction but has recently received attention as a possible remediation strategy at the ORFRC (Beazley et al., 2007; Martinez et al., 2007). Bacterial phosphatase enzymes hydrolyze phosphate moieties from organophosphate substrates to release phosphate and biologically induce precipitation of U(VI) as uranyl phosphate minerals, such as autunite [$Ca(UO_2)_2(PO_4)_2$], chernikovite [$H_2(UO_2)_2(PO_4)_2$], and ankoleite [$K_2(UO_2)_2(PO_4)_2$]. Cell-

bound accumulation of heavy metal phosphates as a result of NSAP activity has been suggested as a possible resistance mechanism to toxic metals (Macaskie et al., 1994).

In a previous study, ORFRC isolates (*Bacillus* sp. strain Y9-2 and *Rahnella* sp. strain Y9602) exhibiting phosphatase-positive phenotypes indicative of constitutive NSAP activity were grown aerobically in synthetic groundwater with nitrate and glycerol-3-phosphate (G3P) as the sole nitrogen, carbon, and phosphorus sources. Both strains liberated sufficient phosphate to precipitate 73 to 95% of uranium between pH 5 and 7 (Beazley et al., 2007; Martinez et al., 2007). Rates of uranium precipitation were highest between pH 5.0 and pH 7.0 because in this pH range the predominant dissolved phosphate species are $H_2PO_4^-$ and HPO_4^{2-} that can form favorable complexes with positively-charged uranyl molecules. Below pH 5.0, however, uranyl precipitation is minimal due to the partial protonation of phosphate and the decrease in cell growth, possibly due to pH stress and uranium toxicity (Suzuki and Banfield, 2004). Analysis by X-ray absorption spectroscopy (XAS) identified the precipitate formed in oxic conditions as a U(VI) autunite/meta-autunite group mineral (Beazley et al., 2007).

Dissolved oxygen is typically low (< 31 μM) in deep ORFRC contaminated soils, but can range up to 125 μM in more shallow groundwater recharge areas (http://public.ornl.gov/orifc/sitenarrative.cfm). A microorganism with the ability to induce the precipitation of uranium both in aerobic and anaerobic conditions, in a wide range of pH, and in the presence of high concentrations of nitrate would be advantageous for in situ remediation at the ORFRC. The present study expands our previous work and determines whether *Rahnella* sp. Y9602 isolated from the ORFRC grows anaerobically

and exhibits sufficient phosphatase activity to precipitate uranyl phosphate in moderately low pH conditions.

4.2 Materials and Methods

4.2.1 Subsurface Bacterial Strains and Growth Conditions.

The facultatively anaerobic gram-negative subsurface bacterial strain used in this study, *Rahnella* sp. Y9602, was previously isolated from ORFRC contaminated soils and identified as similar (98% identity) to *Rahnella aquatilis* (ATCC33989) by 16S rDNA sequencing (Martinez et al., 2006). Phosphatase phenotypes were previously determined by histochemical screening (Martinez et al., 2007). Cells were grown in pH-buffered synthetic groundwater consisting of 50 mM 2-(N-Morpholino)ethanesulfonic acid (MES) (pH 5.5), 2 μM $FeSO_4$, 5 μM $MnCl_2$, 8 μM Na_2MoO_4, 0.8 mM $MgSO_4$, 7.5 mM $NaNO_3$, 0.4 mM KCl, 7.5 mM KNO_3, 0.2 mM $Ca(NO_3)_2$, and amended with 10 mM glycerol-3-phosphate (G3P) (Sigma Aldrich). Nutrient broth (NB) agar (3 g beef extract, 5 g peptone, 15 g agar per liter) was used for the maintenance of the ORFRC strain.

Incubations with *Rahnella* sp. Y9602 were conducted as previously described (Beazley et al., 2007; Martinez et al., 2007), except they were maintained under anoxic conditions in a Coy Laboratory Instruments, Inc. anaerobic chamber maintained at 25 °C under an atmosphere of 1% H_2, 5% CO_2, and 94% N_2. Briefly, triplicate flasks containing 250 mL synthetic groundwater (pH 5.5) amended with 10 mM G3P as the sole carbon and phosphorus source and 15 mM nitrate as the terminal electron acceptor were inoculated with approximately 10^7 cells mL^{-1} of the *Rahnella* sp. Y9602 strain. A set of flasks containing live cells were inoculated in the absence of uranium, while another set of flasks containing actively growing cells were amended with 200 μM uranyl acetate

(Spectrum) 36 h after inoculation. Abiotic and heat-killed cell controls were inoculated simultaneously to identify any matrix and cell membrane interactions with uranium. Subsamples were aseptically removed (24 h time intervals) to determine (1) culturable cell counts, (2) orthophosphate concentrations, (3) nitrite concentrations, (4) pH, and (5) soluble uranium concentrations. Viable cell numbers, reported as colony forming units (CFU), were determined by serially diluting 1 mL subsamples in saline and plating onto NB agar.

4.2.2 Sampling and Analyses

Nitrate reduction and denitrification assays were conducted according to Smibert and Krieg (1994). Briefly, test tubes containing tryptic soy broth (TSB) medium supplemented with 0.1% KNO_3 and 0.17% agar were inoculated with *Escherichia coli* MG1655, *Pseudomonas aeruginosa*, and the ORFRC *Rahnella* sp. Y9602. The *E. coli* and *P. aeruginosa* strains were used as positive controls for nitrate respiration and denitrification, respectively. In this assay, the presence of nitrite was determined from the reaction of nitrite with an aromatic amine leading to the formation of a diazonium compound that forms a pink azo dye with a second amine (Smibert and Krieg, 1994). Dissolved U(VI) concentrations were measured by inductively-coupled plasma mass spectrometry (ICP-MS) with an Agilent 7500a Series system. Samples were filtered (0.2 μm pore size, AcetatePlus; GE Water and Process Technologies) and acidified with 2% nitric acid (trace metal grade, Fisher) diluted in Nanopure water (Barnstead). Holmium and bismuth (SPEX certiPrep) were used as internal standards and River Water Certified Reference Material for Trace Metals (SLRS-4, National Research Council Canada, Ottawa, Canada) for quality controls. Analytical error on triplicate samples was <3%

relative standard deviation (RSD). Total free phosphate (ΣPO_4^{3-}) concentrations were determined by spectrophotometry (Murphy and Riley, 1962). Analytical error on duplicate samples was <4% RSD. Nitrite (NO_2^-) concentrations were determined by spectrophotometry (Grasshoff, 1983) with an analytical error on duplicate samples of <5% RSD. Ammonium (NH_4^+) concentrations were determined colorimetrically according to Strickland and Parsons (1972).

4.2.3 X-Ray Analyses

The precipitate formed during the incubations was collected by centrifugation at the conclusion of the experiments, and analyzed by X-ray absorption spectroscopy (XAS) and X-ray diffraction (XRD) at the Stanford Synchrotron Radiation Laboratory (SSRL), and compared to precipitate formed abiotically. The abiotic uranyl phosphate precipitate was prepared by combining 200 μM uranyl acetate with 1 mM dihydrogen phosphate and allowed to equilibrate for 48 h. The precipitate was collected by centrifugation and washed with deionized water to remove excess phosphate. Uranium L_{III}-edge XAS spectra were collected on wet samples at SSRL beam line 10-2 using a forced X-ray beam with a 23 keV harmonic rejection cutoff. The incident energy was selected with a Si(220) monochromator. Transmission and fluorescence data were collected simultaneously. All extended X-ray absorption fine structure (EXAFS) data were reduced using SIXPACK (Webb, 2005). O_{ax} and O_{eq} shells for uranium were fit initially and subtracted from the raw data to create second-shell residual spectra. This technique allows for a more sensitive response of the fitting procedure to the second-shell contributions in the sample spectra. Phase and amplitude files for the EXAFS fitting were created with FEFF7 (Ankudinov et al., 1998; Zabinsky et al., 1995). Since the

Debye-Waller factors (σ) correlated highly with coordination numbers (N), σ's for some shells were each fixed at their average values. The $U{=}O_{ax}{=}U{=}O_{ax}$ transdioxo multiple scattering path (Hudson et al., 1996) was included in all fits.

To identify crystalline uranium phases, XRD intensity data were collected on wet samples using the two-circle diffractometer on SSRL beam line 2-1 (using a Bicron NaI(Tl) detector equipped with Soller slits). The diffractometer was calibrated with LaB_6 and the incident X-ray beam was tuned to $\lambda = 1.034$ Å.

4.2.4 Electron Microscopy

Upon completion of *Rahnella* sp. Y9602 uranium biomineralization incubations, 40 ml of culture was pelletted and re-suspended in 1 mL fixative (2.5% glutaraldehyde in 0.1 M cacodylate buffer). After 2 hours fixation at 4°C, bacteria were washed with the same buffer and post-fixed with buffered 1% osmium tetroxide at room temperature for 60 minutes. Samples were also prepared without osmium tetroxide to verify that electron dense regions on cell surfaces were due to uranium and not the osmium stain. Following buffer washes, the bacteria were dehydrated, infiltrated, and embedded in Spurr's resin (Ted Pella Inc., Redding CA). Ultrathin sections of uranium-associated bacteria were cut at a thickness of 100 nm with a Leica Ultracut S mictrome. Examination of the ultrathin sections was carried out on a Hitachi HD2000 transmission electron microscope (TEM, Hitachi High Technologies America, Inc., Pleasanton, CA) with an accelerating voltage of 200 kV and equipped with an Oxford INCA Energy 200 energy-dispersive X-ray (EDX) spectrometer.

Analysis of *Rahnella* sp. Y9602 biomineralized uranium was also conducted with a Hitachi S3500N variable-pressure scanning electron microscope (VP-SEM) equipped

with an Oxford INCA Energy 200 energy-dispersive X-ray spectrometer. An accelerating voltage of 20 kV and a chamber pressure of 20 Pa were used for all analyses. Upon completion of uranium biomineralization incubations, 300 µl of the uranium-associated cell pellet was placed on a glass fiber filter and visualized. The uranium-associated cell pellets were not fixed or sputter-coated with metal stains for visualization.

4.3 Results

4.3.1 Nitrate Respiration

The nitrate respiration and denitrification assays (Figure 4.1a) showed that, after 24 h of inoculation, *Rahnella* sp. Y9602 was capable of nitrate respiration but unable to denitrify when compared to *P. aeruginosa*. Anaerobic batch reactor incubations confirmed that *Rahnella* sp. Y9602 respired on nitrate as evidenced by the increase of nitrite concentrations in live cell incubations. Nitrite accumulated up to 3.5 mM during growth in U-free media and to 2.5 mM in media containing U (Figure 4.1b). NH_4^+ was not detected in anaerobic incubations (Figure 4.1b) indicating that *Rahnella* sp. Y9602 is not able to respire using the dissimilatory nitrate reduction to ammonium (DNRA) pathway.

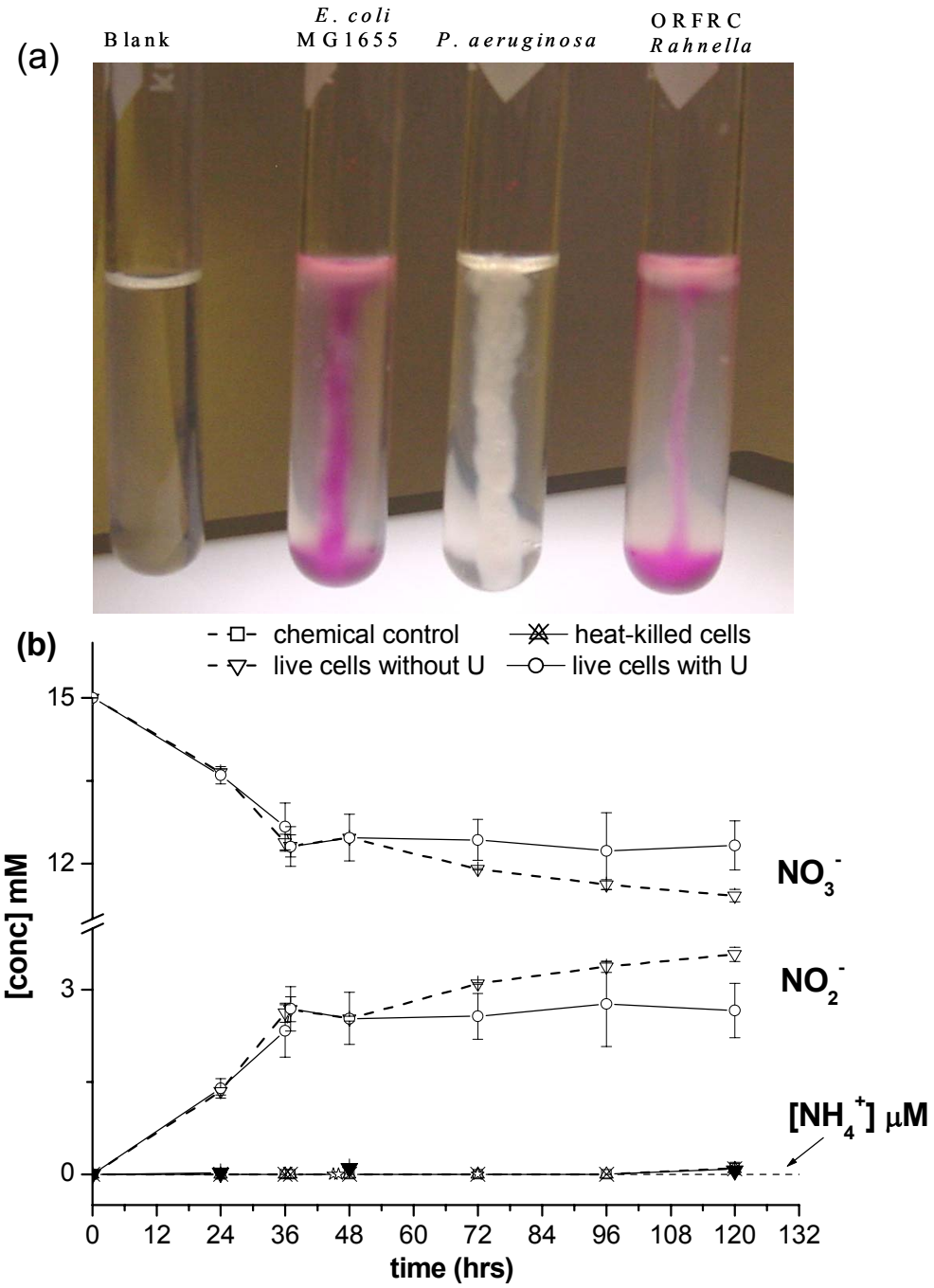

Figure 4.1 (a) Nitrate reduction and denitrification assays used to test the ability of *Rahnella* sp. to respire on nitrate and denitrify. Pink color indicates the accumulation of nitrite 24 h after inoculation. *Rahnella* sp. tested positive for nitrate respiration, but negative for denitrification when compared to *E. coli* (positive control for nitrate respiration and negative control for denitrification) and *P. aeruginosa* (positive control for denitrification). (b) Nitrate, nitrite, and ammonium concentrations in anaerobic (open symbols) and aerobic incubations (closed symbols) of *Rahnella* sp. in synthetic groundwater at pH 5.5 with 10 mM G3P and 200 μM UO_2^{2+} (standard deviation represents variations of triplicate incubations).

4.3.2 Anaerobic metabolism in the presence and absence of U(VI)

Colony forming units (CFUs) were determined at each time interval to monitor culturable cells throughout the incubations (Figure 4.2a). In the absence of U, *Rahnella* sp. Y9602 cell densities increased 6-fold within the first 24 h of incubation under anoxic conditions. After 24 h, however, anaerobic growth ceased and CFUs gradually decreased to approximately 10^6 cells mL^{-1} after 120 h incubation. Anaerobic CFUs were 250 times lower than aerobic CFUs after 120 h. In the presence of U, both aerobic and anaerobic CFUs demonstrated the same dramatic decrease in culturable cells to approximately 10^3 cells mL^{-1} within 12 h after the addition of uranium. While CFUs from aerobic incubations rebounded once uranium was removed from solution, CFUs decreased to 10^1 cells mL^{-1} after 120 h in anaerobic conditions.

Approximately 80% total uranium precipitated anaerobically within one hour of uranyl addition in live cell incubations, and up to 95% precipitated after 120 h. Anaerobic precipitation of U was 2.4 times greater within one hour of U addition compared to aerobic precipitation. After 48 h, however, 95% total U was removed from both aerobic and anaerobic incubations. U precipitation was negligible in heat-killed cell and abiotic controls (Figure 4.2b).

Phosphate liberation by *Rahnella* sp. Y9602 was consistently greater aerobically than anaerobically at all time points (Figure 4.2c). Aerobically-grown cells produced approximately 1.3 times greater phosphate than cells grown under anaerobic conditions after 24 h. This difference steadily increased over the course of the incubations until concentrations reached approximately 2.4 times greater levels in aerobic conditions than anaerobic conditions by the end of the experiment. Phosphate concentrations increased steadily in live cell incubations throughout the anaerobic experiment to a final

concentration of 1.7 mM in the absence of uranium and 1 mM in the presence of uranium. Both aerobic and anaerobic incubations containing U consistently produced less phosphate than samples without U. Abiotic hydrolysis of G3P did not occur as evidenced by the absence of orthophosphate in chemical and heat-killed cell controls (Figure 4.2c).

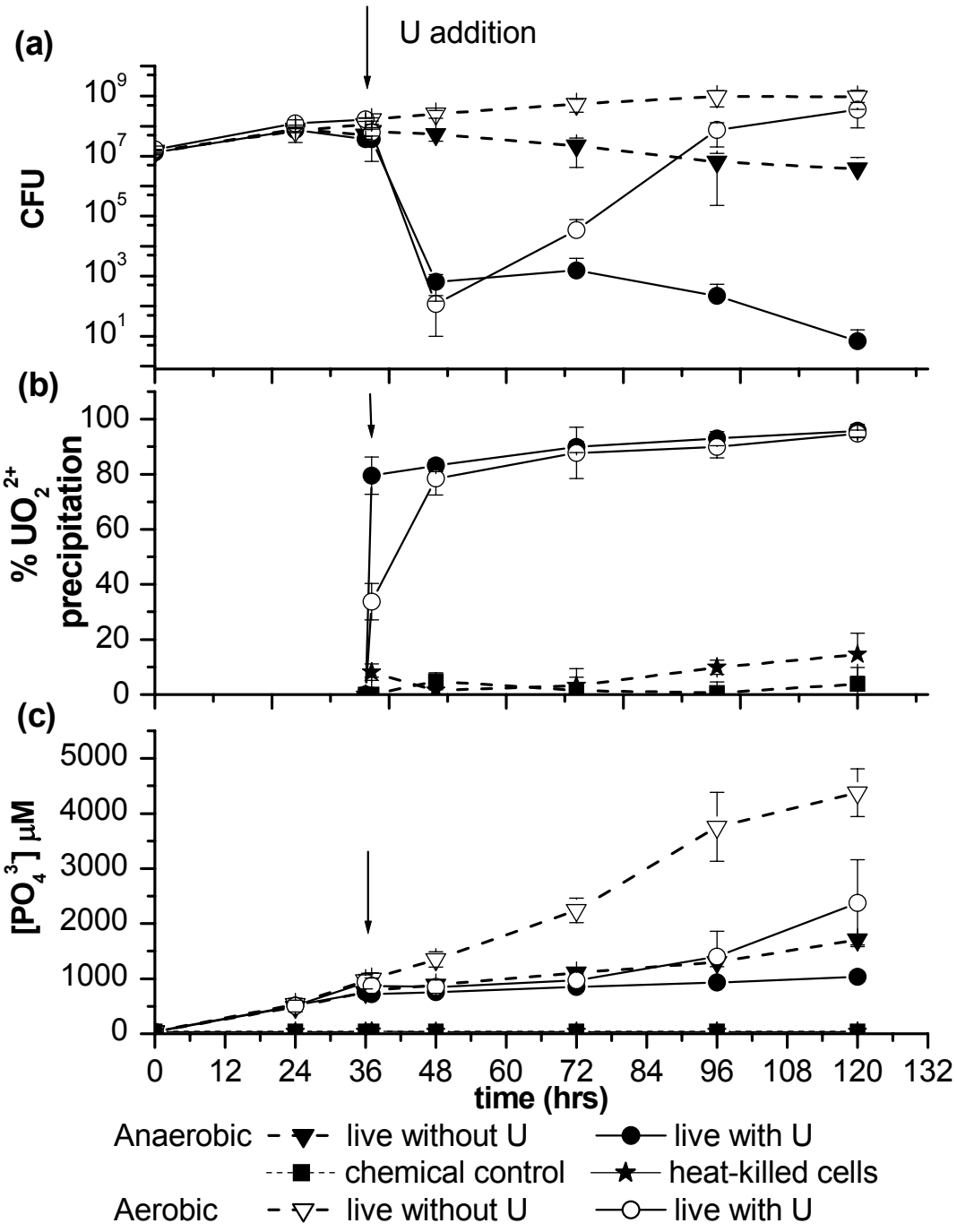

Figure 4.2 (a) Average colony forming units (CFU), (b) percent U(VI) precipitation, and (c) phosphate concentrations produced by *Rahnella* sp. incubated in synthetic groundwater under anaerobic conditions (dark symbols) and aerobic conditions (open symbols) at pH 5.5 with 200 μM UO_2^{2+} and 10 mM G3P (standard deviation represents variations of triplicate incubations). Aerobic data from Beazley et al. 2007.

4.3.3 Solid-Phase Analysis

Synchrotron-based XRD results of the biotic uranyl phosphate precipitate formed anaerobically were compared to abiotic and biotic uranyl phosphate precipitates formed aerobically (Figure 4.3). XRD indicated the presence of chernikovite [$H_2(UO_2)_2(PO_4)_2$] in all three samples when compared to published data (Ross, 1955; Van Haverbeke et al., 1996) and the International Centre for Diffraction Data (ICDD) file 08-0296 (Figure 4.3). Chernikovite has a tetragonal crystal system with axial length designations $a = b \neq c$ (where a, b, and c correspond to unit cell vectors in the x, y, and z planes, respectively) (Cullity, 1978). Calculated unit cell parameters for the three precipitates are listed in Table 4.1 along with estimated particle sizes for the major reflections as determined using the Scherrer formula (Cullity, 1978). Calculated unit cell dimensions were: a = 7.01 Å, b = 7.01 Å, and c = 8.98 Å for the abiotic and aerobic biotic samples and a = 7.01 Å, b = 7.01 Å, and c = 9.04 Å for the anaerobic biotic sample. These calculations were in good agreement with Ross (1955) providing further evidence of the presence of chernikovite in the samples. The broad and low intensity peaks of the biotic samples (Figure 4.3) indicated smaller particle sizes compared to the abiotic sample. Particle sizes along the x and y planes in the biotic samples were larger than those in the z plane (demonstrated by sharper peaks in the 110 and 200 reflections), suggesting a "sheet-like" precipitate was formed during the incubations.

Table 4.1 Calculated Unit Cell Parameters for U-P precipitates

abiotic: a = 7.01 Å, b = 7.01 Å, c = 8.98 Å
aerobic biotic: a = 7.01 Å, b= 7.01 Å, c = 8.98 Å
anaerobic biotic: a = 7.01 Å, b = 7.01 Å, c = 9.04 Å

	abiotic	**aerobic biotic**	**anaerobic biotic**
hkl	**t (Å)**	**t (Å)**	**t (Å)**
001	409	90.2	72.9
110	774	621	297

a, b, and c correspond to unit cell vectors in the x, y, and z planes, respectively
t = particle size in Å as calculated using the Scherrer formula
hkl represent plane designation by Miller indices

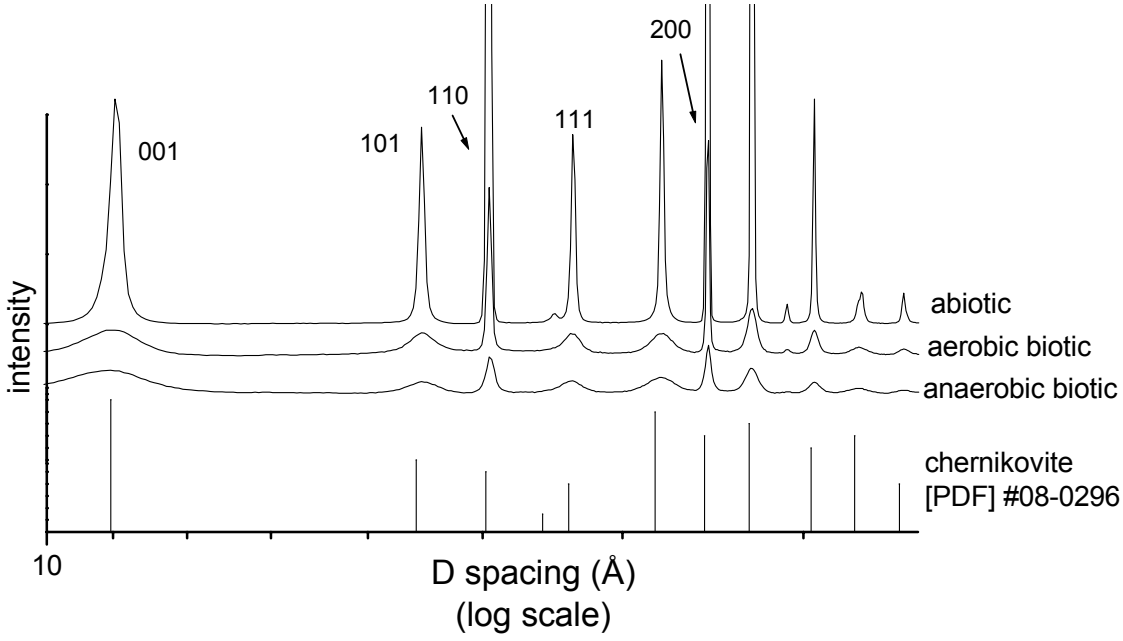

Figure 4.3 X-ray diffraction patterns of U(VI)-phosphate precipitates obtained during anaerobic and aerobic incubations with *Rahnella* sp. in synthetic groundwater at pH 5.5 in the presence of 200 μM UO_2^{2+} and 10 mM G3P compared to an abiotic uranyl phosphate precipitate and the ICDD file 08-0296.

U L_{III}-edge XANES analysis of both aerobic and anaerobic biotic samples displayed the characteristic shoulder of U(VI) oxidation state between 17,180 and 17,200 eV and were similar to an abiotic uranyl phosphate control precipitate (Figure 4.4a). EXAFS fitted parameters (Table 4.2) showed general agreement among the three precipitates with regard to O_{eq} R distances (~ 2.26 Å), P coordination numbers (~ 1.4), U-P distances (~ 3.60 Å), and P-O distances (~ 1.62 Å) (Figure 4.4b). The *k*-space fitted region from 8.5 to 10.5 $Å^{-1}$ was indicative of the autunite/meta-autunite mineral group (Figure 4.4c).

The aerobic biotic precipitate formed in the presence of *Rahnella* sp. Y9602 appeared representative of an amorphous mineral, characterized by ~ 1μm void spaces that may have resulted from the presence/absence of rod-shaped *Rahnella* sp. Y9602 cells or areas on the mineral surface that did not fully crystallize (Figure 4.5a). TEM images displaying a 2-dimensional view of the progress of crystallization as a function of time along with EDX elemental analyses of the crystals (Figure 4.5b) revealed that U mainly coated the cell surfaces within one hour after addition of U (37 h). TEM samples prepared with and without osmium tetroxide at time 37 h both show electron dense material containing uranium, suggesting that osmium did not interfere with the cell images. Over time, however, U desorbed from the cell surface and precipitated outside the cells. Simultaneously, the electron density of the precipitate increased with time.

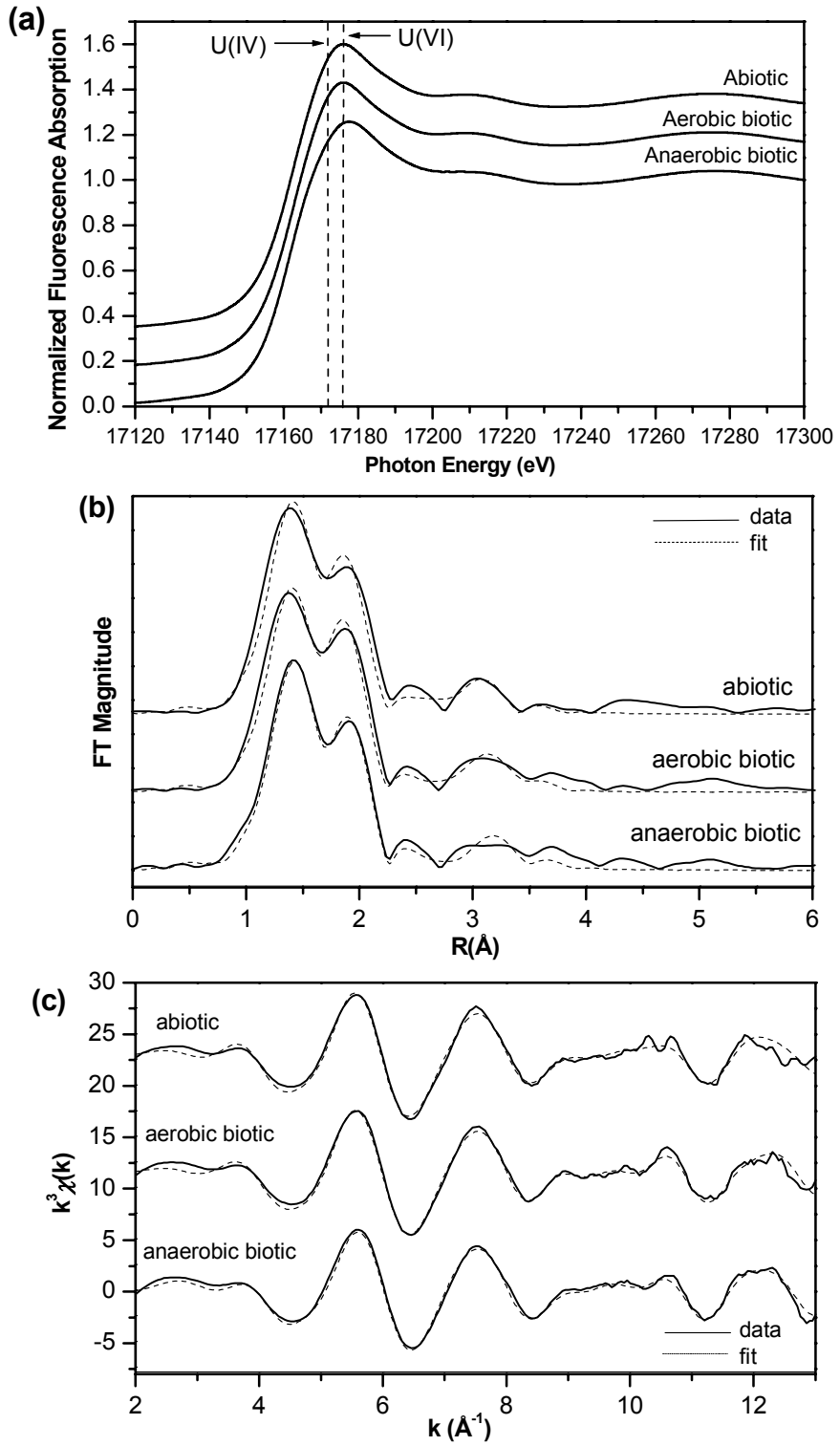

Figure 4.4 Uranium (a) XANES, (b) R-space, and (c) *k*-space diagrams of the L_{III}-edge EXAFS from precipitates obtained during anaerobic and aerobic incubations with *Rahnella* sp. in synthetic groundwater at pH 5.5 in the presence of 200 μM UO_2^{2+} and 10 mM G3P compared to an abiotic uranyl phosphate precipitate.

Table 4.2 Parameters derived from fitting U L_{III}-edge EXAFS for U-P precipitates

Sample		O_{ax}	O_{eq}	P	POU MS*	OPOU MS*	PO dist†	Rfactor	ΔE_0
abiotic	N	2	3.2 (0.7)	1.3 (0.8)	2.6	1.3	1.57 (0.12)	0.0189	-0.99 (2.2)
	R(Å)	1.78 (0.004)	2.27 (0.01)	3.57 (0.05)	3.71	3.84			
	σ(Å^2)	0.0043 (0.0005)	0.005 (0.001)	0.005	0.005	0.005			
aerobic biotic	N	2	3.2 (0.6)	1.6 (0.8)	3.2	1.6	1.65 (0.7)	0.0144	-1.6 (1.9)
	R(Å)	1.77 (0.008)	2.26 (0.01)	3.61 (0.02)	3.76	3.91			
	σ(Å^2)	0.0047 (0.0005)	0.004 (0.001)	0.005	0.005	0.005			
anaerobic biotic	N	2	2.3 (0.4)	1.2 (0.7)	2.4	1.2	1.65 (0.08)	0.0116	3.2 (1.7)
	R(Å)	1.79 (0.007)	2.28 (0.009)	3.62 (0.02)	3.78	3.94			
	σ(Å^2)	0.0043 (0.0004)	0.003 (0.001)	0.005	0.005	0.005			

Errors are given in parentheses (no error means the value was fixed, or calculated from other parameters)

* MS denotes multiple scattering paths

† PO dist is the distance between the P-O in phosphate coordination (used for the MS paths)

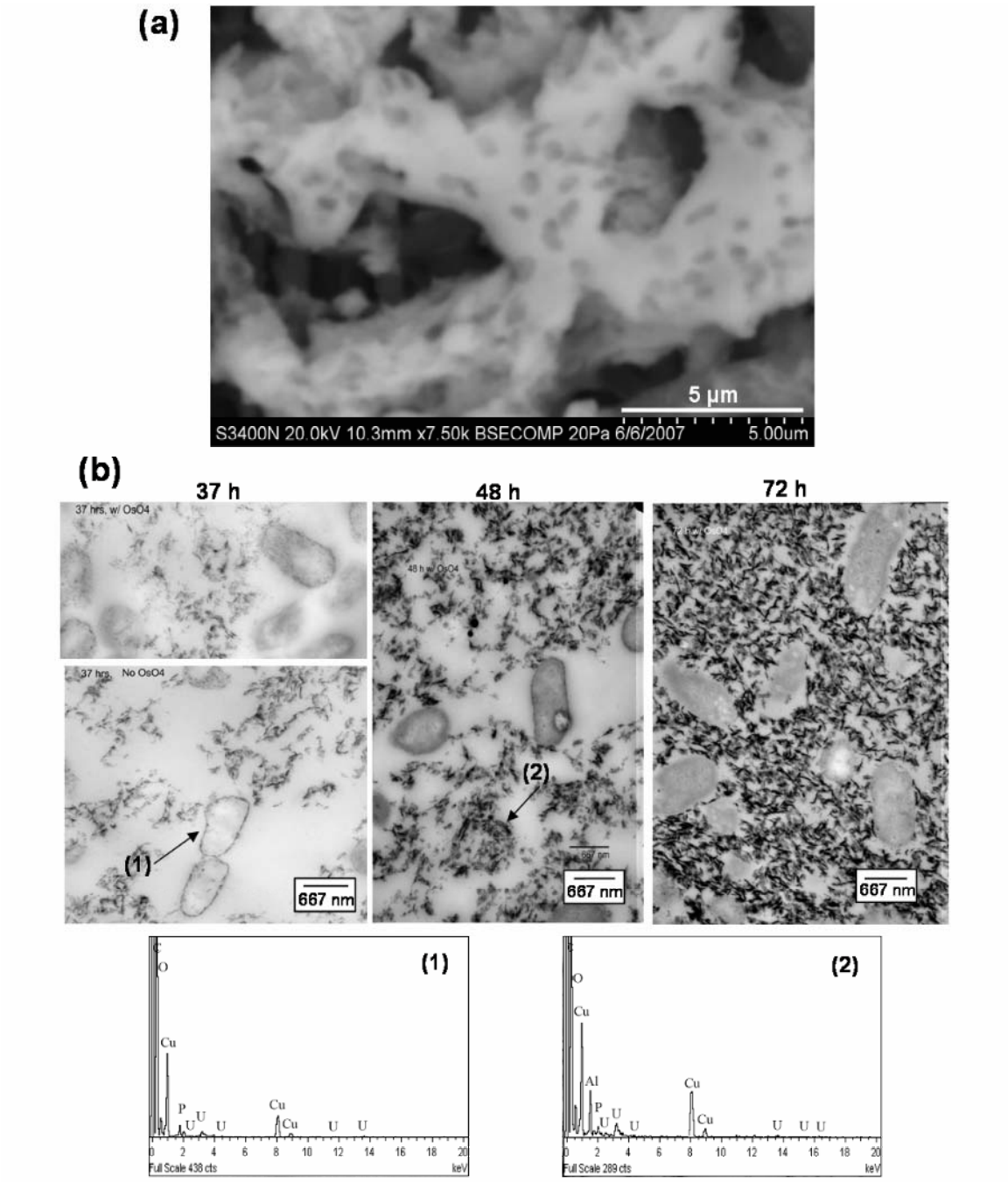

Figure 4.5 Electron microscopic images of aerobic biotic precipitate. (a) VP-SEM image of amorphous U(VI)-phosphate precipitate formed in aerobic biotic incubation after 120 hrs. (b) TEM micrographs of samples collected as a function of time during the incubations showing the progression of U(VI)-phosphate crystallization. Note presence of U surrounding cell membranes at 37 h and absence at 72 h as crystallization proceeds. Time 37 h TEM images treated with (top) and without (bottom) OsO_4 are included to show that electron dense regions on cell surfaces were due to uranium and not the osmium stain. Arrows (1) and (2) indicate the locations of the corresponding EDX analyses.

4.4 Discussion

Previous work has shown that successful remediation strategies of toxic radionuclides such as uranium need to account for the geochemical conditions of each particular subsurface environment (Wu et al., 2006a; Wu et al., 2006b). In areas of the ORFRC, where subsurface soils are characterized by high concentrations of uranium and nitrate and low pH, the precipitation of sparingly soluble uranyl phosphate minerals may be an alternative approach to biotic reduction which occurs preferably at circumneutral pH (Venkateswaran et al., 1999) and low nitrate concentrations (Edwards et al., 2007). Indeed, thermodynamics predicts a wide pH range (4 to 8) for the favorable precipitation of uranyl phosphate minerals (Langmuir, 1978; Sandino and Bruno, 1992). Dissolved inorganic phosphate tends to be limiting in most soil systems due to its incorporation in minerals (Langmuir, 1997) or its complexation by organic compounds (Turner et al., 2002). In such conditions, many microorganisms obtain this essential nutrient through the enzymatic hydrolysis of phosphate from organophosphate substrates (Macaskie et al., 1992). *Rahnella* sp. Y9602, isolated from contaminated areas of the ORFRC, is able to enzymatically hydrolyze up to ~ 7.5 pmol P $cell^{-1}$ from G3P and precipitate 95% of U(VI) in aerobic conditions (Beazley et al., 2007; Martinez et al., 2007). Even though much of the contamination at the ORFRC is within the oxic vadose zone (Stubbs et al., 2006), anaerobic conditions may develop when biological activity is stimulated. Therefore, it would be remedially advantageous if indigenous facultative microorganisms could provide phosphate for uranium precipitation in both aerobic and anaerobic conditions, at low pH, and in the presence of high nitrate concentrations.

In the present study, anaerobic incubations were conducted with the gram-negative facultative anaerobe *Rahnella* sp. Y9602, in the presence of 10 mM G3P and 200 μM UO_2^{2+} at pH 5.5. Our objectives were to determine if (1) *Rahnella* sp. Y9602 could exhibit phosphatase activity in anaerobic conditions, (2) *Rahnella* sp. Y9602 could hydrolyze enough G3P to precipitate uranyl phosphate anaerobically, and (3) the mineral formed was the same as that formed under aerobic conditions. *Rahnella* sp. Y9602 demonstrates robust growth under oxic conditions as evidenced by high concentrations of phosphate and increasing CFUs even in the presence of U and nitrate (Figure 4.2a and c). In the absence of oxygen *Rahnella* sp. Y9602 is able to use nitrate as a terminal electron acceptor for respiration as demonstrated by robust growth following repeated culture passages into rich anoxic media containing 15 mM nitrate (data not shown). Interestingly, *Rahnella* sp. Y9602 is incapable of denitrifying or reducing nitrate to ammonium (Figure 4.1). The inability of *Rahnella* sp. Y9602 to complete denitrification is in agreement with the characterized *Rahnella aquatilis* type strain identified by (Krieg and Holt, 1984). Nitrate reduction rates by *Rahnella* sp. Y9602 followed an apparent first order with respect to nitrate and pseudo-first order rate constants of 2.2×10^{-5} min^{-1} and 3.3×10^{-5} min^{-1} were derived from incubations with and without U, respectively. These rate constants are small compared to the rate constant of 0.18 min^{-1} derived from experiments with *Pseudomonas fluorescens* (Betlach and Tiedje, 1981).

Nitrite toxicity is known to occur among microorganisms and induces a variety of inhibitory effects on bacterial growth, including an increase in the proton permeability of cyctoplasmic membranes in *P. fluorescens* (Sijbesma et al., 1996), inhibition of electron carriers in the respiratory system (Rake and Eagon, 1980), and even inhibition of

denitrification in denitrifying organisms (Bollag and Henninger, 1978; Meijer et al., 1979). Bollag and Henninger (1978) studied the effects of nitrite toxicity under aerobic and anaerobic conditions on a variety of soil bacteria including isolates of a gram-negative, facultatively-anaerobic *Pseudomonas*. They found that tolerance to nitrite (up to 9 mM NO_2^-) was increased in the presence of oxygen but that cell growth was drastically reduced under anaerobic conditions in the presence of 3 mM NO_2^-. In the present study, live cell counts of *Rahnella* sp. Y9602 decrease slightly after 36 h, when nitrite concentrations reach approximately 2.6 mM, demonstrating the possible toxic effects of nitrite. In the presence of U and under anaerobic conditions, however, *Rahnella* sp. Y9602 is unable to overcome the combined toxic effects of both nitrite and U, and growth is completely suppressed (Figure 4.2a). The slow growth of *Rahnella* sp. Y9602 due to the combined toxicity of nitrite and U may have resulted in low nitrate reduction rates. It is important to note that these incubations were conducted in batch reactors where nitrite was able to accumulate in the medium. Bacteria able to respire anaerobically on nitrogen oxide compounds are diverse (Drysdale et al., 1999; Knowles, 1982). The majority of these prokaryotes possess the reductases needed to completely reduce NO_3^- to N_2 or NH_4^+. Some, however, lack NO_3^- reductases and are only able to reduce NO_2^-. Others lack N_2O reductases and produce N_2O as the final product. Finally, some carry the N_2O reductase genes, but cannot reduce NO_3^- or NO_2^- (Bothe et al., 2000; Knowles, 1982). At low pH, NO_2^- is also reduced chemically by Fe(II) (Knowles, 1982) and oxidized by $MnO_{2(s)}$ (Luther and Popp, 2002). Therefore, in natural environments, consortia of microorganisms, groundwater flow, and other geochemical species may

scavenge or distribute nitrite within the system to prevent accumulation of such toxic levels.

Remarkably, *Rahnella* sp. Y9602 hydrolyzes sufficient phosphate, even in the presence of nitrite, to precipitate U(VI) (Figure 4.2b) and the difference in U precipitation at steady state is not significant between aerobic and anaerobic incubations. Anaerobically, however, 80% U precipitates within one hour after addition while only 34% of U(VI) is removed in the aerobic incubations within the same time period. These findings are surprising as cell densities in aerobic conditions are higher and should lead to faster U precipitation rates than in anaerobic conditions. It is possible that higher cell densities in aerobic incubations may provide more cell lysis material which could possibly complex U and prevent initial precipitation. Twelve hours after U addition, however, the concentration of U precipitated is similar in both incubations, suggesting that these initial differences are not significant.

XRD, XANES, and EXAFS analyses (Figures 4.3 and 4.4) of the precipitates formed in the incubations identify the same mineral both aerobically and anaerobically. XANES analysis indicates that all precipitates are of the U(VI) valence state demonstrating that *Rahnella* sp. Y9602 does not reduce U in anaerobic conditions. The average U-P distance of 3.6 Å suggests a monodentate bond formation between U and P (Table 4.2). The *k*-space region from 8.5 to 10.5 $Å^{-1}$ (Figure 4.4c) is characteristic of autunite-type minerals; however due to their similarities they are difficult to distinguish by EXAFS alone (Catalano and Brown Jr., 2004; Fuller et al., 2002). XRD patterns identify the minerals formed as chernikovite [$H_2(UO_2)_2(PO_4)_2$] (Figure 4.3) and the broader peaks of lower intensity show that the biotic precipitates are more amorphous

compared to abiotically-produced uranyl phosphate minerals. VP-SEM also indicates that the chernikovite formed in biotic incubations is more amorphous (Figure 4.5a) than the tabular crystals formed during synthetic production of chernikovite (Van Haverbeke et al., 1996). The incorporation of organic compounds within biomineralized structures has been observed to affect crystallinity (De Yoreo and Vekilov, 2003), suggesting that organic material released by *Rahnella* sp. Y9602 during cell growth and lysis may affect the growth and crystallinity of chernikovite. Particle size estimates suggest all of the precipitates are "sheet-like" minerals with more unit cells stacked in the x and y plane than the z plane.

Interestingly, TEM images show that U coats the cell immediately upon addition of U to the incubations but, then separates from the cell surface over time as uranyl phosphate precipitates in the bulk solution (Figure 4.5b). This observation may explain why CFU counts initially decrease in aerobic incubations, but then rebound over time as U precipitates (Figure 4.2a). EDX elemental analyses of the uranyl coating on the cell surface show the presence of U and P; however, these analyses cannot identify the chemical composition of U. U could be precipitated as uranyl phosphate or adsorbed on the cell surface and the presence of P in the coating could be due to membrane phospholipids or free phosphate as a result of phosphatase activity. EXAFS measurements indicate that at low pH uranyl binds to phosphoryl functional groups on the cell wall of gram-positive *Bacillus subtilis* as an inner-sphere complex (Kelly et al., 2002). Gram-negative bacteria carry a thinner peptidoglycan layer than gram-positive bacteria, yet the concentration of cell wall phosphoryl groups in *Rahnella* sp. Y9602 may still be high enough to adsorb U initially. As phosphate accumulates in the surrounding

media, however, uranyl ions are probably desorbed from the cell surface by stronger ionic attractions with the free negatively-charged orthophosphate. In addition, the same mineral is formed whether *Rahnella* sp. Y9602 is incubated anaerobically or aerobically. These findings suggest that the precipitation of uranyl phosphate is a pure chemical process governed by pH and the concentration of phosphate generated by the microbial hydrolysis of organophosphate by phosphatase enzymes. Thus, the cells may provide a nucleation surface that activates the precipitation of uranyl phosphate and provides for the shape of the subsequent "sheet-like" mineral structure.

The results of this study demonstrate the potential for the bioremediation of uranium catalyzed by the activity of phosphatase enzymes from a facultative microorganism in both aerobic and anaerobic conditions. The *Rahnella* strain used in this study was isolated from ORFRC subsurface soils (Martinez et al., 2006). Sequences related to the *Rahnella* genus have also been identified in a groundwater 16S clone library from Area 3 of the ORFRC (Fields et al., 2005). Together, these findings provide evidence for the importance of Rahnella spp. and other microorganisms that share similar phosphate-liberating physiologies. Uranyl phosphate minerals are sparingly soluble in a wide range of pH (Ohnuki et al., 2004; Wellman et al., 2007; Zheng et al., 2006) and remain stable for long periods of time (Jerden Jr. and Sinha, 2003). In contrast, bioreduction of U(VI) has been shown to occur optimally above pH 7, and its product, uraninite, is easily oxidized in the presence of oxygen and nitrate-reducing conditions (Moon et al., 2007; Senko et al., 2005b; Tokunaga et al., 2008; Wan et al., 2005; Wu et al., 2007). In contaminated areas, such as the ORFRC, where high concentrations of nitrate and low pH may limit or hinder U bioreduction, the biomineralization of U(VI)

phosphate minerals may be a more attractive approach for in situ remediation. Future experiments should examine the competition between bioreduction and non-reductive biomineralization of U in natural systems and the effect of the presence of carbonates on the stability of the minerals formed.

4.5 Conclusions

The results of this investigation illustrate the potential for controlling the solubility of uranium through phosphatase activity by subsurface soil microorganisms in contaminated waste sites in both aerobic and anaerobic conditions. The facultative gram-negative anaerobe, *Rahnella* sp. Y9602, isolated from the ORFRC subsurface demonstrates strong phosphatase activity in both aerobic and anaerobic conditions and in the presence of high nitrate and low pH. The phosphate hydrolyzed from an organophosphate substrate is sufficient to precipitate 95% total U(VI) as the uranyl phosphate mineral chernikovite very rapidly. The precipitation of chernikovite appears to be a pure chemical process, whose kinetics is governed by pH, the concentration of phosphate generated by the microbial hydrolysis of organophosphate by phosphatase enzymes, and probably the adsorption of U(VI) to the cell surfaces. Uranyl phosphates are stable in a wide range of pH for long periods of time and may be preferable to the more reactive and easily oxidized uraninite produced during U(VI) bioreduction.

4.6 Acknowledgements

This research was supported by the Office of Science (BER), U. S. Department of Energy Grant No. DE-FG02-04ER63906. Portions of this research were carried out at the Stanford Synchrotron Radiation Lightsource, a national user facility operated by Stanford

University on behalf of the U.S. Department of Energy, Office of Basic Energy Sciences. The SSRL Structural Molecular Biology Program is supported by the Department of Energy, Office of Biological and Environmental Research, and by the National Institutes of Health, National Center for Research Resources, Biomedical Technology Program. We thank Hong Yi at the Emory School of Medicine Electron Microscopy Core for transmission electron microscopy sample preparation and imaging and Dr. Joan S. Hudson at the Clemson University Electron Microscope Facility for variable-pressure scanning electron microscopy imaging, transmission electron microscopy imaging, and EDX analyses. We also thank the two anonymous reviewers for their valuable comments to improve the manuscript.

CHAPTER 5

THE EFFECT OF pH ON THE REMOVAL OF URANIUM THROUGH THE ACTIVITY OF NATURAL MICROBIAL PHOSPHATASES IN SOILS FROM A URANIUM-CONTAMINATED WASTE SITE

5.1 Abstract

The biomineralization of U(VI) as a result of microbial phosphatase activity has revealed a promising new bioremediation approach to immobilize uranium as uranium phosphate minerals in both aerobic and anaerobic conditions. In this study, two uranium contaminated soils from the Department of Energy Oak Ridge Field Research Center (ORFRC) exposed to low and circumneutral pH groundwater were amended with an organophosphate substrate, as sole carbon and phosphorus source, in small flow-through reactors to determine whether natural phosphatase activity of indigenous soil bacteria was able to promote the immobilization of uranium(VI) phosphate minerals. High concentrations of phosphate were detected in the effluents of flow-through reactors within one day of organophosphate amendments at both low and high pH, compared to negligible phosphate production in control reactors amended with U(VI) only, suggesting that phosphatase-liberating microorganisms were readily stimulated by the

organophosphate substrate. Steady-state concentrations of phosphate were reached within days after addition, suggesting that non-specific acid phosphatase activity was expressed constitutively. A sequential solid-phase extraction scheme, EXAFS measurements, and reactive transport modeling were combined to demonstrate that at both low and high pH, U(VI) was primarily precipitated as uranyl phosphate minerals and partially adsorbed to iron oxides. Precipitated U(VI) was distinguished from adsorbed U(VI) by extraction with both AcOH and hydroxylamine compared to release of adsorbed uranium solely by AcOH in U control reactors. Net phosphate production rates and respective organophosphate consumption rates were highest in low pH soils compared to circumneutral soils providing 3 times more phosphate for U-P precipitation. EXAFS measurements reveal that U(VI) was directly adsorbed to iron oxides at high pH, while U(VI) formed ternary complexes with phosphate pre-adsorbed to iron oxides at low pH. The results of this study indicate that the biomineralization of U(VI) phosphate as a result of natural phosphatase activity in contaminated soils is an effective strategy for the remediation of uranium. Biomineralization of U(VI) phosphate was observed over a wide pH range in the presence of high uranium and nitrate concentrations and may be a complementary remediation approach to bioreduction which requires high pH, low nitrate, and reducing conditions.

5.2 Introduction

The fate and mobility of U in soils and groundwater are determined primarily by its oxidation state, adsorption/desorption reactions at the mineral-water interface, precipitation/dissolution, and complexation reactions (Langmuir, 1997). All of these factors are influenced by pH, redox conditions, biological activity, soil matrix composition, and groundwater constituents. The combination of these parameters contributes to the complexity of natural systems and makes remediation of contaminated areas difficult. U contamination is a concern at Department of Energy (DOE) sites across the United States, but it is a primary environmental problem at the Oak Ridge National Laboratory Reservation at Oak Ridge, Tennessee. Soils and groundwater at the Oak Ridge Field Research Center (ORFRC) are heavily contaminated by chemical wastes, including high concentrations of depleted U (up to 252 μM) and nitrate (up to 645 mM) as a result of more than 30 years of U enrichment at the facility (Brooks, 2001). The cleanup of U and other toxic heavy metals and radionuclides at the ORFRC is a major environmental challenge, and the development of remediation strategies has been ongoing for the past 15 years (NABIR, 2003).

Subsurface conditions at the ORFRC are primarily oxidizing, and U(VI) is the dominant oxidation state in most areas (Stubbs et al., 2006). ORFRC soils are mainly fine textured silt and clay derived from limestone and shale parent rock, containing organic matter and iron and aluminum oxide mineral coatings, that are exposed to groundwater with pHs ranging from 3.5 to circumneutral depending on location and depth in the subsurface (Roh et al., 2000). Characterization of ORFRC soils by electron

microbeam identifies the major U-bearing solid-phases as Fe oxyhydroxides, mixed Mn-Fe oxides, and uranium phosphates (Stubbs et al., 2006).

In oxic conditions, U exists as the highly soluble uranyl ion, UO_2^{2+}. Below circumneutral pH, uranyl is positively charged and forms the soluble species UO_2^{2+} and UO_2OH^+. Above pH 7, uranyl carbonate complexes dominate as $UO_2(CO_2)_3^{4-}$ and $UO_2(CO_3)_2^{2-}$ (Langmuir, 1997). The formation of these strong, highly soluble uranyl carbonate complexes increases U(VI) mobility by preventing the adsorption of U(VI) on mineral surfaces (Fox et al., 2006; Langmuir, 1978) and promoting U(IV) and U(VI) mineral dissolution (De Pablo et al., 1999; Sowder et al., 2001).

The adsorption of U(VI) to Fe oxides is favorable between pH 4 and 8 (low adsorption edge at pH 4 to 5 and maximum adsorption at pH 6 to 7) (Hsi and Langmuir, 1985; Langmuir, 1997) and can be enhanced at lower pH by the sorption of negatively-charged functional groups, such as carboxylate and hydroxyl functional groups (two of the main components of NOM) as well as phosphoryl ligands (Cheng et al., 2004; Lenhart and Honeyman, 1999; Payne et al., 1996; Warren and Haack, 2001), to the Fe oxide surface. Phosphoryl groups carry a negative charge between pH 2 and 12 (Benjamin, 2002), carboxylate groups deprotonate between pH 3 and 5 (Perdue, 1985), and hydroxyls deprotonate above pH 7 (Benjamin, 2002). Therefore, in the typical range of pHs of natural systems (5 to 7), phosphate and NOM are negatively charged and available for adsorption to oxide surfaces. The sorption of negatively-charged functional groups promotes the adsorption of positively-charged metal species, such as uranyl. Hence, the addition of phosphate to ferrihydrite ((Payne et al., 1996), goethite-coated sand (Cheng et al., 2004; Cheng et al., 2006), and alumina (Zhijun et al., 2006) greatly

increases U(VI) adsorption due to the formation of U(VI) phosphate ternary complexes that shift the low U(VI) adsorption edge to pH 3 to 4. Adsorption of U(VI) is also increased on ferrihydrite in the presence humic acid (HA) (up to pH 7) by shifting the low adsorption edge to low pHs (Payne et al., 1996).

U(VI) is immobilized by reduction to U(IV) either chemically by Fe(II) adsorbed onto mineral surfaces (Boyanov et al., 2007; Jeon et al., 2005; Liger et al., 1999; O'Loughlin et al., 2003) or biologically by dissimilatory metal-reducing bacteria (DMRB) and sulfate-reducing bacteria (SRB) (Fredrickson et al., 2000; Lovley and Phillips, 1992; Lovley et al., 1991; North et al., 2004; Wade Jr. and DiChristina, 2000) to form the insoluble mineral uraninite. Unfortunately, uraninite is rapidly oxidized to the more mobile and reactive uranyl ion (UO_2^{2+}) in oxic conditions (Langmuir, 1997; Murphy and Shock, 1999), and more slowly oxidized under nitrate-reducing conditions by nitrite or reactive Fe(III) oxyhydroxides formed by chemical oxidation of Fe(II) by nitrite (Senko et al., 2002; Senko et al., 2005a; Senko et al., 2005b). Previous remediation studies conducted at the ORFRC have demonstrated the potential for in situ bioremediation of U by reduction through the stimulation of iron- and sulfate-reducing bacteria (Wu et al., 2006a; Wu et al., 2006b; Wu et al., 2007). However, these studies had to overcome numerous obstacles, including low pH and high nitrate concentrations that may limit or hinder U(VI) reduction (Finneran et al., 2002; Istok et al., 2004; Senko et al., 2002). Before U bioreduction could be stimulated during the pilot test study conducted at the ORFRC, groundwater in the treatment zone had to be extracted and treated above ground to remove aqueous aluminum (to prevent Al-hydroxide formation at pH > 4.5), calcium (to prevent stable aqueous Ca-U-CO_3 complex formation), and nitrate

(to remove a more favorable terminal electron acceptor). The groundwater pH was then adjusted from pH 3.5 to > 6 to promote microbial growth of the iron- and sulfate-reducing bacteria. From these studies, it is clear that the cleanup of U at this site is a major challenge, and it is important to consider all the biogeochemical processes unique to these soils when developing new remediation strategies

U(VI) forms highly insoluble minerals in a 1:1 stoichiometry with phosphate that are sparingly soluble in a wide range of pH (Ohnuki et al., 2004; Wellman et al., 2007; Zheng et al., 2006). These minerals comprise members of the autunite/meta-autunite group minerals, which include calcium autunite [$Ca(UO_2)_2(PO_4)_2$], chernikovite [$H_2(UO_2)_2(PO_4)_2$], saléeite [$Mg(UO_2)_2(PO_4)_2$], and ankoleite [$K_2(UO_2)_2(PO_4)_2$], and remain stable for long periods of time (Jerden Jr. and Sinha, 2003), suggesting that uranyl phosphates may provide a long-term sink for U at contaminated waste sites. Phosphate addition to contaminated soils, however, was accompanied by a 30% decrease in hydraulic conductivity of the subsurface as a result of phosphate precipitation at the injection site, suggesting that the precipitation of U-P minerals may be restricted to short distances from the injection points in a real subsurface (Wellman et al., 2006).

The biomineralization of U(VI) as a result of phosphatase activity is another biologically-induced mechanism that can reduce the solubility of U(VI). Microorganisms that display metal-resistant phenotypes can survive in the presence of up to 200 μM U(VI) when stimulated with a labile organophosphate source (Martinez et al., 2007) and U-P precipitation through the activity of microbial phosphatases may occur over a wide range of pH (Beazley et al., 2007). Aerobic soil slurries of ORFRC soil amended with organophosphate resulted in up to 91% of total organophosphate hydrolysis and

stimulated 1084 phyla demonstrating the high diversity of microorganisms in these soils (Martinez, 2008). Previous laboratory experiments with the bacterial species *Rahnella* sp. Y9602 isolated from the ORFRC have shown that > 97% of U(VI) is precipitated at pH 5.5 as the uranyl phosphate mineral chernikovite in both aerobic and anaerobic conditions when phosphatase activity is stimulated with an organophosphate compound (Beazley et al., 2007; Beazley et al., 2009; Martinez et al., 2007). These studies demonstrate the potential for in situ bioremediation of uranyl phosphate as a result of microbial phosphatase activity through the introduction of an organophosphate source. The overall objective of this work was to investigate the potential for in situ biomineralization of uranyl phosphate at conditions representative of the ORFRC, including low pH, high nitrate concentrations, and in aerobic conditions, through the injection of an organophosphate substrate to stimulate indigenous microbial phosphatase activity.

Flow-through reactors have proven useful to study biogeochemical transformations in sediments and soils (Barnett et al., 2000; Carey and Taillefert, 2005; Hansel et al., 2003; Roychoudhury, 2001; Roychoudhury et al., 2003; Roychoudhury et al., 1998) when actual in situ work may be difficult to conduct or experimental conditions have to be tested before in situ stimulation. In addition, geochemical parameters, such as pH, carbon, nutrients, and oxygen concentrations, can be adjusted easily to determine their effects on soil and sedimentary environments. Finally, flow-through reactors can also provide information about the transport of pore waters that can be used in mathematical models.

In this study, ORFRC soils from Area 3 were used with flow-through reactors and in situ conditions were simulated by pumping synthetic groundwater containing high concentrations of nitrate (10 and 15 mM) and U(VI) (200 μM) into the reactors. The objective of this work was to determine (1) if indigenous soil bacteria displayed phosphatase activity when supplied an organophosphate source, (2) if the pH of the soil affected natural phosphatase activity, (3) if the solubility of U(VI) was reduced through the precipitation of uranyl phosphates and (4) if soil permeability changed as a result of organophosphate amendments.

5.3 Materials and Methods

5.3.1 Reactors

The soil flow –through reactors consisted of cylinders 8 and 12 cm in length with an inside diameter of 3.8 cm (Figure 5.1 and Figure 5.2). Each end of the cylinder was capped with identical screw covers containing an O-ring, a plastic mesh screen, and a 0.45 μm filter (Micro Filtration Systems). The influent was pumped by a high-precision multi-channel pump (IsmaTec®) through Teflon tubing into an opening in the base of the cylinder and funneled through radial grooves designed to ensure uniform distribution of the solution in the cross-section of the reactor base. The solution then entered the soil through the mesh screen and filter of the reactor where it was forced upward through an identical filter, screen, and opening at the top of the reactor. The effluent exiting the reactor was pumped through a homemade PEEK™ flow cell ca. 7.4 cm in length that can accommodate a PEEK™ mercury gold (Au/Hg) microelectrode for the in-line measurements of O_2, Mn^{2+}, Fe^{2+}, and ΣH_2S (Luther et al., 2002). The counter and reference electrodes were placed in a saline solution (0.02 M NaCl) at the outflow of the

flow cell during measurements to provide the necessary electrical contact between the three electrodes. After the effluent was pumped through the flow cell, it was collected in polypropylene Falcon® tubes with a fraction collector (Eldex) at a rate of two to four samples per day for each reactor. Samples were analyzed for anion composition and pH on the day of collection, and samples for U analysis were acidified in 2% trace metal grade HNO_3 (Fisher).

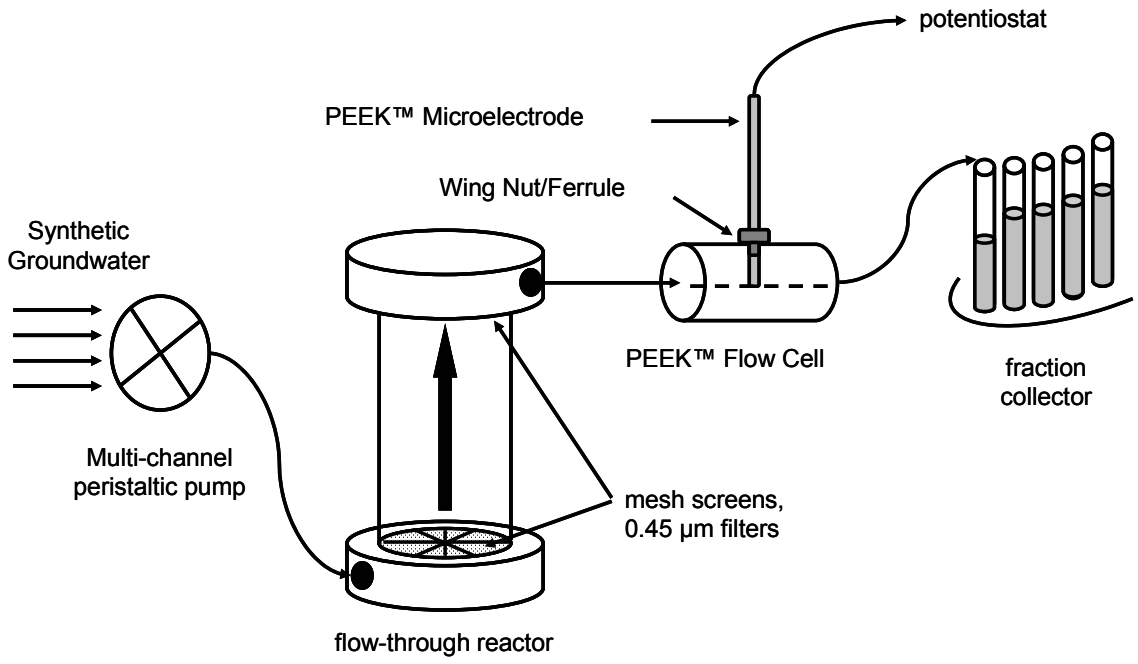

Figure 5.1 Schematic of a flow-through reactor experimental set-up. Synthetic groundwater was pumped into the base of each reactor through a mesh screen and 0.45 µm filter. The flow was directed upwards into the reactor into a flow cell positioned after the output of the reactor that contained a voltammetric Au/Hg microelectrode to monitor O_2, Mn^{2+}, Fe^{2+}, and ΣH_2S. The effluent was then collected with a fraction collector.

Figure 5.2. Photograph of the flow-through reactor experimental set-up showing, from left to right, the synthetic groundwater influent, multi-channel peristaltic pump, and three flow-through reactors and flow cells. A voltammetric Au/Hg microelectrode was positioned in the flow cell during oxygen measurements and the effluent was collected periodically with a fraction collector (not pictured).

5.3.2 Experimental Design

Two different sets of experiments were conducted with soils collected from Area 3 of the ORFRC.

(1) Four 12-cm reactors were filled with homogenized soil (~ 190 g) from core FB069 (courtesy of D. Watson, ORNL). The natural pH of the soil was ca. 7 and influent was pumped through the reactors at a flow rate of ca. 1.35 mL h^{-1} for 30 to 35 days. The influent was made of aerated and unbuffered synthetic groundwater consisting of 2 μM $FeSO_4$, 5 μM $MnCl_2$, 8 μM Na_2MoO_4, 0.8 mM $MgSO_4$, 7.5 mM $NaNO_3$, 0.4 mM KCl, 7.5 mM KNO_3, 0.2 mM $Ca(NO_3)_2$, and 20 mM NaBr (conservative tracer). The influent of three of the reactors was amended with 10 mM glycerol-3-phosphate (G3P) (Sigma

Aldrich) at day 6 and 200 μM uranyl acetate (Spectrum) at day 9 of the experiment. G3P concentration in the influent was reduced to 5 mM at day 9. The fourth reactor (control) was run for 35 days with influent consisting of synthetic groundwater amended only with U added at day 6.

(2) Four 8-cm cores were filled with homogenized soil (~ 120 g) from core FWB120-06-48 (courtesy of D. Watson, ORNL). The natural pH of the soil was ca. 3.7 and influent was pumped through the reactors at a flow rate of ca. 1.2 mL h^{-1}. The influent consisted of the aerated synthetic groundwater described above adjusted as follows: it was buffered at pH 5.5 with 50 mM 2-(N-Morpholino)ethanesulfonic acid (MES); nitrate and bromide concentrations were decreased to 10 mM; and glycerol-2-phosphate (G2P) was used as the organophosphate source as G3P was no longer commercially available. The concentration of MES was decreased to 25 mM once the effluent stabilized at pH 5.5. Synthetic groundwater without bromide was pumped through all the reactors until the pH increased from 3.7 to 5.5 (28 days). The influent of three of the reactors was amended continuously with G2P after day 28 and all reactors (including the control) were supplied with 200 μM uranyl acetate solution after day 51. The bromide tracer was added with G2P, removed from the solution at day 44, and reintroduced with U at day 51 to determine whether the transport of pore waters (i.e., retardation factor, diffusion coefficient, and advection) changed with time.

All chemicals used were reagent grade. Necessary sterile procedures were undertaken to ensure no outside contamination was introduced to the soils inside the reactors. All solutions were autoclaved or filter-sterilized. Reactor parts, filters, tubing, and influent containers were autoclaved or UV-irradiated. Reactors were run on the lab

bench at room temperature and covered with aluminum foil to avoid light interferences. Upon completion of the experiments, the reactors were disassembled and the soils removed in 1-2 cm sections in an anaerobic chamber (Coy Laboratory Instruments, Inc.) to prevent oxidation of any reduced U. The soil sections were analyzed for U by sequential extraction and synchrotron X-ray absorption spectroscopy.

The results of these experiments are reported separately below and designated as "high pH" for the reactors run at pH 7.0 and "low pH" for the reactors run at pH 5.5. Each set included three reactors continuously amended with organophosphate and U(VI) and one reactor continuously supplemented with U(VI) only. The reactors amended with organophosphate are referred to as "org-P amended" and the U(VI)-amended reactors as the "U-control". Error bars represent the standard deviations from the average measurements in the three org-P amended reactors. It was logistically difficult to run more than four reactors at one time; therefore, only one control was run with each experiment.

5.3.3 Analytical Methods

5.3.3.1 Analyses of effluent pore waters

The pH of collected pore waters was determined with an Orion pH electrode by measuring the potential and temperature with a pH meter (Orion model 290Aplus). A certified buffer reagent (pH 7) (Fisher) was used as a standard for all pH measurements, and pH was calculated from the Nernst equation. Dissolved U(VI) concentrations were measured by inductively-coupled plasma mass spectrometry (ICP-MS) with an Agilent 7500a Series system. Samples were acidified with 2% nitric acid (trace metal grade, Fisher) diluted in Nanopure water (Barnstead). Holmium and bismuth (SPEX certiPrep)

were used as internal standards and River Water Certified Reference Material for Trace Metals (SLRS-4, National Research Council Canada, Ottawa, Canada) for quality controls. Analytical error on triplicate samples was <3% relative standard deviation (RSD). Total free phosphate (ΣPO_4^{3-}) concentrations were determined by spectrophotometry (Murphy and Riley, 1962). Analytical error on duplicate samples was <4% RSD. Nitrite (NO_2^-) concentrations were determined by spectrophotometry (Grasshoff, 1983) with an analytical error on duplicate samples of <5% RSD. Bromide (Br^-), chloride (Cl^-), nitrate (NO_3^-), and sulfate (SO_4^{2-}) were analyzed by capillary electrophoresis (CE) (Beckman P/ACE MDQ series) for the pH 7 experiments using chromate (5 mM) as electrolyte (Diress and Lucy, 2005). The anions and G2P from the pH 5.5 experiments were analyzed by ion chromatography (IC) using a Dionex, DX-300 series equipped with a Dionex IonPac® AS4A chromatography column, AG4A guard column, and AMMS III suppressor. Anions were measured with a bicarbonate buffer (1 mM $NaHCO_3$ and 8 mM Na_2CO_3) at a flow rate of 1 mL min^{-1} and a regenerant solution of 25.8 mM H_2SO_4. Mass balance calculations for total nitrogen (N) removal from the low pH experiments were determined by adding the measured concentrations of nitrate and nitrite at each time point in the effluent and dividing by total nitrate added to the influent.

5.3.3.2 In-line voltammetric measurements

Dissolved oxygen and reduced species, such as Fe^{2+}, Mn^{2+}, and ΣH_2S, were analyzed voltammetrically in-line in the flow cell with a computer-operated DLK-100A or DLK-60 potentiostat (Analytical Instrument Systems). All measurements were performed with Au/Hg solid-state microelectrode, a platinum counter electrode, and an

Ag/AgCl reference electrode fabricated as described in Brendel and Luther (1995). The working microelectrodes consisted of a 100-µm-diameter Au wire housed in 3-mm PEEK tubing connected via a copper conducting wire to a potentiostat. The Au surface was polished with diamond pastes of 15, 6, 1, and 0.25 µm (Buehler), mercury plated at -0.1 V in a $Hg(NO_3)_2$ solution, and then polarized at -9 V for 90 s to form a good amalgam between the Au and Hg (Brendel and Luther, 1995). Finally, electrodes were tested for quality and calibrated for dissolved oxygen O_2 by linear sweep voltammetry, then Mn^{2+} by cathodic square wave voltammetry in degassed 0.02 M NaCl. Both the O_2 (MDL ≈ 4 µmol L^{-1}) and Mn^{2+} (MDL ≈ 15 µM) calibrations were run from -0.1 to -1.75 V with a scan rate of 200 mV s^{-1} in 0.02 M NaCl. A pre-conditioning potential of -0.1 V for 10 s was applied to all O_2 and Mn^{2+} measurements to clean the surface of the microelectrodes between measurements (Brendel and Luther, 1995). The Mn^{2+} calibration curves were used to elucidate the concentrations of other species with the pilot ion method (Brendel and Luther, 1995).

5.3.3.3 Solid phase characterization

The soil samples collected from reactors conducted at pH 7 and amended with G3P were chemically extracted using the sequential method of Tessier et al. (1979). Soil samples from each of the 1-2 cm core sections were weighed (~ 0.5 g) and placed in a 50-mL polypropylene Falcon® tube. The following procedures were conducted sequentially (after each procedure the sample was centrifuged, the supernatant removed for analysis, and the remaining sample weighed): (1) 4 mL of $MgCl_2$ was added to the sample and rotated for 1 h at 20°C to obtain the exchangeable fraction or the fraction loosely adsorbed to soil; (2) 4 mL of sodium acetate (NaOAc) adjusted to pH 5 with acetic acid

(AcOH) was added to the residue and rotated for ca. 15 h at 20°C to obtain carbonate or phosphate mineral fraction; (3) 10 mL of $NH_2OH{\cdot}HCl$ in 25% (v/v) AcOH for 6 h at 96°C in a water bath (Fisher Scientific) with occasional agitation to obtain the fraction of U(VI) associated with Fe and Mn oxides; (4) 1.5 mL of 0.02 mol L^{-1} HNO_3 and 2.5 mL of 25% H_2O_2 (pH 2) for 2 h at 96°C, a second 1.5 mL aliquot of 25% H_2O_2 for 3 h at 96°C, and 5 mL of 2.5 mol L^{-1} NH_4OAc in 20% (v/v) HNO_3 rotated for 1 h at 20°C to extract the fraction bound to organic matter; (5) finally, 5 mL concentrated HNO_3 for 3 h at 96°C to extract the residual U. The supernatant from each of the fractions was analyzed for dissolved metal species by ICP-MS.

To carefully examine the solid phase speciation of U(VI) obtained with this extraction scheme, adsorption of U(VI) onto ORFRC soils was tested using batch adsorption experiments conducted in 50-mL Falcon® tubes. The experiments were performed in duplicate to check the reproducibility of the results. The samples were prepared by adding 0.5 g of FB069 or FWB120-06 soil to 2 mL of deionized water containing 0.5 mM uranyl acetate (2 μmol g^{-1}). The FB069 samples were maintained at pH 7 and the pH of the FWB120-06 samples was adjusted to 5.5. The samples were rotated at room temperature for 48 h and then centrifuged. The supernatant was then removed, filtered (0.2 μm pore size, AcetatePlus; GE Water and Process Technologies), and analyzed for U by ICP-MS. The soil was then sequentially extracted as described above and analyzed for U and phosphate.

Chemically-formed uranyl phosphate precipitates were mixed with ORFRC soils in batch experiments to identify the extraction step of the sequential procedure that quantifies precipitated U(VI)-phosphate. The experiments were performed in duplicate

to check the reproducibility of the results. Uranyl phosphate precipitate was prepared by adding 0.5 mM uranyl acetate to 0.5 mM phosphate (from K_2HPO_4 stock; pH adjusted to 5.5), allowed to equilibrate for 48 h, and then centrifuged. The supernatant was then filtered and analyzed for U by ICP-MS to determine U concentration in the precipitate. The uranyl phosphate precipitate was transferred with deionized water (2 mL) to 0.5 g of FB069 or FWB120-06 soil in 50-mL Falcon® tubes. The FB069 and FWB120-06 samples were maintained at pH 7 and 5.5, respectively. The samples were rotated at room temperature for 48 h, centrifuged, and the supernatant removed, filtered, and analyzed for U and phosphate. The soil was sequentially extracted as described above and analyzed for U and phosphate.

Selected samples from all of the reactor experiments were analyzed by X-ray absorption spectroscopy (XAS) and X-ray Microprobe (μ-XANES) at the Stanford Synchrotron Radiation Laboratory (SSRL). Samples for XAS were loaded in windowed Lexan sample holders and sealed with Kapton tape. Samples from reactors run at pH 5.5 were maintained anoxic in a sealed jar for transport to SSRL and under N_2 atmosphere at the beam line. Uranium L_{III}-edge XAS spectra were collected at SSRL beam line 10-2 using a forced X-ray beam with a 23 keV harmonic rejection cutoff and a 13 element Ge detector. The incident energy was selected with a Si(220) monochromator crystal. Transmission and fluorescence data were collected simultaneously. All extended X-ray absorption fine structure (EXAFS) data were reduced using SIXPACK (Webb, 2005). Phase and amplitude files for the EXAFS fitting were created with FEFF7 (Ankudinov et al., 1998; Zabinsky et al., 1995). Since the Debye-Waller factors (σ) correlated highly with coordination numbers (N), σ's for some shells were each fixed at their average

values. The $U{=}O_{ax}{=}U{=}O_{ax}$ transdioxo multiple scattering path (Hudson et al., 1996) was included in all fits.

Elemental imaging and μ-XANES analysis was conducted on selected samples at SSRL beam line 2-3 using a Si(111) monochromator and a motorized three element monolithic Germanium (Ge 3) detector. Elemental data was acquired by continuous scan across the sample grid with a focused beam of 2 μm diameter. Soil samples were thin-sectioned by Spectrum Petrographics, Inc. prior to analysis.

5.4 Results

5.4.1 Speciation of U(VI) in the solid phase

5.4.1.1 U and P composition of initial ORFRC soils

The ORFRC soils were obtained from two different sites within Area 3 of the ORFRC. FB069 was from an area characterized by low porosity (0.20), high pH (~7), low U and high nitrate concentrations. The initial concentrations of soil U and PO_4^{3-} were 0.063 and 3.10 μmol g^{-1}, respectively. FWB120-06 soils were characterized by mid porosities (0.49), low pH (~3.7), high U and high nitrate concentrations. The initial concentrations of soil U and PO_4^{3-} were 0.223 and 0.36 μmol g^{-1}, respectively. The two soils displayed distinct differences in their uranium speciation (Figure 5.3a). U in the acidic soil was more loosely bound to the solid surfaces as displayed by > 60% U extracted in the exchangeable and AcOH-extracted fractions and decreasing concentrations found in the more tightly bound fractions. In contrast, more U was bound to OM (28%) and in the residual portion (22%) of the neutral soil compared to the relatively even distribution (~15%) of the first three more loosely bound fractions (Figure

5.3a). Phosphate in both soils was primarily extracted with hydroxylamine and associated with OM (Figure 5.3b). More phosphate was extractable with hydroxylamine than associated with OM in the low pH soil compared to a more even distribution of phosphate between the two fractions in the high pH soil.

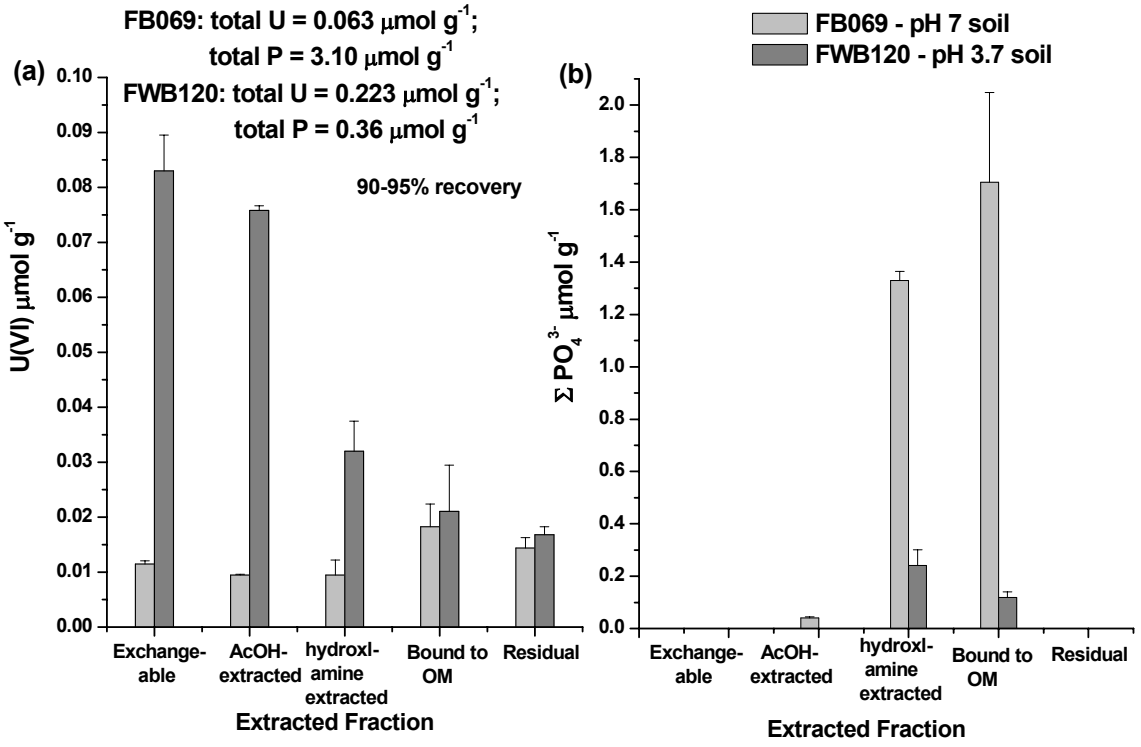

Figure 5.3. Total μmol g^{-1} (a) U and (b) phosphate sequentially extracted from the original ORFRC soils. FB069 soil displayed a natural pH ca. 7, lower U and higher P concentrations compared to the acidic FWB120-06 soil (pH 3.7) that contained higher U and lower P concentrations. The two soils demonstrated distinct differences in solid U speciation. The neutral soil contained higher U concentrations in the more strongly bound fractions (30% bound to OM and 22% in the residual) compared to the acidic soil where 36 and 33% of the U was found in the exchangeable and AcOH-extracted fractions, respectively. Phosphate in both soils was primarily extracted with hydroxylamine and associated with OM. Error bars represent the standard deviations from the average measurements in duplicate samples.

5.4.1.2 U(VI) adsorption onto ORFRC soils in acidic and circumneutral pH conditions

Batch adsorption experiments conducted with FB069 and FWB120-06 soils at pH 7 and 5.5 resulted in a concentration of 1.61 (± 0.3) μM U(VI) in the supernatant of the high pH soil and 153 (± 8.6) μM in the low pH soil, indicating the majority of the U(VI) was adsorbed onto the soil. U(VI) adsorbed more strongly to the high pH soil as evidenced by the low exchangeable fraction (3%) and the 93% removal in the AcOH-extracted fraction (Figure 5.4). In contrast, U(VI) adsorbed more loosely to the acidic soil as evidenced by 65% U(VI) removed in the exchangeable fraction and 28% extracted in the AcOH-extracted fraction (Figure 5.4).

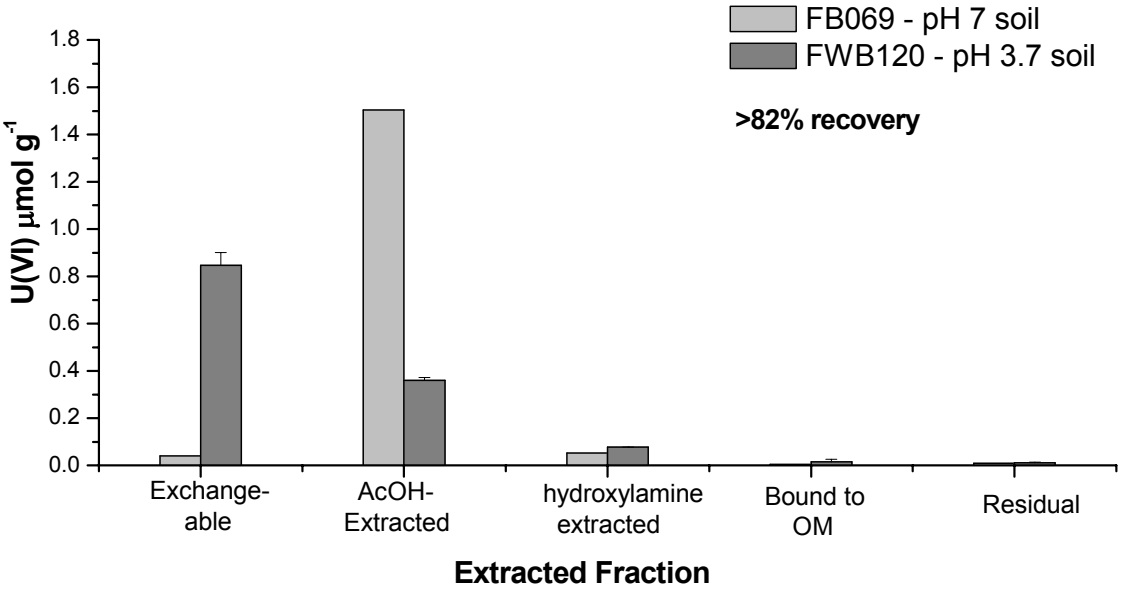

Figure 5.4 Speciation of U(VI) equilibrated for 48 h with ORFRC soils (2 μmol g^{-1}) in batch reactors (70 and 99% total U(VI) was adsorbed to the low and high pH soils after equilibration). FB069 soil incubated at pH 7 revealed 93% of total U in the AcOH-extracted fraction. FWB120-06 soils incubated at pH 5.5 displayed 65% total U in the exchangeable fraction and 28% in the AcOH-extracted fraction.

5.4.1.3 Extraction of uranyl phosphate precipitates equilibrated with ORFRC soils

Laboratory-prepared uranyl phosphate precipitates (2 μmol g^{-1}) were mixed with ORFRC soil at pH 7 (FBO69) and 5.5 (FWB120-06) and sequentially extracted to identify the extraction step that leaches U-P minerals. U-P precipitates were extracted with AcOH and hydroxylamine in both soils (Figure 5.5a and b).

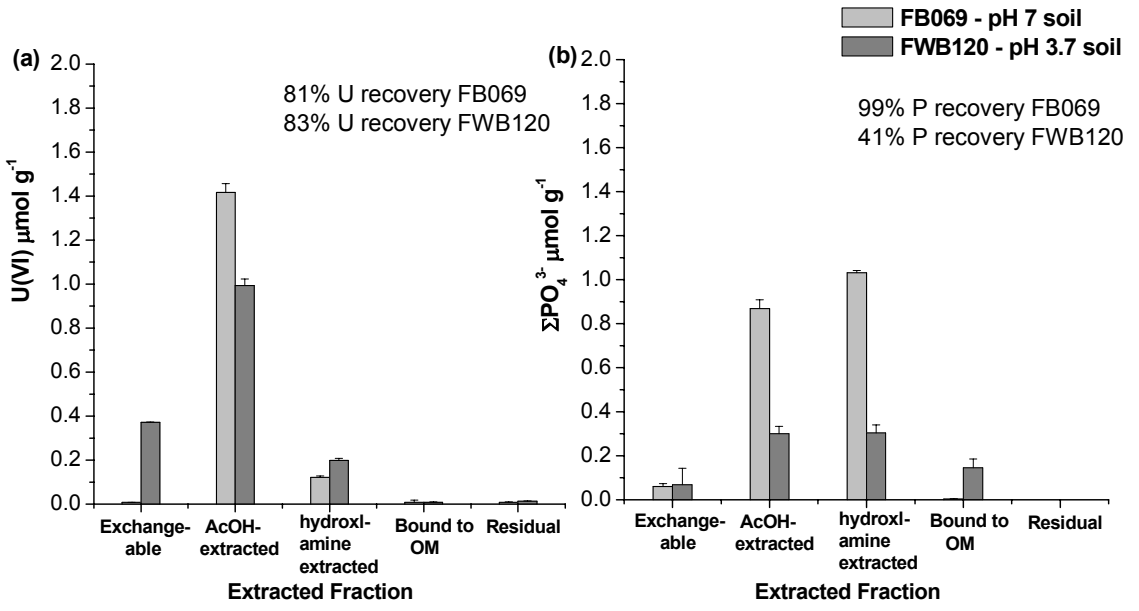

Figure 5.5 Uranyl phosphate precipitate (2 μmol g^{-1}) equilibrated with ORFRC soils in batch reactors was sequentially extracted to determine what extraction dissolves U-P precipitates. U-P precipitates were released by AcOH and hydroxylamine in ORFRC soils at pH 5.5 and 7.

5.4.2 Removal of uranium in flow-through columns at circumneutral pH

5.4.2.1 Dissolved constituents in the effluent

The pH remained relatively constant between 6.5 and 7.0 throughout the experiment in both control and org-P amended reactors (Figure 5.6a). Dissolved oxygen decreased from saturation to ca. 60 μM in org-P amended reactors within 6 d after G3P

was added to the influent (Figure 5.6b). Reduced species Fe^{2+}, Mn^{2+}, and ΣH_2S were not detected in the effluent indicating that conditions in the flow-through reactors were not favorable for microbial iron reduction or sulfate reduction.

Bromide was added as a conservative tracer (Roychoudhury et al., 1998) to determine transport parameters, including the retardation factor, diffusion coefficient, and advection rate, and to establish residence time of the synthetic groundwater in the reactors. Bromide was injected at day 1 and demonstrated conservative behavior throughout the experiment (Figure 5.6c). Residence time as determined from the bromide breakthrough curve was ca. 5 days in the org-P amended reactors.

Chloride concentrations remained relatively constant throughout the experiments (Figure 5.7a). The effluent of the org-P reactors contained slightly more chloride than the control due to the addition of hydrochloric acid (HCl) to adjust the pH of G3P in the influent solution. Nitrate concentrations decreased by ca. 3 mmol L^{-1} after the addition of G3P in amended reactors and remained steady for the rest of the experiment. After U addition, the difference between nitrate concentrations in the control and amended reactors was negligible (Figure 5.7b). Sulfate remained constant throughout the experiment and behaved as a conservative tracer demonstrating a 5 d breakthrough curve (Figure 5.7c).

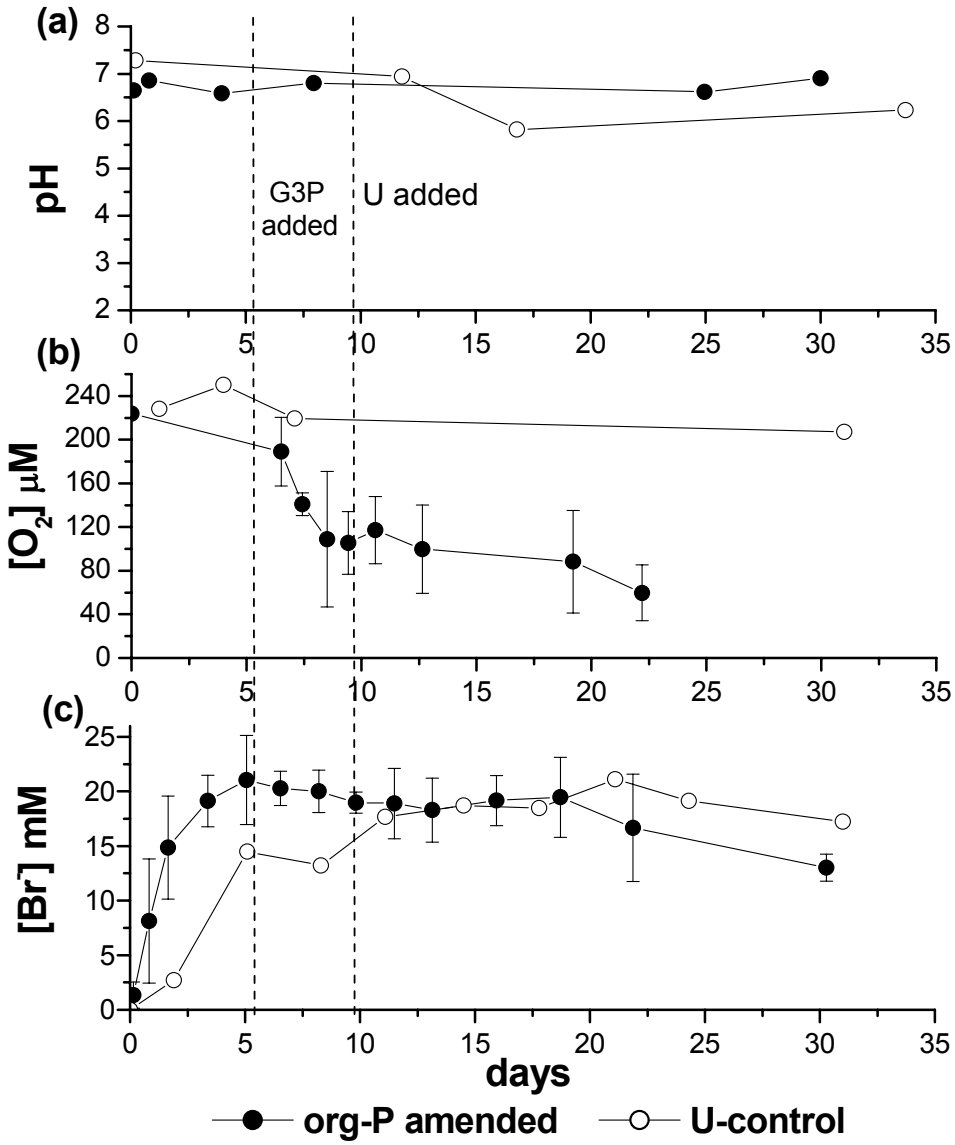

Figure 5.6 Average (a) pH, (b) dissolved oxygen, and (c) bromide measured as a function of time in the effluents of the org-P amended flow-through reactors containing high pH soils compared to the U-control. Oxygen was consumed in org-P amended reactors after G3P was injected. Bromide (20 mM) was injected at day 1 in all reactors. Error bars represent the standard deviations from the average measurements in the three org-P amended reactors. Dashed lines indicate the addition of G2P and U(VI).

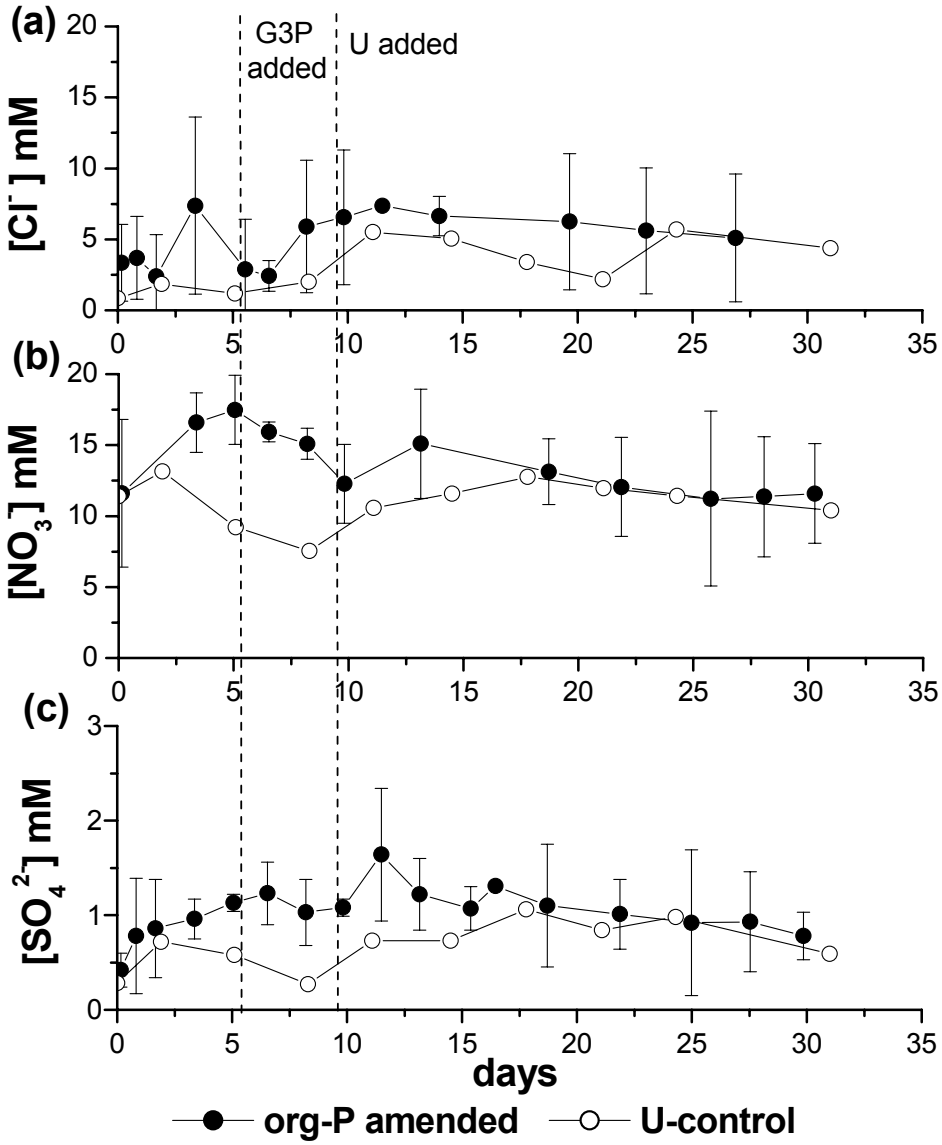

Figure 5.7. Average (a) chloride, (b) nitrate, and (c) sulfate concentrations measured as a function of time in the effluents of the org-P amended flow-through reactors containing high pH soils compared to the U-control. Error bars represent the standard deviations from the average measurements in the three org-P amended reactors. Dashed lines indicate the addition of G2P and U(VI).

Phosphate was not detected in the effluent of the reactors prior to G3P addition nor in the control reactor (Figure 5.8a) indicating little or no exchangeable phosphate on the soils. After G3P was added, however, phosphate concentrations in the effluent increased to > 0.5 mM in less than one day (Figure 5.8a). At day 10, phosphate concentrations reached ca. 1 mM, gradually decreased to ca. 0.5 mM at day 15, and then gradually increased again to >1 mM by 25 d.

U concentrations in the effluent of org-P amended reactors increased to > 15 μM initially, then decreased to < 4 μM at day 17, and remained stable at ca. 1 μM until the end of the experiment (Figure 5.8b). In contrast, U concentration in the control reactor effluent gradually increased to ca. 40 μM over the duration of the experiment (Figure 5.8b). These data show that approximately 97% of U(VI) introduced to the system is retained in the org-P amended reactors, while only approximately 80% U(VI) is retained in the U-control.

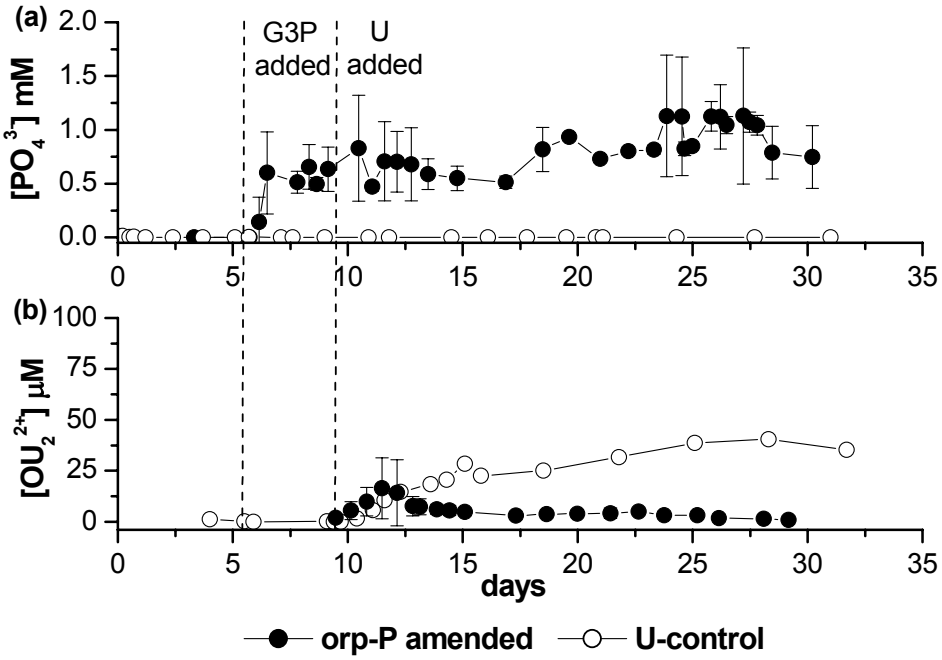

Figure 5.8. Average (a) phosphate and (b) U concentrations measured as a function of time in the effluents of the org-P amended flow-through reactors containing high pH soils compared to the U-control. Phosphate was not detected in the control effluent, but the hydrolysis of 10 mM G3P produced up to 1 mM ΣPO_4^{3-} in the org-P amended effluents. U (200 µM) was added on day 9 and approximately 97% U was retained in the org-P amended reactors compared to 80 % U retention in the control reactor by the end of the experiment. Error bars represent the standard deviations from the average measurements in the three org-P amended reactors. Dashed lines indicate the addition of G2P and U(VI).

5.4.2.2 Speciation of solid uranium in high pH flow-through column studies

Soil in the flow-through reactors was removed in cm-length sections after the experiments were completed. Each section was sequentially extracted and analyzed for U(VI) and P to determine the fraction(s) they were associated with (see Appendix C, Figures C.1-6 for extractions of individual reactors). Approximately 0.62 (± 0.07) µmol g^{-1} U(VI) was added to the soils and more than 97% was retained on the org-P amended columns compared to 88% retention on the U control soil. In addition, highest concentrations of total U(VI) added to the soils was found closest to the flow-through

reactors' inlet and decreased dramatically as distance from the reactors' inlets increased (Figure 5.9). U(VI) in org-P amended reactors was extracted with a combination of AcOH and hydroxylamine indicative of the release of U-P minerals (Figure 5.9a). In contrast, U(VI) in the U control reactor was extracted primarily with AcOH indicative of the release of adsorbed U(VI) (Figure 5.9b).

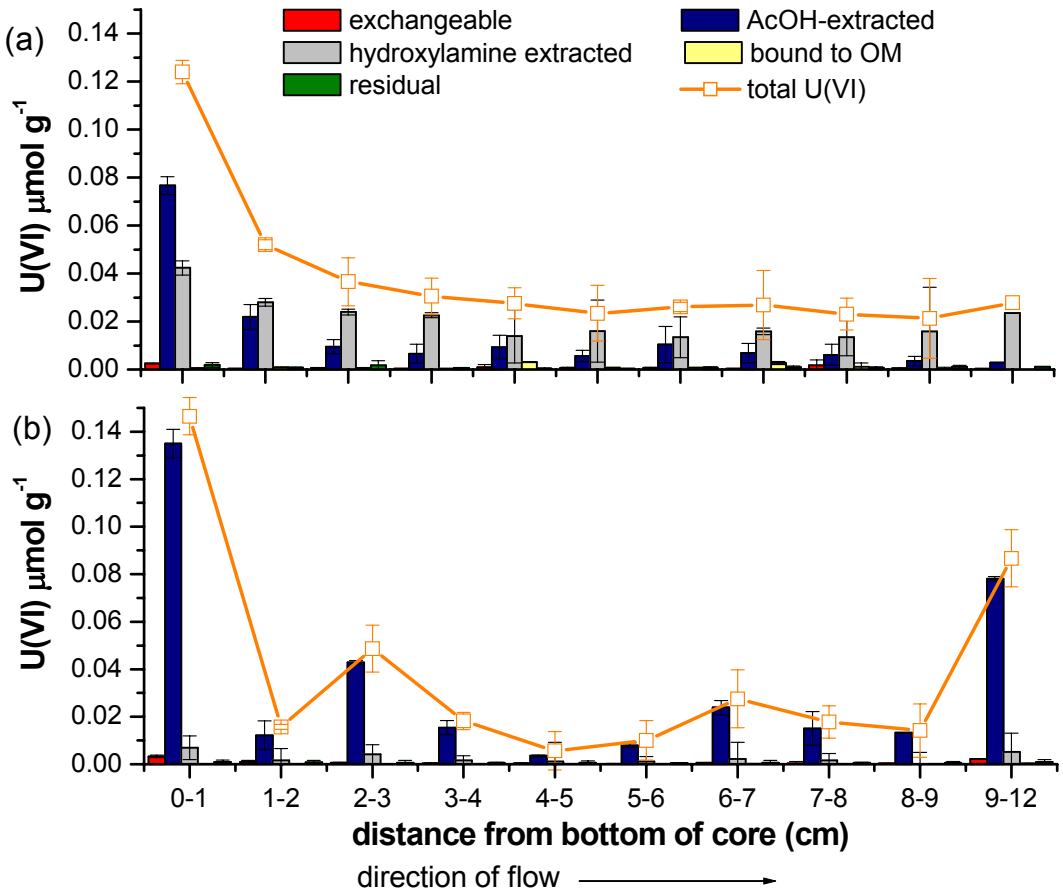

Figure 5.9 Average U (µmol g^{-1}) distributions in soil sections from (a) org-P amended and (b) U control high pH flow-through reactors as determined by sequential extraction. Soil sections nearest the influent inlet contained the highest concentrations of total. U(VI) in org-P amended reactors was released by a combination of AcOH and hydroxylamine indicative of U-P mineral precipitation. U(VI) in U control reactor was released primarily by AcOH indicative of U adsorbed to mineral surfaces.

Comparatively, total phosphate (ca. 4 (± 0.2) µmol g^{-1} total retained on the columns) and exchangeable phosphate were distributed evenly across the length the reactors (Figure 5.10), and the soil layers the closest to the inlets were equally extracted by AcOH and hydroxylamine. Phosphate associated with the AcOH-extracted fraction decreased from 0.18 µmol g^{-1} in sections nearest the reactors' inlet to 0.08 µmol g^{-1} at the end of the reactors, while phosphate extracted by hydroxylamine remained relatively constant across the length of the reactor.

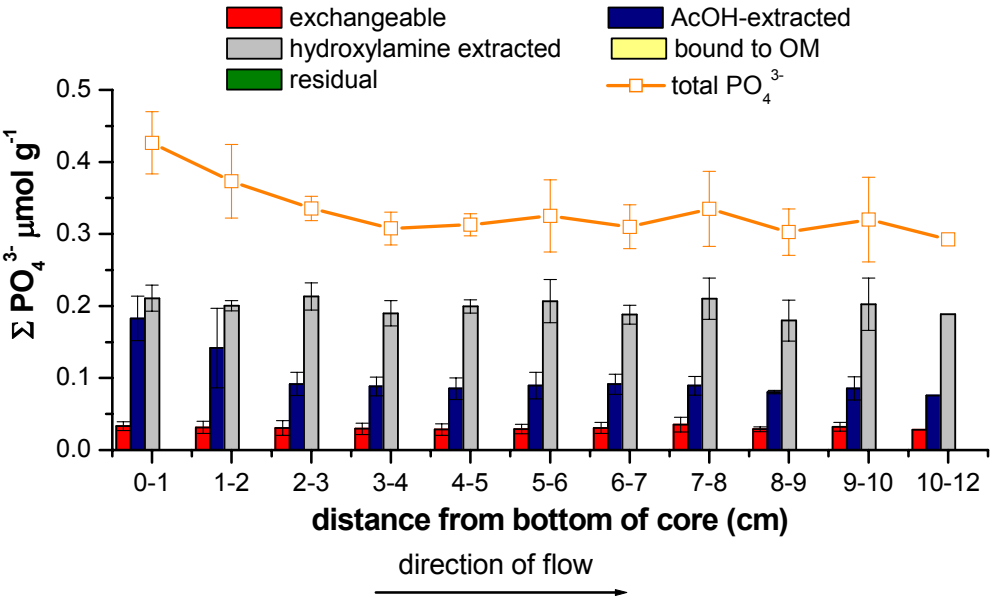

Figure 5.10 Average total phosphate (µmol g^{-1}) distribution in soil sections from the high pH flow-through reactor experiments as determined by sequential extraction. Phosphate concentrations were spread evenly across the length of the reactor and displayed a similar trend as U, with concentrations in the AcOH-extracted fraction highest in sections nearest to the flow inlet (where precipitation occurred), changing to the hydroxylamine extracted fraction as distance from the inlet increased.

The 0-1 cm soil sections from each of the org-P amended and the U amended control flow-through reactors were analyzed by synchrotron X-ray absorption

spectroscopy (XAS). The oxidation state of U in the soil samples was determined by U L_{III}-edge X-ray absorption near-edge structure (XANES). The normalized and background subtracted spectra of the samples (Figure 5.11) displayed the characteristic shoulder between 17,180 and 17,190 eV, which is consistent with U(VI) oxidation state.

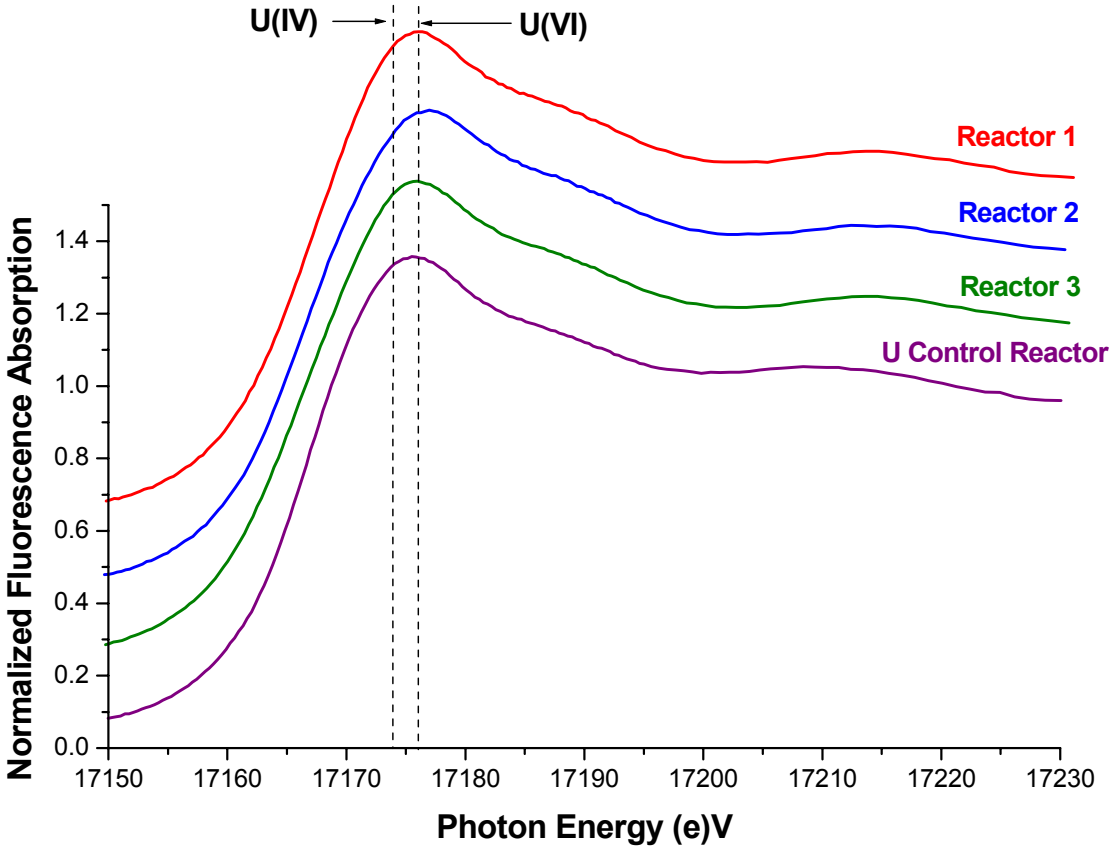

Figure 5.11 Uranium L_{III}-edge XANES spectra of the soil samples from the three org-P amended and the U(VI) amended control flow-through reactors conducted at pH 7.

The k^3-weighted extended X-ray absorption fine structure (EXAFS) data and fits for the four soil samples are shown in Figure 5.12 and Figure 5.13. Fitting parameters are listed in Table 5.1. The FEFF7 phase and amplitude files (Ankudinov et al., 1998;

Zabinsky et al., 1995) used for the fitting of EXAFS in the natural soil samples of this study were first tested on a known chernikovite sample and good agreement was reached with previous fittings (Beazley et al., 2007; Beazley et al., 2009).

All samples show the presence of the O_{ax} shell at ~1.80 Å (Table 5.1) and two different equatorial oxygen shells observed at ~2.30 Å and between ~2.39 and 2.47 Å. The coordination numbers of O_{eq} atoms at 2.30 Å and 2.46 Å are approximately equally distributed in the control reactor compared to higher coordination numbers at ~2.30 Å in the org-P amended reactors.

Synchrotron microprobe elemental mapping of a soil sample from the high pH Reactor 1 is shown in Figure 5.14. The green areas represent uranium distribution on the surface of the soil particle while red represents the iron substrate. U is distributed in discrete areas on the surface of the soil and appears to collect in micropores. XANES analysis performed in the areas indicated with white arrows identified U(VI) as the oxidation state of uranium (data not shown).

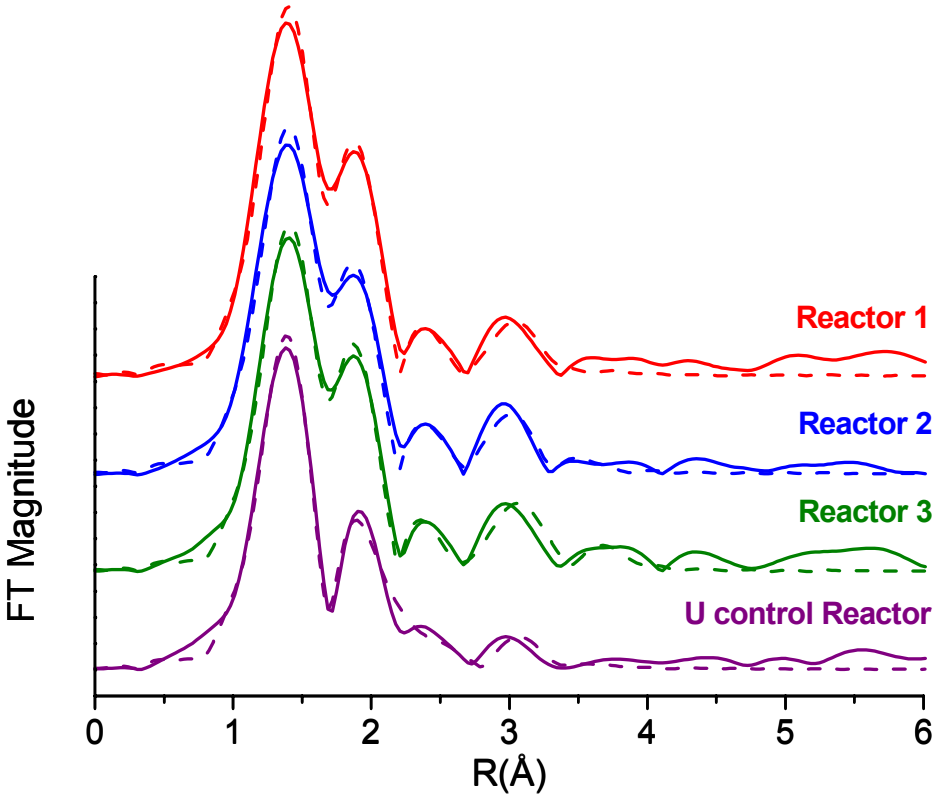

Figure 5.12 Uranium R-space diagrams of the L_{III}-edge EXAFS of the soil samples from the three org-P amended flow-through reactors compared to the U(VI) amended control reactor conducted at pH 7. Solid lines represent experimental data and dashed lines represent the fitted data.

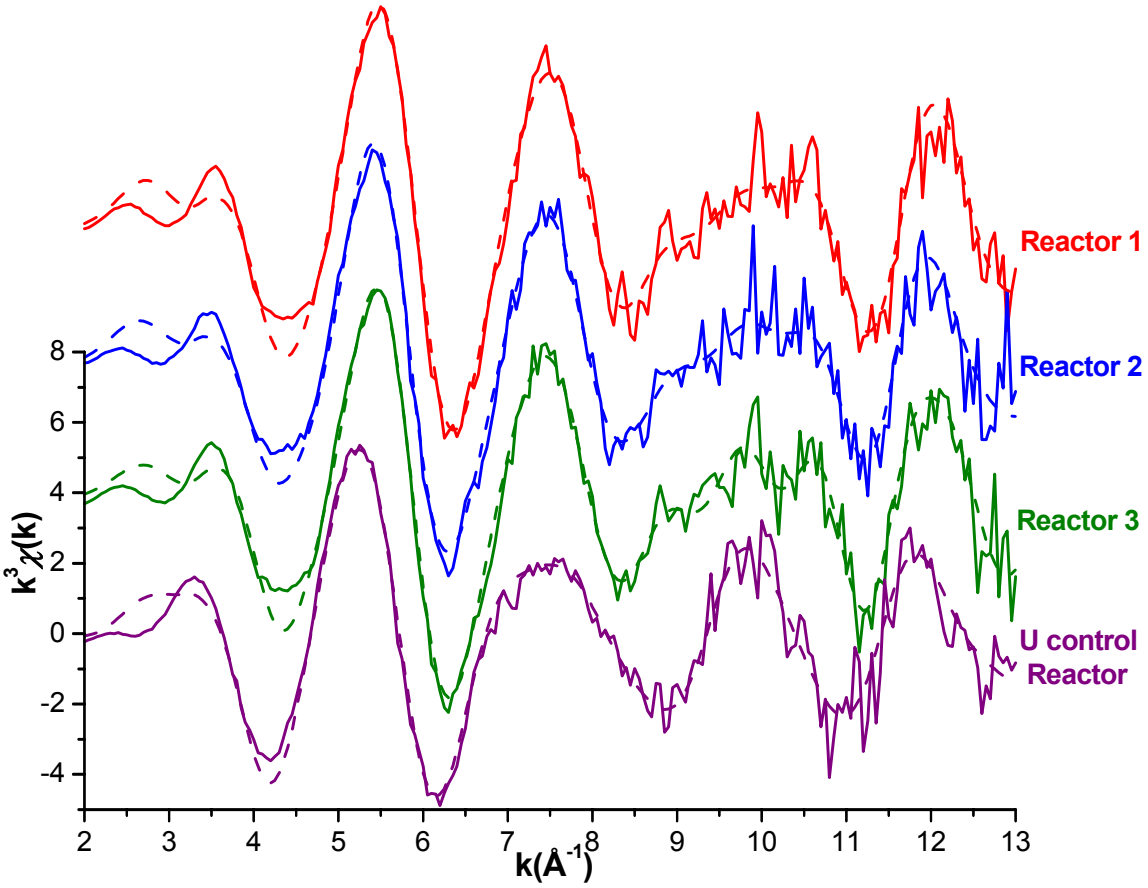

Figure 5.13 Uranium *k*-space diagrams of the L_{III}-edge EXAFS of the soil samples from the three org-P amended flow-through reactors compared to the U(VI) amended control reactor conducted at pH 7. Solid lines represent experimental data and dashed lines represent the fitted data.

Table 5.1 Parameters derived from fitting of U L_{III}-edge EXAFS of flow-through reactor soil samples conducted at pH 7.

Reactor	Shell	N	R (Å)	σ^2 (Å^2)	ΔE_0 (eV)	χ_v^2	R factor
U amended control 0-1 cm	O_{ax}	2	1.80 (0.006)	0.003 (0.0009)	8.68 (1.3)	0.203	0.0112
	O_{eq}	1.52 (0.34)	2.33 (0.02)	0.003			
	O_{eq}	1.48 (0.48)	2.46 (0.01)	0.003			
	C	1.27 (0.38)	2.94 (0.02)	0.003			
	Fe	0.14 (0.1)	3.46 (0.04)	0.003			
Reactor 1 0-1 cm	O_{ax}	2	1.80 (0.009)	0.004 (0.001)	10.9 (2)	0.227	0.0141
	O_{eq}	2.47 (0.6)	2.29 (0.01)	0.003			
	O_{eq}	0.14 (0.4)	2.39 (0.25)	0.003			
	C	1.38 (1.6)	2.90 (0.06)	0.003			
	Fe	0.25 (0.17)	3.42 (0.03)	0.003			
	P	0.27 (0.45)	3.68 (0.11)	0.005			
	POU MS*	0.54	3.77 (0.06)	0.005			
	OPOU MS*	0.27	3.85 (0.05)	0.005			
	PO dist**	1.56 (0.05)					
Reactor 2 0-1 cm	O_{ax}	2	1.80 (0.009)	0.005 (0.001)	10.4 (1.8)	1.629	0.0134
	O_{eq}	2.17 (0.57)	2.29 (0.02)	0.003			
	O_{eq}	0.17 (0.35)	2.41 (0.2)	0.003			
	C	1.37 (1.5)	2.92 (0.08)	0.003			
	Fe	0.34 (0.11)	3.43 (0.02)	0.003			
	P	0.21 (0.16)	3.55 (0.43)	0.005			
	POU MS*	0.42	3.62 (0.17)	0.005			
	OPOU MS*	0.21	3.99 (0.06)	0.005			
	PO dist**	1.7 (0.06)					
Reactor 3 0-1 cm	O_{ax}	2	1.80 (0.01)	0.004 (0.001)	10.9 (2.1)	0.275	0.0110
	O_{eq}	2.68 (0.7)	2.30 (0.01)	0.003			
	O_{eq}	0.42 (0.5)	2.45 (0.06)	0.003			
	C	1.67 (2.2)	2.90 (0.05)	0.003			
	Fe	0.40 (0.11)	3.44 (0.02)	0.003			
	P	2.56 (1.9)	3.79 (0.7)	0.005			
	POU MS*	5.11	3.89 (0.05)	0.005			
	OPOU MS*	2.56	3.98 (0.03)	0.005			
	PO dist**	1.68 (0.03)					

Errors are given in parentheses (no error means the value was fixed, or calculated from other parameters)

* MS denotes multiple scattering paths

** PO dist is the distance between the P-O in phosphate coordination (used for the MS paths)

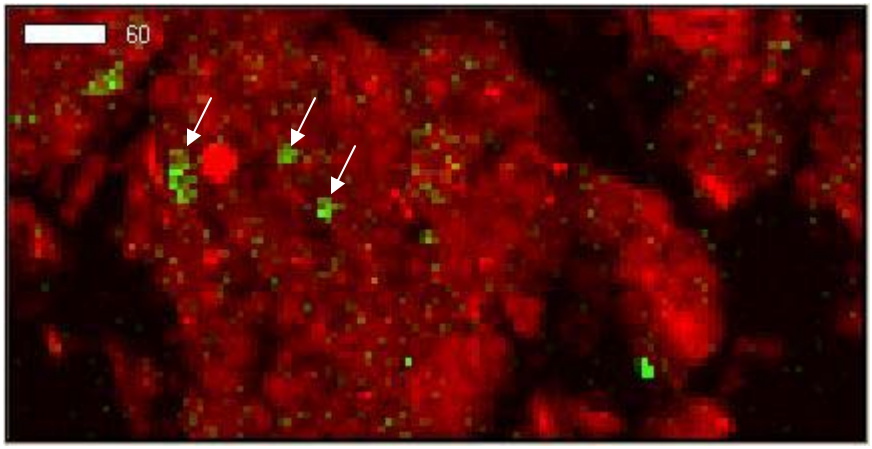

Figure 5.14 Synchrotron microprobe elemental mapping of a soil sample from the high pH Reactor 1. Green areas denote U and red represent Fe. U is distributed on the surface of the soil in discrete areas and appears to collect in micropores. White arrows signify areas of the surface analyzed by µ-XANES. Scalebar units: µm.

5.4.3 Removal of uranium in flow-through columns at low pH

5.4.3.1 Dissolved constituents in the effluent

ORFRC soil used in the low pH reactors displayed an initial pH of ca. 3.7 when equilibrated with synthetic groundwater buffered at pH 5.5. The synthetic groundwater was pumped through the reactors for 28 d to raise the effluent of the reactors to pH 5.5 (Figure 5.15a). During that time, no reactions were observed among the species of interest. Effluent pH remained relatively constant for the remainder of the experiment. Dissolved oxygen concentrations decreased to ca. 60 µM in the org-P amended reactors between days 28 and 40, but remained constant after U was added to the system on day 51. The U-control reactor demonstrated a slight decrease in dissolved oxygen between 30 and 40 d, but returned to saturated concentrations by the end of the experiment (Figure 5.15b). Reduced species Fe^{2+}, Mn^{2+}, and ΣH_2S were not detected in the effluent,

indicating that conditions in the flow-through reactors were not favorable to metal and sulfate reducers.

Bromide was added as a conservative tracer to the influent at day 28, was removed at day 44, and reintroduced at day 51 to determine if the porosity of the soil changed with time. Bromide demonstrated conservative behavior and the breakthrough curve indicated a 4 d residence time in both org-P amended and control reactors (Figure 5.15c).

Chloride concentrations remained relatively constant throughout the experiments (Figure 5.16a), but the effluent of the org-P reactors contained ca. 7 mM more chloride than the control due to the addition of HCl to adjust the pH of G2P in the influent solution. Sulfate concentrations remained constant throughout the experiment in both org-P amended and control reactors, indicating that sulfate reducing conditions were not favored in these experiments (Figure 5.16b). Average nitrate concentrations in the org-P amended reactors decreased dramatically (> 60%) after G2P addition, and an increase (up to 3 mM) in nitrite concentrations was observed simultaneously (Figure 5.16c). Nitrate concentrations in the effluent of the U-control reactor remained constant, and nitrite was never detected during these experiments (Figure 5.16c).

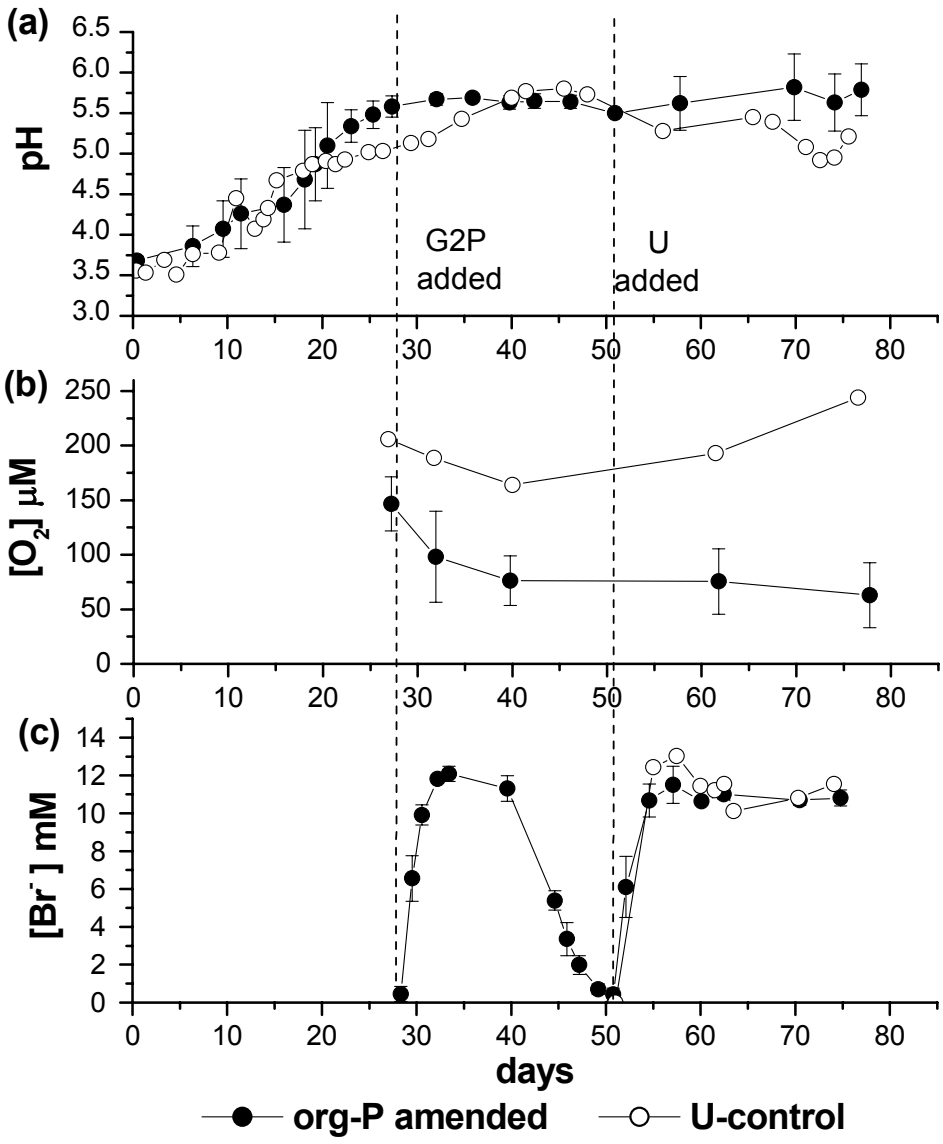

Figure 5.15. Average (a) pH, (b) dissolved oxygen, and (c) bromide measured as a function of time in the effluents of the org-P amended flow-through reactors containing low pH soils compared to the U-control. Oxygen was consumed in org-P amended reactors after G2P was injected. Bromide (10 mM) was injected at day 28, removed at day 44, and reintroduced at day 51 to determine if soil porosity had changed in the org-P amended soils. Bromide was injected simultaneously with U(VI) only at day 51 in the U-control reactor. Error bars represent the standard deviations from the average measurements in the three org-P amended reactors. Dashed lines indicate the addition of G2P and U(VI).

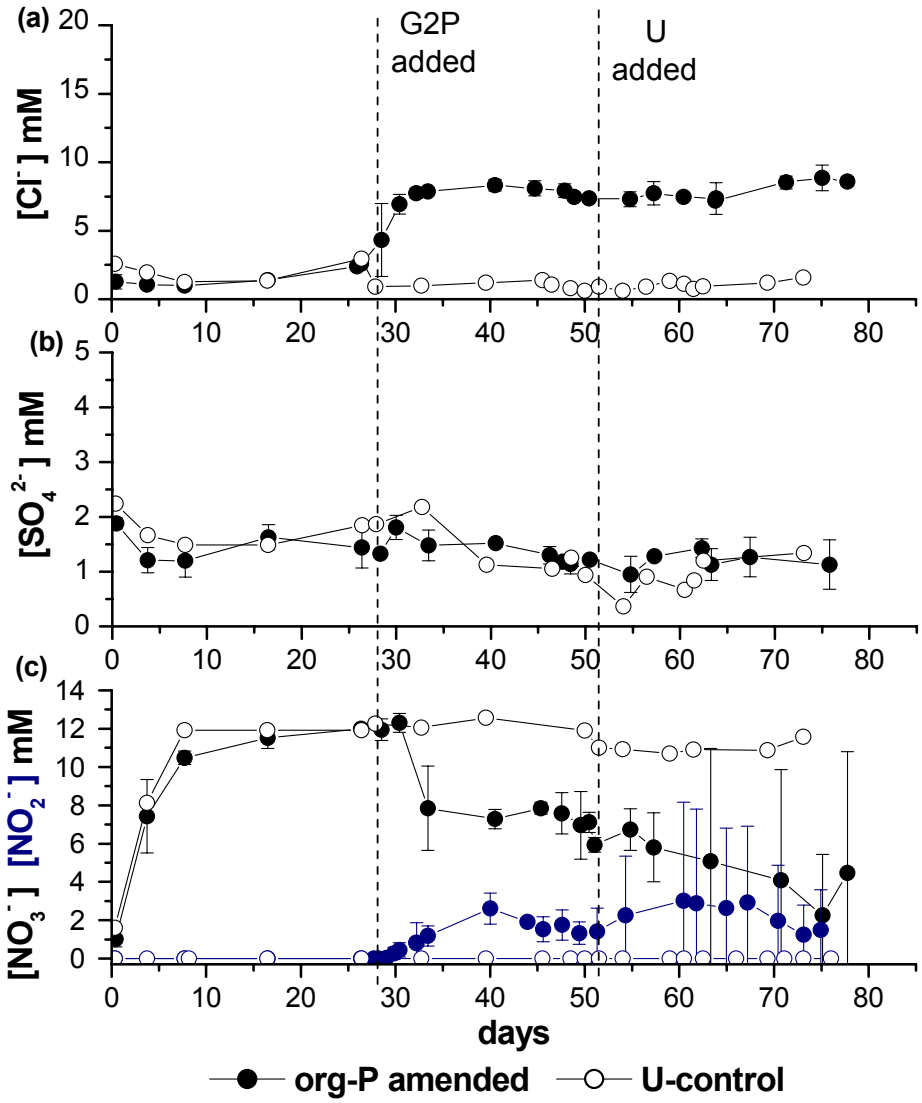

Figure 5.16. Average (a) chloride, (b) sulfate, and (c) nitrate and nitrite measured as a function of time in the effluents of the org-P amended flow-through reactors containing low pH soils compared to the U-control. The org-P amended reactors contained higher concentrations of chloride due to the addition of HCl to adjust the pH of G2P. Sulfate concentrations remained relatively constant in all reactors throughout the experiment. Nitrate (10 mM) was continuously pumped into the flow-through reactors and average nitrate concentrations in org-P amended reactors decreased with a corresponding net nitrite production after G2P (10 mM) was injected. Nitrate concentration remained constant and nitrite was not detected throughout the incubations in the control reactor. Error bars represent the standard deviations from the average measurements in the three org-P amended reactors. Dashed lines indicate the addition of G2P and U(VI).

The high error bars associated with the average concentrations of nitrate and nitrite (Figure 5.16c) are due to the significant differences between the three flow-through reactors amended with org-P. Nitrate was introduced to the reactors at a constant concentration of 10 mM in all four reactors throughout the experiment, yet nitrate and nitrite behaved differently in each reactor (Figure 5.17).

Nitrate concentrations in the effluent of all reactors stabilized at ca. 12 mM prior to G2P addition, but nitrate was consumed in all reactors after G2P was introduced to the influent (Figure 5.17). After U was added to the reactors, nitrate consumption continued in Reactors 2 and 3 until day 60, when nitrate concentrations at the output of these two reactors was negligible (Figure 5.17 b and c), while nitrate concentrations returned to 9 mM in the effluent of Reactor 1 (Figure 5.17a). Nitrite increased to ca. 2 -3 mM in the three reactors after G2P addition but, while nitrite was consumed in Reactor 1 and 3 by days 55-60 (Figure 5.17a and Figure 5.17c), a net nitrite production of up to 9 mM was observed by day 61 in Reactor 2. Mass balance calculations of total nitrogen (N) added to the system (Figure 5.18) indicate significant removal (> 80%) of total N in Reactors 2 and 3 by a mechanism other than nitrate reduction. Loss of N was most probably due to the formation of other denitrification products, such as N_2O, NO, and N_2, or NH_4^+ during dissimilatory nitrate reduction to NH_4^+ (DNRA).

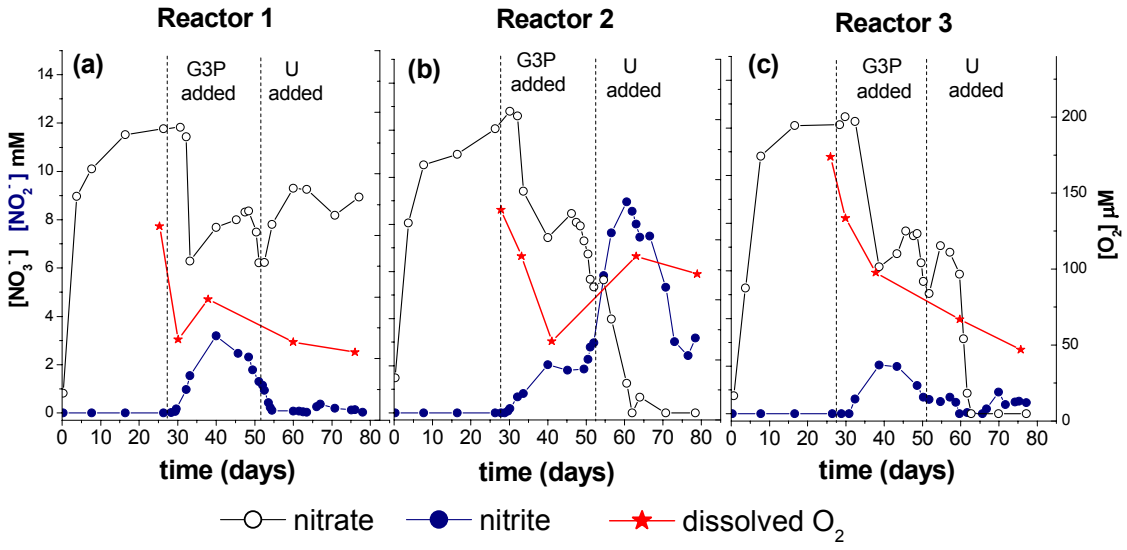

Figure 5.17. Nitrate, nitrite, and dissolved oxygen concentrations of org-P amended reactors containing low pH soil as a function of time in (a) Reactor 1, (b) Reactor 2, and (c) Reactor 3. The concentration of nitrate (10 mM) in the flow-through reactor influent was held constant throughout the experiment. Dashed lines indicate the addition of G2P and U(VI). Dashed lines indicate the addition of G2P and U(VI).

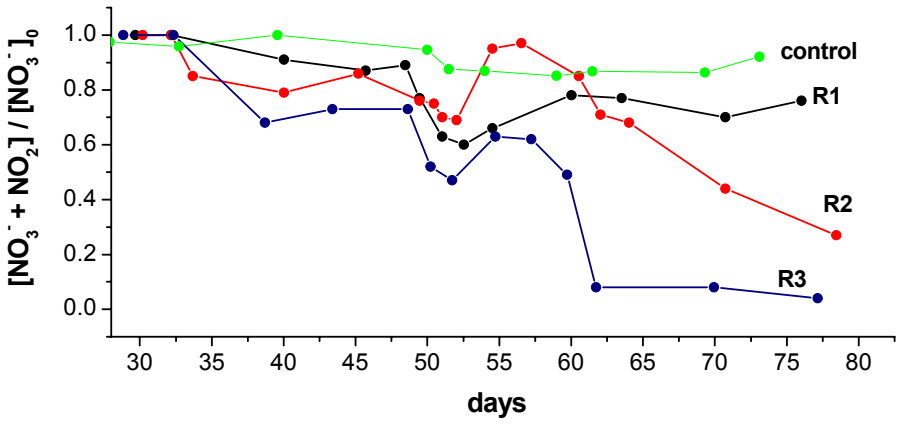

Figure 5.18. Mass balance of total N in the org-P amended flow-through reactors containing low pH soil compared to the unamended control. Total N (10 mM) is balanced prior to G2P addition (10 mM). At the end of the experiment, ca. 80 % of total N is accounted for in Reactor 1, 20 % in Reactor 2, and only 4 % in Reactor 3.

Average G2P concentrations in the effluent increased up to ca. 8 mM with a 5 d breakthrough curve (Figure 5.19a) and remained relatively constant (between 5 to 7 mM) for the rest of the experiment. Phosphate was not detected in the effluent of the reactors prior to G2P addition; indicating little or no exchangeable phosphate on the soils. After G2P was added, however, phosphate concentrations in the effluent raised to > 0.2 mM in one day, then gradually to ca. 3 mM by day 45, and remained between 2 and 3 mM throughout the rest of the experiment (Figure 5.19a). U concentrations in the effluent of the control reactor suddenly increased to ca. 34 μM within 24 d after U injection (Figure 5.19b), corresponding to approximately 85% of the total input of U(VI) removed in the reactors. Average U concentrations in the org-P reactors demonstrated more variability over the same time period but they appeared to stabilize at approximately 15 μM by the end of the experiment, thus demonstrating a constant removal of approximately 95% at steady state.

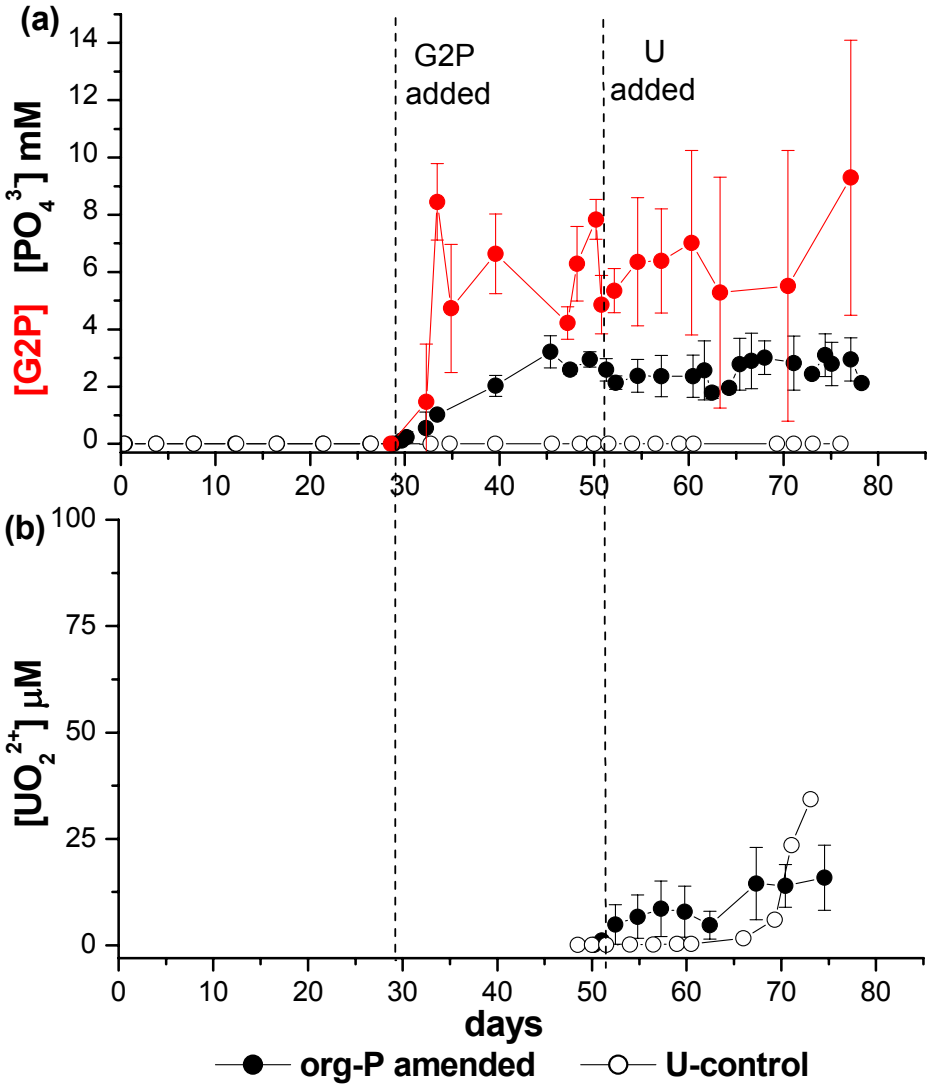

Figure 5.19. (a) Average G2P and phosphate concentrations measured as a function of time in the effluents of the org-P amended flow-through reactors containing low pH soils compared to the U-control. G2P (10 mM) was added at day 28 and average G2P concentrations increased within 5 d of G2P injection and remained relatively constant between 5 and 7 mM for the rest of the experiment. Phosphate increased to ca. 3 mM in org-P amended reactors, but was not detected in the control reactor. (b) U concentrations measured in control and org-P amended flow-through reactors after U injection (200 µM) at day 51. Error bars represent the standard deviations from the average measurements in the three org-P amended reactors. Dashed lines indicate the addition of G2P and U(VI).

5.4.3.2 Speciation of solid uranium in low pH flow-through column studies

Soil in the flow-through reactors was removed in cm-length sections after the experiments were completed. Each section was sequentially extracted and analyzed for U(VI) and P to determine the fraction(s) they were associated with (see Appendix C, Figures C.7-12 for extractions of individual reactors). Approximately 1.1 (± 0.1) μmol g^{-1} U(VI) was added to the soils and more than 95% was retained on the org-P amended columns compared to 95% retention on the U control soil. In addition, highest concentrations of total U(VI) added to the soils was found closest to the flow-through reactors' inlet and decreased dramatically as distance from the reactors' inlets increased (Figure 5.20). U(VI) in org-P amended reactors was extracted with a combination of AcOH and hydroxylamine indicative of the release of U-P minerals (Figure 5.20a). In contrast, U(VI) in the U control reactor was extracted primarily with AcOH indicative of the release of adsorbed U(VI) (Figure 5.20b).

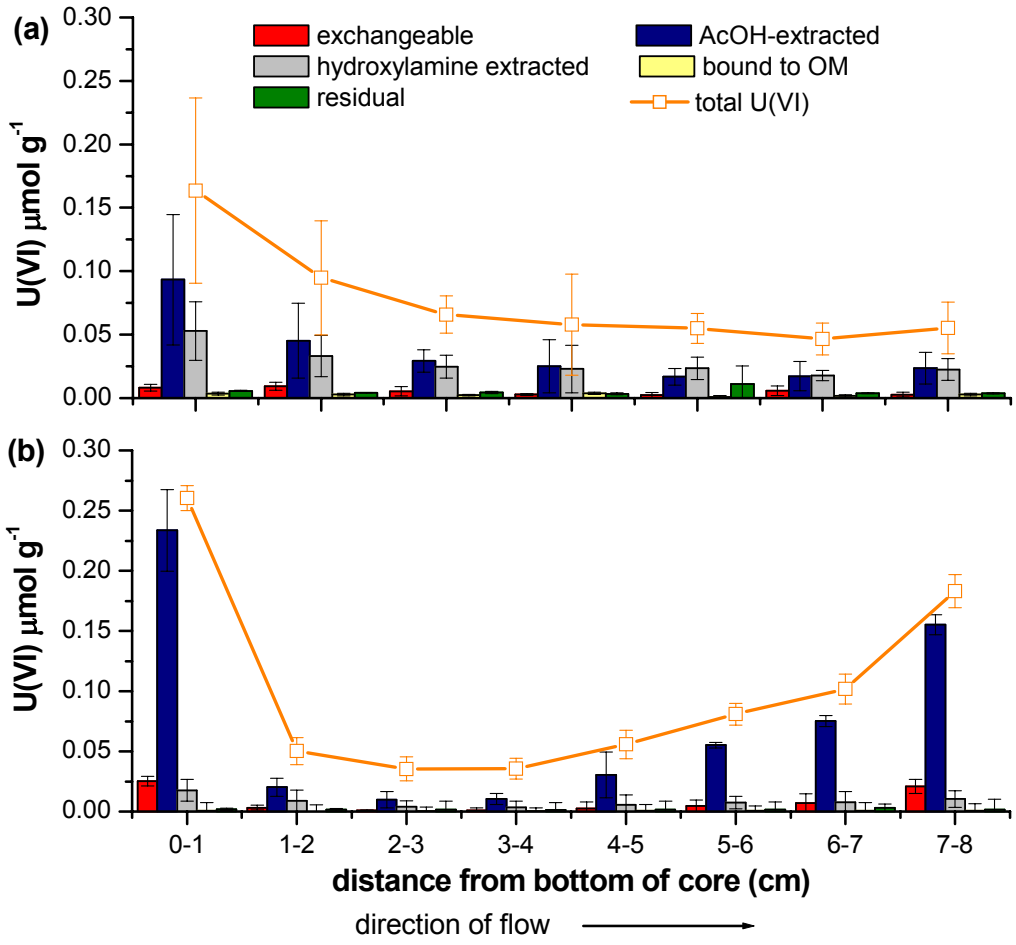

Figure 5.20 Average U (µmol g^{-1}) distributions in soil sections from (a) org-P amended and (b) U control low pH flow-through reactors as determined by sequential extraction. Soil sections nearest the influent inlet contained the highest concentrations of total. U(VI) in org-P amended reactors was released by a combination of AcOH and hydroxylamine indicative of U-P mineral precipitation. U(VI) in U control reactor was released primarily by AcOH indicative of U adsorbed to mineral surfaces.

Comparatively, total phosphate (ca. 8 (± 0.7) µmol g^{-1} total retained on the columns) and exchangeable phosphate were distributed evenly across the length the reactors (Figure 5.21). Phosphate released by AcOH and hydroxylamine was also distributed relatively evenly within the reactor indicative of U-P minerals.

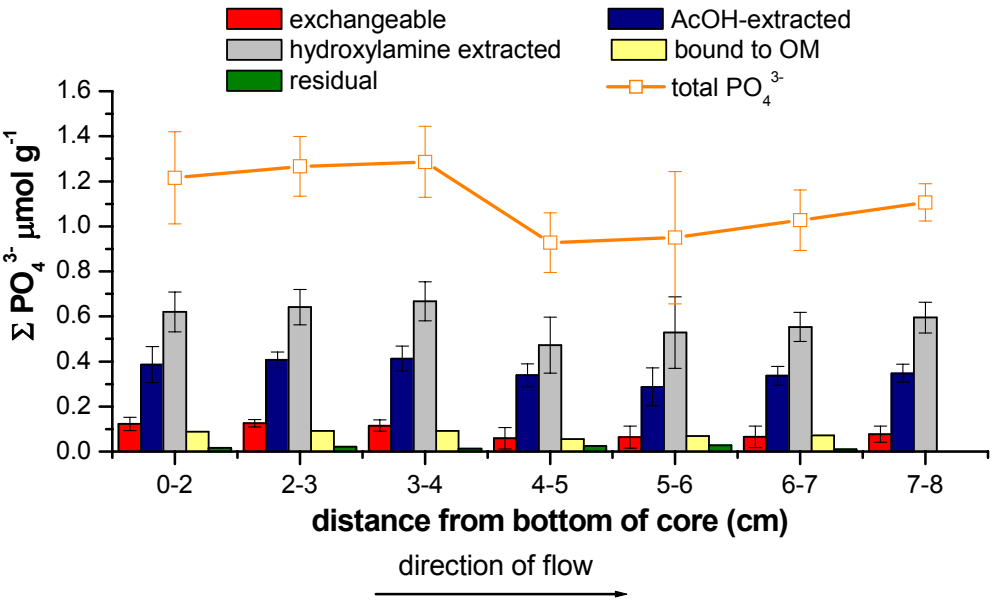

Figure 5.21 Average total phosphate (µmol g^{-1}) distribution in soil sections from the low pH flow-through reactor experiments as determined by sequential extraction. Phosphate concentrations were spread evenly across the length of the reactor and released primarily by AcOH and hydroxylamine.

Soil sections from each of the org-P amended and the U amended control flow-through reactors were analyzed by synchrotron X-ray absorption spectroscopy (XAS). The oxidation state of U in the soil samples was determined by U L_{III}-edge X-ray absorption near-edge structure (XANES). The normalized and background subtracted spectra of the samples (Figure 5.22) displayed the characteristic shoulder between 17,180 and 17,190 eV, which is consistent with U(VI) oxidation state.

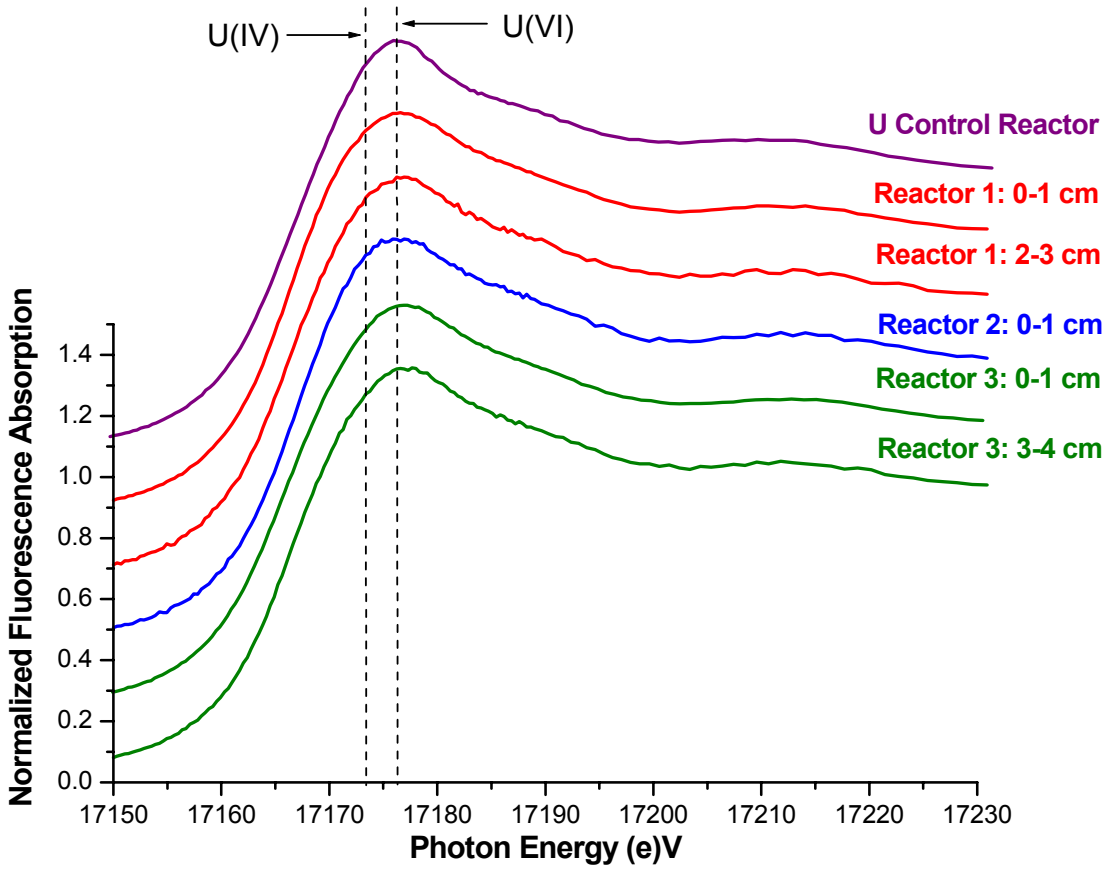

Figure 5.22 Uranium L_{III}-edge XANES spectra of the soil samples from the three org-P amended and the U(VI) amended control flow-through reactors conducted at pH 5.5. The cm designation indicates the reactor section that was analyzed as measured in cm from the inlet of the reactor.

The k^3-weighted extended X-ray absorption fine structure (EXAFS) data and fits for the soil samples from the low pH reactors are shown in Figure 5.23 and Figure 5.24. Fitting parameters are listed in Table 5.2. All samples show the presence of the O_{ax} shell at ~1.80 Å and the equatorial oxygen shells are split with 2 U-O_{eq} shells at ~2.30 Å and ~2.39 to 2.47 Å, except for the low pH Reactor 3 at 3-4 cm that has only one U-O_{eq} shell at 2.31 Å. The coordination numbers of O_{eq} atoms at 2.30 Å and 2.46 Å are approximately equally distributed in the control reactor compared to higher coordination numbers at ~2.30 Å in the org-P amended reactors. C was prevalent in all samples with shells at ~2.92 Å and Ns of 1 to 1.75. Fe shells at ~ 3.43 Å were found in the U-control,

Reactor 2, and Reactor 3, but not in the fit of Reactor 1. Instead, a Mn shell was included in the fit at 3.33 Å in Reactor 1.

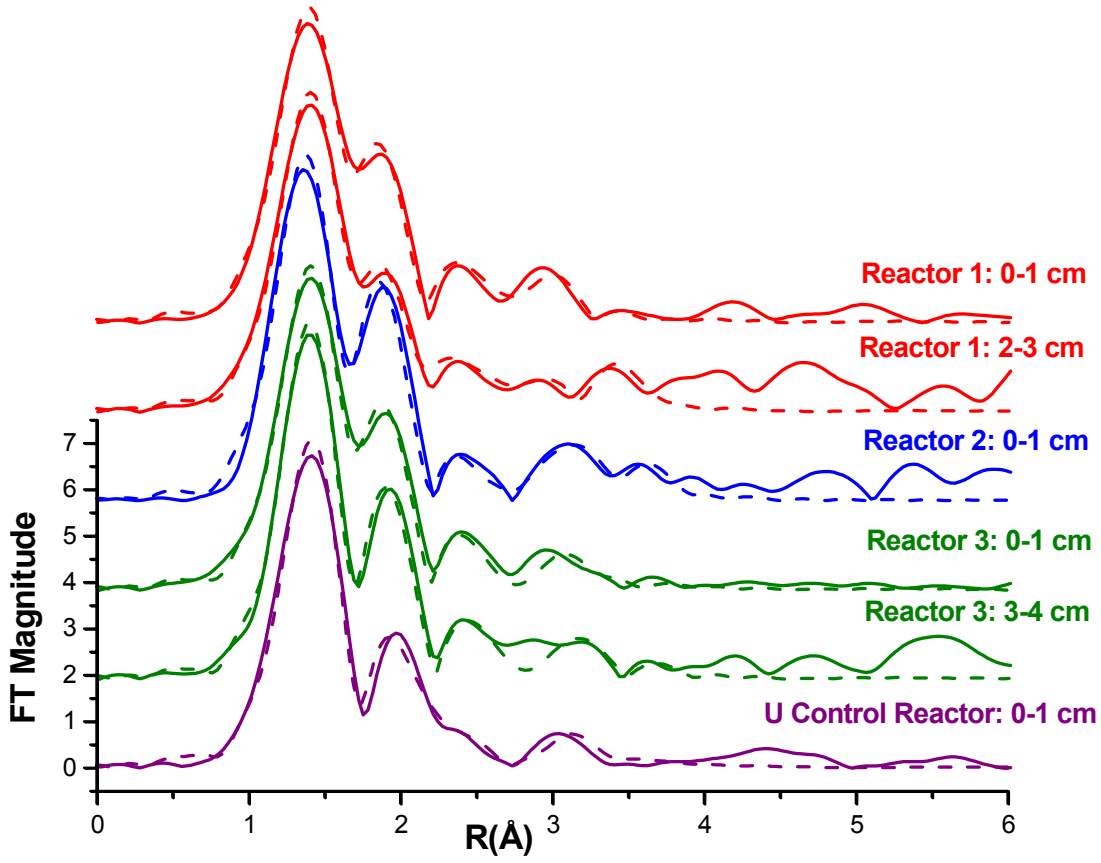

Figure 5.23 Uranium R-space diagrams of the L_{III}-edge EXAFS of the soil samples from the three org-P amended flow-through reactors compared to the U(VI) amended control reactor conducted at pH 5.5. Solid lines represent experimental data and dashed lines represent the fitted data. The cm designation indicates the reactor section that was analyzed as measured in cm from the inlet of the reactor.

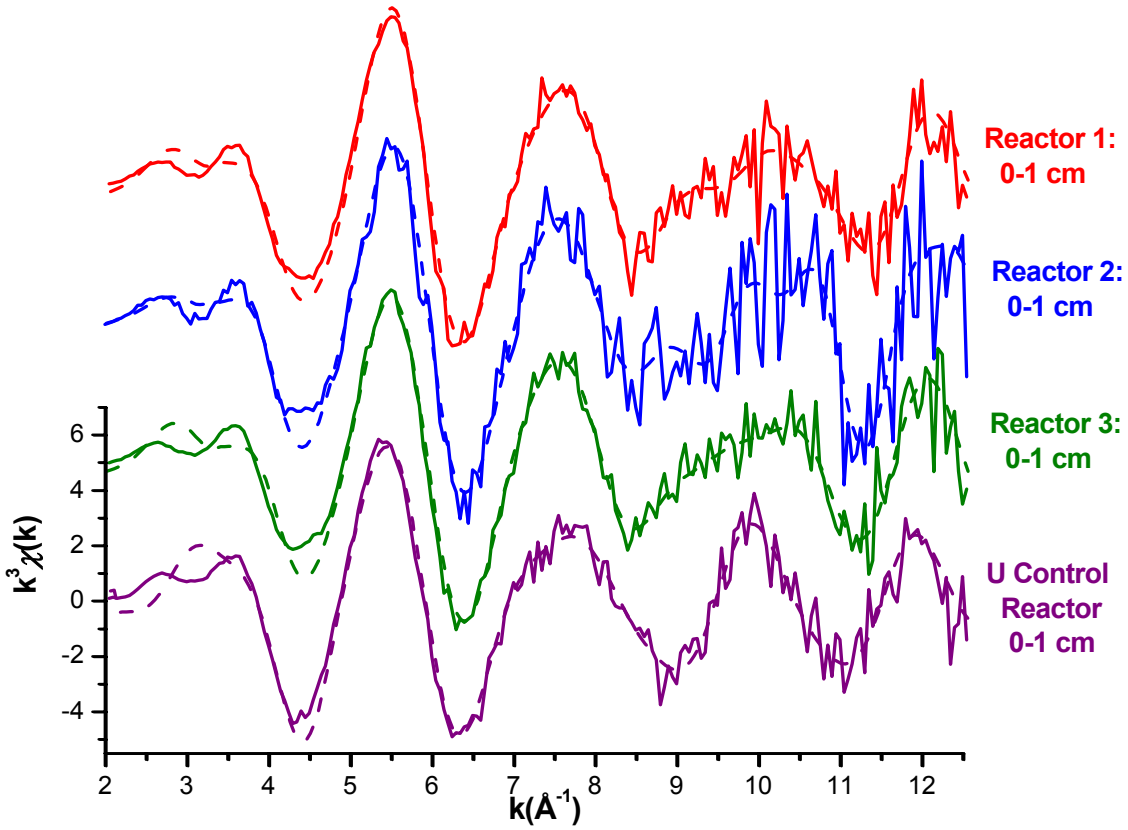

Figure 5.24 Uranium *k*-space diagrams of the L_{III}-edge EXAFS of the soil samples from the three org-P amended flow-through reactors compared to the U(VI) amended control reactor conducted at pH 5.5. Solid lines represent experimental data and dashed lines represent the fitted data. The cm designation indicates the reactor section that was analyzed as measured in cm from the inlet of the reactor.

Table 5.2 Parameters derived from fitting of U L_{III}-edge EXAFS of flow-through reactor soil samples conducted at pH 5.5.

Reactor	Shell	N	R (Å)	σ^2 (Å^2)	ΔE_0 (eV)	χ_v^2	R factor
U amended control	O_{ax}	2	1.80 (0.007)	0.004 (0.0009)	17.3 (1.53)	0.630	0.0130
	O_{eq}	1.28 (0.49)	2.35 (0.04)	0.003			
	O_{eq}	1.04 (0.55)	2.47 (0.05)	0.003			
	C	1.01 (0.4)	2.92 (0.02)	0.003			
	Fe	0.15 (0.1)	3.47 (0.04)	0.003			
Reactor 1	O_{ax}	2	1.79 (0.008)	0.005 (0.001)	12.7 (1.5)	0.735	0.0111
0-1 cm	O_{eq}	2.17 (0.6)	2.29 (0.01)	0.003			
	O_{eq}	0.64 (0.43)	2.45 (0.03)	0.003			
	C	1.44 (0.7)	2.93 (0.05)	0.003			
	Mn	0.29 (0.1)	3.39 (0.02)	0.003			
	Fe	N/A					
	P	0.25 (0.28)	3.5 (0.27)	0.005			
	POU MS*	0.5	3.58 (0.1)	0.005			
	OPOU MS*	0.25	3.71 (0.09)	0.005			
	PO dist**	1.42 (0.09)					
Reactor 1	O_{ax}	2	1.80 (0.01)	0.005 (0.002)	14.8 (2.9)	0.0162	0.0172
2-3 cm	O_{eq}	1.74 (0.6)	2.30 (0.03)	0.003			
	O_{eq}	0.93 (0.6)	2.45 (0.06)	0.003			
	C	1.05 (0.8)	2.93 (0.03)	0.003			
	Mn	0.19 (0.13)	3.33 (0.04)	0.003			
	Fe	N/A					
	P	0.98 (1.5)	3.62 (0.12)	0.005			
	POU MS*	1.96	3.72 (0.06)	0.005			
	OPOU MS*	0.98	3.86 (0.03)	0.005			
	PO dist**	1.56 (0.04)					
Reactor 2	O_{ax}	2	1.77 (0.01)	0.003 (0.001)	9.2 (2.4)	0.264	0.0129
0-1 cm	O_{eq}	2.70 (0.71)	2.28 (0.02)	0.003			
	O_{eq}	0.18 (0.5)	2.40 (0.2)	0.003			
	C	1.74 (0.6)	2.88 (0.02)	0.003			
	Mn	N/A					
	Fe	0.15 (0.23)	3.43 (0.06)	0.003			
	P	2.49 (1.9)	3.70 (0.05)	0.005			
	POU MS*	4.98	3.83 (0.02)	0.005			
	OPOU MS*	2.49	3.94 (0.02)	0.005			
	PO dist**	1.66 (0.03)					

Table 5.2 (cont)

Reactor	Shell	N	R (Å)	σ^2 (Å^2)	ΔE_0 (eV)	χ_v^2	R factor
Reactor 3	O_{ax}	2	1.79 (0.006)	0.004 (0.001)	12.9 (1.3)	0.263	0.0118
0-1 cm	O_{eq}	2.25 (0.5)	2.30 (0.009)	0.003			
	O_{eq}	0.33 (0.4)	2.48 (0.06)	0.003			
	C	1.5 (0.5)	2.93 (0.02)	0.003			
	Mn	N/A					
	Fe	0.12 (0.3)	3.41 (0.16)	0.003			
	P	0.07 (0.08)	3.68 (0.23)	0.005			
	POU MS*	0.15	3.86	0.005			
	OPOU MS*	0.07	3.91	0.005			
	PO dist**	1.61					
Reactor 3	O_{ax}	2	1.79 (0.008)	0.002 (0.001)	13.4 (1.9)	0.086	0.012
3-4 cm	O_{eq}	2.48 (0.9)	2.31 (0.01)	0.003 (0.002)			
	O_{eq}	N/A					
	C	1.75 (0.9)	2.95 (0.04)	0.003			
	Mn	N/A					
	Fe	0.22 (0.1)	3.49 (0.03)	0.003			
	P	1.55 (1.9)	3.77 (0.1)	0.005			
	POU MS*	3.10	3.87 (0.07)	0.005			
	OPOU MS*	1.55	3.96 (0.06)	0.005			
	PO dist**	1.65 (0.06)					

Errors are given in parentheses (no error means the value was fixed, or calculated from other parameters)

* MS denotes multiple scattering paths

** PO dist is the distance between the P-O in phosphate coordination (used for the MS paths)

cm denotes section of reactor analyzed as measured in cm from bottom of reactor (inlet end).

N/A indicates fitting of the shell did not improve the fit

2 C-O-U MS paths (not listed) improved the fitting for all samples

5.5 Discussion

Previous studies have demonstrated that microbial phosphatase activity promotes the immobilization of uranium phosphate minerals in pure cultures (Beazley et al., 2007; Beazley et al., 2009; Martinez et al., 2007) and contaminated soil slurries (Martinez, 2008). To develop a successful in situ remediation strategy, it is necessary to determine whether natural phosphatases can be expressed in soils from the contaminated waste site. Flow-through reactors have been successfully used to study the biogeochemical cycling of chemical species in soils and sediments (e.g. Carey and Taillefert, 2005; Roychoudhury, 2001; Roychoudhury et al., 1998). With these devices, parameters such as flow rate, pH, concentration of reactants, and oxygen concentration, can be adjusted to reflect in situ conditions or alter biogeochemical processes. In this study, flow-through reactor experiments were undertaken with soils from the ORFRC to determine whether (1) indigenous soil bacteria display phosphatase activity when supplied an organophosphate source, (2) pH and high nitrate concentrations affect natural phosphatase activity, (3) the solubility of U(VI) can be reduced through the precipitation of uranyl phosphate, and (4) soil permeability changes as a result of organophosphate amendments.

5.5.1 Phosphate production by phosphatase activity

The flow-through reactor experiments were conducted with soils from two different locations within the contaminated zone (Area 3) of the ORFRC. These soils represent the heterogeneity of subsurface environments at the ORFRC and were chosen for their distinct differences in pH (pH 3.7 and 7) and U content (0.22 and 0.063 μmol g^{-1}). Microbial diversity and abundance of phylotypes at the ORFRC are dependent on the

geochemistry of the soils (Akob et al., 2007; Madden et al., 2007), and previous PhyloChip microarray studies of soil slurry incubations conducted with ORFRC soil from the same location identified high microbial diversity at low pH, even among replicate samples (Martinez, 2008). Therefore, it is expected that these soils may contain distinctly different microbial assemblages and that phosphatase activity is affected by differences in pH and U(VI) concentration. Even though preliminary studies with flow-through reactors demonstrated the production of phosphate after amendment with organophosphate in the pH 3.7 soils (data not shown), the pH was raised in these experiments to accelerate reaction rates.

Phosphate concentrations in the reactor effluents reached ca. 500 μM within one day of organophosphate addition to both high and low pH flow-through reactors and continued to increase to steady state concentrations (ca. 1 to 3 mM) in 10 days compared to the negligible phosphate production observed in the U-control reactors (Figure 5.8 and Figure 5.19). Phosphate production remained relatively constant for the remainder of the experiments, suggesting that non-specific acid phosphatase (NSAP) activity is expressed constitutively in these soils. The presence of constitutively-expressed NSAPs may be advantageous for U(VI) bioremediation because phosphate production in these conditions is only limited by the concentration of the organophosphate substrate. In contrast, phosphatases induced only in limiting phosphate conditions (i.e. regulated phosphatases) should be deactivated at high phosphate concentrations (Vershinina and Znamenskaya, 2002) and may not provide the necessary amount of phosphate needed for U-P precipitation. Interestingly, phosphate concentrations were 50 – 60% higher in the effluent of the low pH flow-through reactors compared to the high pH reactors and were

not significantly affected by the addition of 200 μM U(VI). In turn, phosphate concentrations decreased by ca. 0.5 mM at both pH immediately after U(VI) addition, possibly due to a combination of U-P precipitation and U(VI) toxicity. Within ca. 10 days after U(VI) addition, however, phosphate production returned to previous intensity and even increased in the high pH reactors by ca. 50%. Previous studies with pure cultures of NSAP-carrying *Rahnella* sp. demonstrated a similar decrease in phosphate in aerobic conditions, as well as a reduction in cell viability immediately upon U(VI) addition to incubations and a rebound to previous concentrations within ca. 48 hr (Beazley et al., 2007). The rebound in cell viability was attributed to the fact that U(VI), initially adsorbed to cell membranes, was desorbed from the cell surface as U-P precipitated from the solution (Beazley et al., 2009). Although difficult to demonstrate, U(VI) addition to the flow-through reactors may have had the same effect on bacterial cells.

The addition of organophosphate to the flow-through reactors also provided a carbon substrate that stimulated microbial activity. The hydrolysis of G2P produces glycerol that can in turn be used as a carbon source by various microbes. Thus, the constitutively-expressed NSAPs may have supplied a carbon source for aerobic microorganisms in the high pH soils (Figure 5.7) and nitrate-reducing bacteria in the low pH soils (Figure 5.17). Nitrate reduction was observed in the low pH soils, even though the reactors remained oxic (Figure 5.15), suggesting that the higher activity of NSAPs in the low pH conditions compared to the high pH soils may have promoted nitrate reducing conditions in suboxic or anoxic niches (Patureau et al., 2000; Tiedje et al., 1982). In addition, uranium reducing conditions may have developed as a result of NSAP activity

and the depletion of nitrate in two of the low pH reactors (Figure 5.17). U XANES analysis, however, identified the U(VI) valence state in soils from these reactors (Figure 5.22) as well as in the high pH soils (Figure 5.11). Unless uraninite was in the colloidal form (Suzuki et al., 2002) in anaerobic niches in the low pH reactors, these results suggest that the majority of uranium remained oxidized.

5.5.2 Speciation of U(VI) in the solid phase

Our past studies on the biomineralization of U(VI) as a result of phosphatase activity were conducted in pure culture incubations in synthetic groundwater, and the characterization of the precipitate formed was straightforward. Distinctive yellow precipitate was observed after centrifugation of the incubation media and further analysis by synchrotron-based XRD and XAS identified the relatively pure mineral as chernikovite (Beazley et al., 2007; Beazley et al., 2009). In turn, adsorption of U(VI) to mineral surfaces is likely significant in soils and sediments, and distinguishing adsorption from precipitation of U(VI) in natural systems may be difficult. In this study, a sequential chemical extraction was compared with synchrotron-based XAS measurements to characterize the speciation of uranium in the solid-phase.

Only small concentrations of U(VI) were measured in the effluents of both soils amended with organophosphate compared to the U(VI)-amended controls (Figure 5.8 Figure 5.19), indicating that U(VI) was removed from solution by adsorption onto the solid phase or precipitation as uranium phosphate mineral. Interestingly, ca. 30% of the total U(VI) extracted from the high and low pH reactors was found within one cm of the reactor influent inlet (Figures 5.9 and 5.20), indicating that U(VI) was removed from solution immediately upon introduction, even if 200 μM U(VI) was continuously added

to the soils. In addition, the U(VI) within this section was extracted by both AcOH and hydroxylamine in the org-P amended reactors suggesting the release of U-P minerals. In contrast, the U(VI) in the U control reactors was released primarily by AcOH indicative of adsorbed U(VI). These findings are consistent with previous biomineralization incubations that demonstrated the rapid precipitation of uranyl phosphate within 1 hr of addition to incubations containing hydrolyzed phosphate (Beazley et al., 2007; Beazley et al., 2009). XAS measurements also confirmed that higher concentrations of U(VI) in the low pH reactors were found near the reactor inlet as the resolution of XANES and EXAFS spectra decreased dramatically 3 to 4 cm away from the inlet (data not shown). In contrast to the accumulation of U(VI) near the reactors' inlet, phosphate was distributed evenly throughout the soil (Figures 5.10 and 5.21) and found in high concentrations in the effluent (Figure 5.8). As previously observed (Wellman et al., 2006), phosphate added in similar flow-through columns is readily precipitated onto the soils near the injection points. Together with the steady-state production of phosphate at the output of the reactors, these findings suggest that phosphatase activity was occurring homogeneously throughout the reactor. The uniform distribution of phosphatase activity through the reactors is most advantageous for remediation purposes. It demonstrates that organophosphate can be spread over significant distances before being hydrolyzed.

The chemical extractions of phosphate in the original soils reveal most phosphate is either adsorbed to iron oxides (released by hydroxylamine) or bound to organic matter compounds (released by H_2O_2) while the fraction of phosphate extracted with AcOH is negligible in both soils (Figure 5.3). In turn, sequential extractions conducted with the same soils amended with uranium phosphate precipitates showed that uranium phosphate

is dissolved during sequential extraction with AcOH and hydroxylamine (Figure 5.5). Together, these data indicate that the fractions of phosphate extracted by AcOH and hydroxylamine represent the true fraction of uranium phosphate precipitated during the incubations. Thus, the precipitation of U-P minerals at low and circumneutral pH, identified by the fractions of phosphate extracted by AcOH and hydroxylamine, occurred primarily within the first 1 cm of the reactors' inlets (Figures 5.10 and 5.21), the soil layers displaying also the highest U(VI) concentrations extracted by AcOH and hydroxylamine (Figures 5.9 and 5.20).

Soil samples are heterogeneous and probably contain a mixture of surface complexes and precipitates. Therefore, the fitting of the EXAFS spectra of such samples reflect this complexity by producing lower U-ligand coordination numbers than that observed in pure phases (Bostick et al., 2002). P shells were included in all EXAFS fits of org-P amended reactor samples with radial U-P distances of ~3.6 Å that are indicative of monodentate coordination with phosphorus. U-P minerals are composed of sheets of square bipyramidal uranyl and tetrahedral phosphate $[(UO_2)(PO_4)]^-$ attached by interlayer charge-balancing cations (Catalano and Brown Jr., 2004; Locock and Burns, 2003), and higher P coordination numbers reflect the formation of these structured U-P sheets. As precipitation of U-P is more thermodynamically favorable at low pH (Figure 1.5), it is expected that higher P coordination numbers (N>1) should be observed in these samples. In fact, 3 of the low pH reactor samples contained P coordination numbers ≥ 1 (Table 5.2), and their corresponding EXAFS spectra demonstrated signals in the *k*-space region from 8.5 to 10.5 $Å^{-1}$ (Figure 5.24) characteristic of autunite-type minerals (Fuller et al., 2002). Interestingly, an N of 2.56 is observed in the fitting of the soil from the one of the

high pH org-P amended reactors (Table 5.1), suggesting that uranyl is coordinated by 2.56 P atoms. This data is in good agreement with the stoichiometric U:P ratio determined from chemical extractions of these soils (Figure 5.10) and indicative of U-P precipitation as observed in previous incubations with *Rahnella* sp. incubations (Table 4.2). In addition, the EXAFS spectra of soil samples from the high pH reactors demonstrate the typical autunite-type *k*-space region from 8.5 to 10.5 $Å^{-1}$ (Figure 5.13). These findings from both EXAFS fittings and chemical extractions suggest that U-P biomineralization occurred in both the high and low pH reactors.

Simultaneously, some samples from both high and low pH soils display P coordination numbers (N<1) (Table 5.1 and Table 5.2) that are common for U-P adsorption because uranyl coordination in such interactions is shared between phosphate and atoms associated with the soil surface. Though it is difficult to distinguish adsorption and precipitation processes by EXAFS alone (Arey et al., 1999; Bostick et al., 2002), the EXAFS spectra clearly show that U(VI) is coordinated with phosphate at both pH across each reactor (Table 5.1 and Table 5.2). Synchrotron microprobe analysis indicates that U(VI) is distributed in discrete areas on the surface of the soil and appears to collect in micropores (Figure 5.14). It is suggested that adsorption of U(VI) to mineral surfaces in the presence of phosphate may be a precursor to the precipitation of uranyl phosphate minerals (Sato et al., 1997), and these surface pockets may provide the ideal environment for U-P precipitation. In fact, previous electron microprobe and TEM analysis of ORFRC soils determined that U-P precipitates in shale micropores contained 2 orders of magnitude more uranium than that adsorbed onto iron oxide surfaces (Stubbs et al., 2006).

U(VI) was more tightly bound to the original high pH soils compared to the original low pH soils (Figure 5.3), and U(VI) adsorption experiments with the same soils confirmed this behavior (Figure 5.4). These data suggest that U(VI) strongly adsorbs to mineral surfaces such as iron oxides, present in high concentrations in ORFRC soils (Stubbs et al., 2006), that display maximum U(VI) adsorption between pH 6 and 7 (Hsi and Langmuir, 1985; Langmuir, 1997). Indeed, at pH > 7, deprotonation of iron oxide surfaces provides negatively-charged surface sites for complexation with positively-charged aqueous uranyl species UO_2^{2+}, UO_2OH^+, and $(UO_2)_2(OH)_2^{2+}$ in the absence of carbonate (Barnett et al., 2002; Cheng et al., 2006). Simultaneously, negatively-charged phosphate does likely not adsorb significantly to iron oxides at circumneutral pH because their surface charge is most probably neutral or slightly negatively charged (Stumm and Morgan, 1996). U(VI) in the original low pH soil (35% extracted by Mg^{2+} and 30% extracted by AcOH) was loosely bound (Figure 5.3), suggesting that much of the U(VI) was attached to the mineral surface as weak outer-sphere electrostatic complexes that are easily desorbed by competing cations. U(VI) adsorption experiments performed on the same soils confirm that most uranium is exchangeable by Mg^{2+} (Figure 5.4). At lower pH, both uranyl and mineral surfaces tend to be positively charged, and strong surface complexation may not be as favorable as at high pH unless phosphate is pre-adsorbed to iron oxides (Cheng et al., 2004). Phosphate adsorbs readily to iron oxides at low pH because iron oxides are positively charged ($pH_{ZPC} \leq 7$) and phosphate is negatively charged (Stumm, 1997). Indeed, the majority of phosphate in the original low pH soil was extracted by hydroxylamine (Figure 5.3), suggesting that phosphate is primarily adsorbed to iron oxides in these soils. Adsorption column studies of U(VI) and

phosphate on goethite-coated sand in low pH conditions demonstrated that the adsorption of phosphate onto mineral surfaces prior to U(VI) addition greatly and irreversibly enhances uranyl adsorption by formation of ternary complexes (Cheng et al., 2007). Thus, from the sequential extractions of the original soils, it appears that uranium adsorption to the soils should be favored at circumneutral pH, provided that carbonates are not produced in significant concentrations by microbial processes, while phosphate adsorption should be favored at low pH.

EXAFS fittings of the soil samples indicated split O_{eq} shells (at ~ 2.3 and 2.45 Å) in all but one sample (3-4 cm section of the low pH Reactor 3) (Table 5.1 and Table 5.2). Uranyl equatorial oxygen atoms typically display U-O_{eq} distances of ~2.30 Å; however, uranyl surface complexes can stretch some of the O_{eq} and thus increase bond distances up to ~ 2.45 Å depending on the ligand, which splits the O_{eq} shells. Split equatorial oxygen shells are common in uranyl complexes with minerals including, alumina silicates (Hudson et al., 1999; Sylwester et al., 2000), apatite (Fuller et al., 2003), and iron oxides (Waite et al., 1994). In the latter complexes, two of the shorter O_{eq} are bound to two neighboring iron oxide edge oxygens in a bidentate fashion, forming Fe-O_{eq}-U angles of ca. 112º (Bargar et al., 2000). The formation of Fe-O_{eq}-U complexes leads to U-Fe radial distances of ~3.43 Å that are observed in the majority of the reactor samples at both pHs, suggesting that uranyl adsorbs to iron oxides as an inner-sphere complex. Higher Fe coordination numbers are observed in soils from the high pH reactors compared to the low pH soils, suggesting that U-Fe adsorption is more prevalent at high pH than at low pH. These findings are in good agreement with the bulk extraction data that showed

adsorbed U(VI) at high pH requires a stronger extracting reagent than adsorbed U(VI) at lower pH (Figure 5.4).

O_{eq} atoms at ~2.45 Å are also common in coordination complexes with carbonates (U-C radial distance ~2.90 Å) and indicate the bidentate sharing of two oxygen atoms between uranyl and carbonate. Ternary complexes of Fe-U-C (Bargar et al., 2000) are common in natural systems (Waite et al., 1994) and are observed in ORFRC soils (Bostick et al., 2002). The higher O_{eq} coordination numbers at ~ 2.45 Å in the two U-control samples suggests that Fe-U-C ternary complexes are more abundant at both pHs in soils amended with U(VI) only than in soils amended with both U(VI) and org-P. This is not surprising as adsorption to mineral surfaces is likely the primary removal mechanism for U(VI) in the control samples. Yet, the C shell at ~2.90 Å is pronounced in all org-P amended reactors, and coordination numbers of C atoms (~1.48) are comparable at both pH. Carbonate is expected to play a more significant role at high pH due to the formation of uranyl carbonate complexes that may prevent adsorption of U(VI) in the high pH soils and thus promote reactivity of U(VI) with phosphate. However, these findings also suggest that the high microbial activity observed at low pH produced large enough quantities of bicarbonate to complex U(VI) and favor removal of U(VI) by adsorption.

EXAFS fittings of the low pH soil samples also indicate a lower number of Fe atoms in coordination with U(VI) than in high pH samples. In fact, Fe could not be included in the fit of two samples from one of the reactors amended with org-P. These findings suggest that U(VI) adsorption to iron oxides is not a dominant mechanism at low pH or that >Fe-P-U ternary complexes are formed on iron oxide surfaces (Cheng et al.,

2006). Overall, the prevalence of the 2.30 Å equatorial oxygen in the org-P amended reactors at both pH suggests that, even in the presence of high concentrations of carbonate and adsorption to iron oxides, uranyl is primarily bound to phosphate. These findings suggest that, at high pH, uranyl precipitates with phosphate and, at low pH, uranyl is primarily associated with phosphate as both adsorbed onto Fe and Mn oxides and precipitated as U-P minerals.

In summary, the bulk extraction and EXAFS data, thus far are both indicative of U-P mineral formation at both low and high pH. In the next section, a reactive transport model is presented to calculate net rates of production and consumption of uranium, phosphate, and all other species that could be used to differentiate the mechanisms of U(VI) and phosphate removal on the solid phase.

5.5.3 Transport parameters and net reaction rates of organophosphate hydrolysis, nitrate reduction, and U(VI) precipitation

The fate of a chemical species through a porous medium is determined by its transport through the medium and its reactivity. Transport is described by advection, or the movement of the fluid through the pores at some velocity, and dispersion, including both molecular and mechanical dispersion (Schnoor, 1996) and can be determined with chemical tracers using transport models (Roychoudhury, 2001; Roychoudhury et al., 1998). For this study, a one-dimensional advection-dispersion model (Equation 5-1) was used to determine the dispersion coefficient (D), the advection rate (v), and the retardation factor (R) within the reactors (Roychoudhury et al., 1998), using the bromide breakthrough curve.

$$R\frac{dC}{dt} = D\frac{\partial^2 C}{\partial x^2} - v\frac{\partial C}{\partial x} \qquad (5\text{-}1)$$

The analytical solution to the governing equation (Van Genuchten, 1981) was used with an optimization procedure to calculate the three parameters. The optimization procedure, written in Matlab™, minimizes the difference between the data and the analytical solution of the differential equation to determine the three unknown parameters. The boundary conditions consistent with a flow-through reactor with continuous input of chemical species include:

$$C(x,0) = 0 \qquad C(0,t) = C_0 \qquad \frac{\partial}{\partial x}C(L,t) = 0 \qquad (5\text{-}2)$$

where x is the spatial variable in the reactor, t is time, L is the total length of the reactor, and C_0 is the input concentration of bromide.

The model was used to determine transport parameters R, D, and v in the flow-through reactors using the bromide breakthrough curves. Bromide was introduced at day 1 in the high-pH flow-through reactors, and its concentration in the influent remained constant throughout the experiment. Bromide was introduced at day 28 in the low-pH flow-through reactors, removed at day 44, and re-introduced at day 51. The modeled average bromide concentrations fit the data well for both high-pH and low-pH reactors (Figure 5.25). Table 5.3 lists the average transport parameters, R, D, and v, for each system (see Table C. 1 in Appendix C for transport parameters determined for individual reactors).

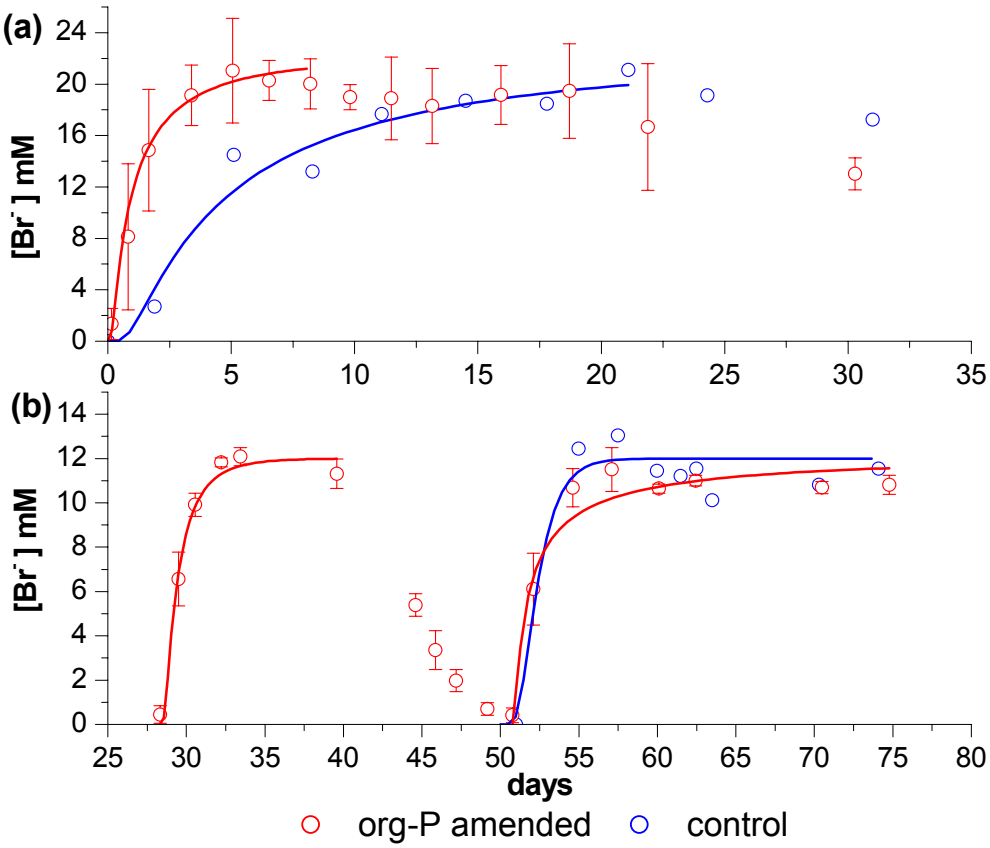

Figure 5.25 Bromide breakthrough curve modeled (solid lines) with a one-dimensional transport equation (Equation 5-2) from average bromide concentrations from flow-through reactors at pH (a) 7 and (b) 5.5. The open circles represent the experimental data (red for org-P amended and blue for controls) and error bars represent the standard deviations from the average measurements in the three org-P amended reactors.

Table 5.3 Average transport parameters determined with a one-dimensional advection-dispersion model of the average bromide concentrations in the effluent of flow-through reactors.

	Reactor	Retardation Factor (R)	Dispersion coefficient (D) (cm^2 sec^{-1})	Advection Rate (υ) (cm sec^{-1})
High pH	org-P amended	0.99	9.8 (± 8) 10^{-4}	7.4 (± 7.7) 10^{-5}
	U-control	0.99	1.7 10^{-4}	1.6 10^{-5}
Low pH	org-P amended	0.99	3.2 (± 3) 10^{-4}	6.3 (± 0.8) 10^{-5}
	org-P amended	0.99	1.5 (± 0.7) 10^{-4}	2.2 (± 2.9) 10^{-5}
	U-control	0.99	3.3 10^{-5}	3.6 10^{-5}

As expected, the retardation factors for all reactors are ca. 1 indicating that the mean transport of bromide through the flow-through reactors is not affected by adsorption of bromide. Diffusion coefficients indicate diffusion is dispersive. The calculated advection rate and dispersion coefficients in the low pH soils amended with org-P are respectively 3 times and one-half lower after day 50 than between day 28 and 40 during the incubations, indicating the porosity of the soil decreased over time probably due to mineral precipitation.

The net production or consumption rates of phosphate, U(VI), G2P, nitrate, and nitrite were determined for time periods during which some of the species of interest were constantly injected into the reactors and chemical changes were observed in the effluents of the reactors. The boundary conditions were (Equation 5-3),

$$C(x,t_0) = C_r \qquad -D\frac{\partial C}{\partial x} + vC\big|_{x=0} = vC_0 \qquad \frac{\partial}{\partial x}C(L,t) = 0 \qquad (5\text{-}3)$$

where $t_0 \geq 0$ is the initial time selected to determine rates during a particular time period, C_r is the concentration of the species of interest across the reactor assuming that the concentration of the effluent is representative of the concentration in the reactors, and all

other parameters are the same as previously. The transport parameters calculated from the bromide breakthrough curves were averaged for each reactor and used with the analytical solution to the governing equation (Van Genuchten, 1981) to determine net reaction rates in each reactor by fitting the experimental data in Matlab™ using the least-squares optimization procedure described previously. A typical example of the type of fitting and rates obtained with these calculations is presented in Figure 5.26. (See Appendix C, Figures C.13-20 for individual reactor fittings).

Table 5.4 Net reaction rates for dissolved PO_4^{3-}, G2P, UO_2^{2+}, NO_2^-, and NO_3^- in the flow-through reactors conducted at pH 5.5 as determined by the one-dimensional reactive transport model. Positive and negative rates indicate production and consumption of a species, respectively.

Reactor	Days	PO_4^{3-} (mM d^{-1})	G2P (mM d^{-1})	UO_2^{2+} (μM d^{-1})	NO_2^- (mM d^{-1})	NO_3^- (mM d^{-1})
Low pH						
U-control	28 - 78	0	0		0	-0.46
	28 - 50	0	0		0	
	50 - 60	0	0		0	
	60 - 78	0	0	-0.87	0	
Reactor 1	28 - 78	0.92	-1.4			
	28 - 50				1.0	-2.0
	50 - 60				$-2.0\ 10^{-6}$	
	60 - 78			-8.6		
Reactor 2	28 - 78	0.69	-1.1			
	28 - 50				0.4	-1.3
	50 - 60				2.1	-3.2
	60 - 78			-6.9	$-2.7\ 10^{-6}$	
Reactor 3	28 - 78	0.60	-1.3			
	28 - 50				0.5	-1.4
	50 - 60				$-2.8\ 10^{-6}$	-3.2
	60 - 78			-6.9		
Average org-P amended	28 - 78	0.73 ± 0.17	-1.3 ± 0.15			
	28 - 50				0.63 ± 0.3	-1.6 ± 0.4
	50 - 60					-2.6 ± 0.98
	60 - 78			-7.5 ± 0.98	$-2.5\ (\pm 0.4)\ 10^{-7}$	
High pH						
U-control	6 - 30	0		-9.3	0	0
Reactor 1	6 - 30	0.29		-80	0	0
Reactor 2	6 - 30	0.23		-29	0	0
Reactor 3	6 - 30	0.79		-15	0	0
Average org-P amended	6 - 30	0.43 ± 0.31		-41 ± 34	0	0

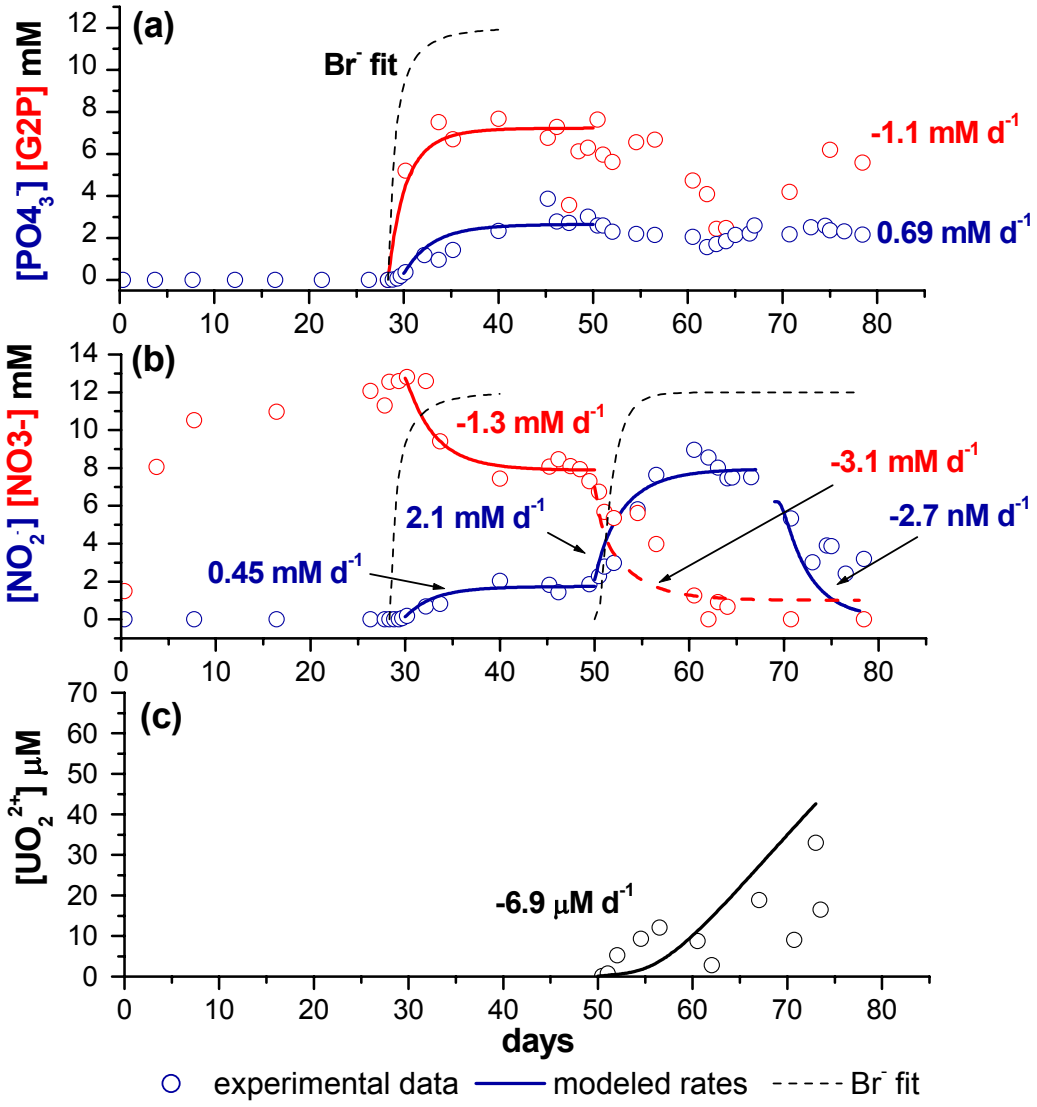

Figure 5.26 Reactor 2 experimental (open circles) vs. modeled (solid lines) data from a one-dimensional reactive transport model for (a) G2P and PO_4^{3-}, (b) NO_2^- and NO_3^-, and (c) PO_4^{3-} and UO_2^{2+} (solid red line represents total net consumption rate (adsorption + precipitation; dashed red line represents net consumption rate from precipitation only). Positive and negative rates indicate net production and consumption of a species, respectively. Dashed black lines represent the modeled bromide breakthrough curves.

Net phosphate production rates within ca. 10 days after organophosphate amendments in the low pH soils (0.73 ± 0.17 mM d^{-1}) were approximately 1.7 times higher compared to the high pH soils (0.43 ± 0.31 mM d^{-1}), suggesting that the indigenous microorganisms in the more contaminated low pH soil were using phosphatase activity as a defense mechanism against toxic U(VI) (Macaskie et al., 1994; Montgomery et al., 1995; Powers et al., 2002; Sobecky et al., 1996; Yong and Macaskie, 1999). In addition, 3 times as much phosphate was extracted from low pH soils compared to the circumneutral soils (Figures 5.10 and 5.21) confirming higher phosphate production rates at the lower pH. The greater average net rate of G2P consumption (-1.3 ± 0.15 mM d^{-1}) in the low pH soils compared to the average net production of phosphate, suggests that an average 0.57 (± 0.23) mM d^{-1} phosphate was consumed by other reactions, such as adsorption and precipitation. Interestingly, a much higher net phosphate production rate is observed for the high pH Reactor 3 (0.79 mM d^{-1}) that agrees with higher P coordination numbers as determined by EXAFS (Table 5.1), suggesting the removal of P by U-P precipitation.

The introduction of G2P also induced microbial denitrification at low pH (Figure 5.17), and net nitrate consumption rates of -1.6 (± 0.38) mM d^{-1} were calculated compared to corresponding net nitrite production rates of 0.63 (± 0.3) mM d^{-1} between days 28 and 50. These data suggest that nitrate was reduced further to NH_4^+ or N_2 and by-products of denitrification. Nitrate and nitrite reduction continued throughout the remainder of the experiment in Reactors 2 and 3, while both processes ceased in Reactor 1 (Figure 5.27). Nitrate concentrations followed the same trend as G2P concentrations in each reactor suggesting the respiration of G2P was driving nitrate reduction (Figure

5.27). The high rates of nitrate reduction coupled to G2P respiration likely introduced high levels of carbonate and contributed to the carbon signal observed in the EXAFS data at low pH (Table 5.2). .

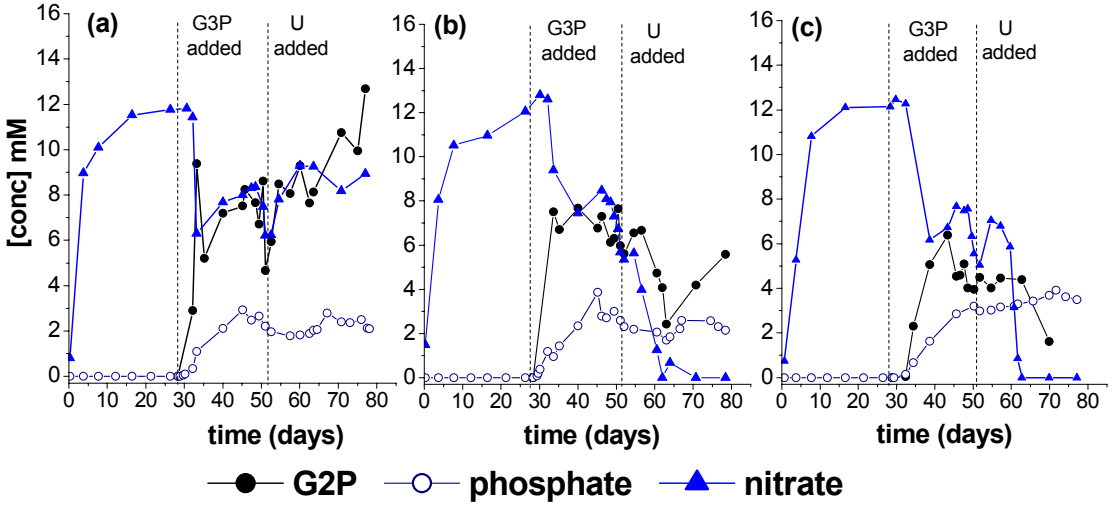

Figure 5.27. G2P, phosphate, and nitrate concentrations in the effluents of org-P amended reactors containing low pH soils as a function of time in (a) Reactor 1, (b) Reactor 2, and (c) Reactor 3. G2P (10 mM) was added at day 28 and 10 mM nitrate was continuously pumped into the reactors from day 1. Dashed lines indicate the addition of G2P and U(VI).

Batch U(VI) adsorption experiments conducted with ORFRC soils revealed that the high pH soil adsorbed more U(VI) as determined by the remaining soluble U(VI) in the supernatant (Figure 5.4). Distribution coefficients, K_D, for the two soils were determined using Equation 5-4 (Knox et al., 2008)

$$K_D = \frac{V_{spike}(C_{spike} - C_{final})}{C_{final} * M_{mineral}} \quad (5\text{-}4)$$

where C_{spike} is the U(VI) concentration in the solution prior to soil addition (mg L^{-1}), C_{final}

is the U(VI) concentration in the solution after contact with the soil (mg L^{-1}), $M_{mineral}$ is the soil mass (g), and V_{spike} is the volume of the solution (mL). K_D values of 1218 mL g^{-1} and 8.9 mL g^{-1} were found for the high and low pH soils, respectively, in agreement with previously reported K_D values ranging between 15 and 10000 mL g^{-1} (pH 1 to 7) for ORFRC soils (Barnett et al., 2002).

The transport of a chemical species through a porous medium is affected by both the porosity of the medium and adsorption on to the solid phase and can be described by the retardation factor, R (Schnoor, 1996) according to Equation 5-5:

$$R = 1 + \frac{\rho_B K_D}{\phi} \qquad (5\text{-}5)$$

where ρ_B is the bulk density of the soil (g/cm^3), K_D is the distribution coefficient, and ϕ is the porosity of the soil (mL/g). The R values calculated from Equation 5-5 using the batch U(VI) adsorption experiments indicate that the high pH soil displayed a much higher retardation factor (R = 9136) compared to the low pH soil (R = 30.7). These calculations suggest that the transport of U(VI) should be much slower in the high pH soils compared to the low pH soils. Indeed the net removal rates of U(VI), including both adsorption and precipitation of U-P minerals (when the retardation factor is set at 0.99), in the org-P amended reactors at high pH (-41 ± 34 μM d^{-1}) are much higher than in the low pH reactors (-7.5 ± 0.98 μM d^{-1}) (Table 5.4). In addition, the net U(VI) removal rates in the U-control reactors were lower at both pH than the corresponding removal rates in the org-P amended reactors, indicating that the precipitation of U-P minerals increased removal rates by 88 and 77%, respectively, in the low and high pH soils.

The combination of the solid phase extractions, EXAFS analyses, and transport model data show that uranium phosphate precipitation is the major mechanism of

removal of U(VI) in the high pH soils, while U(VI) is also removed by adsorption onto iron oxides through formation of ternary U-P-Fe complexes in the low pH soils. Uranium was primarily released with AcOH and hydroxylamine (the extractants shown to dissolve uranium phosphate minerals) during sequential extraction of the high and low pH soils compared to release by AcOH only in U control reactors. The coordination number of uranium to phosphorus measured by EXAFS is greater than one in most samples of both soils, suggesting the precipitation of U-P minerals.

5.6 Conclusions

Flow-through reactor experiments with contaminated soils from the ORFRC were conducted to determine whether (1) indigenous soil bacteria displayed phosphatase activity when supplied an organophosphate source, (2) pH and high nitrate concentrations affected natural phosphatase activity, (3) the solubility of U(VI) was reduced through the precipitation of uranyl phosphates, and (4) soil permeability changes as a result of organophosphate amendments. The results clearly indicate that the addition of an organophosphate substrate as sole carbon and phosphorus source to ORFRC soils promotes the expression of indigenous phosphatases. High concentrations of phosphate were detected in flow-through reactor effluents within one day of G2P and G3P amendments at both low and high pH, compared to negligible phosphate production in U-control reactors, indicating that phosphatase-carrying microorganisms are readily stimulated by the organophosphate substrate. Steady-state concentrations of phosphate were reached within days after addition, suggesting that non-specific acid phosphatase activity was expressed constitutively. In addition, phosphate was distributed evenly

throughout the reactor columns, demonstrating that organophosphate hydrolysis occurred homogeneously inside the soil reactors. These findings have important implications for the development of future in situ bioremediation strategies. First, addition of a labile organophosphate, such as G2P/G3P, should not impede hydraulic flow and clog injection valves observed with the addition of free orthophosphate. Second, the solubility and lability of G2P/G3P allows for greater surface coverage, thereby increasing the bioavailability of the organophosphate for hydrolysis. Finally, the presence of constitutively-expressed phosphatases in ORFRC soils represents advantage because phosphate production should only be limited by organophosphate availability.

Despite the continuous input of aerated groundwater to the soils, dissolved oxygen concentrations decreased in both soils as additional evidence that microbial activity was intense during these incubations. In fact, nitrate and nitrite reduction were observed in two of the reactors at low pH, suggesting that nitrate reducing conditions were occurring in small anaerobic microniches. Interestingly, phosphatase activity was not affected by nitrate and nitrite reduction, and higher net phosphate production rates were observed at lower pH compared to higher pH suggesting that indigenous microorganisms in the more contaminated low pH soil were using phosphatase activity as a defense mechanism against U(VI).

XANES and μ-XANES analyses of soils indicated uranium maintained the U(VI) oxidation state throughout the experiments even on a micron-scale, suggesting that conditions were not favorable for microbial U(VI) reduction. Spatial elemental mapping of soils amended with org-P in the presence of phosphatase activity, demonstrated that U(VI) was distributed discretely on soil surfaces and appeared to collect in small

micropores. These small concentrated areas of uranyl may provide the ideal environment for the mineralization of uranium phosphate.

The combination of solid-phase extractions schemes, EXAFS measurements, and reactive transport modeling demonstrated that U(VI) was primarily precipitated as uranyl phosphate minerals at high pH and precipitated as uranyl phosphate and partially adsorbed to iron-phosphate complexes at low pH.

The results of this study indicate that the biomineralization of U(VI) phosphate as a result of phosphatase activity in contaminated soils is an effective strategy for the remediation of uranium. Biomineralization of U(VI) phosphate was observed over a wide pH range and in the presence of high uranium and nitrate concentrations, and may be a complementary approach to bioreduction which requires high pH and low nitrate conditions.

5.7 Acknowledgements

This research was supported by the Office of Science (BER), U. S. Department of Energy Grant No. DE-FG02-04ER63906. Portions of this research were carried out at the Stanford Synchrotron Radiation Lightsource, a national user facility operated by Stanford University on behalf of the U.S. Department of Energy, Office of Basic Energy Sciences. The SSRL Structural Molecular Biology Program is supported by the Department of Energy, Office of Biological and Environmental Research, and by the National Institutes of Health, National Center for Research Resources, Biomedical Technology Program.

CHAPTER 6

CONCLUSIONS

The cleanup of uranium contaminated groundwater and soils at DOE facilities across the United States is a major undertaking and research over the past 15 years has focused on new and innovative methods of remediation. This dissertation examines the potential of a new and effective strategy for the bioremediation of uranium via microbial phosphatase activity. The strategy involves the addition of organophosphate compound as sole carbon and phosphorus source in soils to activate non-specific acid phosphatases that would result in the chemical precipitation of uranium phosphate minerals in both aerobic and anaerobic conditions. The main hypotheses tested in this thesis include:

1. Bacterial isolates from a contaminated waste site express phosphatase activity when provided an organophosphate substrate as sole C and P source in both pure cultures and contaminated soils.
2. Sufficient phosphate is hydrolyzed to precipitation U-P minerals.
3. Phosphatase activity and U-P biomineralization are affected by pH.

Pure culture incubations in aerobic conditions were conducted with three microbial isolates from the DOE ORFRC contaminated waste site. The objectives of this work were to (1) determine whether the strains hydrolyzed sufficient phosphate from an organophosphate substrate to precipitate uranium, (2) determine whether pH has an effect on phosphatase activity and U(VI) precipitation, and (3) identify the uranium solid phase

formed during biomineralization. Two of the bacterial strains studied, *Rahnella* sp. Y9602 and *Bacillus* sp. Y92 displayed phosphatase activity but *Rahnella* sp. Y9602 hydrolyzed 9 times more G3P than *Bacillus* sp. Y92 after 120 h regardless of the presence of uranium. Phosphate production was sufficient to precipitate 73 to 95% total U(VI) at pH 5.5 in the presence of 15 mM nitrate within 1 h of the addition of U(VI) to incubations.

Incubations of *Rahnella* sp. Y9602 were also conducted at different pH to determine the most favorable pH for phosphatase activity and uranium precipitation. Hydrolysis of G3P demonstrated a dependence on pH and uranium addition. *Rahnella* sp. Y9602 hydrolyzed 1.5 times more G3P at pH 7.0 compared to pH 4.5 in the absence of U(VI) most probably due to the expression of both alkaline and acidic phosphatases. In the presence of U(VI), however, 4 times more G3P was hydrolyzed at pH 7.0 than at pH 4.5. U(VI) precipitation was also dependent on pH. Only 28% of initial U(VI) was precipitated at pH 4.5 compared to 90 to 97% precipitation at pH 5.5 and 7.0, respectively. U-P precipitation is more favorable at pH 5.5 to 7.0 due the increased electronegativity of phosphate at the higher pH.

Solid-phase analysis by synchrotron-based XAS identified the mineral formed during uranyl biomineralization as an autunite/meta-autunite type mineral with a monodentate bond formed between the uranyl and phosphate molecules. The precipitates formed at pH 5.5 contained ~3 more P coordinating molecules than the precipitates at pH 7.0, suggesting the existence of a mixture of uranyl phosphate and uranyl hydroxide minerals. The biological uranyl phosphate displayed approximately the same EXAFS structure as a chemical uranyl phosphate precipitate at pH 5.5, indicating that the

precipitation of uranyl phosphate was a chemical process, though induced by the microbial hydrolysis of organophosphate. This work demonstrated that microbial phosphatase activity hydrolyzed sufficient phosphate to precipitate a highly insoluble uranyl phosphate mineral even at low pH and in the presence of high nitrate concentrations provided that aerobic conditions were maintained during the incubations.

Pure culture incubations were then conducted with *Rahnella* sp. Y9602 in anaerobic conditions to determine whether (1) the microbe could grow anaerobically with nitrate as the terminal electron acceptor, (2) sufficient phosphate was hydrolyzed to precipitate U(VI), and (3) the same mineral was formed as in aerobic conditions. *Rahnella* sp. Y9602 was able to respire anaerobically on nitrate as a terminal electron acceptor in the presence of G3P as the sole carbon and phosphorus source and produced nitrite as reduced metabolite which eventually proved toxic to the organism. Even in the presence of nitrite, *Rahnella* sp. Y9602 hydrolyzed sufficient phosphate to precipitate 95% total U(VI) at pH 5.5.

Synchrotron-based solid-phase analyses demonstrated that the same mineral was formed during both aerobic and anaerobic incubations with *Rahnella* sp. Y9602.. XANES analysis of the anaerobic precipitate indicated a U(VI) oxidation state demonstrating that *Rahnella* sp. Y9602 did not reduce U(VI). EXAFS analysis identified the precipitate formed as an autunite/meta-autunite mineral with a structure approximately the same as that of the aerobic mineral formed during aerobic incubations with *Rahnella* sp. Y9602. Further analysis by synchrotron-based XRD identified the uranyl phosphate mineral as amorphous chernikovite [$H_2(UO_2)_2(PO_4)_2$]. TEM images indicated that U(VI) coated the microbial cell membranes immediately upon addition to

incubations and separated from the cell surface over time as uranyl phosphate precipitated in the bulk solution, suggesting the cells provided a nucleation surface that activated precipitation. This work further demonstrated the potential for the bioremediation of uranium facilitated by the activity of phosphatase-carrying microorganisms in both aerobic and anaerobic conditions at low pH and in the presence of high nitrate concentrations.

Finally, flow-through reactors were used to determine how natural microbial communities react to organophosphate amendment in quasi natural conditions. Parameters such as pH and nitrate concentrations were adjusted to assess their effect on phosphatase activity. The objectives of this part of the study were to determine whether (1) indigenous microorganisms in a contaminated soil hydrolyzed phosphate from an organophosphate substrate, (2) pH and nitrate concentrations affected phosphatase activity, (3) enough phosphate was produced to precipitate U(VI), and (4) organophosphates could be transported sufficiently far in soils to generate U(VI) precipitate on a wide spatial scale.

The addition of an organophosphate substrate to contaminated ORFRC soils at both high and low pH resulted in the immediate production of high concentrations of phosphate, compared to U-control reactors amended with U(VI) only. In general, millimolar concentrations of phosphate were hydrolyzed at both pH, but higher rates of phosphate production were observed at low pH. Organophosphate hydrolysis reached steady state within ca. 10 days and was maintained throughout the experiment indicating constitutively-expressed phosphatases were active at both pHs. Uranium was precipitated as uranium phosphate mineral in both soils, but a fraction of the uranium was

removed by adsorption onto iron oxides (high pH soil) or by ternary complex formation with phosphate pre-adsorbed onto iron oxides (low pH soils). Microprobe analysis of soils from the high pH experiments indicated that U(VI) was distributed discretely on mineral surfaces and collected in micropores, suggesting that localized mineral surfaces may be ideal environments for the precipitation of U-P minerals. Uranium removal rates were much higher at high pH compared to low pH, suggesting that overall the immobilization of U(VI) through the activity of natural microbial phosphatases was most efficient in the high pH soils.

Overall, the results of this study demonstrate the biomineralization of U(VI) phosphate as a result of microbial phosphatase activity is efficient in both pure cultures and soils from a contaminated waste site. High levels of phosphatase activity were observed across a wide range of pH, in both aerobic and anaerobic conditions, and in the presence of high nitrate and uranium concentrations. The nonreductive biomineralization of U(VI) provides a promising new approach for in situ uranium bioremediation in low pH, high nitrate, and aerobic conditions that could be complementary to U(VI) bioreduction in high pH, low nitrate, and reducing environments.

6.1 Recommendations for future research

Several questions have arisen from the present study, and suggestions for future research in the area of U(VI) biomineralization are provided below. This study demonstrated the potential for the bioremediation of U(VI) phosphate as a result of microbial phosphatase activity. The mineral formed in the pure culture incubations was quasi amorphous with organic material from microbial cells incorporated into the mineral matrix. The stability of this mineral to changes in pH, redox conditions, ionic strength, temperature, and ligands (such as carbonate) has to be investigated to assess its use as a long term repository for uranium in the subsurface.

Adsorption of phosphate onto these soils should be investigated in flow-through control incubations to differentiate the rate of phosphate adsorption independently from uranium phosphate mineral precipitation.

Analysis of the changes in the soil microbial populations before and at the conclusion of the experiments should be conducted to shed light on the type of microorganisms affected by the addition of organophosphate.

The addition of different organophosphate substrates may help determine the most feasible phosphorus source for uranium biomineralization. Eventually, the use of natural organophosphates (i.e. phytate) should be envisioned to determine how natural phytases could be stimulated in natural soils.

The stability of the uranium phosphate biomineralized product could be studied by alternating the redox conditions of the reactor and stimulate more realistic in situ conditions. The addition of high concentrations of phosphate to soils may affect the overall geochemistry and microbiology of these systems. Phosphate adsorbs very

efficiently to mineral surfaces and may decrease the bioavailability of iron surface for bioreduction. In addition, the increase in a limiting nutrient, such as phosphate, may stimulate otherwise dormant microbial communities that may out-compete other bacterial assemblages that may or may not have negative impacts on the system.

Finally, as demonstrated above, it is difficult to distinguish between adsorbed and precipitated uranyl phosphate minerals using X-ray absorption spectroscopy (XAS). Future work in this area should concentrate on determining the best combination of analytical tools to help make this distinction. Imaging techniques such as scanning and transmission electron microscopy (SEM and TEM) may be combined with XAS (both U and P) and new chemical extraction methods.

APPENDIX A

SUPPLEMENTAL INFORMATION FOR CHAPTER 3

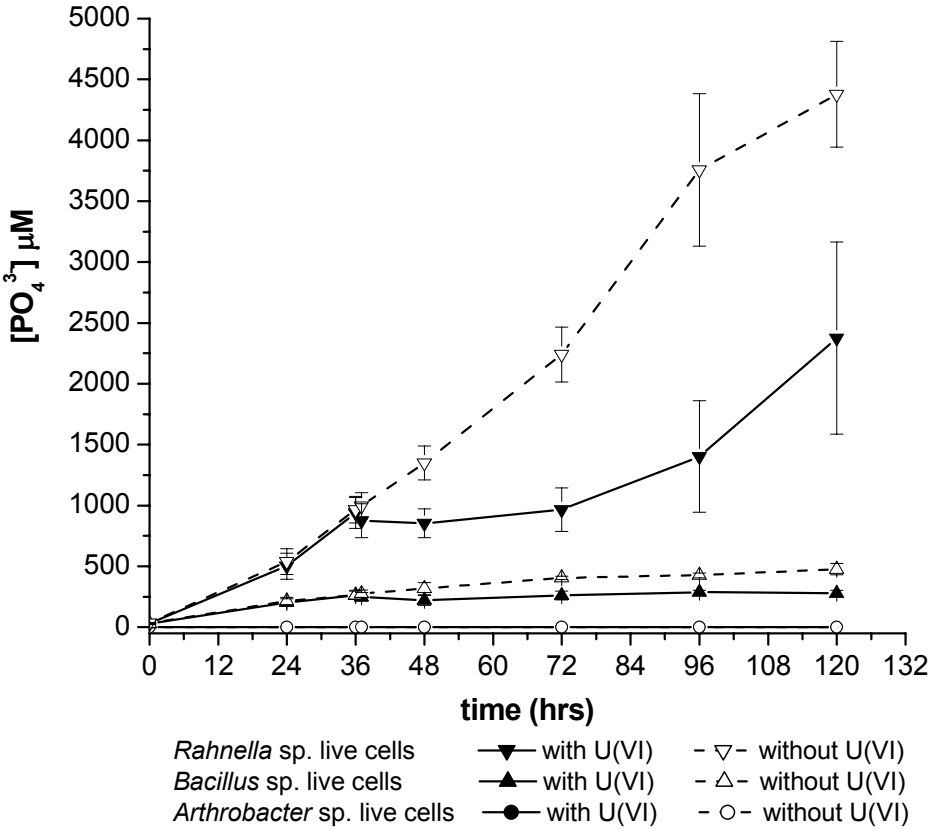

Figure A. 1 Average phosphate concentrations in aerobic incubations of three bacterial species in simulated groundwater at pH 5.5, in the presence of 10 mM G3P, with and without 200 µM UO_2^{2+} (standard deviation represents variations of triplicate incubations). Closed and open symbols represent incubations with UO_2^{2+} and without UO_2^{2+}, respectively.

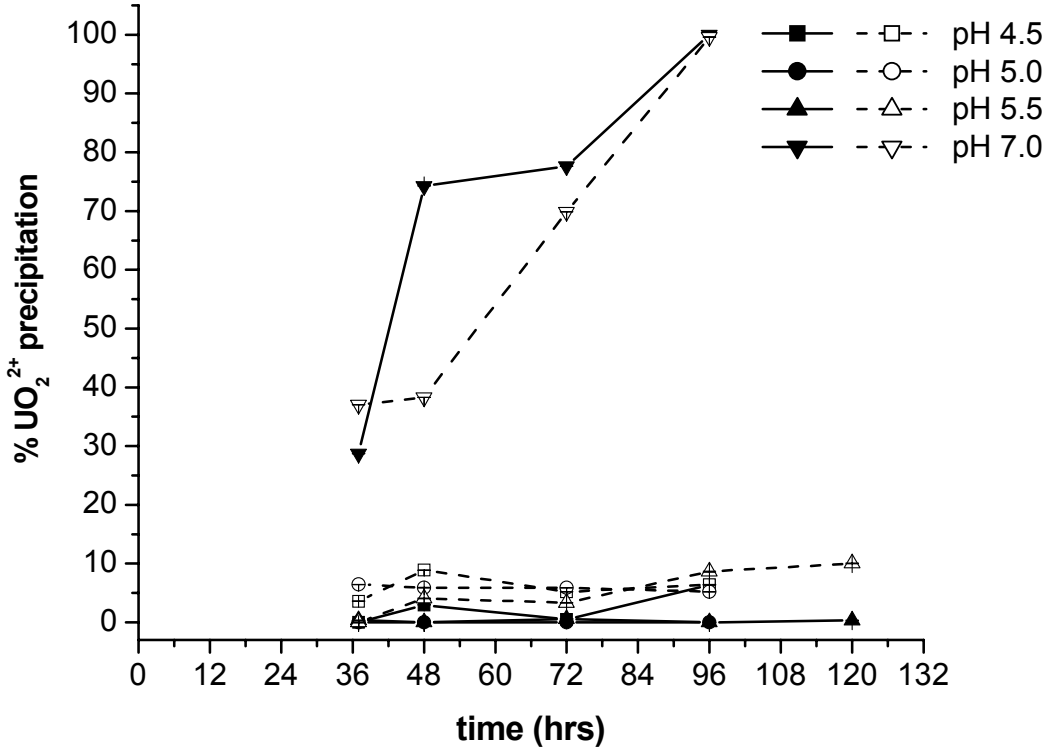

Figure A. 2 Average $\%UO_2^{2+}$ precipitation in chemical (closed symbols) and heat-killed (open symbols) control incubations as a function of pH with *Rahnella* sp. in the presence of 200 μM UO_2^{2+} and 10 mM G3P in simulated groundwater (standard deviation represents variations of triplicate incubations). $\%UO_2^{2+}$ precipitation increases at pH 7.0 as a result of the chemical precipitation of uranyl hydroxide.

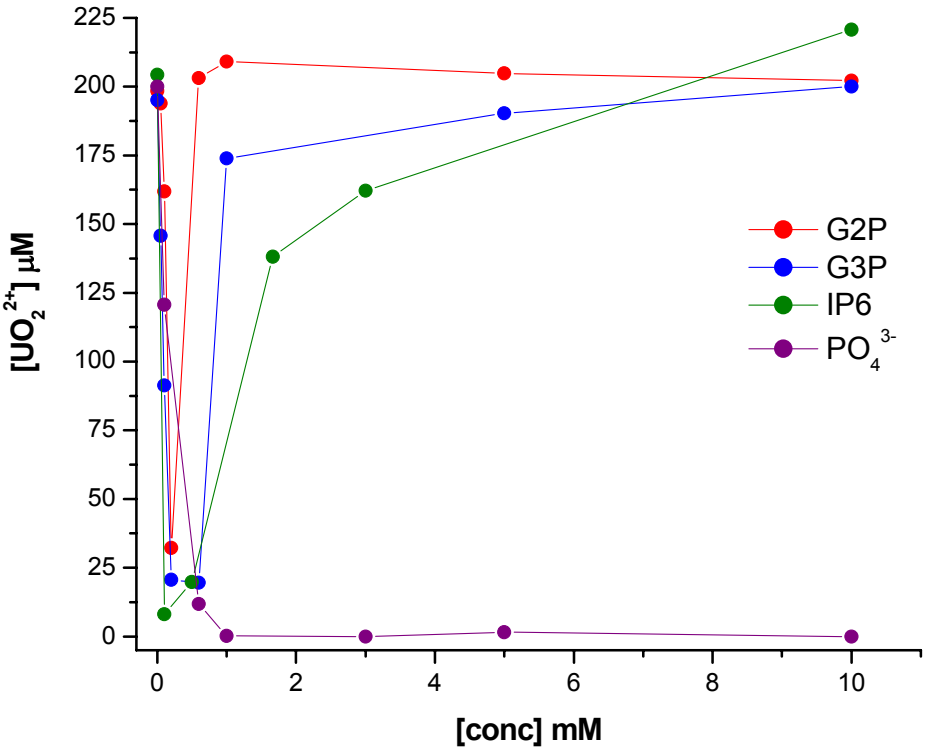

Figure A. 3 Solubility of uranyl as a function of G2P, G3P, IP6 (phytic acid), and PO_4^{3-} concentration.

Table A. 1 Parameters derived from fitting of U LIII-edge EXAFS for samples collected from aerobic pure culture incubations.

Sample		O_{ax}	O_{eq}	P	POU MS*	OPOU MS*	PO dist†	Rfactor	ΔE_0
A *Rahnella* sp. pH 5.5	**N**	2	2.7 (0.4)	1.2 (0.4)	2.4	1.2	1.57 (0.06)	0.009	-5 (1.4)
	R(Å)	1.79 (0.005)	2.28 (0.007)	3.59 (0.02)	3.72	3.84			
	σ(Å²)	0.003 (0.0003)	0.003 (0.00009)	0.003	0.003	0.003			
B *Rahnella* sp. pH 7.0	**N**	2	3.1 (0.7)	0.7 (1.3)	1.5	0.7	1.4 (0.4)	0.0207	-6.4 (2.1)
	R(Å)	1.78 (0.01)	2.28 (0.01)	3.54 (0.06)	3.62	3.7			
	σ(Å²)	0.0036 (0.0005)	0.004 (0.002)	0.003	0.003	0.003			
C abiotic U-P pH 5.5	**N**	2	3.7 (0.7)	1.6 (0.9)	3.1	1.6	1.56 (0.07)	0.0174	-5.4 (1.9)
	R(Å)	1.79 (0.009)	2.27 (0.01)	3.58 (0.03)	3.71	3.84			
	σ(Å²)	0.0047 (0.0006)	0.005 (0.002)	0.003	0.003	0.003			
D abiotic pH 7.0 (no P)	**N**	2	1.6 (1)	1.7 (1)				0.0497	-0.8 (3.1)
	R(Å)	1.81 (0.01)	2.31 (0.04)	2.47 (0.04)					
	σ(Å²)	0.0038 (0.0006)	0.005 (0.005)	0.005					

Errors are given in parentheses (no error means the value was fixed, or calculated from other parameters)

* MS denotes multiple scattering paths

† PO dist is the distance between the P-O in phosphate coordination (used for the MS paths)

APPENDIX B

DESCRIPTIONS OF TRANSPORT MODELS

B.1 Bromide breakthrough curve model

The Matlab™ code for the one-dimensional advection-dispersion model used to model the bromide breakthrough curves in the flow-through reactors in Chapter 5. The main routine "TracerBr" and subroutine "funPFR" are described below.

```
% This program calculates the breakthrough curve of a tracer (Bromide) in a PFR
clear
global x time n BrCexp Br0 v
R = 0.99;
D = 1e-5;                          % cm2/sec
Br0 = 12e-3;                       % M
Q = 1.2;                           % ml/hr
fi = 0.49;                         % Porosity
A = (3.86/2)^2*pi;                 % Surface area cm^2
% Load the data for each reactor
%
load Bromide14.txt -ascii
load Bromide15.txt -ascii
load Bromide16.txt -ascii
load Bromide17.txt -ascii

time141 = (Bromide14(1:6,1)-Bromide14(1,1))*86400;              % Correct for t0 = 0 - [sec]
time142 = (Bromide14(12:length(Bromide14),1)-Bromide14(12,1))*86400;  % Correct for t0 = 0
time151 = (Bromide15(1:6,1)-Bromide15(1,1))*86400;
time152 = (Bromide15(11:length(Bromide15),1)-Bromide15(11,1))*86400;
time161 = (Bromide16(1:6,1)-Bromide16(1,1))*86400;
time162 = (Bromide16(12:length(Bromide16),1)-Bromide16(12,1))*86400;
time171 = (Bromide17(1:5,1)-Bromide17(1,1))*86400;
time172 = (Bromide17(12:length(Bromide17),1)-Bromide17(12,1))*86400;


BrC11 = Bromide14(1:6,2);                                       % Load the Bromide data
BrC12 = Bromide14(12:length(Bromide14),2);
BrC21 = Bromide15(1:6,2);
BrC22 = Bromide15(11:length(Bromide15),2);
BrC31 = Bromide16(1:6,2);
BrC32 = Bromide16(12:length(Bromide16),2);
BrC41 = Bromide17(1:5,2);
BrC42 = Bromide17(12:length(Bromide17),2);
```

```
% Analytical solution for bromide
X0 = [R;D;v];            % vector containing the parameters to optimize
dx = 0.05;               % node space - [cm]
x = (0:dx:8)';           % length of the reactor - [cm]
n = length(x);
P = v*dx/D               % Peclet #
%
% Optimize R, D, and v to minimize the least square difference between the data
% and the modeled Bromide concentration at the output of the PFR
LB = [0;0];
UB = [1;1e-2];
for i = 1:2              % i represents the two Br- amendments in the same reactor
   for j = 1:4           % j represents the reactor number
      eval(['time = [0:max(time' num2str(13+j) num2str(i) ')/48:max(time' num2str(13+j)
       num2str(i) ')];']);                                    % Define a new time vector
      time = time';                                           % time vector in sec
      eval(['BrC' num2str(j) num2str(i) 'i = interp1(time' num2str(13+j) num2str(i) ',BrC'
      num2str(j) num2str(i) ',time)*1e-3;'])  % Interpolate the concentration
      eval(['BrC' num2str(i) ' (:,' num2str(j) ' )= BrC' num2str(j) num2str(i) 'i;']);
      eval(['BrCexp = BrC' num2str(i) '(:,j);']);
      X = lsqnonlin('funPFR',X0,LB,UB);                       % Use a least square non linear method
   %
   % Analytical solution for bromide
   %
      R = X(1);
      D = X(2);
      v = X(3);
      par(:,4*(i-1)+j) = X
      Br(:,1) = zeros(n,1);
      for p = 2:length(time)
         m = length(time);
         A1 = 1/2*erfc((R*x-v*time(p))/(2*(D*R*time(p))^0.5));
         A2 = 1/2*exp(v*x/D).*erfc((R*x+v*time(p))/(2*(D*R*time(p))^0.5));
         A = A1+A2;
         Br(:,p) = Br0*A;
      end
      BrCopt = [time/86400 Br(n,:)'];      % Regroup time and data at output reactor into a matrix
      clear X

      figure(1)
      surf(time(2:m)/86500,x,Br(:,2:m))
      xlabel('time - [days]')
      ylabel('depth - [cm]')
      zlabel('Bromide - [M]')
      pause(5)

      figure(2)
      eval(['B = BrC' num2str(j) num2str(i) ';']);
      eval(['t1 = time' num2str(13+j) num2str(i) ';']);
      if j == 1;
         plot(time/86500,Br(n,:)'/1e-3,'b',t1/86400,B,'bo')
```

```
        hold on
      elseif j == 2;
        plot(time/86500,Br(n,:)'/1e-3,'r',t1/86400,B,'ro')
        hold on
      elseif j == 3;
        plot(time/86500,Br(n,:)'/1e-3,'g',t1/86400,B,'go')
        hold on
      else
        plot(time/86500,Br(n,:)'/1e-3,'m',t1/86400,B,'mo')
        hold on
      end
   %
   % Save calculated values and plot the data
   %
      filename = ['BrC' int2str(j) int2str(i) 'opt.txt'];
      eval(['save ' filename ' BrCopt -ascii']);
   end
   title('Bromide Tracer Breakthrough Curves in Reactors C1, C2, C3, and C4')
   xlabel('time - [days]')
   ylabel('Bromide - [mM]')
   legend('C1','C2','','C3','','C4','')
end
%
% Save parameters R, D, and v
%
save paramRDv.txt par –ascii
```

Subroutine funPFR :

```
% Subroutine to calculate Bromide breakthrough curve and optimize the parameters
% R, D, and v to minimize the theoretical and experimental data
%
function F = funPFR(X)
global x time n BrCexp Br0 v
% Analytical solution for bromide
R = X(1);
D = X(2);
v = X(3);
Br(:,1) = zeros(n,1);
for i = 2:length(time)
    A1 = 1/2*erfc((R*x-v*time(i))/(2*(D*R*time(i))^0.5));
    A2 = 1/2*exp(v*x/D).*erfc((R*x+v*time(i))/(2*(D*R*time(i))^0.5));
    A = A1+A2;
    Br(:,i) = Br0*A;
end
F = Br(n,:)'-BrCexp;
```

B.2 Reactive transport model

The Matlab™ code for the one-dimensional reactive transport model used to determine net production/consumption rates in the flow-through reactors in Chapter 5. The main routine "ratecalc" and subroutine funPFRRate are described below.

```
% This program calculates the net rate of reactions of NO3-, NO2-, PO4 3-, G2P, and dissolved
uranium in a PFR using Gemuchten's analytical solutions. It optimizes the difference between the
data and the model for two cases:  zero-order production (k>0) or consumption (k<0). k is in fact
the reaction rate
%
clear
global x ta n Cexp C0 Ci v D R

Q = 1.2;                        % Measured flow rate - [ml/hr]
fi = 0.49;                      % Porosity of the soil
A = (3.86/2)^2*pi;              % Surface area of the Reactor - [cm^2]
L = 8;                          % Length of the Reactor - [cm]
U0 = 200e-6;                    % Concentration of U(VI) introduced in the reactor at t=0
G0 = 0.01;
% Load the optimized parameters using Bromide as tracer
load paramRDv.txt -ascii
R = paramRDv(1,:);  % Retardation coefficient optimized with Br-
D = paramRDv(2,:);  % Difussion coefficient optimized with Br- - [cm2/sec]
v = paramRDv(3,:);  % Advection optimized with Br- [cm/s]
% Load the data for each reactor
load R14NO2NO3.txt -ascii
load R14Udiss.txt -ascii
load R14PO4.txt -ascii
load R15NO2.txt -ascii
load R15NO3.txt -ascii
load R15Udiss.txt -ascii
load R15PO4.txt -ascii
load R15G2P.txt -ascii
load R16NO2.txt -ascii
load R16NO3.txt -ascii
load R16Udiss.txt -ascii
load R16PO4.txt -ascii
load R16G2P.txt -ascii
load R17NO2.txt -ascii
load R17NO3.txt -ascii
load R17Udiss.txt -ascii
load R17PO4.txt -ascii
load R17G2P.txt -ascii

t14NO2 = [0;R14NO2NO3(:,1)]*86400;    % Reactor 14 - Time vector corrected for t0 = 0 - [sec]
t14NO3 = [0;R14NO2NO3(:,3)]*86400;
t14U = [0;R14Udiss(:,1)]*86400;
```

```
t14P = [0;R14PO4(:,1)]*86400;

t15NO2 = [0;R15NO2(:,1)]*86400;          % Reactor 15 - Time vector corrected for t0 = 0 - [sec]
t15NO3 = [0;R15NO3(:,1)]*86400;
t15U = [0;R15Udiss(:,1)]*86400;
t15P = [0;R15PO4(:,1)]*86400;
t15G = [0;R15G2P(:,1)]*86400;

t16NO2 = [0;R16NO2(:,1)]*86400;          % Reactor 16 - Time vector corrected for t0 = 0 - [sec]
t16NO3 = [0;R16NO3(:,1)]*86400;
t16U = [0;R16Udiss(:,1)]*86400;
t16P = [0;R16PO4(:,1)]*86400;
t16G = [0;R16G2P(:,1)]*86400;

t17NO2 = [0;R17NO2(:,1)]*86400;          % Reactor 17 - Time vector corrected for t0 = 0 - [sec]
t17NO3 = [0;R17NO3(:,1)]*86400;
t17U = [0;R17Udiss(:,1)]*86400;
t17P = [0;R17PO4(:,1)]*86400;
t17G = [0;R17G2P(:,1)]*86400;

NO214 = [0;R14NO2NO3(:,2)]*1e-3;         % Reactor 14 - NO2, NO3, U(VI), PO4 data
NO314 = [0;R14NO2NO3(:,4)]*1e-3;
U14 = [0;R14Udiss(:,2)]*1e-6;
P14 = [0;R14PO4(:,2)]*1e-3;

NO215 = [0;R15NO2(:,2)]*1e-3;            % Reactor 15 - NO2, NO3, U(VI), PO4, G2P data
NO315 = [0;R15NO3(:,2)]*1e-3;
U15 = [0;R15Udiss(:,2)]*1e-6;
P15 = [0;R15PO4(:,2)]*1e-3;
G15 = [0;R15G2P(:,2)]*1e-3;

NO216 = [0;R16NO2(:,2)]*1e-3;            % Reactor 16 - NO2, NO3, U(VI), PO4, G2P data
NO316 = [0;R16NO3(:,2)]*1e-3;
U16 = [0;R16Udiss(:,2)]*1e-6;
P16 = [0;R16PO4(:,2)]*1e-3;
G16 = [0;R16G2P(:,2)]*1e-3;

NO217 = [0;R17NO2(:,2)]*1e-3;            % Reactor 17 - NO2, NO3, U(VI), PO4, G2P data
NO317 = [0;R17NO3(:,2)]*1e-3;
U17 = [0;R17Udiss(:,2)]*1e-6;
P17 = [0;R17PO4(:,2)]*1e-3;
G17 = [0;R17G2P(:,2)]*1e-3;
%
% Plot the data and ask for what species and time interval the calculation needs to be done
%
p = input('What reactor do you want to determine the reaction rates (14 control, 15 rep 1, 16 rep
2, or 17 rep 3)?');
eval(['t1 = t' num2str(p) 'NO2;']);
eval(['NO2 = NO2' num2str(p) ';']);
eval(['t2 = t' num2str(p) 'NO3;']);
eval(['NO3 = NO3' num2str(p) ';']);
```

```
eval(['t3 = t' num2str(p) 'U;']);
eval(['U = U' num2str(p) ';']);
eval(['t4 = t' num2str(p) 'P;']);
eval(['P = P' num2str(p) ';']);
if p == 14
   R = mean(R);            % Derive the retardation coefficient as the average of the retardation
coefficients in R15, R16, and R17
   D = mean(D);    % Derive the diffusion coefficient as the average of the diffusion coefficients
in R15, R16, and R17
   v = mean(v);       % Derive the advection as the average of the advection in R15, R16, and R17
   else
   R = mean(R(2*p-29:2*p-28));    % Derive the retardation coefficient as the average of the
retardation coefficients of the two tracer injections in R15, R16, or R17
   D = mean(D(2*p-29:2*p-28));    % Derive the diffusion coefficient as the average of the
diffusion coefficients of the two tracer injections in R15, R16, or R17
   v = mean(v(2*p-29:2*p-28));    % Derive the advection as the average of the advection of the
two tracer injections in R15, R16, or R17
   eval(['t5 = t' num2str(p) 'G;']);
   eval(['G = G' num2str(p) ';']);
end

figure(1)
if p ==14                          % This is for Reactor 14 only (the control without G2P)
   subplot(4,1,1)
   plot(t1/86400,NO2/1e-3,'sr')
   title('NO2-, NO3-, and PO43- at the output of PFR')
   ylabel('NO2- - [mM]')
   subplot(4,1,2)
   plot(t2/86400,NO3/1e-3,'vb')
   ylabel('NO3- - [mM]')
   subplot(4,1,3)
   plot(t3/86400,U/1e-6,'^b')
   ylabel('U(VI) - [uM]')
   subplot(4,1,4)
   plot(t4/86400,P/1e-3,'^k')
   ylabel('PO43- - [mM]')
   xlabel('Time - [days]')
else                               % This is for Reactors 15, 16, or 17
   subplot(5,1,1)
   plot(t1/86400,NO2/1e-3,'sr')
   title('NO2-, NO3-, PO43-, and G2P at the output of PFR')
   ylabel('NO2- - [mM]')
   subplot(5,1,2)
   plot(t2/86400,NO3/1e-3,'vb')
   ylabel('NO3- - [mM]')
   subplot(5,1,3)
   plot(t3/86400,U/1e-6,'^b')
   ylabel('U(VI) - [uM]')
   subplot(5,1,4)
   plot(t4/86400,P/1e-3,'^k')
   ylabel('PO43- - [mM]')
```

```
   subplot(5,1,5)
   plot(t5/86400,G/1e-3,'dg')
   xlabel('Time - [days]')
   ylabel('G2P - [mM]')
end
j = input('What species do you want to determine the rate (NO2 = 1; NO3 = 2; U(VI) = 3; PO43- = 4; G2P = 5)?');
ti = input('At what time you wish to start the calculation?');
tf = input('At what time you wish to finish the calculation?');
h = input('Do you want to calculate a net consumption (0) or a production (1) rate');
close
%
% Analytical solution for 1-D transient reactive transport equation with simple source or sink term
%
dx = 0.1;
x = (0:dx:L)';                          % length of the reactor - [cm]
n = length(x);
dt = 86400*(tf-ti)/160;
t = (86400*ti:dt:86400*tf)';            % time - [sec]
ta = t-t(1);                            % apparent time set to zero to start calculation anywhere
m = length(ta);
NO2i = interp1(t1,NO2,t);
NO3i = interp1(t2,NO3,t);
Ui = interp1(t3,U,t);
Pi = interp1(t4,P,t);
if exist('G')
   Gi = interp1(t5,G,t);
   Ciall = [NO2i NO3i Ui Pi Gi];
   Ci0all = [0 max(NO3) U0 0 G0];
   else
   Ciall = [NO2i NO3i Ui Pi];
   Ci0all = [0 max(NO3) 0 0];
end
%
% Optimize k (first order rate constant) to minimize the least square difference between the data
% and the modeled NO2-, NO3-, U(VI), PO43-, or G2P concentration at the output of the PFR
%
Cexp = Ciall(:,j);              % Experimental data used to fit the parameter
C0 = Ci0all(j);                 % Initial reactor input concentration at x = 0
Ci = Ciall(1,j);                % Initial concentration at all x taken as the first output data
                                % from the reactors, assuming the reactors are first homogeneous
if h == 0                       % Consumption Case
   k = -1.5e-5;% -1.5e-5
   LB = -1e-3; %-1e-3           % Format parameters for the non-linear least-square optimization
   UB = 0;
elseif h == 1                   % Production Case
   k = 1.5e-5;
   LB = 0;                      % Format parameters for the non-linear least-square optimization
   UB = 1e-3;
else
```

```
   break
end
X0 = k;                          % vector containing the parameters to optimize
[X,resnorm,residual,exitflag,output,lambda,jacobian] = lsqnonlin('funPFRRate',X0,LB,UB);
% Use a least square non linear method of optimization of the rate of removal or production.
k = X(1);
%
% Calculate analytical solution
%
C(:,1) = Ci*ones(n,1);
for i = 2:length(ta)       % THIS CASE IS FOR C(x,0) = Ci; FLUX CONDITION AT x = 0 AT
ALL t; AND ZERO-ORDER SOURCE (k NOT 0) - CASE C1
   A1 = 1/2*erfc((R*x-v*ta(i))/(2*sqrt(D*R*ta(i))))+sqrt(v^2*ta(i)/(pi*D*R))*exp(-(R*x-
v*ta(i)).^2/(4*D*R*ta(i)));
   A2 = 1/2*(1+v*x/D+v^2*ta(i)/(D*R)).*exp(v*x/D).*erfc((R*x+v*ta(i))/(2*sqrt(D*R*ta(i))));
   A3 = A1-A2;

   A4 = (ta(i)/2-R*x/(2*v)-D*R/(2*v^2)).*erfc((R*x-v*ta(i))/(2*sqrt(D*R*ta(i))));
   A5 = sqrt(ta(i)/(4*pi*D*R))*(R*x+v*ta(i)+2*D*R/v).*exp(-(R*x-v*ta(i)).^2/(4*D*R*ta(i)));
   A6 = (ta(i)/2-
D*R/(2*v^2)+(R*x+v*ta(i)).^2/(4*D*R)).*exp(v*x/D).*erfc((R*x+v*ta(i))/(2*sqrt(D*R*ta(i))));
   A7 = k/R*(ta(i)-A4-A5+A6);
   C(:,i) = Ci+(C0-Ci)*A3+A7;
end
%
% Save calculated values and plot the data
%
Copt = [t/86400 C(n,:)'];
filename = ['C' int2str(p) '_Spec' int2str(j) 't' int2str(ti) '_' int2str(tf) 'opt.txt'];
eval(['save ' filename ' Copt -ascii']);
figure(1)
surf(t([1:m])/86500,x,C(:,[1:m]))
xlabel('time - [days]')
ylabel('depth - [cm]')
zlabel('Concentration - [M]')

figure(2)
if p ==14                  % This is for Reactor 14 only (the control without G2P)
   subplot(4,1,1)
   plot(t1/86400,NO2/1e-3,'sr')
   title('NO2-, NO3-, and PO43- at the output of PFR')
   ylabel('NO2- - [mM]')
   hold on
   subplot(4,1,2)
   plot(t2/86400,NO3/1e-3,'vb')
   ylabel('NO3- - [mM]')
   hold on
   subplot(4,1,3)
   plot(t3/86400,U/1e-6,'^b')
   ylabel('U(VI) - [uM]')
   hold on
```

```
    subplot(4,1,4)
    plot(t4/86400,P/1e-3,'^k')
    ylabel('PO43- - [mM]')
    xlabel('Time - [days]')
    hold on
    if j == 1;
       subplot(4,1,1)
       plot(t/86400,C(n,:)*1e3,'r')
    elseif j == 2;
       subplot(4,1,2)
       plot(t/86400,C(n,:)*1e3,'b')
    elseif j == 3;
       subplot(4,1,3)
       plot(t/86400,C(n,:)*1e6,'b')
    else
       subplot(4,1,4)
       plot(t/86400,C(n,:)*1e3,'k')
    end
else                                % This is for Reactors 15, 16, or 17
    subplot(5,1,1)
    plot(t1/86400,NO2/1e-3,'sr')
    title('NO2-, NO3-, PO43-, and G2P at the output of PFR')
    ylabel('NO2- - [mM]')
    hold on
    subplot(5,1,2)
    plot(t2/86400,NO3/1e-3,'vb')
    ylabel('NO3- - [mM]')
    hold on
    subplot(5,1,3)
    plot(t3/86400,U/1e-6,'^b')
    ylabel('U(VI) - [uM]')
    hold on
    subplot(5,1,4)
    plot(t4/86400,P/1e-3,'^k')
    ylabel('PO43- - [mM]')
    hold on
    subplot(5,1,5)
    plot(t5/86400,G/1e-3,'dg')
    xlabel('Time - [days]')
    ylabel('G2P - [mM]')
    hold on
    if j == 1;
       subplot(5,1,1)
       plot(t/86400,C(n,:)*1e3,'r')
    elseif j == 2;
       subplot(5,1,2)
       plot(t/86400,C(n,:)*1e3,'b')
    elseif j == 3;
       subplot(5,1,3)
       plot(t/86400,C(n,:)*1e6,'b')
    elseif j == 4;
```

```
      subplot(5,1,4)
      plot(t/86400,C(n,:)*1e3,'k')
   else
      subplot(5,1,5)
      plot(t/86400,C(n,:)*1e3,'g')
   end
end
disp('k = ')
disp(k*86400)
disp('mole/day')
```

Subroutine funPFRRate:

```
% Subroutine to calculate rate of reaction for NO2-, NO3-, U(VI), PO43-, and G2P
transformation and optimize the parameter k to minimize the theoretical and experimental data
%
function F = funPFRRate(X)
global x ta n Cexp C0 Ci v D R
%
% Analytical solution for Fe(II), SO42-, or H2S
%
k = X(1);
C(:,1) = Ci*ones(n,1);
for i = 2:length(ta)        % THIS CASE IS FOR C(x,0) = Ci; FLUX CONDITION AT x = 0 AT
ALL t; AND ZERO-ORDER SOURCE (k NOT 0) - CASE C1
   A1 = 1/2*erfc((R*x-v*ta(i))/(2*sqrt(D*R*ta(i))))+sqrt(v^2*ta(i)/(pi*D*R))*exp(-(R*x-
v*ta(i)).^2/(4*D*R*ta(i)));
   A2 = 1/2*(1+v*x/D+v^2*ta(i)/(D*R)).*exp(v*x/D).*erfc((R*x+v*ta(i))/(2*sqrt(D*R*ta(i))));
   A3 = A1-A2;

   A4 = (ta(i)/2-R*x/(2*v)-D*R/(2*v^2)).*erfc((R*x-v*ta(i))/(2*sqrt(D*R*ta(i))));
   A5 = sqrt(ta(i)/(4*pi*D*R))*(R*x+v*ta(i)+2*D*R/v).*exp(-(R*x-v*ta(i)).^2/(4*D*R*ta(i)));
   A6 = (ta(i)/2-
D*R/(2*v^2)+(R*x+v*ta(i)).^2/(4*D*R)).*exp(v*x/D).*erfc((R*x+v*ta(i))/(2*sqrt(D*R*ta(i))));
   A7 = k/R*(ta(i)-A4-A5+A6);
   C(:,i) = Ci+(C0-Ci)*A3+A7;
end
F = (C(n,:)'-Cexp)*1e3;
disp('F = ')
disp(norm(F))
```

APPENDIX C

SUPPLEMENTAL INFORMATION FOR CHAPTER 5

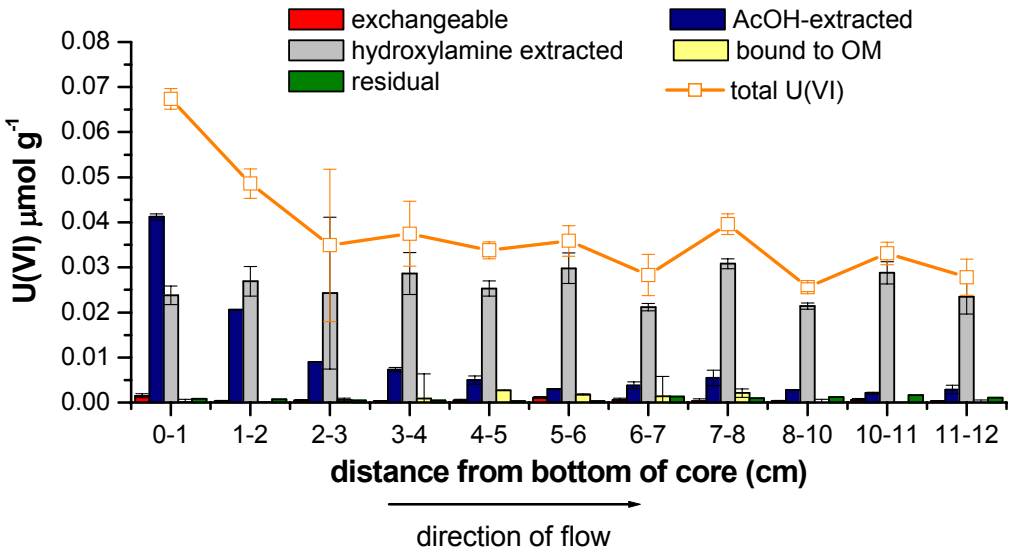

Figure C. 1 U distribution in soil from Reactor 1 of the high pH flow-through reactor experiments as determined by sequential extraction.

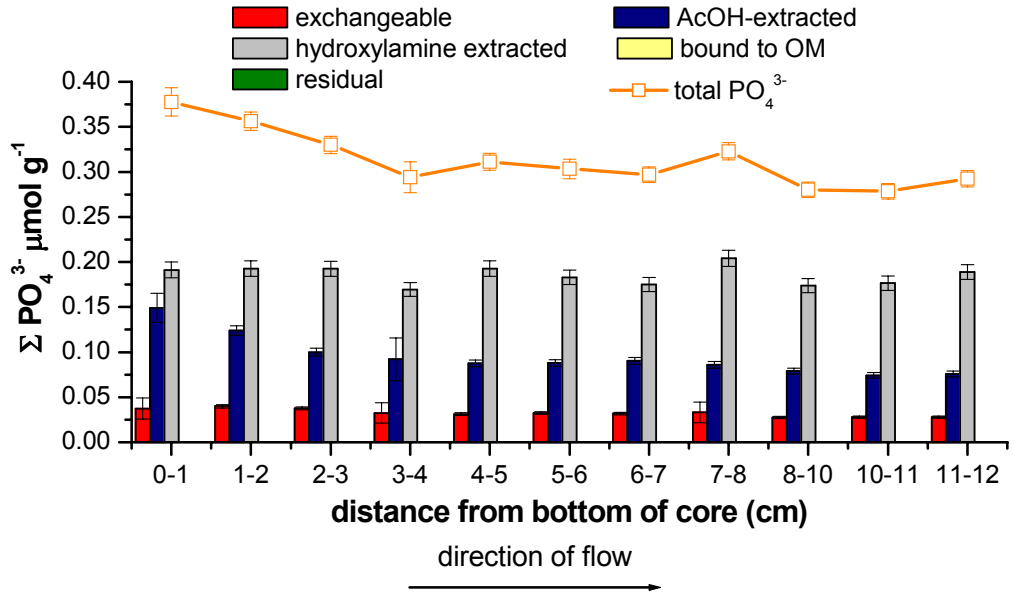

Figure C. 2 Phosphate distribution in soil from Reactor 1 of the high pH flow-through reactor experiments as determined by sequential extraction.

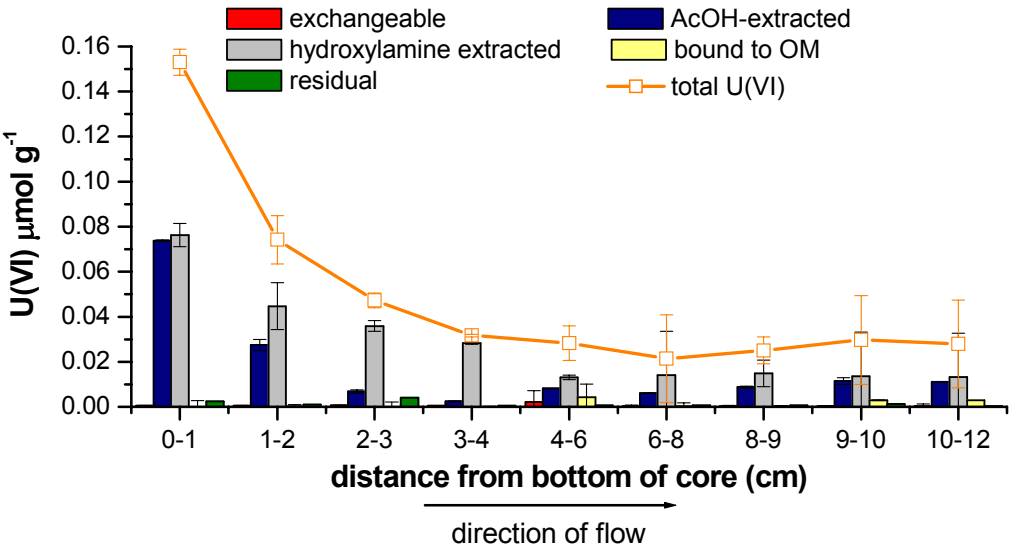

Figure C. 3 U distribution in soil from Reactor 2 of the high pH flow-through reactor experiments as determined by sequential extraction.

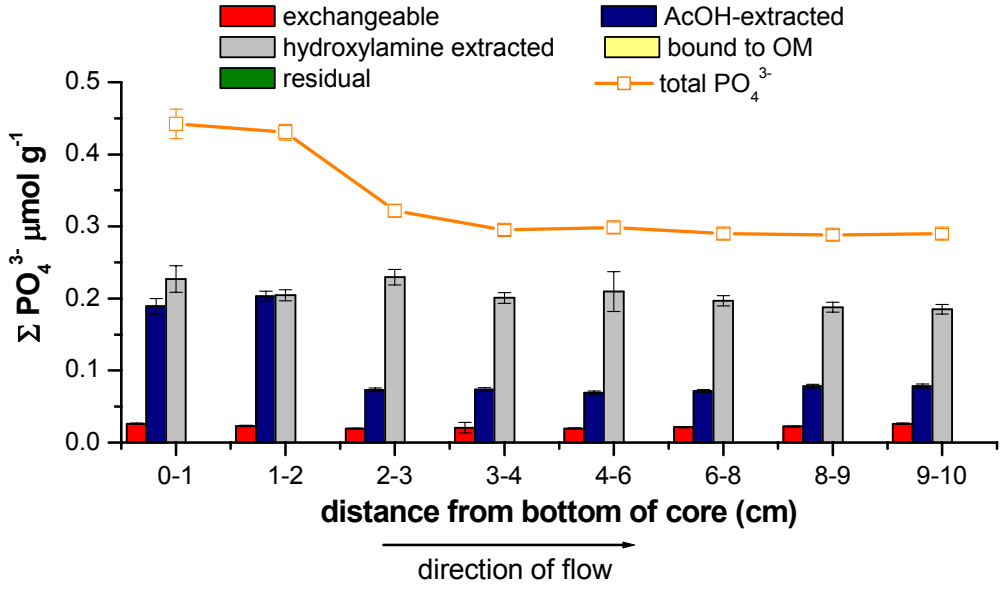

Figure C. 4 Phosphate distribution in soil from Reactor 2 of the high pH flow-through reactor experiments as determined by sequential extraction.

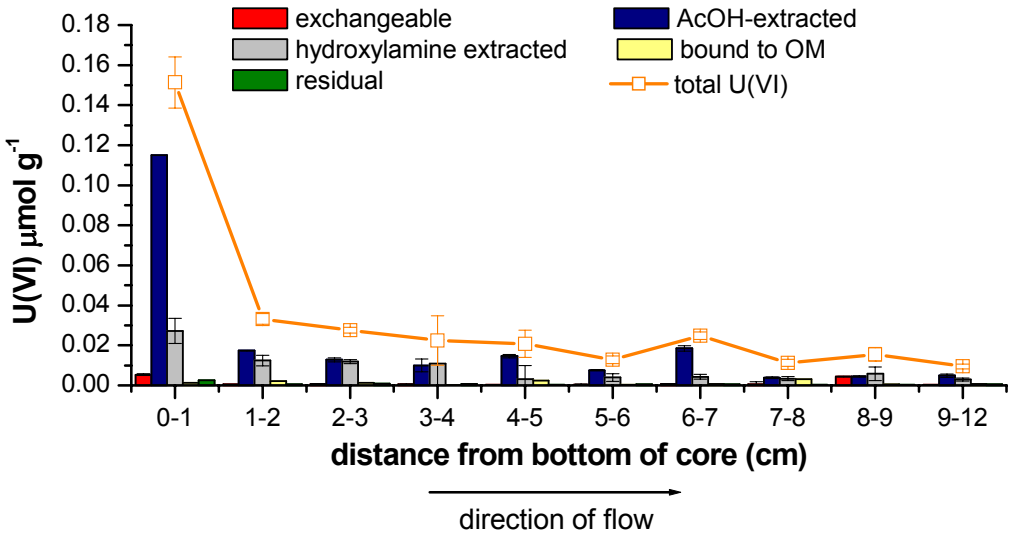

Figure C. 5 U distribution in soil from Reactor 3 of the high pH flow-through reactor experiments as determined by sequential extraction.

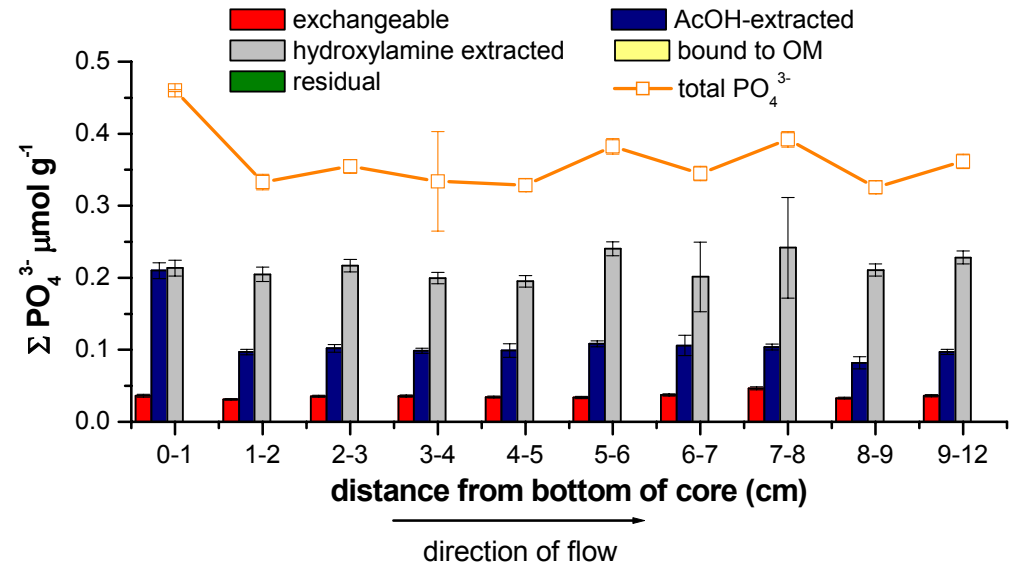

Figure C. 6 Phosphate distribution in soil from Reactor 3 of the high pH flow-through reactor experiments as determined by sequential extraction.

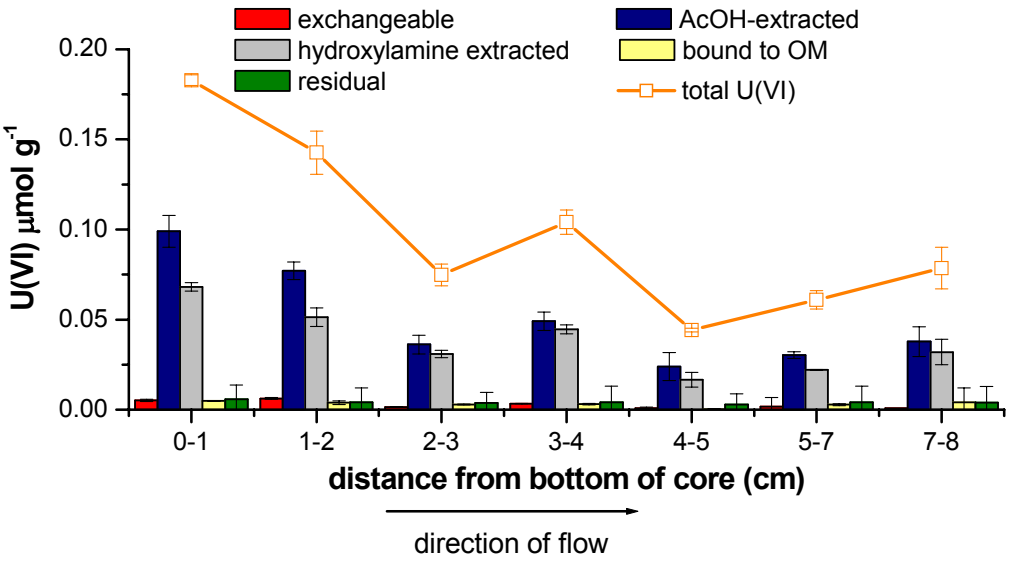

Figure C. 7 U distribution in soil from Reactor 1 of the low pH flow-through reactor experiments as determined by sequential extraction.

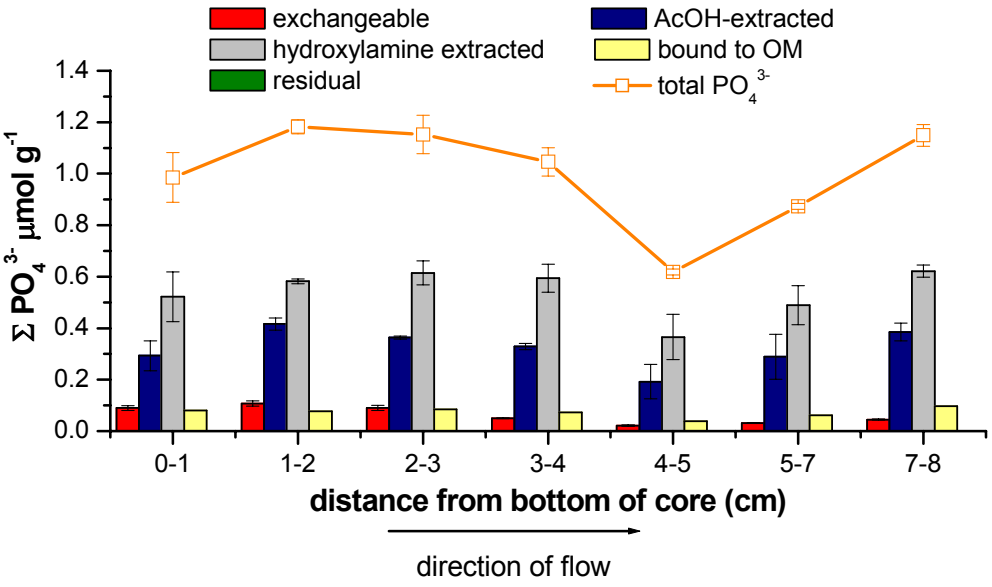

Figure C. 8 Phosphate distribution in soil from Reactor 1 of the low pH flow-through reactor experiments as determined by sequential extraction.

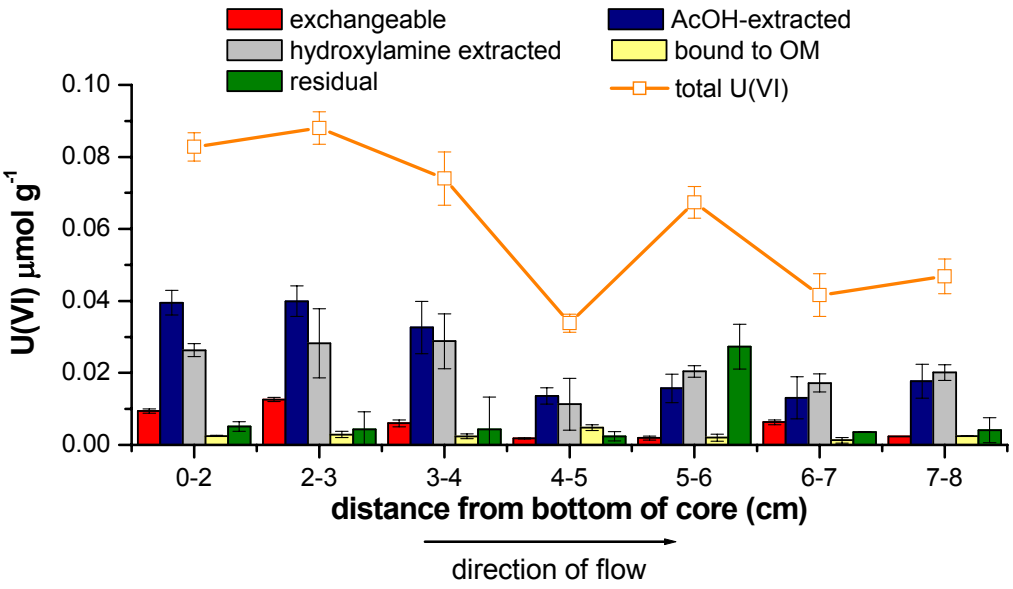

Figure C. 9 U distribution in soil from Reactor 2 of the low pH flow-through reactor experiments as determined by sequential extraction.

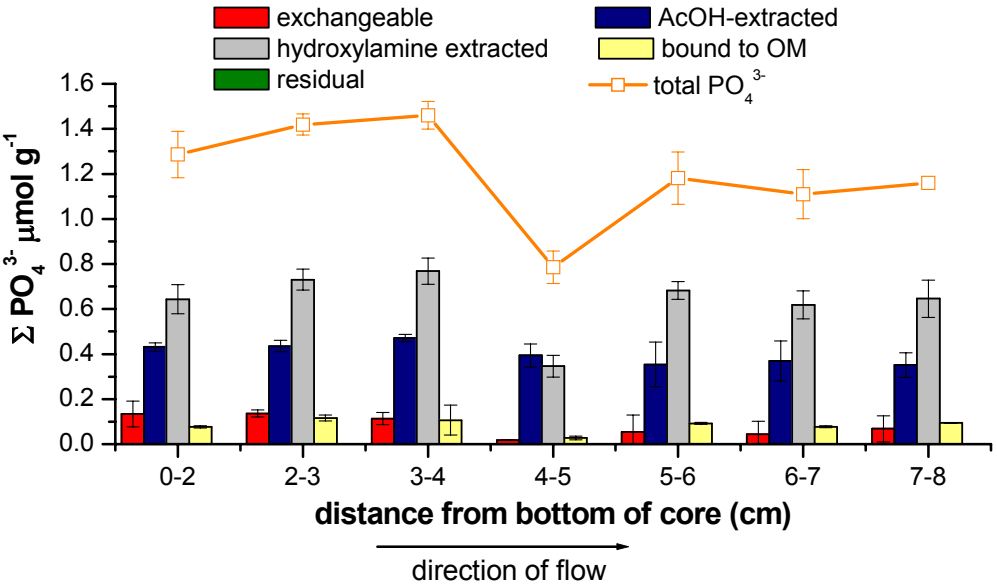

Figure C. 10 Phosphate distribution in soil from Reactor 2 of the low pH flow-through reactor experiments as determined by sequential extraction.

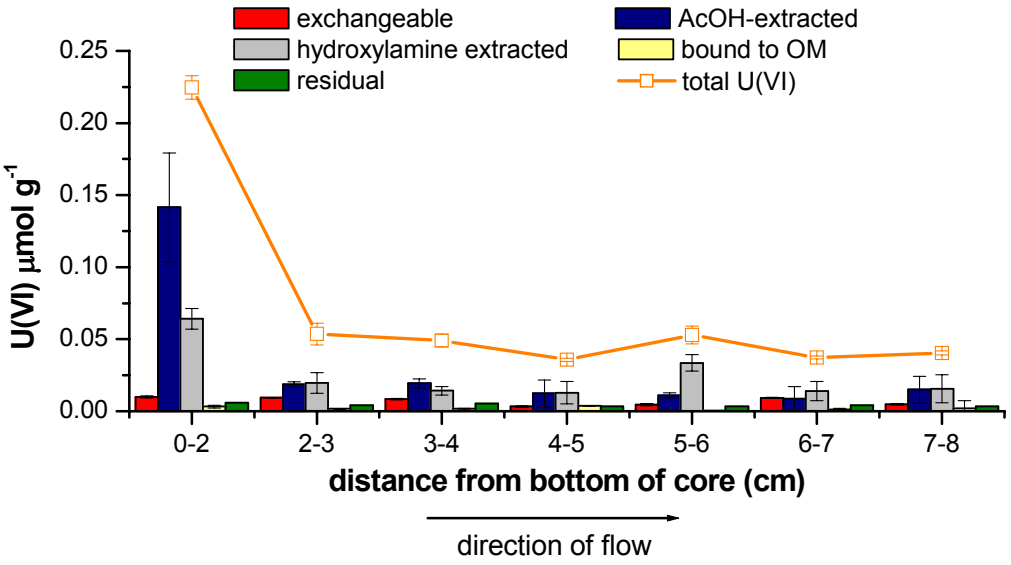

Figure C. 11 U distribution in soil from Reactor 3 of the low pH flow-through reactor experiments as determined by sequential extraction.

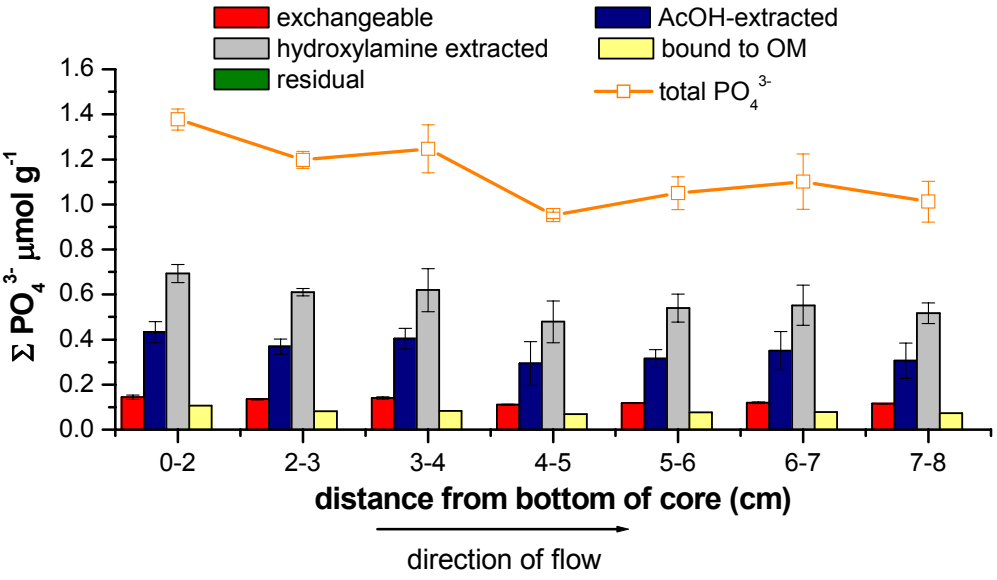

Figure C. 12 Phosphate distribution in soil from Reactor 3 of the low pH flow-through reactor experiments as determined by sequential extraction.

Table C. 1 Transport parameters determined from a one-dimensional advection-dispersion model for individual reactors.

Reactor	Retardation Factor (R)	Dispersion coefficient (D) (cm^2/sec)	Advection rate (v) (cm/sec)
High-pH org-P amended (averaged)	0.99	9.8 (± 7.5) 10^{-4}	1.1 (± 0.78) 10^{-4}
- Reactor 1	0.99	3.3 10^{-4}	6.7 10^{-5}
- Reactor 2	0.99	8.2 10^{-4}	4.7 10^{-5}
- Reactor 3	0.99	1.8 10^{-3}	1.9 10^{-4}
High-pH control	0.99	1.7 10^{-4}	1.6 10^{-5}
Low-pH org-P amended (curve 1) (averaged)	0.99	3.2 (± 2.8) 10^{-4}	6.1 (± 0.8) 10^{-5}
- Reactor 1	0.99	1.8 10^{-4}	6.6 10^{-5}
- Reactor 2	0.99	6.4 10^{-4}	6.6 10^{-5}
- Reactor 3	0.99	1.4 10^{-4}	5.2 10^{-5}
Low-pH org-P amended (curve 2) (averaged)	0.99	1.5 (± 0.7) 10^{-4}	2.9 (± 1.6) 10^{-5}
- Reactor 1	0.99	1.2 10^{-4}	1.8 10^{-5}
- Reactor 2	0.99	1.0 10^{-4}	4.8 10^{-5}
- Reactor 3	0.99	2.3 10^{-4}	2.2 10^{-5}
Low-pH control	0.99	3.3 10^{-5}	3.6 10^{-5}

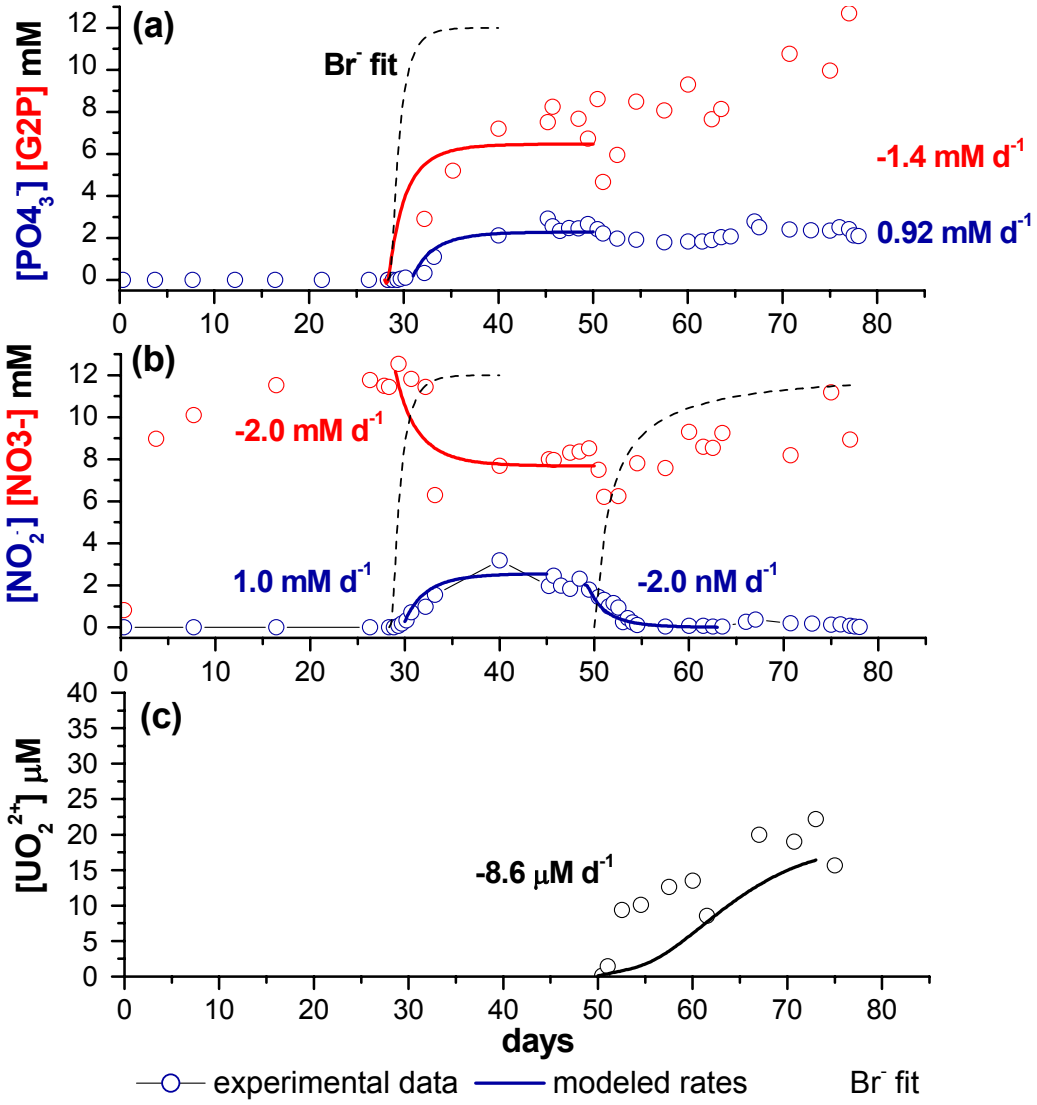

Figure C. 13 Low pH Reactor 1 continuously amended with 10 mM G2P and 200 µM UO_2^{2+}. Experimental (open circles) vs. modeled (solid lines) data from a one-dimensional advection-dispersion transport model: (a) G2P and PO_4^{3-}, (b) NO_2^- and NO_3^-, and (c) and UO_2^{2+}. Positive and negative rates indicate net production and consumption of a species, respectively. Dashed black lines are the modeled bromide breakthrough curves.

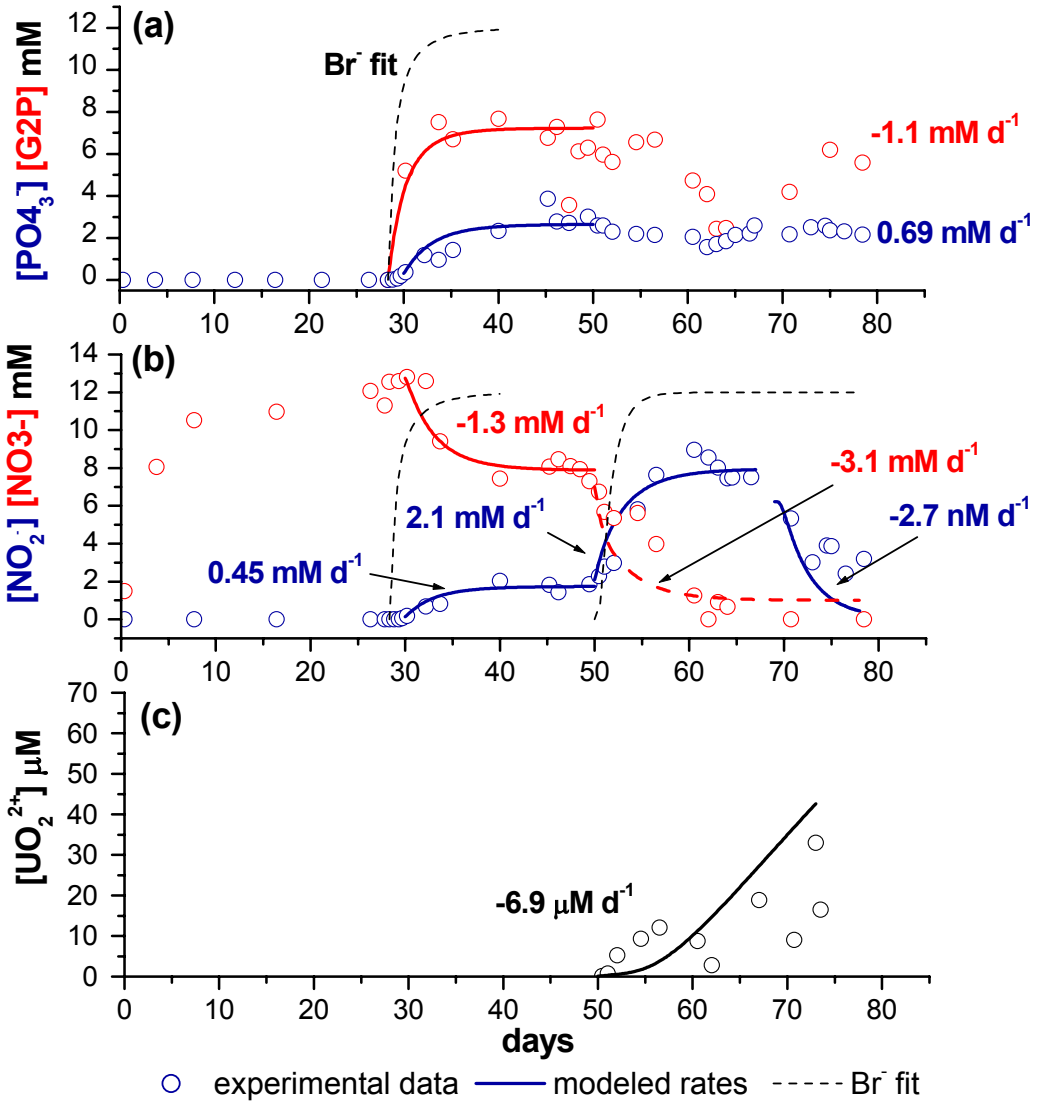

Figure C. 14 Low pH Reactor 2 continuously amended with 10 mM G2P and 200 µM UO_2^{2+}. Experimental (open circles) vs. modeled (solid lines) data from a one-dimensional advection-dispersion transport model: (a) G2P and PO_4^{3-}, (b) NO_2^- and NO_3^-, and (c) UO_2^{2+}. Positive and negative rates indicate net production and consumption of a species, respectively. Dashed black lines are the modeled bromide breakthrough curves.

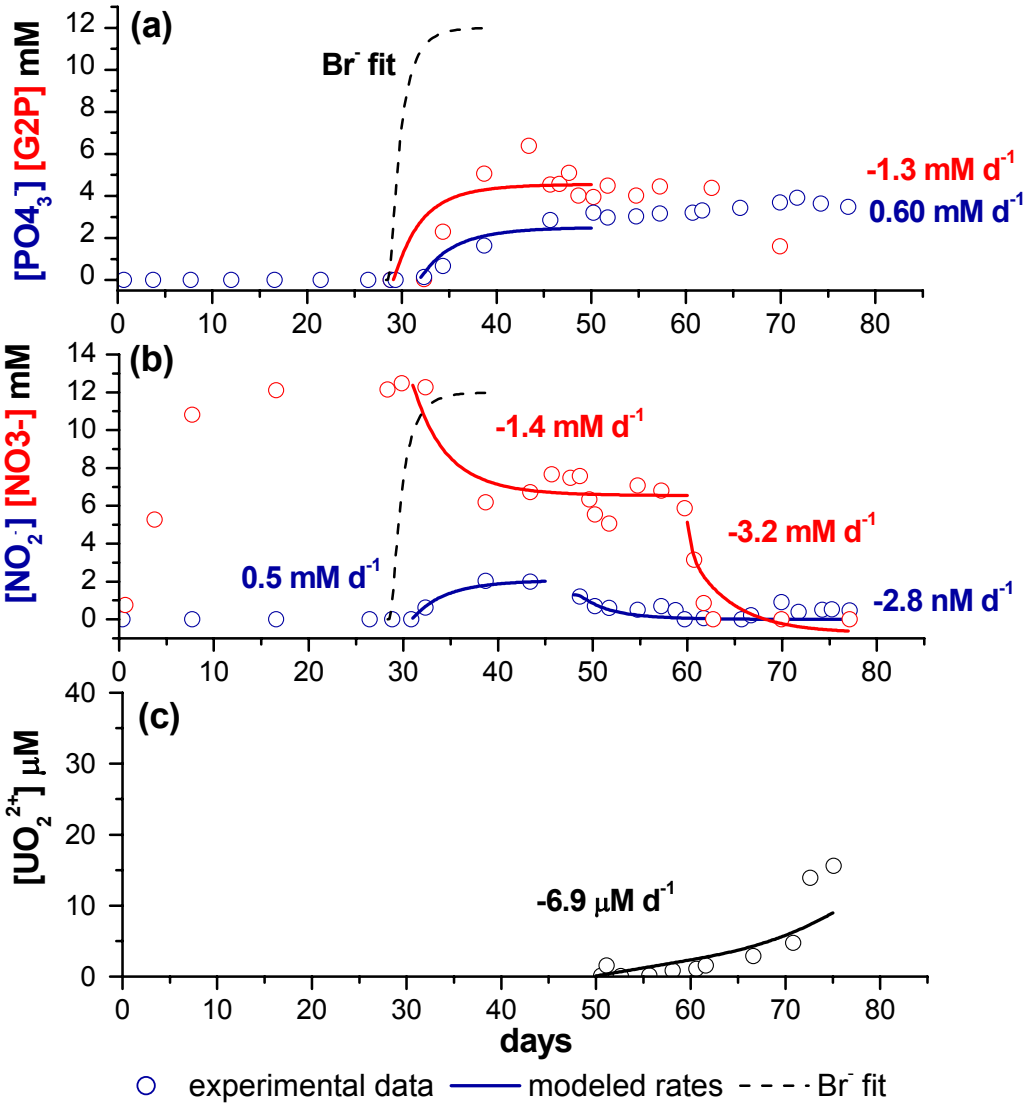

Figure C. 15 Low pH Reactor 3 continuously amended with 10 mM G2P and 200 µM UO_2^{2+}. Experimental (open circles) vs. modeled (solid lines) data from a one-dimensional advection-dispersion transport model: (a) G2P and PO_4^{3-}, (b) NO_2^- and NO_3^-, and (c) UO_2^{2+}. Positive and negative rates indicate net production and consumption of a species, respectively. Dashed black lines are the modeled bromide breakthrough curves.

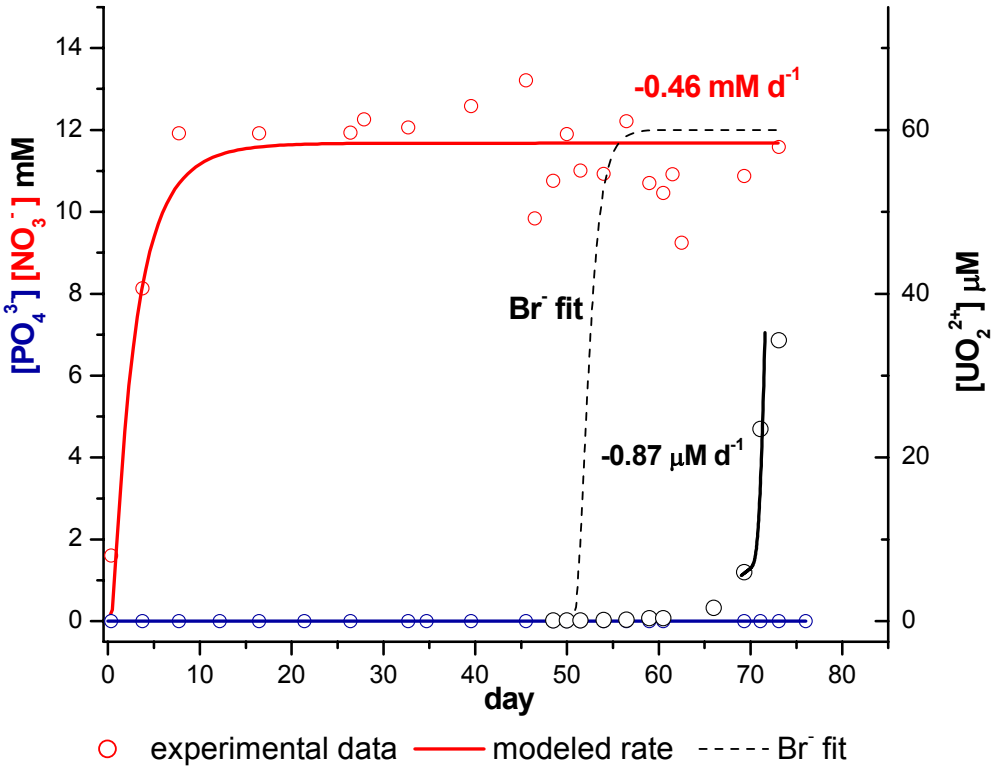

Figure C. 16 Low pH control reactor continuously amended with 200 µM UO_2^{2+}. Experimental (open circles) vs. modeled (solid lines) data from a one-dimensional advection-dispersion transport model: PO_4^{3-}, NO_3^-, and UO_2^{2+}. Positive and negative rates indicate net production and consumption of a species, respectively. Dashed line is the modeled bromide breakthrough curve.

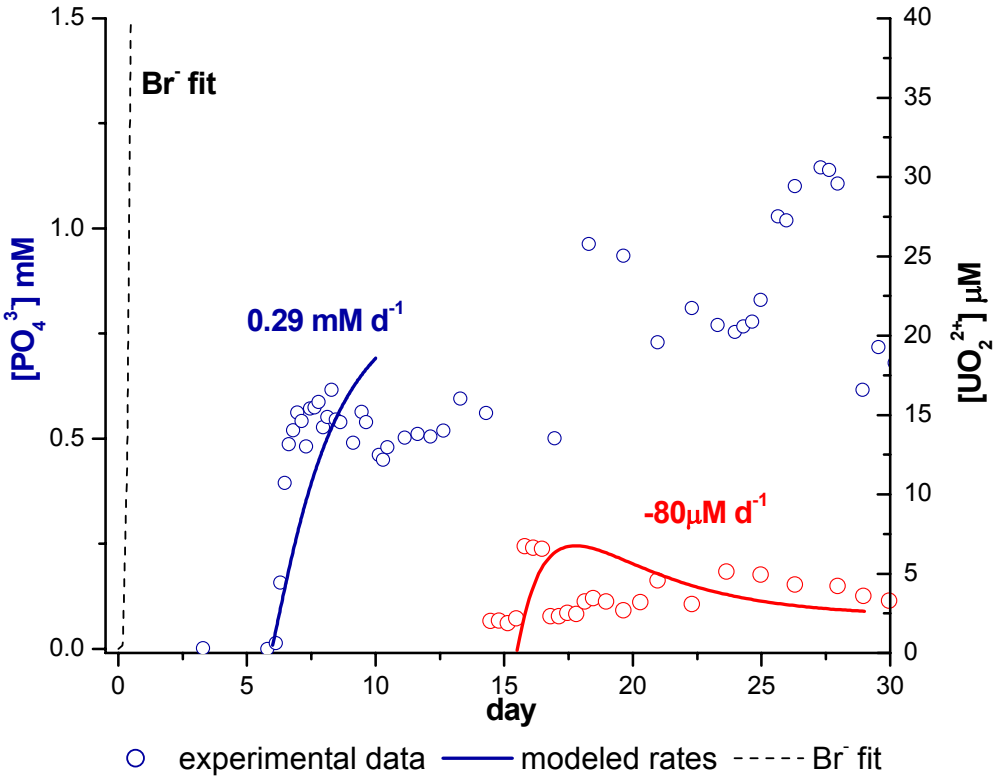

Figure C. 17 High pH Reactor 1 continuously amended with 10 mM G3P and 200 μM UO_2^{2+}. Experimental (open circles) vs. modeled (solid lines) data from a one-dimensional advection-dispersion transport model: PO_4^{3-} and UO_2^{2+}. Positive and negative rates indicate net production and consumption of a species, respectively. Dashed black lines are the modeled bromide breakthrough curves.

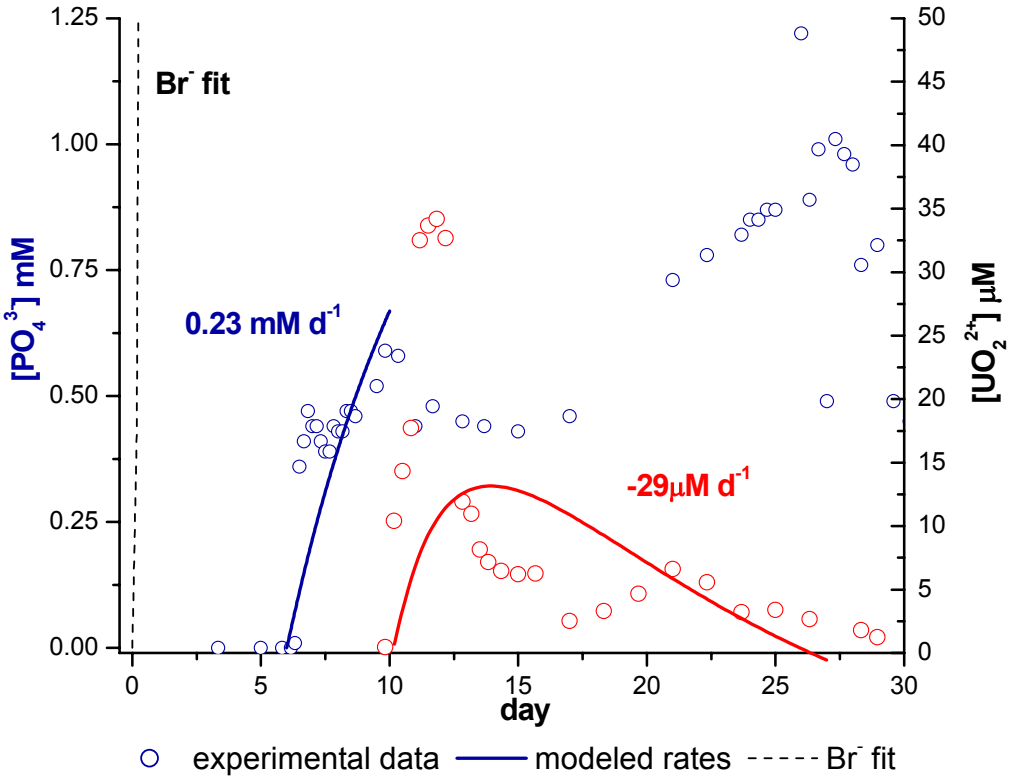

Figure C. 18 High pH Reactor 2 continuously amended with 10 mM G3P and 200 μM UO_2^{2+}. Experimental (open circles) vs. modeled (solid lines) data from a one-dimensional advection-dispersion transport model: PO_4^{3-} and UO_2^{2+}. Positive and negative rates indicate net production and consumption of a species, respectively. Dashed black line is the modeled bromide breakthrough curves.

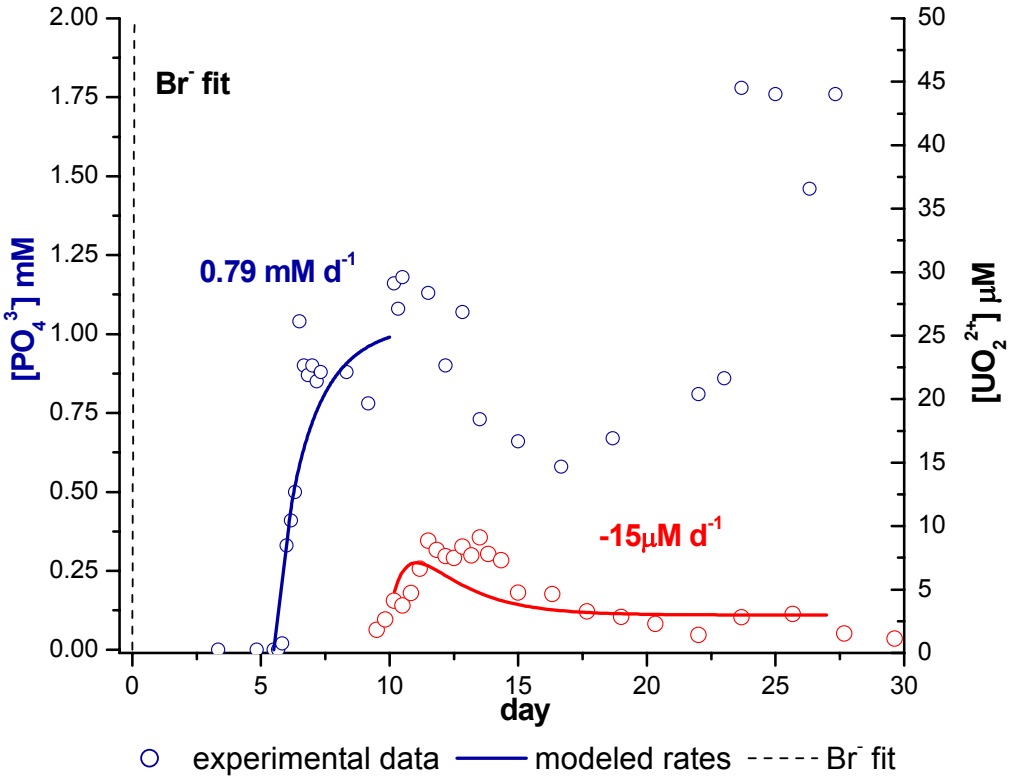

Figure C. 19 High pH Reactor 3 continuously amended with 10 mM G3P and 200 µM UO_2^{2+}. Experimental (open circles) vs. modeled (solid lines) data from a one-dimensional advection-dispersion transport model: PO_4^{3-} and UO_2^{2+}. Positive and negative rates indicate net production and consumption of a species, respectively. Dashed black line is the modeled bromide breakthrough curves.

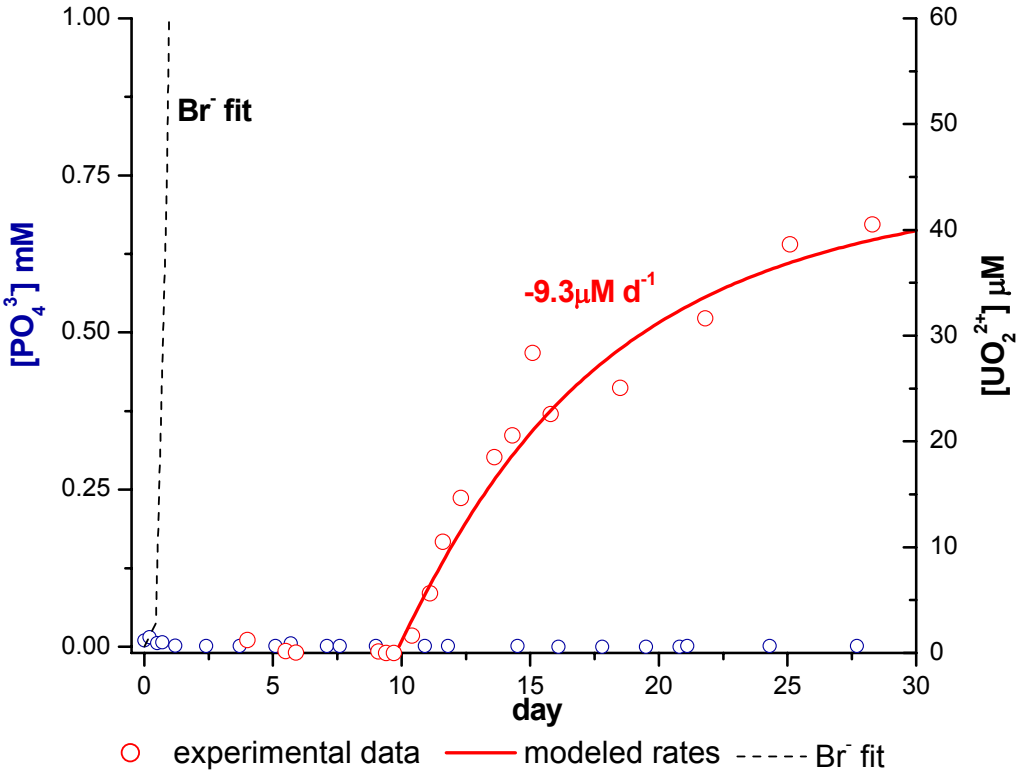

Figure C. 20 High pH U-control reactor continuously amended with 200 µM UO_2^{2+}. Experimental (open circles) vs. modeled (solid lines) UO_2^{2+} data determined from a one-dimensional advection-dispersion transport model. (Positive and negative rates indicate net production and consumption of a species, respectively. Dashed black line is the modeled bromide breakthrough curves.

REFERENCES

Akob, D. M., Mills, H. J., and Kostka, J. E., 2007. Metabolically active microbial communities in uranium-contaminated subsurface sediments. *FEMS Microbiol. Ecol.* **59**, 95-107.

Alexander, M., 1981. Biodegradation of chemicals of environmental concern. *Science* **211**, 132-138.

Ankudinov, A. L., Ravel, B., Rehr, J. J., and Conradson, S. D., 1998. Real space multiple scattering calculation of XANES. *Phys. Rev. B* **58**, 7565.

Arai, Y., Marcus, M. A., Tamura, N., Davis, J. A., and Zachara, J. M., 2007. Spectroscopic evidence for uranium bearing precipitates in vadose zone sediments at the Hanford 300-Area site. *Environ. Sci. Technol.* **41**, 4633-4639.

Arey, J. S., Seaman, J. C., and Bertsch, P. M., 1999. Immobilization of uranium in contaminated sediments by hydroxyapatite addition. *Environ. Sci. Technol.* **33**, 337-342.

Balkwill, D. L. and Boone, D. R., 1997. Identity and diversity of microorganisms cultured from subsurface environments. In: Amy, P. S. and Haldeman, D. L. Eds., *The Microbiology of the Terrestrial Deep Subsurface*. CRC Lewis Publishers, Boca Raton
New York.

Bargar, J. R., Reitmeyer, R., Lenhart, J. J., and Davis, J. A., 2000. Characterization of U(VI)-carbonato ternary complexes on hematite: EXAFS and electrophoretic mobility measurements. *Geochim. Cosmochim. Acta* **64**, 2737-2749.

Barnett, M. O., Jardine, P. M., and Brooks, S. C., 2002. U(VI) adsorption to heterogeneous subsurface media: Application of a surface complexation model. *Environ. Sci. Technol.* **36**, 937-942.

Barnett, M. O., Jardine, P. M., Brooks, S. C., and Selim, H. M., 2000. Adsorption and transport of uranium(VI) in subsurface media. *Soil Science Society of America Journal* **64**, 908-917.

Beazley, M. J., Martinez, R. J., Sobecky, P. A., Webb, S. M., and Taillefert, M., 2007. Uranium biomineralization as a result of bacterial phosphatase activity: Insights from bacterial isolates from a contaminated subsurface. *Environ. Sci. Technol.* **41**, 5701-5707.

Beazley, M. J., Martinez, R. J., Sobecky, P. A., Webb, S. M., and Taillefert, M., 2009. Nonreductive biomineralization of uranium(VI) phosphate via microbial phosphatase activity in anaerobic conditions. *Geomicrobiol. J.*

Beller, H. R., 2005. Anaerobic, nitrate-dependent oxidation of U(IV) oxide minerals by the chemolithoautotrophic bacterium *Thiobacillus denitrificans*. *Appl. Environ. Microbiol.* **71**, 2170-2174.

Benjamin, M. M., 2002. *Water Chemistry*. McGraw-Hill, New York.

Bernhard, G., Geipel, G., Brendler, V., and Nitsche, H., 1996. Speciation of uranium in seepage waters of a mine tailing pile studied by time-resolved laser-induced fluorescence spectroscopy (TRLFS). *Radiochim. Acta* **74**, 87-91.

Bertsch, P. M., Hunter, D. B., Sutton, S. R., and Bajt, S., 1994. *In situ* chemical speciation of uranium in soils and sediments by micro X-ray absorption spectroscopy. *Environ. Sci. Technol.* **28**, 980-984.

Betlach, M. R. and Tiedje, J. M., 1981. Kinetic explanation for accumulation of nitrite, nitric oxide, and nitrous oxide during bacterial denitrification. *Appl. Environ. Microbiol.* **42**, 1074-1084.

Bollag, J.-M. and Henninger, N. M., 1978. Effects of nitrite toxicity on soil bacteria under aerobic and anaerobic conditions. *Soil Biol. Biochem.* **10**, 377-381.

Borch, T., Masue, Y., Kukkadapu, r. K., and Fendorf, S., 2007. Phosphate imposed limitations on biological reduction and alteration of ferrihydrite. *Environ. Sci. Technol.* **41**, 166-172.

Bostick, B. C., Fendorf, S., Barnett, M. O., Jardine, P. M., and Brooks, S. C., 2002. Uranyl surface complexes formed on subsurface media from DOE facilities. *Soil Science Society of America Journal* **66**, 99-108.

Bothe, H., Jost, G., Schloter, M., Ward, B. B., and Witzel, K.-P., 2000. Molecular analysis of ammonia oxidation and denitrification in natural environments. *FEMS Microbiol. Rev.* **24**, 673-690.

Boyanov, M. I., O'Loughlin, E. J., Roden, E. E., Fein, J. B., and Kemner, K. M., 2007. Adsorption of Fe(II) and U(VI) to carboxyl-functionalized microspheres: The influence of speciation on uranyl reduction studied by titration and XAFS. *Geochim. Cosmochim. Acta* **71**, 1898-1912.

Brendel, P. J. and Luther, G. W., III, 1995. Development of a gold amalgam voltammetric microelectrode for the determination of dissolved Fe, Mn, O_2, and S(-II) in porewaters of marine and freshwater sediments. *Environ. Sci. Technol.* **29**, 751-761.

Brooks, S. C., 2001. Waste Characteristics of the Former S-3 Ponds and Outline of Uranium Chemistry Relevant to NABIR Field Research Center Studies. Technical Report; NABIR FRC.

Brooks, S. C., Fredrickson, J. K., Carroll, S. L., Kennedy, D. W., Zachara, J. M., Plymale, A. E., Kelly, S. D., Kemner, K. M., and Fendorf, S., 2003. Inhibition of bacterial U(VI) reduction by calcium. *Environ. Sci. Technol.* **37**, 1850-1858.

Bruno, J., De Pablo, J., Duro, L., and Figuerola, E., 1995. Experimental study and modeling of the U(VI)-Fe(OH)$_3$ surface precipitation/coprecipitation equilibria. *Geochim. Cosmochim. Acta* **59**, 4113-4123.

Burns, P. C., 1999. The crystal chemistry of uranium. In: Burns, P. C. and Finch, R. Eds., *Uranium: Mineralogy, Geochemistry and the Environment*. Mineralogical Society of America, Washington, D.C.

Carey, E. A. and Taillefert, M., 2005. The role of soluble Fe(III) in the cycling of iron and sulfur in coastal marine sediments. *Limnology and Oceanography* **50**, 1129-1141.

Catalano, J. G. and Brown Jr., G. E., 2004. Analysis of uranyl-bearing phases by EXAFS spectroscopy: Interferences, multiple scattering, accuracy of structural parameters, and spectral differences. *Am. Mineral.* **89**, 1004-1021.

Catalano, J. G., McKinley, J. P., Zachara, J. M., Heald, S. M., Smith, S. C., and Brown Jr., G. E., 2006. Changes in uranium speciation through a depth sequence of contaminated Hanford sediments. *Environ. Sci. Technol.* **40**, 2517-2524.

Cheng, T., Barnett, M. O., Roden, E. E., and Zhuang, J., 2004. Effects of phosphate on uranium(VI) adsorption to goethite-coated sand. *Environ. Sci. Technol.* **38**, 6059-6065.

Cheng, T., Barnett, M. O., Roden, E. E., and Zhuang, J., 2006. Effects of solid-to-solution ratio on uranium(VI) adsorption and its implications. *Environ. Sci. Technol.* **40**, 3243-3247.

Cheng, T., Barnett, M. O., Roden, E. E., and Zhuang, J., 2007. Reactive transport of uranium(VI) and phoshate in a goethite-coated sand column: An experimental study. *Chemosphere* **68**, 1218-1223.

Chernyaev, I. I., 1966. Complex compounds of uranium. Israel Program for Scientific Translations, Jerusaleum.

Coleman, J. E., 1992. Structure and mechanism of alkaline phosphatase. *Annu Rev Biophys Biomol Struct* **21**, 441-83.

Cotton, F. A., Wilkinson, G., Murillo, C. A., and Bochmann, M., 1999. *Advanced Inorganic Chemistry*. John Wiley & Sons, Inc., New York.

CRC, 1997. *CRC Handbook of Chemisty and Physics*. CRC Press, Boca Raton.

Cullity, B. D., 1978. *Elements of X-Ray Diffraction*. Addison-Wesley Publishing Company, Inc., Menlo Park, CA.

Dawson, G. and Gilman, J., 2001. Land reclamation technology - expanding the geotechnical engineering envelope. *Proceedings of the Institution of Civil Engineering-Geotechnical Engineering* **149**, 49-61.

De Pablo, J., Casas, I., Giménez, J., Molera, M., Rovira, M., Duro, L., and Bruno, J., 1999. The oxidative dissolution mechanism of uranium dioxide. I. The effect of temperature in hydrogen carbonate medium. *Geochim. Cosmochim. Acta* **63**, 3097-3103.

De Yoreo, J. J. and Vekilov, P. G., 2003. Principles of crystal nucleation and growth. In: Dove, P. M., De Yoreo, J. J., and Weiner, S. Eds., *Biomineralization*. Mineralogical Society of America, Washington, D.C.

Dideriksen, K. and Stipp, S. L. S., 2003. The adsorption of glyphosate and phosphate to geothite: A molecular-scale atomic force microscopy study. *Geochim. Cosmochim. Acta* **67**, 3313-3327.

Diress, A. and Lucy, C. A., 2005. Study of the selectivity of inorganic anions in hydro-organic solvents using indirect capillary electrophoresis. *Journal of Chromatography A* **1085**, 155-163.

DOE, 1997. Linking Legacies - Connecting the cold war nuclear weapons production processes to their environmental consequences. Office of Environmental Management - The U.S. Department of Energy, Washington, D.C.

Dong, W. and Brooks, S. C., 2006. Determination of the formation constants of ternary complexes of uranyl and carbonate with alkaline earth metals (Mg^{2+}, Ca^{2+}, Sr^{2+}, and Ba^{2+}) using anion exhange method. *Environ. Sci. Technol.* **40**, 4689-4695.

Drysdale, G. D., Kasan, H. C., and Bux, F., 1999. Denitrification by heterotrophic bacteria during activated sludge treatment. *Water SA* **25**, 357-362.

Edwards, L., Küsel, K., Drake, H., and Kostka, J. E., 2007. Electron flow in acidic subsurface sediments co-contaminated with nitrate and uranium. *Geochim. Cosmochim. Acta* **71**, 643-654.

Ewing, R. C., 1999. Radioactivity and the 20th Century. In: Burns, P. C. and Finch, R. Eds., *Uranium: Mineralogy, Geochemistry and the Environment*. Mineralogical Society of America, Washington, D.C.

Fields, M. W., Yan, T., Rhee, S.-K., Carroll, S. L., Jardine, P. M., Watson, D. B., Criddle, C. S., and Zhou, J., 2005. Impacts on microbial communities and cultivable isolates from groundwater contaminated with high levels of nitric acid-uranium waste. *FEMS Microbiol. Ecol.* **53**, 417-428.

Finch, R. and Murakami, T., 1999. Systematics and paragenesis of uranium minerals. In: Burns, P. C. and Finch, R. Eds., *Uranium: Mineralogy, Geochemistry and the Environment*. Mineralogical Society of America, Washington, D.C.

Finneran, K. T., Housewright, M. E., and Lovley, D. R., 2002. Multiple influenences of nitrate on uranium solubility during bioremediation of uranium-contaminated subsurface sediments. *Environ. Microbiol.* **4**, 510-516.

Fox, P. M., Davis, J. A., and Zachara, J. M., 2006. The effect of calcium on aqueous uranium(VI) speciation and adsorption to ferrihydrite and quartz. *Geochim. Cosmochim. Acta* **70**, 1379-1387.

Francis, A. J., Dodge, C. J., Gillow, J. B., and Papenguth, H. W., 2000. Biotransformation of uranium compounds in high ionic strength brine by a halophilic bacterium under denitrifying conditions. *Environ. Sci. Technol.* **34**, 2311-2317.

Fredrickson, J. K., Zachara, J. M., Kennedy, D. W., Duff, M. C., Gorby, Y. A., Li, S.-M. W., and Krupka, K. M., 2000. Reduction of U(VI) in goethite (α-FeOOH) suspensions by a dissimilatory metal-reducing bacterium. *Geochim. Cosmochim. Acta* **64**, 3085-3098.

Fredrickson, J. K., Zachara, J. M., Kennedy, D. W., Liu, C., Duff, M. C., Hunter, D. B., and Dohnalkova, A., 2002. Influence of Mn oxides on the reduction of uranium (VI) by the metal-reducing bacterium *Shewanella putrefaciens*. *Geochim. Cosmochim. Acta* **66**, 3247-3262.

Fuller, C. C., Bargar, J. R., and Davis, J. A., 2003. Molecular-scale characterization of uranium sorption by bone apatite materials for a permeable reactive barrier demonstration. *Environ. Sci. Technol.* **37**, 4642-4649.

Fuller, C. C., Bargar, J. R., Davis, J. A., and Piana, M. J., 2002. Mechanisms of uranium interactions with hydroxyapatite: Implications for groundwater remediation. *Environ. Sci. Technol.* **36**, 158-165.

Ganesh, R., Robinson, K. G., Chu, L., Kucsmas, D., and Reed, G. D., 1999. Reductive precipitation of uranium by *Desulfovibrio desulfuricans*: Evaluation of cocontaminant effects and selective removal. *Water Research* **33**, 3447-3458.

Grasshoff, K., 1983. Determination of nitrite. In: Grasshoff, K., Ehrhardt, M., and Kremling, K. Eds., *Methods of Seawater Analysis*. Verlag Chemie GmbH, Weinheim.

Grenthe, I., Fuger, J., Konings, R. J. M., Lemire, R. J., Mueller, A. B., Nguyen-Trung, C., and Wanner, H., 1992. *Chemical Thermodynamics of Uranium*. Nuclear Energy Agency, Paris, France.

Gu, B., Brooks, S. C., Roh, Y., and Jardine, P. M., 2003. Geochemical reactions and dynamics during titration of a contaminated groundwater with high uranium, aluminum, and calcium. *Geochim. Cosmochim. Acta* **67**, 2749-2761.

Guillaumont, R., Fanghänel, T., Fuger, J., Grenthe, I., Neck, V., Palmer, D. A., and Rand, M. H., 2003. *Chemical Thermodynamics 5. Update on the Chemical Thermodynamics of Uranium, Neptunium, Plutonium, Americium and Technetium*. Elsevier, Amsterdam.

Haas, J. R. and Northup, A., 2004. Effects of aqueous complexation on reductive precipitation of uranium by *Shewanella putrefaciens*. *Geochemical Transactions* **5**, 41-48.

Hansel, C. M., Benner, S. G., Neiss, J., Dohnalkova, A., Kukkadapu, R. K., and Fendorf, S., 2003. Secondary mineralization pathways induced by dissimilatory iron reduction of ferrihydrite under advective flow. *Geochim. Cosmochim. Acta* **67**, 2977-2992.

Harris, D. C., 1999. *Quantitative Chemical Analysis*. W. H. Freeman and Company, New York.

Hsi, C.-K. D. and Langmuir, D., 1985. Adsorption of uranyl onto ferric oxyhydroxides: Application of the surface complexation site-binding model. *Geochim. Cosmochim. Acta* **49**, 1931-1941.

Hudson, E. A., Allen, P. G., Terminello, L. J., Denecke, M. A., and Reich, T., 1996. Polarized x-ray-absorption spectroscopy of the uranyl ion: Comparison of experiment and theory. *Phys. Rev. B* **54**, 156-165.

Hudson, E. A., Terminello, L. J., Viani, B. E., Denecke, M., Reich, T., Allen, P. G., Bucher, J. J., Shuh, D. K., and Edelstein, N. M., 1999. The structure of U^{6+} sorption complexes on vermiculite and hydrobiotite. *Clays and Clay Minerals* **47**, 439-457.

Istok, J. D., Senko, J. M., Krumholz, L. R., Watson, D., Bogle, M. A., Peacock, A., Chang, Y.-J., and White, D. C., 2004. In situ bioreduction of technetium and uranium in a nitrate-contaminated aquifer. *Environ. Sci. Technol.* **38**, 468-475.

Jardine, P. M., Watson, D. B., Blake, D. A., Beard, L. P., Brooks, S. C., Carley, J. M., Criddle, C. S., Doll, W. E., Fields, M. W., Fendorf, S. E., Geesey, G. G., Ginder-Vogel, M., Hubbard, S. S., Istok, J. D., Kelly, S., Kemner, K. M., Peacock, A. D., Spalding, B. P., White, D. C., Wolfe, A., Wu, W., and Zhou, J., 2006. Techniques for assessing the performance of in situ bioreduction and immobilization of metals and radionuclides in contaminated subsurface envionments. Technical Report; NABIR FRC.

Jeon, B.-H., Dempsey, B. A., Burgos, W. D., Barnett, M. O., and Roden, E. E., 2005. Chemical reduction of U(VI) by Fe(II) at the solid-water interface using natural and synthetic Fe(III) oxides. *Environ. Sci. Technol.* **39**, 5642-5649.

Jeong, B. C., Hawes, C., Bonthrone, K. M., and Macaskie, L. E., 1997. Localization of enzymically enhanced heavy metal accumulation by *Citrobacter* sp. and metal accumulation *in vitro* by liposomes containing entrapped enzyme. *Microbiology* **143**, 2497-2507.

Jerden Jr., J. L. and Sinha, A. K., 2003. Phosphate based immobilization of uranium in an oxidizing bedrock aquifer. *Appl. Geochem.* **18**, 823-843.

Kelly, S. D., Kemner, K. M., Fein, J. B., Fowle, D. A., Boyanov, M. I., Bunker, B. A., and Yee, N., 2002. X-ray absorption fine structure determination of pH-dependent U-bacterial cell wall interactions. *Geochim. Cosmochim. Acta* **66**, 3855-3871.

Kelly, S. D., Kemner, K. M., O'Loughlin, E. J., Boyanov, M. I., Watson, D. B., Jardine, P. M., and Phillips, D. H., 2005. U L_3-Edge EXAFS Measurements of Sediment Samples from Oak Ridge National Laboratory, Tennessee, U.S.A. Technical Report; NABIR FRC.

Kertesz, M. A., Cook, A. M., and Leisinger, T., 1994. Microbial metabolism of sulfur- and phosphorus-containing xenobiotics. *FEMS Microbiol. Rev.* **15**, 195-215.

Kim, E. E. and Wyckoff, H. W., 1991. Reaction mechanism of alkaline phosphatase based on crystal structures: Two-metal ion catalysis. *Journal of Molecular Biology* **218**, 449-464.

Knowles, R., 1982. Denitrification. *Microbiol. Rev.* **46**, 43-70.

Knox, A. S., Brigmon, R. L., Kaplan, D. I., and Paller, M. H., 2008. Interactions among phosphate amendments, microbes and uranium mobility in contaminated sediments. *Science of the Total Environment* **295**, 63-71.

Koban, A., Geipel, G., Roßberg, A., and Bernhard, G., 2004. Uranium (VI) complexes with sugar phosphates in aqueous solution. *Radiochim. Acta* **92**, 903-908.

Krieg, N. R. and Holt, J. G., 1984. Bergey's Manual of Systematic Bacteriology. In: Krieg, N. R. and Holt, J. G. Eds.). Williams & Wilkins, Baltimore, MD.

Lack, J. G., Chaudhuri, S. K., Kelly, S. D., Kemner, K. M., O'Connor, S. M., and Coates, J. D., 2002. Immobilization of radionuclides and heavy metals through anaerobic bio-oxidation of Fe(II). *Appl. Environ. Microbiol.* **68**, 2704-2710.

Langmuir, D., 1978. Uranium solution-mineral equilibria at low temperatures with applications to sedimentary ore deposits. *Geochim. Cosmochim. Acta* **42**, 547-569.

Langmuir, D., 1997. *Aqueous Environmental Geochemistry*. Prentice Hall, Upper Saddle River, New Jersey.

Lenhart, J. J. and Honeyman, B. D., 1999. Uranium(VI) sorption to hematite in the presence of humic acid. *Geochim. Cosmochim. Acta* **63**, 2891-2901.

Liger, E., Charlet, L., and Van Cappellen, P., 1999. Surface catalysis of uranium(VI) reduction by iron(II). *Geochim. Cosmochim. Acta* **63**, 2939-2955.

Liu, C., Jeon, B.-H., Zachara, J. M., and Wang, Z., 2007. Influence of calcium on microbial reduction of solid phase uranium(VI). *Biotechnol. Bioeng.* **97**, 1415-1422.

Locock, A. J. and Burns, P. C., 2003. The crystal structure of synthetic autunite, $Ca[(UO_2)(PO_4)]_2(H_2O)_{11}$. *Am. Mineral.* **88**, 240-244.

Lovley, D. R. and Phillips, E. J. P., 1992. Reduction of uranium by *Desulfovibrio desulfuricans*. *Appl. Environ. Microbiol.* **58**, 850-856.

Lovley, D. R., Phillips, E. J. P., Gorby, Y. A., and Landa, E. R., 1991. Microbial reduction of uranium. *Nature* **350**, 413-416.

Luther, G. W., III, Bono, A. B., Taillefert, M., and Cary, S. C., 2002. A continuous flow electrochemical cell for analysis of chemical species and ions at high pressure: Laboratory, shipboard and hydrothermal vent results. In: Taillefert, M. and Rozan, T. F. Eds., *Environmental electrochemistry: Analyses of trace element biogeochemistry*. ACS Symposium Series. American Chemical Society.

Luther, G. W. and Popp, J. I., 2002. Kinetics of the abiotic reduction of polymeric manganese dioxide by nitrite: An anaerobic nitrification reaction. *Aquat.Geochem.* **8**, 15-36.

Macaskie, L. E. and Basnakova, G., 1998. Microbially-enhanced chemisorption of heavy metals: A method for the bioremediation of solutions containing long-lived isotopes of neptunium and plutonium. *Environ. Sci. Technol.* **32**, 184-187.

Macaskie, L. E., Bonthrone, K. M., and Rouch, D. A., 1994. Phosphatase-mediated heavy metal accumulation by a *Citrobacter* sp. and related enterobacteria. *FEMS Microbiol. Lett.* **121**, 141-146.

Macaskie, L. E., Empson, R. M., Cheetham, A. K., Grey, C. P., and Skarnulis, A. J., 1992. Uranium bioaccumulation by a *Citrobacter* sp. as a result of enzymatically mediated growth of polycrystalline HUO_2PO_4. *Science* **257**, 782-784.

Macaskie, L. E., Hewitt, C. J., Shearer, J. A., and Kent, C. A., 1995. Biomass production for the removal of heavy metals from aqueous solutions at low pH using growth-decoupled cells of a *Citrobacter* sp. *International Biodeterioration & Biodegradation* **35**, 73-92.

Mackay, D. M. and Cherry, J. A., 1989. Groundwater remediation: Pump-and-treat remediation. **23**, 630-636.

Madden, A. S., Smith, A. C., Balkwill, D. L., Fagan, L. A., and Phelps, T. J., 2007. Microbial uranium immobilization independent of nitrate reduction. *Environ. Microbiol.* **9**, 2321-2330.

Martinez, R. J., 2008. Multiscale analyses of microbial popluations in extreme environments, Georgia Institute of Technology.

Martinez, R. J., Beazley, M. J., Taillefert, M., Arakaki, A. K., Skolnick, J., and Sobecky, P. A., 2007. Aerobic uranium(VI) bioprecipitation by metal-resistant bacteria isolated from radionuclide- and metal-contaminated subsurface soils. *Environ. Microbiol.* **9**, 3122-3133.

Martinez, R. J., Wang, Y., Raimondo, M. A., Coombs, J. M., Barkay, T., and Sobecky, P. A., 2006. Horizontal gene transfer of P_{IB}-type ATPases among bacteria isolated from radionuclide- and metal-contaminated subsurface soils. *Appl. Environ. Microbiol.* **72**, 3111-3118.

Meijer, E. M., Van Der Zwaan, J. W., Wever, R., and Stouthamer, A. H., 1979. Anaerobic respiration and energy conservation in *Paracoccus denitrificans*. Functioning of iron-sulfur centers and the uncoupling effect of nitrite. *Eur. J. Biochem.* **96**, 69-76.

Merroun, M. L., Raff, J., Rossberg, A., Hennig, C., Reich, T., and Selenska-Pobell, S., 2005. Complexation of uranium by cells and S-layer sheets of *Bacillus sphaericus* JG-A12. *Appl. Environ. Microbiol.* **71**, 5532-5543.

Montgomery, D. M., Dean, A. C. R., Wiffen, P., and Macaskie, L. E., 1995. Phosphatase production and activity in *Citrobacter freundii* and a naturally occurring, heavy-metal-accumulating *Citrobacter* sp. *Microbiology* **141**, 2433-2441.

Moon, H. S., Komlos, J., and Jaffé, P., 2007. Uranium reoxidation in previously bioreduced sediment by dissolved oxygen and nitrate. *Environ. Sci. Technol.* **41**, 4587-4592.

Morris, D. E., Allen, P. G., Berg, J. M., Chisholm-Brause, C. J., Conradson, S. D., Donohoe, R. J., Hess, N. J., Musgrave, J. A., and Tait, C. D., 1996. Speciation of uranium in Fernald soils by molecular spectroscopic methods: Characterization of untreated soils. *Environ. Sci. Technol.* **30**, 2322-2331.

Murphy, J. and Riley, J. P., 1962. A modified single solution method for the determination of phosphate in natural waters. *Anal. Chim. Acta* **27**, 31-36.

Murphy, W. M. and Shock, E. L., 1999. Environmental aqueous geochemistry of actinides. In: Burns, P. C. and Finch, R. Eds., *Uranium: Mineralogy,*

Geochemistry and the Environment. Mineralogical Society of America, Washington, D.C.

NABIR, 2003. Bioremediation of Metals and Radionuclides. DOE.

Nash, K. L., Jensen, M. P., and Schmidt, M. A., 1998. Actinide immobilization in the subsurface environment by in-situ treatment with a hydrolytically unstable organophosphate complexant: Uranyl uptake by calcium phytate. *Journal of Alloys and Compounds* **271-273**, 257-261.

North, N. N., Dollhopf, S. L., Petrie, L., Istok, J. D., Balkwill, D. L., and Kostka, J. E., 2004. Change in bacterial community structure during in situ biostimulation of subsurface sediment cocontaminated with uranium and nitrate. *Appl. Environ. Microbiol.* **70**, 4911-4920.

Noubactep, C., 2006. Effect of selected ligands on the U(VI) immobilization by zerovalent iron. *Journal of Radioanalytical and Nuclear Chemistry* **267**, 13-19.

Noubactep, C., Schoner, A., and Meinrath, G., 2006. Mechanism of uranium removal from the aqueous solution by elemental iron. *Journal of Hazardous Materials* **B132**, 202-212.

O'Loughlin, E. J., Kelly, S. D., Cook, R. E., Csencsits, R., and Kemner, K. M., 2003. Reduction of uranium(VI) by mixed iron(II)/iron(III) hydroxide (green rust): Formation of UO nanoparticles. *Environ. Sci. Technol.* **37**, 721-727.

Ohnuki, T., Kozai, N., Samadfam, M., Yasuda, R., Yamamoto, S., Narumi, K., Naramoto, H., and Murakami, T., 2004. The formation of autunite ($Ca(UO_2)_2(PO_4)_2{\cdot}nH_2O$) within the leached layer of dissolving apatite: incorporation mechanism of uranium by apatite. *Chem. Geol.* **211**, 1-14.

Panak, P. J., Knopp, R., Booth, C. H., and Nitsche, H., 2002. Spectroscopic studies on the interaction of U(VI) with *Bacillus sphaericus*. *Radiochim. Acta* **90**, 779-783.

Panak, P. J., Raff, J., Selenska-Pobell, S., Geipel, G., Bernhard, G., and Nitsche, H., 2000. Complex formation of U(VI) with *Bacillus*-isolates from a uranium mining waste pile. *Radiochim. Acta* **88**, 71-76.

Patureau, D., Zumstein, E., Delgenes, J. P., and Moletta, R., 2000. Aerobic denitrifiers isolated from diverse natural and managed ecosystems. *Microbial Ecology* **39**, 145-152.

Payne, T. E., Davis, J. A., and Waite, T. D., 1996. Uranium adsorption on ferrihydrite - Effects of phosphate and humic acid. *Radiochim. Acta* **74**, 239-243.

Perdue, E. M., 1985. Acidic functional groups of humic substances. In: Aiken, G. R., McKnight, D. M., Wershaw, R. L., and MacCarthy, P. Eds., *Humic Substances in*

Soil, Sediment, and Water: Geochemistry, Isolation, and Characterization. John Wiley & Sons, Inc., New York.

Powers, L. G., Mills, H. J., Palumbo, A. V., Zhang, C., Delaney, K., and Sobecky, P. A., 2002. Introduction of a plasmid-encoded *phoA* gene for constitutive overproduction of alkaline phosphatase in three subsurface *Pseudomonas* isolates *FEMS Microbiol. Ecol.* **41**, 115-123.

Rabinowitch, E. and Belford, R. L., 1964. *Spectroscopy and photochemistry of uranyl compounds*. The Macmillan Company, New York.

Rake, J. B. and Eagon, R. G., 1980. Inhibition, but not uncoupling, of respiratory energy coupling of three bacterial species by nitrite. *J. Bacteriol.* **144**, 975-982.

Robinson, K. G., Ganesh, R., and Reed, G. D., 1998. Impact of organic ligands on uranium removal during anaerobic biological treatment. *Water Science & Technology* **37**, 73-80.

Roh, Y., Lee, S. R., Choi, S.-K., Elless, M. P., and Lee, S. Y., 2000. Physicochemical and mineralogical characterization of uranium-contaminated soils. *Soil and Sediment Contamination* **9**, 463-486.

Ross, V., 1955. Studies of uranium minerals (XXI): Synthetic hydrogen-autunite. *Am. Mineral.* **40**, 917-919.

Rossolini, G. M., Schippa, S., Riccio, M. L., Berlutti, F., Macaskie, L. E., and Thaller, M. C., 1998. Bacterial nonspecific acid phosphohydrolases: physiology, evolution and use as tools in microbial biotechnology. *Cellular and Molecular Life Sciences* **54**, 833-850.

Roychoudhury, A. N., 2001. Dispersion in unconsolidated aquatic sediments. *Estuarine, Coastal and Shelf Science* **53**, 745-757.

Roychoudhury, A. N., Van Cappellen, P., Kostka, J. E., and Viollier, E., 2003. Kinetics of microbially mediated reactions: dissimilatory sulfate reduction in saltmarsh sediments (Sapelo Island, Georgia, USA). *Estuarine, Coastal and Shelf Science* **56**, 1001-1010.

Roychoudhury, A. N., Viollier, E., and Van Cappellen, P., 1998. A plug flow-through reactor for studying biogeochemical reactions in undisturbed aquatic sediments. *Appl. Geochem.* **13**, 269-280.

Rozhon, W. M., Petutschnig, E. K., and Jonak, C., 2006. Isolation and characterization of pHW15, a small cryptic plasmid from Rahnella genomospecies 2. *Plasmid* **56**, 202-215.

Sandino, A. and Bruno, J., 1992. The solubility of $(UO_2)_3(PO_4)_2 \cdot 4H_2O_{(s)}$ and the formation of U(VI) phosphate complexes: Their influence in uranium speciation in natural waters. *Geochim. Cosmochim. Acta* **56**, 4135-4145.

Sato, T., Murakami, T., Yanase, N., Isobe, H., Payne, T. E., and Airey, P. L., 1997. Iron nodules scavenging uranium from groundwater. *Environ. Sci. Technol.* **31**, 2854-2858.

Schecher, W. D. and McAvoy, D. C., 2001. *MINEQL+: A Chemical Equilibrium Modeling System, Version 4.5 for Windows, User's Manual*. Environmental Research Software, Hallowell, Maine.

Schnoor, J. L., 1996. *Environemental modeling: Fate and transport of pollutants in water, air, and soil*. John Wiley & Sons, Inc., New York

Seaman, J. C., Hutchison, J. M., Jackson, B. P., and Vulava, V. M., 2003. In situ treatment of metals in contaminated soils with phytate. *J. Environ. Qual.* **32**, 153-161.

Senko, J. M., Istok, J. D., Suflita, J. M., and Krumholz, L. R., 2002. In-situ evidence for uranium immobilization and remobilization. *Environ. Sci. Technol.* **36**, 1491-1496.

Senko, J. M., Mohamed, Y., Dewers, T. A., and Krumholz, L. R., 2005a. Role for Fe(III) minerals in nitrate-dependent microbial U(IV) oxidation. *Environ. Sci. Technol.* **39**, 2529-2536.

Senko, J. M., Suflita, J. M., and Krumholz, L. R., 2005b. Geochemical controls on microbial nitrate-dependent U(IV) oxidation. *Geomicrobiol. J.* **22**, 371-378.

Shelobolina, E. S., Sullivan, S. A., O'Neill, K. R., Nevin, K. P., and Lovley, D. R., 2004. Isolation, characterization, and U(VI)-reducing potential of a facultatively anaerobic, acid-resistant bacterium from low-pH, nitrate- and U(VI)-contaminated subsurface sediment and description of *Salmonella subterranea* sp. nov. *Appl. Environ. Microbiol.* **70**, 2959-2965.

Sijbesma, W. F. H., Almeida, J. S., Reis, M. A. M., and Santos, H., 1996. Uncoupling effect of nitrite during denitrification by *Pseudomonas fluorescens*: An in vivo ^{31}P-NMR study. *Biotechnol. Bioeng.* **52**, 176-182.

Smibert, R. M. and Krieg, N. R., 1994. Phenotypic Characterization. In: Gerhardt, P., Murray, R. G. E., Wood, W. A., and Krieg, N. R. Eds., *Methods for general and molecular bacteriology*. American Society for Microbiology, Washington, D.C.

Sobecky, P. A., Schell, M. A., Moran, M. A., and Hodson, R. E., 1996. Impact of a genetically engineered bacterium with enhanced alkaline phosphatase activity on marine phytoplankton communities. *Appl. Environ. Microbiol.* **62**, 6-12.

Sowder, A. G., Clark, S. B., and Fjeld, R. A., 2001. The impact of mineralogy in the U(VI)-Ca-PO_4 system on the environmental availability of uranium. *Journal of Radioanalytical and Nuclear Chemistry* **248**, 517-524.

Stec, B., Holtz, K. M., and Kantrowitz, E. R., 2000. A revised mechanism for the alkaline phosphatase reaction involving three metal ions. *Journal of Molecular Biology* **299**, 1303-1311.

Stubbs, J. E., Elbert, D. C., Veblen, D. R., and Zhu, C., 2006. Electron microbeam investigation of uranium-contaminated soils from Oak Ridge, TN, USA. *Environ. Sci. Technol.* **40**, 2108-2113.

Stumm, W., 1997. Reactivity at the mineral-water interface: dissolution and inhibition. *Colloids and Surfaces A: Physiochem. Eng. Aspects* **120**, 143-166.

Stumm, W. and Morgan, J. J., 1996. *Aquatic Chemistry: Chemical Equilibria and Rates in Natural Waters*. John Wiley & Sons, Inc., New York.

Suzuki, Y. and Banfield, J. F., 1999. Geomicrobiology of uranium. In: Burns, P. C. and Finch, R. Eds., *Uranium: Mineralogy, Geochemistry and the Environment*. Mineralogical Society of America, Washington, D.C.

Suzuki, Y. and Banfield, J. F., 2004. Resistance to, and accumulation of, uranium by bacteria from a uranium-contaminated site. *Geomicrobiol. J.* **21**, 113-121.

Suzuki, Y., Kelly, S. D., Kemner, K. M., and Banfield, J. F., 2002. Nanometre-size products of uranium bioreduction. *Nature* **419**, 134.

Sylwester, E. R., Hudson, E. A., and Allen, P. G., 2000. The structure of uranium (VI) sorption complexes on silica, alumina, and montmorillonite. *Geochim. Cosmochim. Acta* **64**, 2431-2438.

Tessier, A., Fortin, D., Belzile, N., DeVitre, R. R., and Leppard, G. G., 1996. Metal sorption to diagenetic iron and manganese oxyhydroxides and associated organic matter: Narrowing the gap betwen field and laboratory measurements. *Geochim. Cosmochim. Acta* **60**, 387-404.

Tiedje, J. M., Sexstone, A. J., Myrold, D. D., and Robinson, J. A., 1982. Denitrification: ecological niches, competition and survival. *Antonie van Leeuwenhoek* **48**, 569-583.

Tokunaga, T. K., Wan, J., Kim, Y., Sutton, S. R., Newville, M., Lanzirotti, A., and Rao, W., 2008. Real-time X-ray absorption spectroscopy of uranium, iron, and manganese in contaminated sediments during bioreduction. *Environ. Sci. Technol.* **42**, 2839-2844.

Turner, B. L., Papházy, M. J., Haygarth, P. M., and McKelvie, I. D., 2002. Inositol phosphates in the environment. *Phil. Trans. R. Soc. Lond. B* **357**, 449-469.

Van Genuchten, M. T., 1981. Analytical solution for chemical transport with simultaneous adsorption, zero-order production and first order decay. *Journal of Hydrology* **43**, 213-233.

Van Haverbeke, L., Vochten, R., and Van Springel, K., 1996. Solubility and spectrochemical characteristics of synthetic chernikovite and meta-ankoleite. *Mineral. Mag.* **60**, 759-766.

Venkateswaran, K., Moser, D. P., Dollhopf, M. E., Lies, D. P., Saffarini, D. A., MacGregor, B. J., Ringelberg, D. B., White, D. C., Nishijima, M., Sano, H., Burghardt, J., Stackebrandt, E., and Nealson, K. H., 1999. Polyphasic taxonomy of the genus *Shewanella* and description of *Shewanella oneidensis* sp. nov. *Int. J. Syst. Bacteriol.* **49**, 705-724.

Vershinina, O. A. and Znamenskaya, L. V., 2002. The Pho regulons of bacteria. *Microbiology* **71**, 497-511.

Wade Jr., R. and DiChristina, T. J., 2000. Isolation of U(VI) reduction-deficient mutants of *Shewanella putrefaciens*. *FEMS Microbiol. Lett.* **184**, 143-148.

Waite, T. D., Davis, J. A., Payne, T. E., Waychunas, G. A., and Xu, N., 1994. Uranium(VI) adsorption to ferrihydrite: Application of a surface complexation model. *Geochim. Cosmochim. Acta* **58**, 5465-5478.

Wan, J., Tokunaga, T. K., Brodie, E., Wang, Z., Zheng, Z., Herman, D., Hazen, T. C., Firestone, M. K., and Sutton, S. R., 2005. Reoxidation of bioreduced uranium under reducing conditions. *Environ. Sci. Technol.* **39**, 6162-6169.

Wanner, B. L., 1993. Gene regulation by phosphate in Enteric bacteria. *Journal of Cellular Biochemistry* **51**, 47-54.

Warren, L. A. and Haack, E. A., 2001. Biogeochemical controls on metal behaviour in freshwater environments. *Earth-Science Reviews* **54**, 261-320.

Webb, S. M., 2005. SIXPACK: A graphical user interface for XAS analysis using IFEFFIT. *Phys. Scr.* **T115**, 1011-1014.

Weinberger, R., 2000. *Practical Capillary Electrophoresis*. Academic Press, San Diego.

Wellman, D. M., Gunderson, K. M., Icenhower, J. P., and Forrester, S. W., 2007. Dissolution kinetics of synthetic and natural meta-autunite minerals, $X_{3\text{-}n}^{(n)+}[(UO_2)(PO_4)]_2 \cdot xH_2O$, under acidic conditions. *Geochem. Geophys. Geosyst.* **8**, Q11001.

Wellman, D. M., Icenhower, J. P., and Owen, A. T., 2006. Comparative analysis of soluble phosphate amendments for the remediation of heavy metal contaminants: Effect on sediment hydraulic conductivity. *Environmental Chemistry* **3**, 219-224.

Wielinga, B., Bostick, B., Hansel, C. M., Rosenzweig, R. F., and Fendorf, S., 2000. Inhibition of bacterially promoted uranium reduction: Ferric (hydr)oxides as competitive electron acceptors. *Environ. Sci. Technol.* **34**, 2190-2195.

Wu, W.-M., Carley, J., Fienen, M., Mehlhorn, T., Lowe, K., Nyman, J., Luo, J., Gentile, M. E., Rajan, R., Wagner, D., Hickey, R. F., Gu, B., Watson, D., Cirpka, O. A., Kitanidis, P. K., Jardine, P. M., and Criddle, C. S., 2006a. Pilot-scale in situ bioremediation of uranium in a highly contaminated aquifer. 1. Conditioning of a treatment zone. *Environ. Sci. Technol.* **40**, 3978-3985.

Wu, W.-M., Carley, J., Gentry, T., Ginder-Vogel, M. A., Fienen, M., Mehlhorn, T., Yan, H., Caroll, S., Pace, M. N., Nyman, J., Luo, J., Gentile, M. E., Fields, M. W., Hickey, R. F., Gu, B., Watson, D., Cirpka, O. A., Zhou, J., Fendorf, S., Kitanidis, P. K., Jardine, P. M., and Criddle, C. S., 2006b. Pilot-scale in situ bioremediation of uranium in a highly contaminated aquifer. 2. Reduction of U(VI) and geochemical control of U(VI) bioavailability. *Environ. Sci. Technol.* **40**, 3986-3995.

Wu, W.-M., Carley, J., Luo, J., Ginder-Vogel, M. A., Cardenas, E., Leigh, M. B., Hwang, C., Kelly, S. D., Ruan, C., Wu, L., Van Nostrand, J., Gentry, T., Lowe, K., Mehlhorn, T., Carroll, S., Luo, W., Fields, M. W., Gu, B., Watson, D., Kemner, K. M., Marsh, T., Tiedje, J., Zhou, J., Fendorf, S., Kitanidis, P. K., Jardine, P. M., and Criddle, C. S., 2007. In situ bioreduction of uranium (VI) to submicromolar levels and reoxidation by dissolved oxygen. *Environ. Sci. Technol.* **41**, 5716-5723.

Yong, P. and Macaskie, L. E., 1995. Enhancement of uranium bioaccumulation by a *Citrobacter* sp. via enzymatically-mediated growth of polycrystalline $NH_4UO_2PO_4$. *J. Chem. Technol. Biotechnol.* **63**, 101-108.

Yong, P. and Macaskie, L. E., 1999. The role of sulfate as a competitive inhibitor of enzymatically-mediated heavy metal uptake by *Citrobacter* sp: implications in the bioremediation of acid mine drainage water using biogenic phosphate precipitant. *J. Chem. Technol. Biotechnol.* **74**, 1149-1156.

Zabinsky, S. I., Rehr, J. J., Ankudinov, A., Albers, R. C., and Eller, M. J., 1995. Multiple-scattering calculations of X-ray absorption spectra. *Phys. Rev. B* **52**, 2995-3009.

Zheng, Z., Wan, J., Song, X., and Tokunaga, T. K., 2006. Sodium meta-autunite colloids: Synthesis, characterization, and stability. *Colloids and Surfaces A: Physiochem. Eng. Aspects* **274**, 48-55.

Zhijun, G., Feihu, G., and Zuyi, T., 2006. Effects of phosphate and ionic strength upon uranium(VI) sorption onto alumina as a function of pH. *Radiochim. Acta* **94**, 223-228.

Zhou, P. and Gu, B., 2005. Extraction of oxidized and reduced forms of uranium from contaminated soils: Effects of carbonate concentration and pH. *Environ. Sci. Technol.* **39**, 4435-4440.